Bremner, Shaun Kennedy (2020) *A role for AMPK in the regulation of mitosis and cytokinesis.* PhD thesis.

https://theses.gla.ac.uk/80254/

Enlighten: Theses
https://theses.gla.ac.uk/
research-enlighten@glasgow.ac.uk

A role for AMPK in the regulation of mitosis and cytokinesis

Shaun Kennedy Bremner MRes, BSc (Hons)

Submitted in fulfilment of the requirements for
the Degree of Doctor of Philosophy

March 2020

School of Medical, Veterinary and Life Science

Institute of Cardiovascular and Medical Science

University of Glasgow

Abstract

AMP-activated protein kinase (AMPK) has a central role in maintaining cellular energy homeostasis. AMPK is activated allosterically by AMP and signals to inhibit ATP consuming pathways while simultaneously promoting ATP producing pathways. As such AMPK exerts an anti-proliferative effect to induce cell cycle arrest when nutrient resources are limited. Although many of the anti-proliferative effects of AMPK have been well documented during interphase, less is known about how AMPK signalling may influence mitosis. A few publications have reported that levels of active phospho-T172 AMPK increase as mitosis progresses and a link has also been reported between AMPK and myosin regulatory light chain (MRLC) in mitosis. In this Thesis, a combination of cellular, genetic and biochemical techniques were used to further characterise the role of AMPK in mitosis.

A novel localisation of the AMPKα1 subunit was described, where AMPKα1 was detected at the microtubule organising centres (MTOCs) during mitosis in both primary human cells and in HeLa cells. AMPKα2 localisation to the midbody was also demonstrated in primary cells and in cell lines. Modulation of AMPK activity by either pharmacological or genetic means caused cell cycle arrest and influenced polyploidy in a number of cell lines.

A yeast genetic approach was utilised to investigate the link between the AMPK pathway and a number of key mitotic regulates. Genetic interactions were detected between the AMPK pathway and *S. pombe* aurora kinase (*ark1*), polo-like kinase (*plo1*), anillin (*mid1*) and components of the endosomal sorting complex required for transport (ESCRT) machinery. Furthermore, a network of cross phosphorylation events were described *in vitro* between the mammalian protein orthologues. This included the phosphorylation of aurora A, aurora B and PLK1 by AMPK and the phosphorylation of aurora A and aurora B by Ca^{2+}/calmodulin-dependent protein kinase kinase ß (CaMKKß).

Considering the localisation of AMPK to mitotic structures and the numerous interactions documented with mitotic proteins, a role for AMPK in the regulation of mitosis is clear although the precise cellular effects remain difficult to discern.

Table of Contents

List of Figures

List of Tables

Acknowledgement

Author's Declaration

I declare that the work presented in this Thesis has been carried out by me, unless otherwise stated. It is entirely of my own composition and has not, in whole or in part, been submitted for any other degree.

Shaun Kennedy Bremner

March 2020

Abbreviations

4E-BP1	eukaryotic initiation factor 4E binding protein
ACC	Acetyl-CoA carboxylase
ADaM	Allosteric drug and metabolite
Ad.AMPK-CA	constitutively active AMPK adenovirus
Ad.AMPK-DN	Dominant negative AMPK adenovirus
Ad.GFP	GFP recombinant adenovirus
Ad.Null	Null adenovirus
ADP	Adenosine diphosphate
AICAR	5-aminoimidazole-4-carboxamide riboside
AID	Auto-inhibitory sequence
ALIX	Apoptosis-linked gene 2-interacting protein
AMP	Adenosine monophosphate
AMPK	AMP-activated protein kinase
ANOVA	Analysis of variance
APS	Ammonium persulphate
ARK	AMPK related kinase
ATP	Adenosine triphosphate
BRSK1/2	brain-specific kinase 1/2
BSA	Bovine serum albumin
CaM	Calmodulin
CaMKK	Calcium calmodulin dependent protein kinase kinase
CBS	Cystathionine β synthase
CBD	Carbohydrate binding domain
cdc	Cell division cycle
CDK	Cyclin-dependant kinase
CDKI	CDK inhibitor
C. elegans	*Caenorhabditis elegans*

CEP55	Centrosomal protein of 55 kDa
CHMP	Charged multivesicular body protein
DMEM	Dulbecco's modified Eagle's medium
DMSO	Dimethyl sulphoxide
DN	Dominant negative
DTT	Dithiothreitol
E. coli	*Escherichia coli*
FBS	Foetal bovine serum
EMM	Edinburgh minimal media
ESCRT	Endosomal sorting complex required for transport
FS-A	Forward scatter by area
G_1-phase	Gap 1-phase
G_2-phase	Gap 2-phase
GAPDH	Glyceraldehyde-3-phosphate dehydrogenase
GFP	Green fluorescent protein
GG	"Glasgow" lab collection number
GLUT4	Glucose transporter 4
HAEC	Human aortic endothelial cells
HEK 293	Human embryonic kidney 293 cell
HIV	Human immunodeficiency virus
HUVEC	Human umbilical vein endothelial cells
ID	Immunodeplete
IF	Immunofluorescence
IgG	Immunoglobulin G
IP	Immunoprecipitation
Ipl1	increase-in-polyploidy 1
KD	Kinase dead
LKB1	Liver kinase B1
LSB	Laemmli sample buffer

MBP	Myelin basic protein
mCherry	Monomeric cherry
ME	Malt extract
MEF	Mouse embryonic fibroblast
MEM	Minimal essential media
MetSal	Metformin and salicylate
M-phase	Mitosis-phase
MO25	Mouse protein-25
MRLC	Myosin regulatory light chain
MTOC	Microtubule organising centre
mTOR	Mammalian target of rapamycin
mTORC1	mTOR complex 1
mTORC2	mTOR complex 2
MVB	Multivesicular bodies
MYPT1	myosin phosphatase targeting-1
NSCLC	Non-small cell lung carcinoma
p70S6K	p70 ribosomal protein S6 kinase 1
PBD	Polo-box domain
PBS	Phosphate buffered saline
PBST	PBS with Tween-20
PCM	Pericentriolar material
PE-A	Phycoerythrin by area
pfu	Plaque forming units
PI	Propidium iodide
PJS	Peutz-Jeghers syndrome
PLK	Polo-like kinase
PP1ß	protein phosphatase 1ß
Sc	Scrambled
S. cerevisiae	*Saccharomyces cerevisiae*

SDS-PAGE	Sodium dodecyl sulphate-polyacrylamide gel electrophoresis
SEM	Standard error of the mean
SGLT2	Sodium/glucose cotransporter 2
siRNA	Small interfering RNA
Snf1	Sucrose non-fermenting1
SnRK1	Snf1-related protein kinase
SPB	Spindle pole body
SSC	Squamous cell carcinoma
STRAD	STE20-related kinase adapter protein
S-phase	Synthesis-phase
S. pombe	*Schizosaccharomyces pombe*
TBS	Tris buffered saline
TBST	TBS with Tween-20
TE	Tris-EDTA
TEMED	N,N,N',N'-tetramethylethylenediamine
TSG101	Tumour susceptibility gene 101
ULK1	Unc-51 like kinase 1
UTR	Untranslated region
Vps	Vacuolar protein sorting
YE	Yeast extract
YFP	Yellow fluorescent protein
YGRC	Yeast genetic resource centre
WT	Wild type
ZMP	5'-aminoimidazole-4-carboxamide ribonucleotide monophosphate

1 Chapter 1-Introduction

1.1 The cell cycle and cytokinesis

1.1.1 Overview of the cell cycle

During the cell cycle, eukaryotic cells sequentially pass through several phases culminating in the formation of two daughter cells. The cell cycle can be divided into four distinct stages; G_1 (gap 1) where cells grow; S (synthesis) phase where DNA replication occurs; G_2 (gap 2) an intermediate phase allowing cells to perform check points and grow before finally M (mitosis) phase, where chromosomes segregate and the cell divides (Figure 1-1) (Alberts *et al.*, 2012). Collectively G_1-, S- and G_2- phase are referred to as interphase.
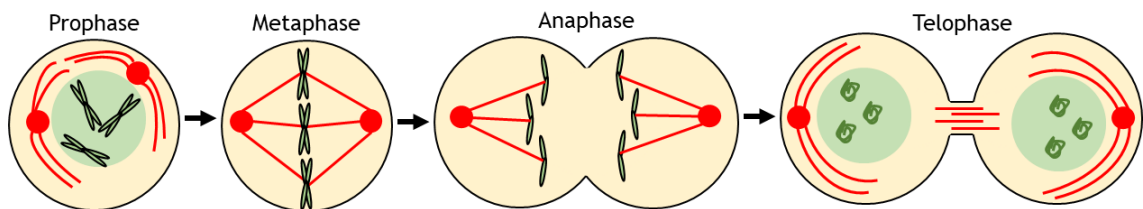
Figure 1-1. Representation of mammalian cell mitosis
During prophase, the nuclear envelope breaks down as chromosomes condense. In metaphase, the chromosomes align at the cell equator as the spindles attach to the centromeres. As mitosis progresses to anaphase, the chromatids are separated as a cleavage furrow forms. Plasma membrane ingression continues into telophase until daughter cells are connected by a thin intracellular bridge. Cytokinesis resolves the intracellular bridge, separating the daughter cells.

Mitosis can also be subdivided into a number of phases; prophase, metaphase, anaphase and telophase (Figure 1-1). During prophase chromosomes condense and spindles begin to form. In metaphase spindle fibres align the chromosomes in the centre of the cell. In anaphase chromatids are separated and begin to move to the poles of the cell. Finally in telophase, chromatids arrive at the poles of the cells and the nuclear envelope reforms. For daughter cells to separate, a cleavage furrow is formed by the ingression of the plasma membrane. Membrane furrowing continues until the daughter cells are connected by a thin intracellular bridge with an array of microtubules at is core, called the central spindle. At the centre of the intracellular bridge, the midbody, a series of signalling pathways culminate in membrane abscission, this will be discussed in more detail in the following Sections (Alberts *et al.*, 2012).

1.1.2 Centrosomes in mitosis

From early investigations, it was apparent that microtubules originate from a distinct subcellular site which was termed the microtubule organising centre (MTOC) (Pickett-Heaps, 1969). MTOCs act as a site for the minus (non-dynamic) end of microtubules to anchor to and nucleate from. The most well defined MTOC is the centrosome which is crucial for karyokinesis. The centrosome is composed of two centrioles and pericentriolar material (PCM). Generally, most mammalian cells contain one MTOC which is replicated in S-phase in dividing cells (Robbins *et al.*, 1968).

Early in mitosis a number of proteins localise to the centrosomes such as cyclin-dependant kinase 1 (CDK1)/cyclin B, aurora A and polo-like kinase 1 (PLK1) (Jackman *et al.*, 2003). Therefore it has been suggested that the centrosomes may act as a platform to integrate mitotic signalling pathways. PLK1 and aurora A play an important role in the maturation of centrioles, which will be discussed further in Section 1.1.4.

1.1.3 Cytokinesis

In mammalian cells the division plane is defined by the microtubules following karyokinesis (Cao and Wang, 1996; Eckley *et al.*, 1997). During the early stages of cytokinesis, the primary ingression occurs to form the intracellular bridge. This process is controlled by the formation of an actomyosin ring beneath the cell membrane at the cell equator. Contraction of the actomyosin ring begins in anaphase and causes invagination of the cell membrane to form the cleavage furrow (Eggert *et al.*, 2006). After chromosome separation, the spindles in the midzone are reorganised to form an array of antiparallel bundles (central spindle) which become the backbone for the intracellular bridge (Guertin *et al.*, 2002). To enable daughter cell separation, the endosomal sorting complex required for transport (ESCRT) machinery is recruited to the midbody to mediate abscission (Eggert *et al,.* 2006). The role of the ESCRT machinery in cytokinesis will be discussed in this Section and other facets of the ESCRT proteins will be discussed further in Section 1.1.4.3.

Briefly, the ESCRT machinery have been described in a number of processes including multivesicular body (MVB) formation, HIV budding and cytokinesis. The ESCRT proteins were originally described in *S. cerevisiae* where mutations in the ESCRT genes caused the missorting of cargo destined for the vacuole causing an abnormal endocytic structure to form (Raymond *et al.*, 1992). Many of these mutated genes were denotes as "vacuolar protein sorting mutants (vps)" (Raymond *et al.*, 1992). The ESCRT proteins can be organised into member of four heteromeric complexes, denoted, ESCRT-0, ESCRT-I, ESCRT-II and ESCRT-III, or form a group of accessory proteins which includes Vps4 an AAA-ATPase (Saksena *et al.*, 2009).

For membrane abscission, centrosomal protein of 55 kDa (CEP55), is recruited to the midbody by the endosomal membrane protein syntaxin 16 (Lee *et al.*, 2008; Neto *et al.*, 2013). The ESCRT-I tumour susceptibility gene 101 (TSG101) is then recruited to the midbody which forms two cortical rings on either side of CEP55 (Figure 1-2) (Lee *et al.*, 2008). ESCRT-III subunits (charged multivesicular body protein 4b (CHMP4B), CHMP2A, CHMP2B and CHMP6) polymerises to form a ringed structure on either side of the midbody (Elia *et al.*, 2011; Guizetti *et al.*, 2011). The initial ESCRT-III polymer structure forms with a diameter greater than 1 μm (Elia *et al.*, 2012). However, ESCRT-III polymer rings favour a diameter of 50 nm, thus the greater diameter puts mechanical stress on the complex. As ESCRT-III assembles, Vps4 remodels the emerging polymer and eventually splits the complex into two distinct structures. The initial structure remains in place at the midbody, whereas the second structure (referred to as the fission complex) constricts to 50 nm as it travels along the intracellular bridge while remaining bound to the membrane (Figure 1-2). As the fission complex relaxes to its more energetically favourable structure, the membrane is deformed to drive membrane fusion (Elia *et al.*, 2012). ESCRT proteins are vital for efficient cytokinesis; disruption of the Cep55/ESCRT-III interaction causes failure of cytokinesis and binucleation (Carlton *et al.*, 2008). Furthermore, depletion of TSG101 or Vps4 overexpression prevents abscission in HeLa cells (Morita *et al.*, 2007).
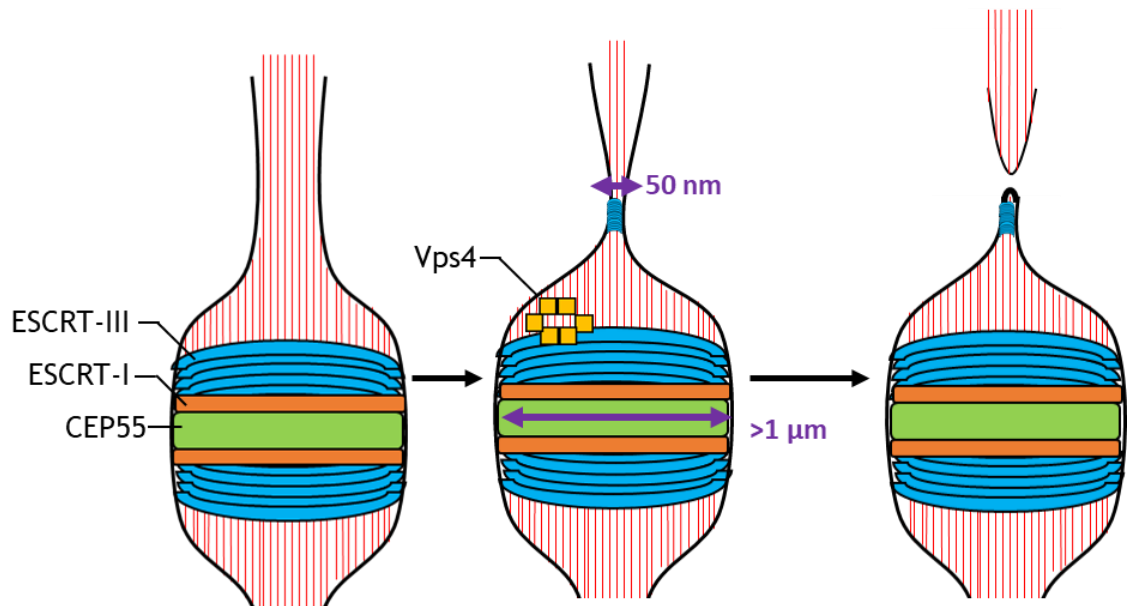
Figure 1-2. Schematic representation of ESCRT-mediated cytokinesis
Following membrane furrowing, newly formed daughter cells are connected by a thin intracellular bridge. At the centre of the intracellular bridge is the midbody where the ESCRT machinery catalyse membrane fusion to separate daughter cells. CEP55 is recruited to the midbody which in turn recruits ESCRT-I components which links to the ESCRT-III machinery. ESCRT-III polymerise to forms cortical rings with a diameter of >1 µm on either side of the midbody. Following remodelling by Vps4, some of the ESCRT-III polymer separates and constricts to a diameter of 50 nm. The deformation forces of this remodelling causes membrane fusion to separate daughter cells. Red lines are microtubules.

1.1.4 Important regulators of cytokinesis

1.1.4.1 Aurora kinases

Aurora was identified as an orthologue of increase-in-polyploidy 1 (Ipl1) in *S. cerevisiae* during a screen for mitotic mutants that failed to segregate chromosomes normally (Chan and Botstein, 1993). The *Drosophila* orthologue is crucial for mitosis to occur efficiently and mutations cause pupal lethality, mitotic arrest and chromosome mis-segregation (Glover *et al.*, 1995). Mammalian cells encode three aurora kinases; aurora A, aurora B and aurora C.

The mammalian aurora paralogues have similar sequences in the C-terminal kinase domain but have differing N-terminal domains (Bischoff *et al.*, 1998; Giet and Prigent, 1999). The three kinases show overlapping yet distinct localisations and functions. Aurora-A associates with the centrosomes, with regions on microtubules proximal to centrosomes and the spindle midzone (Sugimoto *et al.*, 2002). During prophase, aurora A and other mitotic regulators such as PLK1 are

recruited to the MTOC (Petretti *et al.*, 2006). Aurora A then facilitates centrosomal maturation and γ-tubulin recruitment (Hannak *et al.*, 2001). Depletion of aurora A leads to monopolar spindles and delays mitosis (Liu and Ruderman, 2006; Bertolin *et al.*, 2016). As mitosis progresses, aurora A is important for formation of the central spindle (Lioutas and Vernos, 2013; Reboutier *et al.*, 2013).

Aurora-B interacts with centromeric heterochromatin in early mitosis to regulate the interaction between chromosomes and microtubules to ensure proper segregation (Shimada *et al.*, 2016). In anaphase, aurora B accumulates at the cleavage furrow and remains there as the midbody forms (Fuller *et al.*, 2008). Additionally aurora B signalling also coordinates the contraction of the actomyosin ring. (Minoshima *et al.*, 2003). Aurora-C is the least well characterised of the aurora paralogues. The kinase localises to the centrosome, and in late mitosis and is thought to regulate centrosome function (Kimura *et al.*, 1999). Aurora-A has attracted the most attention, due to its overexpression in numerous tumours (Bischoff *et al.*, 1998; Tanner *et al.*, 2000; Goepfert *et al.*, 2002). Overexpression of aurora A also causes polyploidy and centrosome overgrowth (Meraldi, Honda and Nigg, 2002).

1.1.4.2 Polo-like kinase

Polo-like kinase (PLK) was initially identified in *S. cerevisiae* during the screening of a number of cell division cycle (*cdc*) mutants. Temperature sensitive *cdc5* mutant cells have defective cytokinesis with increased instances of binucleation and cell cycle arrest (Hartwell *et al.*, 1973). Later it was discovered that mutations in the *Drosophila* gene *polo* inhibited embryonic development by causing cells to arrest in metaphase (Sunkel and Glover, 1988). Cells presented with multipolar spindles, polyploidy and altered centrosome structure (Sunkel and Glover, 1988). *S. cerevisiae cdc5* was later shown to be the orthologue of *Drosophila* polo and the mammalian PLK1 (Hartwell *et al.*, 1973). In mammalian cells, PLK1 has diverged into five paralogues, denoted PLK1-5. The PLK family are defined by the presence of a polo-box domain (PBD) (Kothe *et al.*, 2007). The five PLK paralogues vary in a number of ways; the number of PBDs, expression in different cells and temporal expression/activity during the cell cycle.

PLK1 has a dynamic subcellular localisation during mitosis; initially localising to the centrosomes, followed by the spindle midzone, the kinetochore of mitotic chromosomes and finally to the midbody (Arnaud *et al.*, 1998). Reflecting the dynamic mitotic localisation, PLK1 regulates a number of processes including centrosome maturation and bipolar spindle formation in late G_2 or prophase (Lane, 1996). PLK1 signalling is also important for mitotic progression past the G_2/M boundary (Abrieu *et al.*, 1998). Depletion of PLK1 delays mitotic entrance, and cells accumulate in a pre-anaphase state which often causes apoptosis (Sumara *et al.*, 2004). Injection of a constitutively active form of Plx1 (*Xenopus* orthologue of PLK1) into *Xenopus* oocytes causes arrest prior to cytokinesis resulting in polyploidy. This suggests that PLK1 must be inactivated for cytokinesis to occur efficiently (Qian *et al.*, 1999). Conversely, PLK1 inhibition during anaphase suppresses cleavage furrow formation and cell division (Burkard *et al.*, 2007).

The other mammalian PLK paralogues can be organised into two families; PLK2, PLK3 and PLK5 belong to the PLK2 subfamily whereas PLK4 is distinct. PLK4 is the most structurally divergent of the PLK family and functions as a regulator of centriole duplication (Habedanck *et al.*, 2005). PLK2 expression peaks in S-phase and is not essential for growth (Ma *et al.*, 2003). PLK3 is important at the G_1/S phase transition and has a role in responding to DNA damage and mitotic spindle disruption (Bahassi *et al.*, 2002). The human gene for PLK5 contains a stop codon within the kinase domain, immediately after this stop codon is a second open reading frame which encodes the rest of PLK5 (Andrysik *et al.*, 2010). PLK5 is downregulated in proliferating cells and ectopic expression caused causes cell cycle arrest in G_1 (Andrysik *et al.*, 2010; de Carcer *et al.*, 2011).

1.1.4.3 ESCRT proteins

As described in Section 1.1.3 the ESCRT machinery plays a central role in cytokinesis. In this Section the ESCRT proteins will be described more broadly. The ESCRT machinery can be divided into four complexes which function with an array of accessory proteins such as Vps4 and apoptosis-linked gene 2-interacting protein (ALIX) an "early acting ESCRT-factor". Vps4 oligomerizes to form a hexameric ring crucial for recycling and remodelling the ESCRT-III polymer (Carlton and Martin-Serrano, 2007; Su *et al.*, 2017).
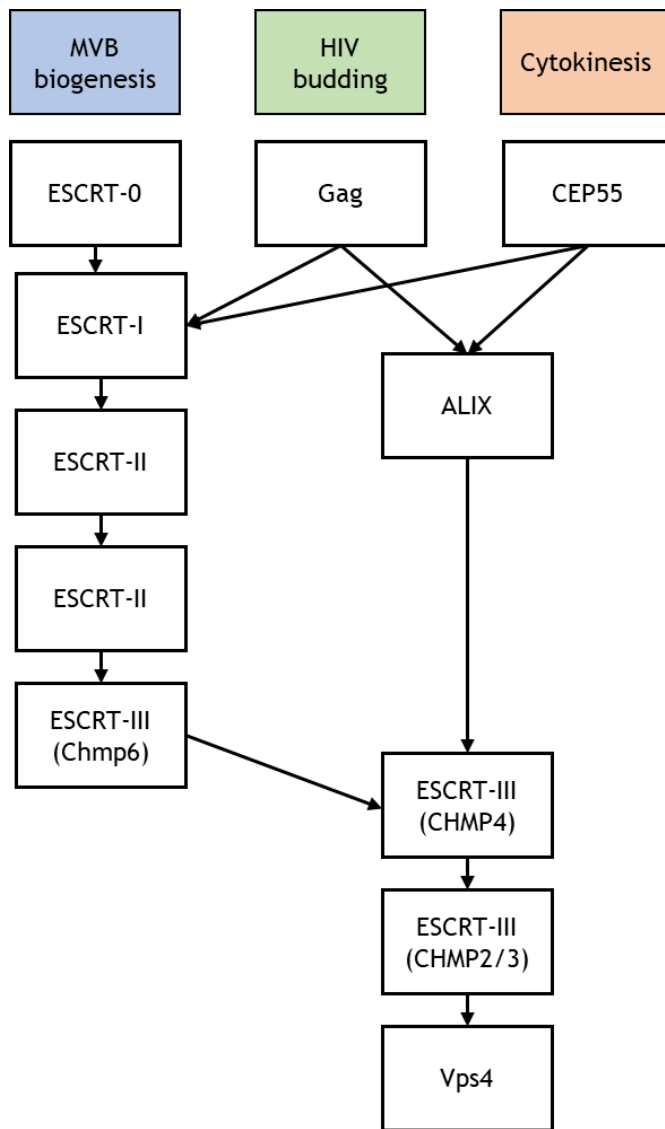
Figure 1-3.Comparison of the ESCRT pathways for MVB biogenesis, virus budding and cytokinesis
Representation of the three main pathways of membranes scission catalysed by the ESCRT machinery. Multivesicular body (MVB) biogenesis occurs by the "canonical" ESCRT pathway in which the ESCRT-0 recognises cargo and sequentially recruits the other complexes culminating in scission being catalysed by ESCRT-III and Vps4. In HIV budding, Gag is the adaptor utilised whereas in cytokinesis, CEP55 is the adaptor for ALIX. Following binding to ALIX, the canonical ESCRT pathway is followed to mediate membrane fusion

Other than cytokinesis, the ESCRT machinery regulates a number of other membrane fusion events including MVB formation, repair of ruptured membranes and by being co-opted during budding of enveloped retroviruses such as HIV. In the canonical ESCRT pathway for MVB biogenesis, HRS/STAM of ESCRT-0 binds to cargo and links to ESCRT-I enabling the sequential recruitment of the ESCRT machinery before membrane abscission is catalysed by ESCRT-III (Katzmann *et al.*, 2001) (Figure 1-3). The retroviral structural protein Gag co-opts the ESCRT machinery by interacting with ALIX to mediate viral budding (Garoff *et al.*, 1998) (Figure 1-3).

ESCRT-III proteins CHMP2A and CHMP4B have been implicated in the reformation of the nuclear envelope following karyokinesis (Olmos *et al.*, 2015). Furthermore, the ESCRT proteins have also been linked to the repair of the nuclear envelope in interphase cells. As mammalian cells migrate, the nuclear envelope can deform causing the exchange of nuclear and cytoplasmic material, these deformations are repaired by the ESCRT machinery (Raab *et al.*, 2016). Finally the ESCRT machinery has also been suggested to have a role in the repair of the plasma membrane following damage (Jimenez *et al.*, 2014; Scheffer *et al.*, 2014).

1.1.4.4 Anillin

Anillin was first described in *Drosophila* as a protein that binds to F-actin (Miller *et al.,*1989). In mammalian cells, anillin localises to the nucleus during interphase and upon the onset of mitosis localises to the cell cortex followed by enrichment at the cleavage furrow in anaphase and telophase (Field and Alberts, 1995; Oegema *et al.*, 2000). Anillin acts as a scaffold protein at the division plane and is involved in the formation of the actomyosin ring (Piekny and Glotzer, 2008). Anillin is necessary to maintain active myosin at the cleavage furrow (Straight *et al.*, 2005; Piekny and Glotzer, 2008). Interestingly, anillin is not required for the initial furrowing but is necessary for myosin accumulation and to maintain furrowing position during ingression (Straight *et al.*, 2005). Downregulation of anillin in HeLa cells causes mislocalization of the contractile ring and binucleation (Straight *et al.*, 2005). Overexpression of anillin has been described in a number of tumours, interestingly anillin expression increases as the pathology progresses (Hall *et al.*, 2005). The *S. pombe* orthologue of anillin (*mid1*) has a critical role in fission yeast cytokinesis and will be discussed in Section 1.4.3.

1.2 AMPK

1.2.1 Structure of AMPK subunits

AMP-activated protein kinase (AMPK) is a heterotrimeric serine/ threonine protein kinase composed of a catalytic α subunit and regulatory β and γ subunits. AMPK is activated allosterically by AMP binding to the γ subunit but for maximal activation, T172 on the α subunit is phosphorylated by liver kinase B1 (LKB1) or Ca^{2+}/calmodulin-dependent protein kinase kinase β (CaMKKβ) (Hawley *et al.*, 2003b, 2005; Townley and Shapiro, 2007).

In humans, multiple of isoforms the AMPK subunits exist; α1, α2, β1, β2, γ1, γ2 and γ3 each encoded by a separate gene. Therefore 12 different AMPK heterotrimer are theoretically possible (Kahn *et al.*, 2005). The expression of the different subunits varies dramatically; the β1 isoform is highly expressed in the liver with very low expression in skeletal muscles, conversely the β2 subunit is the predominant subunit in skeletal muscles (Thornton *et al.,* 1998). The subunit composition can influence AMPK activity and localisation. AMPKα2 containing heterotrimers have a much greater dependence on AMP and shows a nuclear localisation (Salt *et al.*, 1998). The γ1 isoform is the predominant subunit and is thought to represent 80-90% of total AMPK activity in many tissues.(Cheung *et al.*, 2000). The γ2 subunit is the most AMP-dependent isoform whereas the γ3 subunit has the lowest AMP dependence (Cheung *et al.*, 2000).

The N terminus of the α subunit contains the kinase domain (Figure 1-4). On the activation loop there is a critical threonine residue, T172 in AMPKα1 or T174 in AMPKα2 (by convention referred to as T172) important for activation of AMPK (Figure 1-4). The C terminus contains a domain for complex assembly. AMPKα also contains regulatory elements including an autoinhibitory domain (AID) and motifs involved in the allosteric regulation by adenine nucleotides (α linker) (Figure 1-4) (Xiao *et al.*, 2011; Chen *et al.*, 2012, 2013).

The β subunits act as a scaffold for heterotrimer formation and contains a domain for glycogen binding (Figure 1-4) (Hardie *et al.*, 2003; Polekhina *et al.*, 2003). The N-terminus of the β subunits can be myristoylated which may be important for the subcellular localisation of AMPK (Mitchelhill *et al.*, 1997).
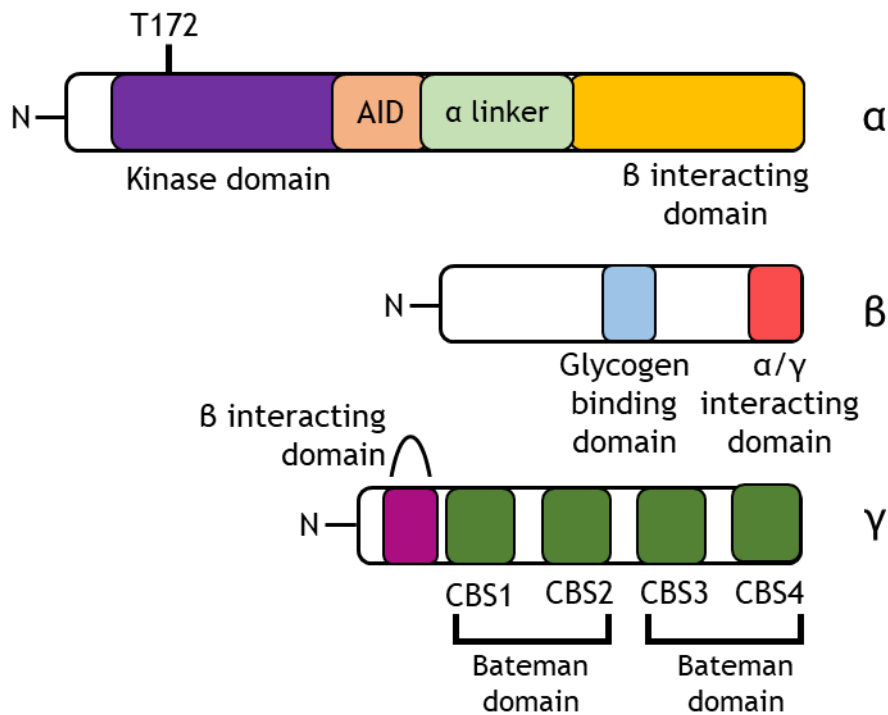
Figure 1-4. Schematic representation of the domain organisation of AMPK subunits
The α subunit contains the kinase domain and a critical threonine (T172) in the activation loop. The α subunit also contains regulatory elements including an autoinhibitory domain (AID) and the α-linker region. At the C-terminus, there is a domain needed for interaction with the β subunit. The β subunit contains a glycogen binding domain and a domain important for heterotrimer formation. The γ subunit contains an N-terminal domain which interacts with the β subunit and contains four cystathionine β-synthase repeats (CBS) which form two Bateman domains.

The γ subunit contain four cystathionine β-synthase repeats (CBS) which interact to form two Bateman domains (Figure 1-4) (Kemp, 2004). The CBS domains are responsible for nucleotide binding and thus control the allosteric activation of AMPK by AMP. Modelling studies have suggested that CBS1 and CBS3 can exchange adenine nucleotides competitively whereas CBS4 has a much high affinity for AMP which may not be exchangeable (Xiao *et al.*, 2011; Chen *et al.*, 2012; Calabrese *et al.*, 2014). CBS2 in non-functional and cannot bind adenine nucleotides as it lacks a critical aspartate. (Xiao *et al.*, 2011).

1.2.2 Control of AMPK activity

1.2.2.1 Binding of adenine nucleotides

AMP activates AMPK by three mechanisms; allosteric activation by binding to the γ domain, promoting phosphorylation of T172 by upstream kinases while inhibiting its dephosphorylation by protein phosphatases (Figure 1-5) (Davies *et al.*, 1995). Binding of AMP to CBS3 causes a conformational change where the α-hook region of the α subunit interacts with CBS3. This interaction displaces the AID from the kinase domain enabling catalytic activity (Chen *et al.*, 2012; Calabrese *et al.*, 2014; Li *et al.*, 2015). The movement of the α-hook lowers the flexibility of the α-linker region, which in turn promotes an interaction between the activation loop with the C terminus of the β domain. This is believed to physically protect T172 from phosphatases (Sanders *et al.*, 2007; Xiao *et al.*, 2011).

While ADP does not allosterically activate AMPK, binding of ADP can prevent T172 dephosphorylation (Xiao *et al.*, 2011; Gowans *et al.*, 2013). However, AMP is a 10-fold more potent inhibitor of T172 dephosphorylation than ADP (Gowans *et al.*, 2013). ATP binding causes the AID to remain in the inhibitory position where T172 remains exposed to phosphatases (Xiao *et al.*, 2011).
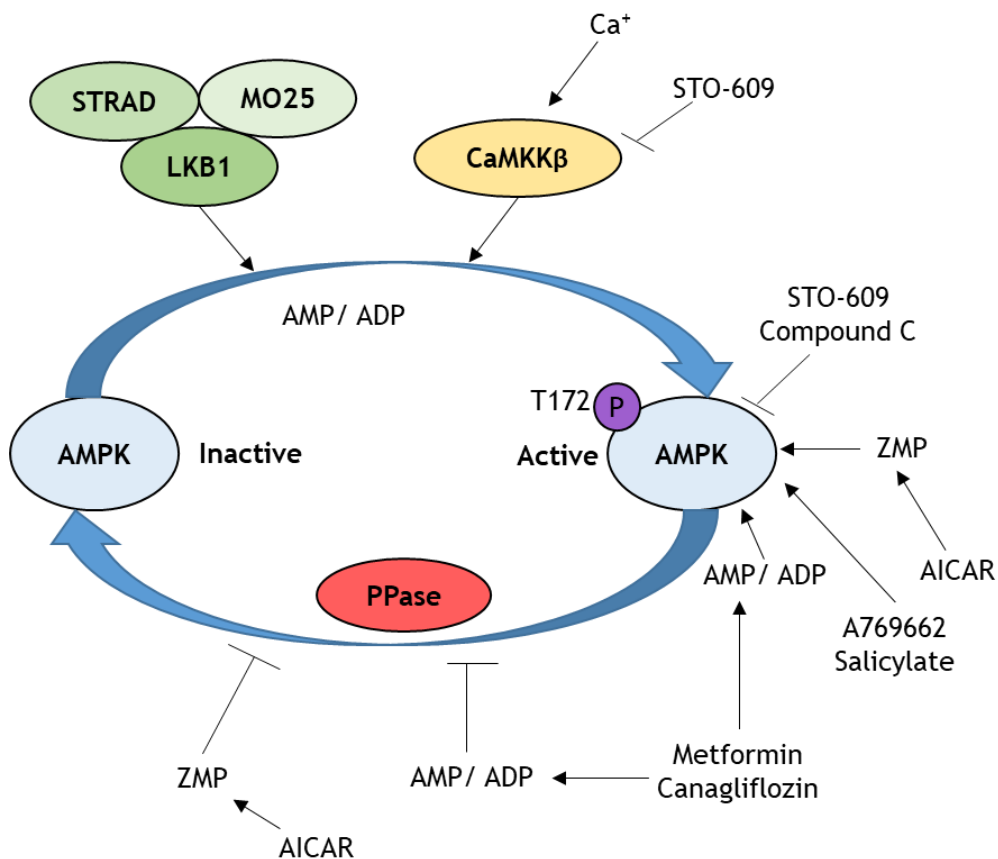
Figure 1-5. Schematic representation of AMPK activation
AMPK is activated allosterically by the binding of AMP or ADP. For maximal activation T172 in the α subunit is phosphorylated by liver kinase B1 (LKB1) which is in a complex with accessory proteins STRAD and MO25. Ca^{2+}/calmodulin-dependent protein kinase kinase β (CaMKKβ) can also phosphorylate T172 in response to increased intracellular calcium. AMP binding also promotes phosphorylation of T172 while preventing dephosphorylation by protein phosphatases (PPase). AMPK activity can be modulated by a number of compounds; STO-609 inhibits CaMKKβ and AMPK; compound C inhibits AMPK; A769662 and salicylate allosterically activate AMPK; AICAR is metabolised by cells to ZMP, an AMP mimetic; metformin and canagliflozin increase AMP levels by inhibiting mitochondrial respiration.

1.2.2.2 Phosphorylation of T172

As described, activation of AMPK involves the phosphorylation of T172 by either LKB1 or CaMKKß (Figure 1-5) (Hawley *et al.*, 2003b; Woods *et al.*, 2005). Allosteric activation by AMP increases AMPK activity by approximately 5-fold, whereas phosphorylation of T172 increases activity over 100-fold (Davies *et al.*, 1994; Suter *et al.*, 2006).

LKB1 was identified as a cause in the development of Peutz-Jeghers syndrome (PJS), a hereditary condition where individuals have a predisposition to tumours (Hemminki *et al.*, 1998). Loss of function LKB1 mutations are often detected in patients with PJS (Hemminki *et al.*, 1998). LKB1 interacts with two accessory proteins; STE20-related adaptor (STRAD) and MO25 (Hawley *et al.*, 2003a). LKB1

is necessary for full AMPK activation in response to increased intracellular AMP or AMP mimetics (Hawley *et al.*, 2003b). However, LKB1 is not itself stimulated by AMP or AMP mimetics, thus LKB1 is considered to be constitutively active (Lizcano *et al.*, 2004; Sakamoto *et al.*, 2004).

The second AMPK kinase to be described *in vivo* was CaMKKß (Figure 1-5). CaMKKß is activated by an increase in intracellular calcium and is not dependent on the energy state of the cell (Hawley *et al.*, 2005). Calcium mediated CaMKKß activation of AMPK is believed to be how many hormones can activate AMPK (Hawley *et al.*, 2005).

1.2.3 Pharmacological activators and inhibitors of AMPK

1.2.3.1 A769662

A769662 is a commonly used allosteric activator of AMPK (Figure 1-5) (Cool *et al.*, 2006). AMPK activation by A769662 is independent of T172 phosphorylation but requires phosphorylation of S108 in the ß1 subunit (Scott *et al.*, 2014). A769662 binds to an allosteric site formed between the glycogen binding motif of the ß subunit and the N-terminal lobe of the kinase domain (Cool *et al.*, 2006; Calabrese *et al.*, 2014; Li *et al.*, 2015). This binding site is referred to as the allosteric drug and metabolite (ADaM) site. A769662 stabilizes the active conformations of the α subunit and displaces the AID from the kinase domain (Calabrese *et al.*, 2014). Binding also induces the formation of an α helix in the ß subunit which interacts with the kinase domain protecting phospho-T172 from dephosphorylation and increases substrate affinity (Göransson *et al.*, 2007; Sanders *et al.*, 2007; Calabrese *et al.*, 2014). A799662 shows considerably higher selectivity for AMPK heterotrimers containing the ß1 subunit over the ß2 isoform (Scott *et al.*, 2008).

1.2.3.2 AICAR

Aminoimidazole-4-carboxamide ribonucleotide (AICAR) is an indirect activator of AMPK. AICAR is transported into cells and phosphorylated by adenylate kinase to generate ZMP, an AMP mimetic (Sullivan *et al.*, 1994; Corton *et al.*, 1995). ZMP has a lower potency than AMP for the γ subunit but stimulates AMPK activity in a similar manner (Figure 1-5) (Day *et al.*, 2007). AICAR/ZMP has also been

reported to stimulate a number of AMP-dependent enzymes other than AMPK such as fructose-1,6-bisphosphatase and 6-phosphofructo-2-kinase (Vincent *et al.*, 1991; Vincent *et al.,* 1992).

1.2.3.3 Canagliflozin

Canagliflozin is a sodium/glucose cotransporter 2 (SGLT2) inhibitor used clinically for the treatment of type 2 diabetes. SGLT2 is located in the proximal convoluted tubule and is responsible for glucose reabsorption from the urine. Thus, by inhibiting SGLT2, canagliflozin increases glucose excretion in urine to effectively lower blood glucose (Rosenwasser *et al.*, 2013). Canagliflozin stimulates AMPK activity whereas other SGLT2 inhibitors such as dapagliflozin and empagliflozin do not activate AMPK to the same extent (Hawley *et al.*, 2016). Activation of AMPK is achieved though inhibition of complex I of the electron transport chain which increases intracellular AMP and ADP levels (Figure 1-5) (Hawley *et al.*, 2016).

1.2.3.4 Compound C

Compound C is a potent ATP-competitive inhibitor of AMPK (Figure 1-5) (Zhou *et al.*, 2001). However, compound C has a number of well documented AMPK-independent effects. *In vitro* compound C inhibits a number of kinases to a greater extent than AMPK (Bain *et al.*, 2007; Emerling *et al.*, 2007; Nam *et al.*, 2008).

1.2.3.5 Metformin

Metformin has been used clinically in the treatment of diabetes for a number of years. Metformin acts as a mild mitochondrial toxin by inhibiting complex I of the electron transport chain, thereby increasing AMP and ADP levels (figure 1-5) (Owen *et al.,* 2000). In doing so hepatic gluconeogenesis is reduced and glucose utilization of peripheral tissues is increased (Owen *et al.,* 2000).

1.2.3.6 Salicylate

Salicylate is a naturally occurring compound found in willow bark and is produced as a metabolite of aspirin (Higgs *et al.*, 1987). Salicylate directly binds to AMPK causing allosteric activation and preventing T172 dephosphorylation

(Figure 1-5) (Hawley *et al.*, 2012). Similarly to A7629662, salicylate binds to the ADaM site, is dependent on S108 phosphorylation in the ß subunit and shows a selectivity for ß1 containing complexes (Hawley *et al.*, 2012). AMPK activation by salicylate is independent of adenine nucleotide ratio (Hawley *et al.*, 2012).

Salicylate and metformin are often used in combination (MetSal) to activate AMPK due to the different mechanisms of stimulating AMPK activity. This synergistic effect can be seen in human and mouse hepatocytes where MetSal causes a large increase in AMPK activity whereas incubation with either compound alone resulted in limited AMPK activation (Hawley *et al.*, 2012).

1.2.3.7 STO-609

STO-609 is an ATP-competitive inhibitor of CaMKK (Figure 1-5) (Tokumitsu *et al.*, 2002). Inhibition of CaMKKß is approximately 5-fold higher than the inhibition of CaMKKα (Tokumitsu *et al.*, 2002). STO-609 therefore represents a mechanism to downregulate AMPK activity by inhibiting one of the upstream kinase. However, as with compound C, STO-609 can inhibit a number of kinases including AMPK directly (Bain *et al.*, 2007).

1.2.4 Function and downstream targets of AMPK

1.2.4.1 Energy homeostasis

As AMPK is activated by increased levels of AMP, AMPK acts as a key sensor of cellular energy levels. AMPK signals to restore energy homeostasis by inhibiting ATP consuming processes such as fatty acid synthesis, gluconeogenesis and protein synthesis. Simultaneously, AMPK promotes ATP producing pathways; fatty acid oxidation, glucose uptake and mitochondrial biogenesis.

One of the principal downstream targets of AMPK is acetyl-CoA carboxylase (ACC) which is phosphorylated on S79 to inhibit its activity. S79 is phosphorylated exclusively by AMPK and as such phospho-S79 ACC has been accepted as a marker of AMPK activity (Ha *et al.*, 1994; Gowans *et al.*, 2013). ACC catalyses the conversion of acetyl-CoA to malonyl-CoA in the lipid synthesis pathway, thus the inhibitory phosphorylation of S79 inhibits lipid synthesis (McGarry, 2002; Munday, 2002). Furthermore, inhibition of ACC reduces the

levels of malonyl-CoA, an inhibitor of fatty acid oxidation. Therefore phosphorylation of ACC inhibits lipid synthesis while promoting fatty acid oxidation to re-establish energy homeostasis (McGarry, 2002; Fediuc *et al.*, 2006).

AMPK increases glucose import into striated muscle by increasing insulin stimulated trafficking of glucose transporter 4 (GLUT4) to the plasma membrane as well as increasing its transcription (Kurth-Kraczek *et al.*, 1999; McGee *et al.*, 2008; Lee *et al.*, 2012). GLUT4 translocation to the plasma membrane increases glucose import and thus ATP synthesis, conversely in adipocytes AMPK inhibits insulin stimulated GLUT4 trafficking which is believed to inhibit fatty acid synthesis, thereby conserving ATP (Salt *et al.*, 2000).

Consistent with the actions of AMPK to increase cellular ATP, a role has been described in mitochondrial biogenesis. One of the key transcription factors which regulate mitochondrial biogenesis is PGC-1α (Wu *et al.*, 1999). A769662 increases PGC-1α expression, whereas in AMPKα knockout cells expression of PGC-1α is impaired (Zhao *et al.*, 2014). Furthermore, pharmacological activation of AMPK in human umbilical vein endothelial cells (HUVECs) upregulates the expression of a number of proteins involved in mitochondrial biogenesis (Kukidome *et al.*, 2006).

1.2.4.2 Cell growth and proliferation

AMPK coordinates a metabolic checkpoint at the G_1/S-phase transition. During glucose limitation, AMPK induces cell cycle arrest by phosphorylating the tumour suppressor p53 at S15 (Jones *et al.*, 2005). Phosphorylation prevents p53 degradation allowing protein levels to accumulate (Shieh *et al.*, 1997). Furthermore, AMPK phosphorylates MDMX at S342, enhancing binding to 14-3-3 (He *et al.*, 2014). MDMX is a negative regulator of p53 which mediates p53 proteasomal degradation. Thus AMPK-induced sequestration of MDMX enables p53 levels to accumulate (He *et al.*, 2014). p53 regulates a number of genes including the cyclin-dependent kinase inhibitor (CDKI) p21[CIP] to cause cell cycle arrest. A metabolic checkpoint at the G_1/S-phase transition ensures cells have sufficient energy to undergo DNA replication and mitosis.

Additionally, AMPK regulates protein synthesis through mammalian target of rapamycin complex 1 (mTORC1). mTORC1 is pro-proliferative and promotes cell growth, lipid biogenesis and protein synthesis. AMPK phosphorylates raptor, one of the components of mTORC1, to inhibit mTORC1 kinase activity to cause cell cycle arrest following energy stress (Gwinn *et al.*, 2008). Furthermore, AMPK also phosphorylates the upstream regulator of mTOR, TSC2 to enhance its Rheb-GAP activity thereby inhibiting mTORC1 (Inoki *et al.*, 2003). Inhibition of mTORC1 causes inhibition of p70 ribosomal protein S6 kinase 1 (p70S6K) thereby inhibiting translation. mTORC1 inhibition also caused activation of eukaryotic initiation factor 4E binding protein (4E-BP1) to inhibits translation (Inoki *et al.*, 2002). Thus, AMPK activation inhibits protein synthesis and limits cell growth.

1.3 AMPK in mitosis and cytokinesis

Phospho-T172 AMPK has been described to localise to the MTOC during mitosis (Vazquez-Martin *et al.*, 2009; Thaiparambil *et al.*, 2012). AMPK has also been reported to be important for the correct positioning of the spindle apparatus, as downregulation of AMPK causes spindle misorientation and mitotic delay (Thaiparambil *et al.*, 2012). In later stages of mitosis, the AMPKα2 subunit and phospho-T172 AMPK has been reported to localise to the midbody (Vazquez-Martin *et al.*, 2009; Pinter *et al.*, 2012). Interestingly, glucose deprivation does not alter phospho-T172 AMPK mitotic localisation (Vazquez-Martin *et al.*, 2012).

Phospho-S79-ACC has been reported to have an identical localisation pattern as phospho-T172 AMPK during mitosis (Vazquez-Martin *et al.*, 2009; Vazquez-Martin *et al.*, 2013). Additionally, levels of S79-phospho-ACC have been shown to be increased during mitosis in an AMPK-dependent manner demonstrating AMPK activity in mitosis (Mao *et al.*, 2013). Fission yeast which have a disrupted ACC gene have impaired nuclear division causing the formation of large polyploid nuclei which arrest at the G2/M transition (Saitoh *et al.*, 1996). Furthermore, inhibition of fatty acid synthesis in HeLa cells causes cell cycle arrest at the G_2/M-phase boundary despite fatty acids being present in the media. Together this may suggest a role for ACC in mitosis either through the coupling of lipogenesis to cell cycle progression or in a yet to be defined role (Scaglia *et al.*, 2014).

A chemical genetic screen identified protein phosphatase 1 regulatory subunit 12C (PPP1R12C) and p21-activated protein kinase (PAK2) as substrates for AMPKα2 phosphorylation on S452 and S20 respectively (Banko *et al.*, 2011). PPP1R12C inhibits myosin regulatory light chain (MRLC), a regulator of mitosis and cytokinesis whereas PAK2 promotes MRLC phosphorylation (Tuazon and Traugh, 1984; Komatsu *et al.*, 2000; Banko *et al.*, 2011). Thus, AMPK may regulate two antagonizing pathways in mitosis (Banko *et al.*, 2011). Both AMPK T172 and PPP1R12C S452 phosphorylation are elevated in prometaphase. Phosphorylation levels of both decrease as mitosis progresses but PPP1R12C phosphorylation increases at the end of mitosis (Banko *et al.*, 2011). Cells which express a phospho-null PPP1R12C (S452A) mutant have an increase in polyploidy (Banko *et al.*, 2011). Phosphorylation of PPP1R12C promotes interaction with 14-3-3 which may inactivate the complex, thus AMPK activity would promote the activation of MRLC (Banko *et al.*, 2011).

PAK2 mediates the phosphorylation of myosin light chain kinase (MLCK) and is involved in cytoskeletal reorganisation (Goeckeler *et al.*, 2000). The inhibitory phosphorylation of MLCK causes stress fibre dissolution (Sanders *et al.*, 1999). PAK2 localises with the centrosomes until metaphase where it activates aurora A and PLK1 facilitating mitotic entry, although a role for AMPK remains elusive at this time (Zhao *et al.*, 2005; Ando *et al.*, 2007; Maroto *et al.*, 2008; May *et al.*, 2014).

Metformin has been shown to alter the transcriptome of the epidermoid cancer cell line A431 cells by causing down regulation of a number of proteins including; auroras kinases, PLKs; kinesin and tubulin (Oliveras-Ferraros *et al.,* 2009). Strikingly, chronic metformin treatment has also been reported cause a reorganisation of nuclei structure forming crescent, ring or lobular shapes (Vazquez-Martin *et al.*, 2009).

1.3.1 AMPK orthologues

AMPK or its orthologues appear to be a fundamental feature of eukaryotic cell life. AMPK orthologues have been described in a range of organisms including fungi and plants, an AMPK orthologue has even been described in the primitive protozoan *Giardia lamblia* (Adam, 2000; Hardie *et al.*, 2003).

In budding yeast, the AMPKα orthologue sucrose non-fermenting 1 (Snf1) is important in the cellular response to low glucose (Hardie *et al.*, 1998). *S. cerevisiae* encode three β subunits (Gal183, Sip1 and Sip2) and one γ orthologue Snf4 (Celenza and Carlson, 1989; Yang *et al.*, 1994). Similar to mammalian AMPK, Snf4 relieves the inhibition of Snf1 by interacting with the AID domain (Leech *et al.*, 2003). The T172 of AMPKα1 is orthologous to T210 in Snf1 which is phosphorylated by three kinases; Sak1, Tos3 and Elm1 (Hong *et al.*, 2003; Sutherland *et al.*, 2003). Interestingly, Snf1 is not allosterically activated by AMP (Wilson *et al.*, 1996). SNF1 is important for a number of cellular processes such as autophagy and the response to a number of environmental stresses including ionic and heat shock (Wang *et al.*, 2001; Portillo *et al.*, 2005; Platara *et al.*, 2006).

AMPK also has an important role in plants, which encode two homologues of the AMPKα subunits, Snf1-related protein kinase (SnRK1) a/b. In the moss *Physcomitella petens* double AMPKα knockout inhibits growth unless kept under constant illumination (Thelander *et al.*, 2004).

AMPK is also well conserved in the fission yeast *Schizosaccharomyces pombe* (*S. pombe*) and will be discussed in detail in Section 1.4.4.

1.4 *S. pombe* and the cell cycle

1.4.1 *S. pombe* overview

S. pombe, or fission yeast, is a unicellular ascomycete fungus. The ascomycete phylum is defined by the production of their sexual spores in a specialised cell wall-like structure called an ascus (derived from the Greek *askos* for bag), this process is discussed further in Section 1.4.3.2 (Hoffman *et* al., 2015). *S. pombe* was originally isolated from an East African beer with "pombe" being the Swahili word for alcohol. *S. pombe* was first used as a model organism in the 1940s by Urs Leupold who researched mating and homothallism (Leupold, 1949). From these early studies, three distinct strains were isolated; 968 h^{90}, 972 h$^-$ and 975 h$^+$, which became the founders for nearly all subsequent *S. pombe* strains used experimentally (Fantes and Hoffman, 2016). As the majority of *S. pombe* research is carried out on the ancestors of these three strains (which were originated from a single isolate), most laboratory strains of *S. pombe* are isogenic. Conversely, in *S. cerevisiae*, the other widely used experimental yeast species, there are differences between the ancestral "wild type" strains, so subsequent genetic alterations could produce different results (Elion *et al.*, 1991; Ralser *et al.*, 2012; Hoffman *et al.*, 2015).

1.4.2 *S. pombe* as a model organism

S. pombe was the sixth eukaryotic organism to have its genome sequenced, confirming fission yeast a popular model for genetic studies (Wood *et al.*, 2002). *S. pombe* generally exist as haploid cells, which is important when assessing the impact of a mutation. Generally a mutation will produce a loss of function effect and be recessive to the wild type allele. Thus, in a diploid organism the effect of a recessive heterozygotic mutation would not readily be detectable, being masked by the wild type gene. Diploid fission yeast cells can however be formed and maintained under controlled certain conditions, important for other genetic analysis, especially with essential genes.

A number of the key genes and proteins have been evolutionarily conserved between *S. pombe* and mammalian cells, emphasising the use of fission yeast as a model organism. In the context of this Thesis, proteins involved in mitosis and

cytokinesis appeared one billion years ago in the common ancestor for amoeba, fungi and animals (Pollard and Wu, 2010).

1.4.3 Cell cycle of *S. pombe*

S. pombe have two cell cycles: an asexual/mitotic cell cycle in which vegetative cells follow and a sexual/meiotic cell cycle that is induced upon nitrogen limitation (Figure 1-6). In the vegetative cell cycle, *S. pombe* cells pass through consecutive G_1-, S-, G_2- and M-phases similar to animal cells. The cells grow by linear extension followed by medial fission once they reach ~14 µm, producing two daughter cells of identical size (Mitchison and Nurse, 1985). During mitosis, a division septum is deposited on the division plane prior to abscission, with this process being analogous to mammalian cytokinesis. Following septation, but prior to separation, cells which have a volume above a critical level rapidly progress through G_1 and S-phases (Nasmyth *et al.*, 1979). Therefore, the short G_1 and S-phase occur between mitosis and separation, meaning that once cells separate at the end of the previous cell cycle they are already in G_2 of the following cell cycle.

After cytokinesis, the newly formed daughter cell grows from the "old end" until mid G_2 when growth begins to occur at the "new end" that was created from the previous cell division. This alteration in growth polarity is termed "new end take-off" (NETO) and represents the switch from monopolar to bipolar growth (Mitchison and Nurse, 1985).
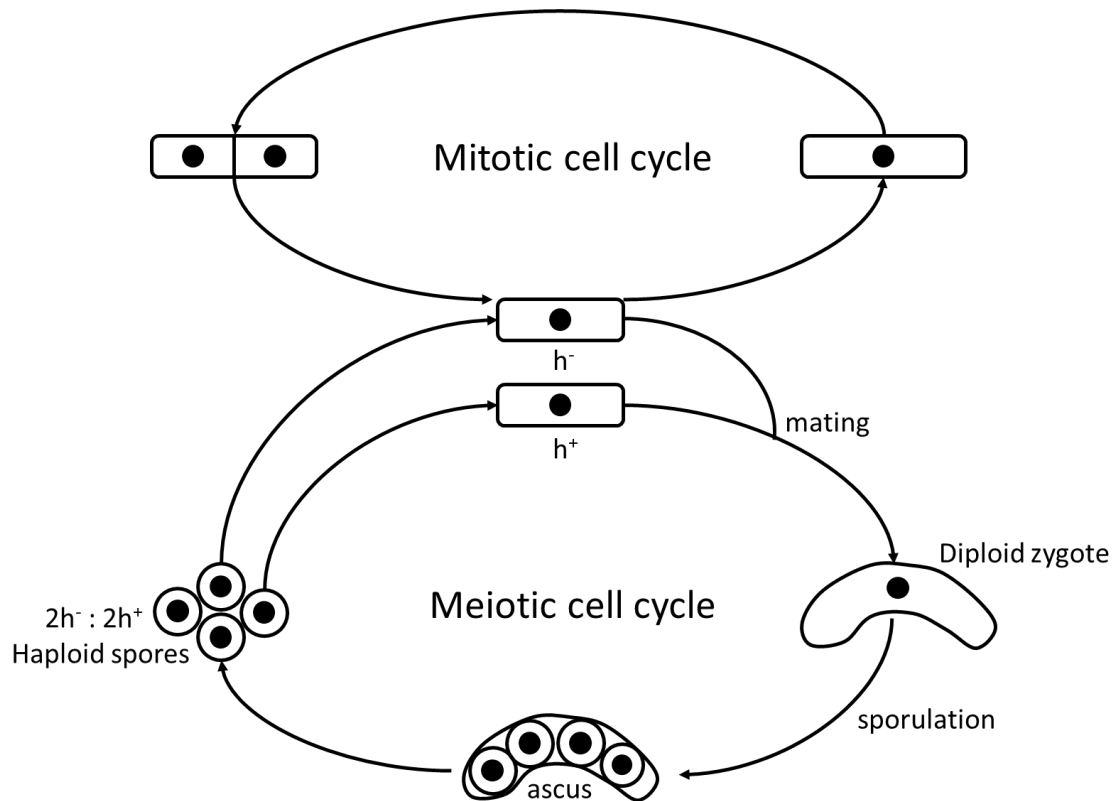
Figure 1-6. *S. pombe* **mitotic and meiotic cell cycles**
In the mitotic cell cycle *S. pombe* progress through G_1-, S-, G_2- and M phase. During cytokinesis a division septa is deposited to enable separation of daughter cells. Under nitrogen limitation cells can undergo the meiotic cell cycle where cells of opposite mating types (h^+ or h^-) undergo sexual differentiation to enable cell conjugation followed by nuclear fusion forming a diploid zygote. Meiosis and sporulation then generates four haploid spores enclosed in an ascus. The ascus is lysed to release the spores.

As cells enter mitosis, medial extension stops and actin redistributes from the growth tips to form a cortical ring at the equator (Marks *et al.*, 1986). *S. pombe* undergo "closed mitosis", in that the nuclear envelope does not breakdown for karyokinesis. Instead, from the cytoplasm, two spindle pole body's (SPBs; analogous to mammalian centrosome) align at either side of the nucleus and produce an intra-nuclear spindle (Figure 1-7) (Ding *et al.*, 1997). The condensed chromosomes adhere to the spindle, and as the spindle elongates the sister chromatids are separated (Bak *et al.*, 1977; Umesono *et al.*, 1983).

In mammalian cells the division site is defined by the microtubules, whereas in *S. pombe* the site of cytokinesis is defined by the position of the nuclei through the signalling of Plo1p (orthologous to mammalian PLK1) and Mid1p (anillin) (Chang *et al.*, 1996; Sohrmann *et al.*, 1996; Bähler *et al.*, 1998). During interphase, Mid1p transitions between the nucleus and the cell cortex (Paoletti and Chang, 2000). Once mitosis begins, Mid1p is phosphorylated by Plo1p and

exits the nucleus to the cortex forming a ring overlying the nucleus and recruits proteins for actomyosin ring formation (Sohrmann *et al.*, 1996; J Bähler *et al.*, 1998). Mutations in *mid1* results in abnormal septum positioning although cells can still divide (Sohrmann *et al.*, 1996).
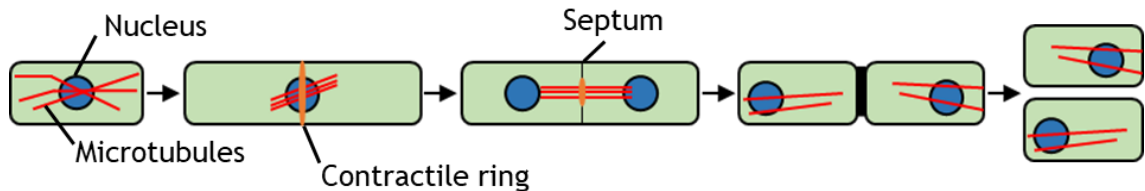
Figure 1-7. Representation of *S. pombe* mitosis and cytokinesis
During *S. pombe* mitosis the nucleus is located at the cell equator. Microtubules separate the nuclei to the cell poles and a contractile actomyosin ring is assembled at the cell equator. As the ring contracts there is deposition of septum material behind the division plane. Enzymatic digestion of the septum material separates the cells. Occasionally, cells will not separate immediately, instead remaining attached with a "delayed separation following septation" phenotype.

1.4.3.1 Septation and cytokinesis

During fission yeast cytokinesis, an actomyosin ring forms on the division plane followed by the formation of the division septa behind the contractile ring (Figure 1-7). The septum is a three-layered structure composed of an inner primary layer with secondary septa on either side. The primary septum is composed of 1,3-ß-glucan and binds strongly to the stain Calcofluor-White whereas the secondary septa consist of 1,3-α-glucan, 1,6-branched 1,3-ß-glucan, 1,6-ß-glucan and galactomannans and is less calcofluor sensitive (Horisberger and Rouvet-Vauthey, 1985; Humbel *et al.*, 2001; Sugawara *et al.*, 2003). As the primary septa is degraded by digestive enzymes, there is increased turgor pressure on the secondary septa generating a physical force to the cells (Sipiczki and Bozsik, 2000; Dekker *et al.*, 2004). Occasionally cells do not immediately separate following division and have a "delayed separation following septation" phenotype (Figure 1-7) (Mitchison and Nurse, 1985; Bhutta *et al.*, 2014).

1.4.3.2 Meiotic cell cycle

When under nutritional stress, calls rapidly progress though the cell cycle before arresting in G_1 at a smaller cell size. Two haploid cells of opposite mating types can then undergo sexual differentiation and mating to form four dormant spores which can survive unfavourable conditions (Egel and Egel-Mitani, 1974) (Figure 1-6). This process has been utilised in a number of genetic screens where two parental strains carrying mutations in separate genes were crossed to produce double mutant progeny.

Mating type is determined by the expression of genes at the *mat-cassette* on chromosome two. The mating types are denoted as h^+, h^- and h^{90}, with h^+ and h^- being heterothallic and h^{90} homothallic. Conjugation of two cells requires the cells to be of opposite mating types. h^{90} is capable with mating with itself but h^+ and h^- cannot, necessitating both mating types to be present (Egel and Gutz, 1981; Beach, 1983). In a population of h^{90} cells, there will be a mixture of both h^+ and h^- cells. *mat-cassette* gene expression is inhibited at G_2, so the genes are only expressed upon nitrogen starvation when G_1 is extended. The cassette control the expression of one of two pheromones and a receptor for the opposite pheromone. Binding of the pheromone to the appropriate receptors induces conjugation of the cells and nuclear fusion. In the now single cell, the pheromones form a heterodimer which triggers meiosis forming four haploid nuclei. A specialised cell walls forms around the spores called the ascus membrane which will eventually lyse enabling the spores to enter the mitotic cell cycle (Hoffman *et al.,* 2015).

1.4.4 The AMPK orthologue in *S. pombe*

Similar to mammalian AMPK, the *S. pombe* orthologue is a heterotrimer composed of Ssp2p (AMPKα subunit orthologue), Amk2p (AMPKß) and Cbs2p (AMPKγ) (Valbuena and Moreno, 2012). Cbs2p contains four CBS domains (Hanyu *et al.*, 2009). Structural analysis of the *S. pombe* AMPK heterotrimer has indicated that adenine nucleotides can bind competitively to a single site in Cbs2p (Townley and Shapiro, 2007). Amk2p can bind ADP but the functional significance is not known (Jin *et al.,* 2007). Ssp2p activity is regulated by a single upstream kinase Ssp1p. Sequence analysis of *S. pombe* identified *ssp1* as

the orthologue of mammalian CaMKKα and CaMKKß. *Ssp1* was first identified as a protein kinase responsible for regulating cell polarity (Matsusaka *et al.*, 1995; Hanyu *et al.*, 2009). In *ssp1* mutant cells, cortical actin was only detected at one end of the cell indicating that the cells failed to alter growth polarity for NETO. Overexpression of wild type *ssp1* caused a random distribution of cortical actin (Matsusaka *et al.*, 1995). Ssp1p phosphorylates T189 in Ssp2p in response to a number of environmental triggers including; glucose depletion, nitrogen limitation and osmotic stress (Hanyu *et al.*, 2009; Valbuena and Moreno, 2012; Davie *et al.*, 2015; Schutt and Moseley, 2017).

Consistent with mammalian studies on AMPK regulation, all three subunits are required for the adaption to low-glucose media (Matsuzawa *et al.*, 2012; Saitoh *et al.*, 2015; Deng *et al.*, 2017). Mutation of T289A in Ssp2p reduces the capacity for cells to grow on low glucose media, which mimics the phenotype of *ssp1Δ* and *ssp2Δ*. Furthermore, *amk2Δ* and *cbs2Δ* reduced cell proliferation and phospho-T189 Ssp2p levels (Deng *et al.*, 2017). This indicates that all the subunits of the AMPK heterotrimer are necessary for the adaption to low glucose and, that T189 must be phosphorylated by Ssp1p. These observations are in line with the established role of *S. cerevisiae* Snf1p in the response to glucose deprivation. Snf1p is essential for growth on media lacking glucose (Carlson *et al.*, 1981). Additionally, Snf1p is also involved in the adaption to low glucose conditions by regulating glucose uptake through the phosphorylation of Mig1p, a transcription factor for hexose transporters (Nicastro *et al.*, 2015; Treitel *et al.*, 1998).

Ssp1p mediated phosphorylation of Ssp2p is required for the adaptation to low nitrogen levels (Davie *et al.*, 2015). Unusually, for the response to nitrogen stress, Amk2p and Cbs2p are not required, nor are alterations in cellular adenine nucleotide levels (Davie *et al.*, 2015). Although each of the Ssp2p heterotrimer subunits and Ssp1p is important for sexual differentiation of *S. pombe* and deletion of each of the proteins dramatically reduced the number of zygotes (Valbuena and Moreno, 2012). Deletion of *ssp2* reduces levels of Ste11p, a transcription factor important for sexual differentiation (Valbuena and Moreno, 2012).

1.5 Aims

A number of publications have suggested a role for AMPK in the regulation of mitosis, however, the signalling pathways in which AMPK regulates have not been fully characterised. As such, this body of work sought to further elucidate the role of AMPK in mitosis and cytokinesis.

By using a combination of cellular, biochemical and genetic techniques the role of AMPK in the control of mitosis was assessed in both mammalian cells and fission yeast. Additionally, to examine the pathways in which AMPK may regulate during the cell cycle, a genetic screen was undertaken using the model organism *S. pombe*.

Thus, the following research questions were investigated:

- Can the reported subcellular localisation of AMPK be replicated in other cell types?

- How does modulation of AMPK activity influence cytokinesis?

- Does *S. pombe* AMPK genetically interact with any of the key regulators of the cell cycle?

- Are the genetic interactions discovered in yeast conserved in a mammalian system?

2 Chapter 2-Materials and methods

2.1 Materials

2.1.1 List of materials and suppliers

Abcam, Cambridge, UK
A769662.

Acros Organics, Thermo Fisher Scientific, Geel, Belgium
Brij-35.

BDH Laboratory supplies, Poole, UK
Coomassie Brilliant Blue G-250, tetra-sodium pyrophosphate.

Beckman Coulter™, High Wycombe, UK
ISOTON, ultra-Clear™ ultracentrifuge tubes.

Bio-rad Laboratories Ltd, Hertfordshire, UK
SureBeads™ Protein A/G magnetic beads

Biotium, Hayward, CA, USA
RedDot2.

Cambridge Biosciance Ltd, Cambridge, UK
Quick Titre™ Adenovirus Titre Immunoassay kit.

ChromoTek, Planegg-Martinsried, Germany
Anti-GFP magnetic beads, anti-RFP magnetic beads, anti-Myc magnetic beads.

Dharmacon Inc, Lafayette, Colorado, USA
AMPKα1 and AMPKα2 siRNA.

Fisher Scientific UK Lts, Loughborough, Leicestershire, UK
Corning tissue culture T25/T75/T150 flasks, Corning 6-well and 12-well plates.

Ibidi, Martinsried, Germany
Ibidi cell culture chambers.

Thermo Fisher Scientific (including Life technologies, Applied Bio Systems, GIBCO and Invitrogen), Carlsbad, Ca, USA
Blasticidin, DMEM, EMEM, FCS, Lipofectamine® 2000 reagent, non-essential amino acids (100x), One Shot chemically competent *E. coli*, Opti-MEM® reduced serum media, Penicillin-Streptomycin (10000 U/ml, 10000 µg/ml), *Taq* DNA Polymerase, Trypsin-EDTA, Immuno-Mount™, zeocin.

Merck Chemicals Ltd, Nottingham, UK
BrdU cell proliferation kit, Compound C, lithium acetate.

New England Biolabs, Ipswich, MA, USA
Prestained protein markers, Lambda protein phosphatase.

Pall Life Science, Pensacola, FL, USA
Nitrocellulose membrane, 0.25 µm pore size.

Perkin Elmer, Beaconsfeild, Buckinghamshire, UK
$[\gamma\text{-}^{32}P]$ ATP.

Promega, Madison, Wisconsin, USA
MTS reagent.

PromoCell, Heidleberg, Germany
MV2 endothelial cell growth media (with supplement).

R&D Systems, Inc (Tocris Bioscience), Minneapolis, MN, USA
STO-609.

Severn Biotech Ltd, Kidderminster, Hereford, UK
Acrylamide: bisacrylamide (37.5:1; 30 % (w/v) acrylamide).

Sigma-Aldrich Ltd, Gillingham, Dorset, UK
ATP, AMP, ampicillin, β-Glucuronidase from *Helix pomatia*, Calcofluor-White stain, benzamidine, propidium iodide, nocodazole, recombinant aurora A,

recombinant aurora B, recombinant CaMKKß, recombinant PLK1, Ribonuclease A, soybean trypsin inhibitor (SBTI), N,N,N',N'-Tetramethylethylenediamine (TEMED), Triton X-100, Tween 20.

<u>Synvolux Products, Leiden, Netherlands</u>
SAINT-sRNA.

<u>Toronto Research Chemicals Inc, Ontario, Canada</u>
AICAR.

<u>VWR International Ltd, Lutterworth, Leicestershire, UK</u>
Falcon brand cell culture plastics.

<u>Qiagen, Venlo, Netherlands</u>
HiPerFect® Transfection reagent.

2.1.2 Standard solutions

Unless stated otherwise, all buffers and reagents were made up with distilled water.

<u>Bradford's reagent</u>
30 mg/l Coomassie Brilliant Blue, 5.0% (v/v) ethanol, 5.1% (v/v) orthophosphoric acid
Note: Bradford's reagent was filtered and stored in the dark

<u>Coomassie Brilliant Blue solution</u>
1 g/l Coomassie Brilliant Blue, 50% (v/v) methanol, 10% (v/v) acetic acid
Note: Coomassie Brilliant Blue solution was filtered prior to use

<u>Destain solution</u>
10% (v/v) acetic acid, 40% (v/v) methanol

<u>Genome extraction buffer</u>
2 % (v/v) Triton X-100, 1 % (w/v) SDS, 100 mM Tris-HCl (pH 8 at room temperature), 1 mM EDTA

HEPES-Brij-DTT

50 mM HEPES (pH 7.4- NaOH), 0.02% (v/v) Brij-35, 1 mM DTT, 1 mM Na_3VO_4

Immunofluorescence (IF) buffer

0.2% (w/v) fish skin gelatin, 0.1% (v/v) goat or donkey serum

Note: solution was made up in PBS. The serum chosen for the buffer was one that was different to the species of the secondary antibodies used in IF staining.

Immunoprecipitation (IP) buffer

50 mM Tris-HCl, pH 7.4 at 4°C, 150 mM NaCl, 50 mM NaF, 5 mM $Na_4P_2O_7$, 1 mM EDTA, 1 mM EGTA, 1 % (v/v) Triton X-100, 1 % (v/v) glycerol, 1 mM DTT, 1 mM Na_3VO_4, 0.1 mM benzamidine, 0.1 mM PMSF, 5 µg/ml SBTI

Kinase assay buffer

5 mM MOPS (pH 7.2), 2.5 mM glycerol 2-phosphate, 250 µM DTT, 1 mM Na_3VO_4

Laemmli sample buffer (LSB) 4x

200 mM Tris-HCl (pH 6.8), 8 % (w/v) SDS, 40 % (v/v) glycerol, 0.4 % (w/v) bromophenol blue, 200 mM DTT

Permeabilization buffer

0.1% (v/v) Triton X-100

Note: solution was made up in PBS. Solution was filtered prior to use.

4% p-formaldehyde

4% (w/v) p-formaldehyde, 1 mM $CaCl_2$, 1 mM $MgCl_2$

Note: solution was made up in PBS

Phosphate-buffered saline (PBS) (pH 7.2)

85 mM NaCl, 1.7 mM KCl, 5 mM Na_2HPO_4, 0.9 mM KH_2PO_4

Ponceau S stain

0.2% (w/v) Ponceau S, 1% (v/v) acetic acid

Quenching buffer

50 mM NH_4Cl

Note: solution was made up in PBS

SDS-polyacrylamide gel electrophoresis (SDS-PAGE) running buffer

190 mM glycine, 62 mM Tris base, 0.1% (w/v) SDS

SDS-PAGE sample buffer (4X)

200 mM Tris-HCl, pH 6.8, 8% (w/v) SDS, 40% (v/v) glycerol, 0.4% (w/v) bromophenol blue, 200 mM DTT

Note: DTT was added on the day of use.

TE buffer

0.1 M Tris-HCl, pH 7.5, 0.1 M EDTA

Transfer buffer

190 mM glycine, 62 mM Tris base

Tris-buffered saline (TBS)

20 mM Tris-HCl, pH 7.5, 137 mM NaCl

Tris-buffered saline + Tween 20 (TBST)

20 mM Tris-HCl, pH7.5, 137 mM NaCl, 0.1% (v/v) Tween 20

Triton X-100 lysis buffer

50 mM Tris-HCl, pH 7.4 at 4°C, 50 mM NaF, 1 mM $Na_4P_2O_7$, 1 mM EDTA, 1 mM EGTA, 1% (v/v) Triton X-100, 250 mM mannitol, 1 mM DTT, 1 mM Na_3VO_4, 0.1 mM benzamidine, 0.1 mM PMSF, 5 µg/ml SBTI

2.1.3 List of antibodies and condition of use

2.1.3.1 Primary antibodies for immunoblotting

Antibodies were diluted in 3% (w/v) Bovine serum albumin (BSA) in TBST. Blots were incubated with antibodies overnight at 4°C.

Epitope	Clonality	Host species	Dilution	Source (product number)
ACC	Monoclonal	Rabbit	1:1000	New England Biolabs, Hertfordshire, UK. (#3676)
Phospho-S79 ACC	Polyclonal	Rabbit	1:1000	New England Biolabs, Hertfordshire, UK. (#3661)
AMPK	Polyclonal	Rabbit	1:1000	New England Biolabs, Hertfordshire, UK. (#2532)
AMPK α1	Polyclonal	sheep	1 μg/ml	A generous gift from Prof. D. G. Hardie, University of Dundee, UK (A Woods *et al.*, 1996)
AMPK α2	Polyclonal	Sheep	1 μg/ml	A generous gift from Prof. D. G. Hardie, University of Dundee, UK (A Woods *et al.*, 1996)
Phospho-T172 AMPK	Monoclonal	Rabbit	1:1000	New England Biolabs, Hertfordshire, UK. (#2535)
Aurora A	Polyclonal	Rabbit	1:1000	Abcam, Cambridgeshire, UK. (#1287)

Aurora B	Polyclonal	Rabbit	1:1000	Abcam, Cambridgeshire, UK. (#2254)
FLAG	Monoclonal	Mouse	10 µg/ml	Merc, Kenilworth, USA. (F-3165)
GAPDH	Monoclonal	Mouse	1:80000	Ambion, Cambridgeshire, UK. (#4300)
GFP	Monoclonal	Mouse	1:4000	Abcam, Cambridgeshire, UK. (#184519)
LKB1	Monoclonal	Rabbit	1:1000	New England Biolabs, Hertfordshire, UK. (#3050)
mCherry	Polyclonal	Rabbit	1:1000	Badrilla, Leeds, UK. (A010-mCherry-5)
PLK1	Polyclonal	Rabbit	0.5 µg/ml	Novus Biologicals, Abingdon, UK. (NB100-547)

Table 2-1: Primary antibodies used for immunoblotting

2.1.3.2 Secondary antibodies for immunoblotting

Antibodies were diluted in 3% (w/v) BSA in TBST. Blots were incubated with secondary antibodies for 1 h at room temperature.

Epitope	Linked molecule	Host species	Dilution	Source (product number)
Mouse IgG	IRDye ®680cw	Donkey	1:10000	Li-COR, Lincoln, USA. (#925-68072).

Rabbit IgG	IRDye ®800cw	Donkey	1:10000	Li-COR, Lincoln, USA. (#926-32213).
Sheep IgG	IRDye ®680cw	Donkey	1:10000	Li-COR, Lincoln, USA. (#925-32214).

Table 2-2: Secondary antibodies used for immunoblotting

2.1.3.3 Primary antibodies for immunofluorescence

Antibodies were diluted in immunofluorescence buffer containing 0.1% (v/v) donkey or goat serum.

Epitope	Clonality	Host species	Dilution	Source (product number)
Phospho-S79 ACC	Polyclonal	Rabbit	1:250	New England Biolabs, Hertfordshire, UK. (#11818)
AMPK α1 (amino acids 344-358)	Polyclonal	Sheep	1 µg/ml	A generous gift from Prof. D. G. Hardie, University of Dundee, UK (A Woods *et al.*, 1996)
AMPK α1 (amino acids 351-366)	Monoclonal	Mouse	1:200	Abcam, Cambridge UK. (ab110036).
AMPK α2 (amino acids 351-366)	Polyclonal	Sheep	1 µg/ml	A generous gift from Prof. D. G. Hardie, University of Dundee, UK (A Woods *et al.*, 1996)

AMPK α2 (amino acids 29-510)	Polyclonal	Rabbit	1:100	Thermo Fisher Scientific, Waltham, USA. (PA5-21494)
Phospho-T172 AMPK	Monoclonal	Rabbit	1:100	New England Biolabs, Hertfordshire, UK. (#2535)
Phospho-T172 AMPK	Polyclonal	Rabbit	1:50	Santa Cruz Biotechnology, INC, Dallas, USA (sc-101630)
Aurora A	Polyclonal	Rabbit	1:100	Abcam, Cambridge UK. (ab1287)
Aurora B	Polyclonal	Rabbit	1 µg/ml	Abcam, Cambridge UK. (ab2254)
Myc	Monoclonal	Mouse	1:50	Santa Cruz Biotechnology, INC, Dallas, USA (sc-40)
PLK1	Polyclonal	Rabbit	0.5 µg/ml	Novus Biologicals, Abingdon, UK. (NB100-547)
Tubulin	Monoclonal	Rabbit	1:50	New England Biolabs, Hertfordshire, UK. (#2125)
Tubulin	Monoclonal	Rat	1:1000	Abcam, Cambridge UK. (ab6160)

Table 2-3: Primary antibodies used for immunofluorescence

2.1.3.4 Secondary antibodies for immunofluorescence

Antibodies were diluted in immunofluorescence buffer containing 0.1% (v/v) donkey or goat serum.

Epitope	Linked molecule	Host species	Dilution	Source (product number)
Mouse IgG	Alexa Flour ® 488	Donkey	1:500	Invitrogen, Carlsbad, USA. (A21202)
Rabbit IgG	Alexa Flour ®568	Donkey	1:500	Invitrogen, Carlsbad, USA. (A11011)
Rabbit IgG	Alexa Flour ®488	Donkey	1:500	Invitrogen, Carlsbad, USA. (A11008)
Rat IgG	Alexa Flour ®568	Goat	1:500	Invitrogen, Carlsbad, USA. (A11077)
Rat IgG	Alexa Flour ®488	Donkey	1:500	Invitrogen, Carlsbad, USA.(A21208)
Sheep IgG	Alexa Flour ®568	Donkey	1:500	Invitrogen, Carlsbad, USA. (A21099)

Table 2-4: Secondary antibodies used for immunofluorescence

2.1.4 PCR primers

Target	Sequence (5' to 3')	Length
fkh2 forward primer	CAACGATAACAAAGACGCATT	21
fkh2 reverse primer	AGCAATTGTGCTGTTGGTGT	20
ssp2 forward deletion primer 1	AATTTAAGCCTTGCTATTAAGGAAAAAAGATTT TATCAATAAACTTTCAATATTGGATTTGCCAAGC GAATAGCTGATACGGATCCCCGGGTTAATTAA	100
ssp2 forward deletion primer 2	ATATTTATCTCACACTCTGAAATTTAAGCCTTGCT ATTAAGGAAAAAAGATTTTATCAATAAACTTTCA ATATTGGATTCGGATCCCCGGGTTAATTAA	100
ssp2 forward deletion primer 3	TTTGCCTTCTACCAAATTATATATTTATCTCACAC TCTGAAATTTAAGCCTTGCTATTAAGGAAAAAAA GATTTTATCAACGGATCCCCGGGTTAATTAA	100
ssp2 reverse deletion primer 1	TGCTATTGAGTAGATTTGTTCAACAATGGGTAAT TAAGGGATGCTTGAAAACAGCGTGTTAAATGGG GAGTTACAATAAAGAATTCGAGCTCGTTTAAAC	100
ssp2 reverse deletion primer 2	AAAAAAATAAAATGTGTCTTTGCTATTGAGTAGA TTTGTTCAACAATGGGTAATTAAGGGATGCTTGA AAACAGCGTGTTGAATTCGAGCTCGTTTAAAC	100
ssp2 forward checking primer	TTGAGTAAAATTCCGCATTGTG	22
Kan*MX6* primer	GCTAGGATACAGTTCTCACATCACATCCG	29

Table 2-5: Primers used for PCR

2.1.5 Plasmids

Description	Plasmid backbone	Source
KD-Aurora A mCherry tagged. Kinase dead, K126R	mCherry-C1	A gift from Michael Davidson, University of California, USA. (Addgene plasmid # 54998)
KD-Aurora B GFP tagged. Kinase dead, K106R	pEGFP-C2	A gift from Susanne Lens, Department of Medical Oncology, Netherlands. (Addgene plasmid # 108493). (Hengeveld *et al.*, 2012).
AMPK α1-GFP	hGFP-S65T	A generous gift from Prof. D. G. Hardie, University of Dundee, UK.
AMPK α2-GFP	hGFP-S65T	A generous gift from Prof. D. G. Hardie, University of Dundee, UK.
CHMP2A-GFP	P643_pmEGFP_N_dest	A gift from Daniel Gerlich, Swiss Federal Institute of Technology, Switzerland. (Addgene plasmid # 31805). (Guizetti *et al.*, 2011).
CHMP2B-GFP	pLNCX2	A gift from Sanford Simon, Rockefeller University, USA. (Addgene plasmid # 115329). (Johnson, Bleck and Simon, 2018)

GFP	peGFT-C2	A generous gift from Prof. D. G. Hardie, University of Dundee, UK.
KanMX6	pFA6a	A gift from Jurg Bahler & John Pringle, University College London, UK. (Addgene plasmid # 39296). (Jürg Bähler *et al.*, 1998).
mCherry	pCDH	System Biosciences, Palo Alto, California USA. Cat CD512B.
KD-PLK1 YFP tagged. Kinase dead, K82R.	pEYFP-C3	A generous gift from J. Pines, Welcome Trust/Cancer Research UK Gordon Institute, Cambridge, UK. (Lindon and Pines, 2004).

Table 2-6: Plasmids used during this investigation

2.1.6 *S. pombe* media

Media was autoclaved prior to use. Solid media was made by the addition of 5% (w/v) agar. *S. pombe* were cultured as previously described (Moreno *et al.*, 1991).

Edinburgh minimal media (EMM)

20 g/L glucose, 5 g/L NH_4Cl, 0.1 g/L Na_2SO_4, 0.1 g/L $MgCl_2$, 15 mg/L $CaCl_2$, 3 g/L potassium hydrogen phthalate, 1.8 g/L Na_2HPO_4, 55 µM inositol, 81 µM nicotinic acid, 2 µM calcium pantothenate, 40 µM biotin, 8.2 µM H_3BO_3, 3.5 µM $MnSO_4$, 2.5 µM $ZnSO_4$, 1.2 µM $FeCl_3$, 900 nM MoO_3, 250 nM $CuSO_4$, 5.2 µM citric acid, 6 nM KI

Malt extract (ME) media

30 g/l malt extract

Yeast extract (YE) media

30 g/l glucose, 5 g/l yeast extract, 0.225 g/l adenine, 0.225 g/l uracil

2.1.7 Bacteria medium

Bacteria were cultured with solid or liquid 2YT media. Solid media was made by the addition of 5% (w/v) agar. Media was autoclaved prior to use.

2YT

1.6% (w/v) tryptone, 1% (w/v) yeast extract, 0.5% (w/v) NaCl

For selection, ampicillin (50-100 μg/ml) or kanamycin (50 μg/ml) was added after autoclaving.

2.2 Mammalian cell culture procedure

2.2.1 Mammalian cell suppliers

Human umbilical vein endothelial cells (HUVECs) were purchased from PromoCell, Heidelberg Germany. HUVECs were supplied as a pool from 6-8 donors. Human embryonic kidney 293 (HEK 293) cells and HeLa CCl-2 cells were obtained from ATCC, Manassas, USA. HeLa cells expressing FLAG-tagged wild type (WT) or kinase dead (KD) LKB1 were a kind gift from Prof. Dario Alessi, University of Dundee, UK (Sapkota *et al.*, 2002). AMPK α1/α2 (AMPK -/-) double knockout and wild type mouse embryonic fibroblasts (MEFs) were a kind gift from Dr. Benoit Viollet, Institute Cochin, Paris France (Laderoute *et al.*, 2006).

2.2.2 Cell culture plastic ware

Cells were maintained in Corning T25, T175 or T150 cell culture flasks. MEFs, HeLa cells and HEK 293 cells were cultured in Corning plastic ware. HUVECs were cultured on Falcon plastic. Alternatively, cells were seeded on 8-well Ibidi chambers.

2.2.3 Cell culture growth media

Cells were maintained at 37°C in a 5% (v/v) CO_2 humidified atmosphere and in the following media;

Cell type	Media and Supplement(s)
HEK 293	DMEM and 10% (v/v) FBS
HeLa CCl2	DMEM and 10% (v/v) FBS
WT/KD-LKB1 HeLa	MEM,10% (v/v) FBS, 2 mM glutamine, 100 U/ml penicillin, 100 µg/ml streptomycin, 2 mM non-essential amino acids, 5 µg/ml blasticidin and 100 µg/ml zeocin
HUVECs	MV2 with supplied 5% (v/v) serum supplement
Wild type and AMPK -/- MEFs	DMEM and 10% (v/v) FBS

Table 2-7: Mammalian cell culture media and supplements

2.2.4 Passaging of cells

When cells were approximately 70% confluent, growth media was aspirated and cells briefly washed with PBS. Cells were incubated with 0.05% (v/v) trypsin (3 ml in T75 flask or 6 ml in T150 flask) until cells began to detach. Trypsin was quenched with growth medium and cells diluted to the desired concentration and seeded onto fresh flasks or plates. HUVECs were cultured up to passage 6. HeLa cells, HEKs and MEFs were cultured up to passage 30.

2.2.5 Cryopreservation of cell stocks

Cell culture media was removed from T75 flasks and cells washed with PBS prior to the addition of 3 ml 0.05% (v/v) trypsin and incubated at 37°C until cells detached. Trypsin was neutralized with 9 ml of the appropriate cell culture

growth media (as described in Section 2.2.3). The cell suspension was transferred to a 15 ml centrifuge tube and cells sedimented at 350 x g for 5 mins. The supernatant was aspirated and cell pellet resuspended in 1 ml of the appropriate media containing 10% DMSO (v/v) and transferred to a 1.8 ml polypropylene cryogenic tube. Cells were stored overnight at -80°C in a Mr. Frosty™ freezing container before being transferred to liquid nitrogen storage.

2.2.6 Resurrection of frozen cell stocks

Cell cryogenic vials were removed from liquid nitrogen storage and thawed in a 37°C water bath. Cells were transferred into a T75 flask containing 11 ml of the appropriate cell culture growth media (as described in Section 2.2.3) and incubated for 4 h. Once cells had attached to the flask, media was aspirated and replaced with fresh medium.

2.3 Preparation of cell lysates

Media was aspirated and cells washed with ice cold PBS. Cells were lysed with 100 µl lysis buffer per well of a 6-well plate or 50 µl lysis buffer per well of a 12-well plate. Wells were scraped using a cell lifter and incubated for 20 mins on ice. Lysate was transferred to cold 1.5 ml microcentrifuge tubes and centrifuged at 21,910 x g for 5 mins at 4°C. The supernatant was collected and stored at -20°C.

2.4 Protein concentration determination

Protein concentration was calculated by spectrophotometric analysis according to the Bradford method (Bradford, 1976). In duplicate, 0.5-5 µl of cell lysate was made up to 100 µl with distilled water in a plastic cuvette, followed by the addition of 1 ml Bradford's reagent. Absorbance was measured at 595 nm using a WPA S2000 spectrophotometer equipped with appropriate filters.

2.5 SDS-PAGE

SDS-PAGE was carried out using 1.5 mm thick acrylamide gels between 8% and 15 % (v/v) with a 5% (v/v) stacking gel of approximately 2 cm. Samples were mixed with LSB and heated at 95°C for 5 min. Electrophoresis was carried out at 80 V

for the stacking gel and 80-150 V through the resolving gel until the dye front had migrated off the gel. Prestained broad range protein markers were used as a reference.

2.6 Western blotting of proteins

2.6.1 Electrophoretic transfer of proteins onto nitrocellulose membranes

Gels were placed on nitrocellulose membrane (0.25 μm pore size) and layered between two sheets of 3 mm filter paper. Sponges were placed outside the filter paper and the ensemble placed in a gel holder cassette. Electrophoretic transfer was carried out at 60 V for 2.25 h or 30 mA overnight. Nitrocellulose membrane was stained with Ponceau S to assess transfer efficiency and equal loading of protein.

2.6.2 Blocking of membranes and incubation with primary antibodies

To prevent non-specific binding of antibodies to the membrane, the nitrocellulose was incubated in 5 % (w/v) Marvel milk powder in TBS for 30 mins at room temperature. Membranes were washed briefly with TBS followed by incubation with primary antibodies overnight at $4^{o}C$ with shaking.

2.6.3 Secondary antibodies and immunodetection of proteins using the LI-COR detection system

Membranes were washes (3 times, 5 min) with TBST and incubated with the appropriate secondary antibodies for 1 h at room temperature with shaking. Membranes were subsequently washed (3 times, 5 min) with TBST. Secondary antibody fluorescence was detected using the LI-COR Odyssey ® SA system.

2.6.4 Stripping of nitrocellulose membranes

When required, antibodies were stripped from the nitrocellulose membranes by incubation with 0.2 mM NaOH for 12 min. Membranes were then washed (3 times, 5 min) in TBST until pH returned to ~7.5. Membranes were stained with Ponceau S to ensure that proteins were not inadvertently stripped from the

membrane during the process. Following stripping, membranes were blocked as described in section 2.6.2 and incubated with primary antibodies.

2.6.5 Densitometric quantification of protein bands

Blots were cropped using Image Studio Lite Version 5.0. Images were imported into ImageJ and band intensity calculated.

2.7 Immunofluorescence

2.7.1 Preparation of coverslips

Glass coverslips (13 mm diameter) were immersed in 100% ethanol and placed upright in the wells of a 12-well plate and air dried in a laminar flow hood. Once dry, plates were agitated allowing the coverslips to fall to the bottom of the wells. Coverslips were exposed to UV light for a minimum of 30 min.

2.7.2 Immunofluorescence staining

Media was aspirated from wells and coverslips washed three times with PBS followed by incubation with 1 ml 4 % (w/v) p-formaldehyde (PFA) for 20 min. Cells were washed three times with PBS and incubated with 1 ml quenching buffer for 10 mins followed by three washes with PBS. Cells were incubated with 1 ml permeabilization buffer for 5 min. Permeabilization buffer was aspirated and cells incubated in 1 ml IF buffer for at least 20 min to block non-specific sites.

2.7.3 Incubation of coverslips with primary and secondary antibodies

Primary antibodies were prepared in IF buffer, 35 µl of antibody solution was pipetted onto Parafilm. Coverslips were removed from the wells, inverted and placed onto the antibody solution using fine pointed tweezers. Coverslips were incubated with the primary antibody for 1 h at room temperature. Coverslips were returned to the wells and washed three times with IF buffer.

Secondary antibodies were prepared in the same manner as primary antibodies but coverslips were only incubated for 30 min. Following incubation with

antibodies, coverslips were returned to their wells and washed three times with IF buffer. During incubation with the primary and secondary antibodies, the Parafilm was covered to reduce evaporation and prevent photobleaching of secondary antibodies

2.7.4 Staining of DNA

DNA was stained with either 4',6-diamidino-2-phenylindol (DAPI) or RedDot2. DAPI staining was carried out following incubation with the secondary antibody; cells were incubated with 1 µg/ml DAPI for 10 min. Alternatively RedDot2 was diluted 1:200 and co-incubated with secondary antibodies.

2.7.5 Mounting coverslips on slides

A drop of Immuno-Mount was applied to a glass microscope slide and using fine tweezers, coverslips were placed cell-side down onto the Immuno-Mount. Slides were left to dry overnight in the dark.

2.7.6 Preparation of samples in ibidi® µ slides

For staining carried out in 8-well ibidi® µ slides, the protocol described in Section 2.7.2 can be followed but volumes adjusted to 300 µl. Antibody solutions (150 µl) were added directly to the chamber wells. Finally, three drops of ibidi® mounting medium was added to each chamber to preserve samples.

2.7.7 Confocal microscopy and image acquisition

Images were acquired using a Zeiss LSM Exciter laser scanning microscope with a 63X/1.4 NA oil DIC objective lens. Images were processed using ImageJ.

2.8 Recombinant adenoviruses

2.8.1 Adenoviruses used

Adenoviruses used during the course of this project are outlined in Table 2-8.

Virus	Tag	Details	Reference
Ad.AMPKα1-dominant negative (DN)	Myc	Encodes full length AMPKα1 containing a D157A mutation	A generous gift from Dr. F. Foufelle, Centre Biomedical des Cordelier, Paris (Woods *et al.*, 2000).
Ad.AMPKα1-consitutively active (CA)	GFP	Encodes for amino acids 1-312 of AMPKα1 containing a T172D mutation	A generous gift from Dr. F. Foufelle, Centre Biomedical des Cordelier, Paris (Woods *et al.*, 2000).
Ad.GFP	N/A	Encodes for GFP	A generous gift from Dr. F. Foufelle, Centre Biomedical des Cordelier, Paris (Woods *et al.*, 2000).
Ad.Null	N/A	Empty capsid virus	A generous gift from Dr. F. Foufelle, Centre Biomedical des Cordelier, Paris (Woods *et al.*, 2000).

Table 2-8: Adenoviruses used during this investigation

2.8.2 Adenovirus propagation and purification

Two T150 flasks of HEK 293 cells were infected with 2 µl of virus and incubated for 48 h. Cells were detached by pipetting and collected in 50 ml Falcon tubes. Cells were sedimented at 340 x *g* for 15 min and the supernatant discarded. Pellets were pooled and resuspended in 10 ml PBS before being mixed with 10 ml Arklone P (1,1,1-trichloro-1,2,2-trifluroethane) and gently inverted for 10 sec.

The cell-Arklone P mixture was centrifuged at 340 x *g* for 15 min and the upper layer containing the virus isolated. The virus layer was diluted in 600 ml DMEM containing 10% (v/v) FBS and distributed between 25 T150 flasks of HEK 293 cells and incubated for 48 h. Cells were detached by pipetting and collected in 50 ml Falcon tubes. Cells were sedimented at 340 x *g* for 15 min and the supernatant discarded. Cell pellets were pooled and resuspended in 20 ml PBS. Cells were lysed with 10 ml of Arklone P and centrifuged at 340 x *g* for 15 min. The upper layer containing the virus was layered onto a CsCl gradient consisting of 2.5 ml of CsCl in TE buffer with a density of 1.33 g/ml layered on top of 1.5 ml CsCl in TE buffer with a density of 1.45 g/ml in a centrifuge tube. This was centrifuged at 100,000 x *g* in a SW40 rotor using an Optima™ XL-80K ultra centrifuge for 90 min at 20ºC. The centrifuge tube was punctured with a 19-gauge needle just below the virus layer and collected into a 1 ml syringe. Viruses were transferred to a float-a-lyzer to dialyse against TE buffer overnight at 4ºC. The following morning, the float-a-lyzer was transferred to 10% (v/v) glycerol in TE buffer to dialyse for 2 h. Purified virus was stored at -80ºC. Virus concentration was calculated using an adenovirus titration kit from Clontech according to the manufacturer's guidelines.

2.8.3 Adenovirus infection of mammalian cells

Adenoviruses were diluted to the required concentration in the appropriate cell culture media (Section 2.2.3) and added directly wells. Cells were incubated with viruses for 24-48 h before experiments were conducted

2.9 siRNA-mediated knockdown of gene expression

HUVECs were seeded in 6-well plates 24 h prior to transfection. siRNA (40 μl of 200 nM) was diluted in 500 μl Opti-MEM® with 40 μl SAINT-sRNA transfection reagent. The mixture was briefly vortexed and incubated at room temperature for 5 min. Cells were washed with 1 ml Opti-MEM® and siRNA solution added dropwise to cells. Cells were incubated for 3 h at 37ºC. Following incubation, 1.5 ml MV2 media was added to each well and cells cultured for 48 h.

2.10 Transfection of plasmid DNA

HeLa cells or HEK 293 cells were plated 24 h prior to transfection. Plasmid DNA and Lipofectamine® 2000 was diluted in Opti-MEM® media, the volumes and quantities are described in Table 2-9. Media was vortex mixed briefly and incubated at room temperature for 20 min. Cells were washed once with Opti-MEM® and DNA-lipid complexes added dropwise. Cells were incubated for 4 h at 37°C. Opti-MEM® was aspirated and cells incubated in the appropriate media (Section 2.2.3) for 24-48 h.

	Lipofectamine® 2000	Plasmid DNA	Opti-MEM®
1 well of a 12-well plate	4 µl	1.6 µg	200 µl
1 well of a 6-well plate	10 µl	2.5 µg	500 µl
10 cm dish	60 µl	24 µg	3 ml

Table 2-9. Volumes and quantities of Lipofectamine® 2000 and plasmid DNA used for the transfection of mammalian cells.

2.11 Cell synchronisation

2.11.1   Thymidine and nocodazole block

Cells were seeded in 20 T150 flasks and grown to 40% confluency, then incubated with 5 mM thymidine overnight. Flasks were washed three times with PBS and once with the appropriate growth media (Section 2.2.3). Flasks were incubated with the appropriate media for 8 h. Cells were then incubated with 10 ng/ml nocodazole overnight. The following day, media was aspirated and cells detached by agitation. Flasks were washed with PBS and cells collected in 50 ml tubes. Cells were washed three times with PBS and once with the appropriate cell culture growth media. Cells were plated as required and incubated until cells reached the desired point of the cell cycle.

2.11.2   Double thymidine block

HUVECs were plated in either 6-well or 12-well plates and grown to 30% confluency. Thymidine (2 mM) was added to media and cells incubated for 18 h. Cells were washed twice with PBS and once with MV2 media, followed by incubation in media for 9 h. Thymidine (2 mM) was added to media and cells incubated for 15 h. Cells were washed twice with PBS and once with MV2 media. Cells were then cultured at 37°C until they reached the desired point of the cell cycle.

2.12 Flow cytometry

Cells were detached from wells by mechanical agitation using a cell scraper and collected into 15 ml centrifuge tubes. Cells were sedimented at 350 x *g* for 5 min and fixed by the addition of 5 ml ice cold 70% (v/v) ethanol while vortex mixing and incubated at 4°C for a minimum of 20 min. Cells were sedimented at 350 x *g* for 5 min and resuspended in 1 ml PBS containing 50 μg/ml RNase A and 50 μg/ml propidium iodide (PI). PI fluorescence was measures using a BD Biosciences FACSCanto II System with Fluidics Cart (6-color, blue/red) flow cytometer.

2.13 Cell viability assay (MTS assay)

Cells were seeded into a 96-well plate and incubated for 4-6 h to allow cells to adhere to plastic, followed by the addition of the required small molecule activator/inhibitors. After 18-24 h, 20 μl MTS reagent was added to each well (100 μl media/well). Cells were incubated with MTS reagent as follows; HUVECs for 2 h, HeLa cells 3 h and MEFs 4 h. Absorbance was measured at 489 nm using a BMG Labtech FLUOstar Optima spectrophotometer microplate reader.

2.14 Cell proliferation assay (BrdU assay)

Cell proliferation was assayed using a BrdU Assay Kit as directed by the manufacturer's protocol. Briefly, cells were seeded into a 96-well plate and incubated for 4-6 h, to allow cells to adhere to plastic. BrdU reagent was diluted 1:500 in the appropriate cell culture media (Section 2.2.3) and 20 μl added per well of a 96-well containing 100 μl media. Cells were cultured at 37°C for 18-24

h. Cells were fixed with the supplied fixing solution for 30 min. Plates were washed three times and incubated with supplied anti-BrdU antibody for 1 h. Plated were washed three times and incubated with supplied HRP-conjugated antibody for 30 min. Following washing, plates were incubated with a peroxidase substrate for 30 min in the dark. Reaction was terminated using supplied acidic stop solution. Detection was performed using a PHERAstar FS spectrophotometer microplate reader. Absorbance was measured at 450 nm and corrected by subtracting absorbance at 550 nm.

2.15 Immunoprecipitation

2.15.1   FLAG-tag immunoprecipitation

HeLa cells expressing FLAG-tagged KD-LKB1 were cultured in 10 cm dishes until confluent. Cells were lysed with 500 µl lysis buffer as described in Section 2.3. Lysates were incubated with 10 µg anti-FLAG antibody (Merc, Kenilworth, USA. Catalogue number F-3165) and 20 µl magnetic protein G beads overnight on a rotating mixer at 4°C. Beads were washed three times with PBS and protein complexes were either eluted from the beads by the addition of 2X LSB or resuspended in either HEPES-Brij DTT or kinase assays buffer.

2.15.2   Immunoprecipitation using conjugated nanobodies

Fusion proteins tagged with either GFP/YFP, Myc or RFP (mCherry) were immunoprecipitated using ChromoTek nanobodies conjugated to magnetic beads. Beads (20 µl of packed volume) were washed twice with 1 ml PBS and added to 500 µl of cell lysate. Lysates were incubated for 1 h at 4°C with mixing by rotation. Beads were washed three times with 1 ml PBS. Protein complexes were either eluted from the beads by the addition of 2X LSB or resuspended in either HEPES-Brij DTT or kinase assays buffer.

2.16 *In vitro* Phosphorylation assays

2.16.1   Substrate generation

HEK-293 cells were transfected with plasmids encoding tagged proteins (KD-aurora A-mCherry, KD-aurora B-GFP, KD-PLK1-GFP, CHMP2A) or infected with

Ad.AMPK-DN adenoviruses and lysates prepared (Section 2.3). Fusion proteins were immunoprecipitated as described in Section 2.15.2 using ChromoTek anti-myc, anti-GFP or anti-RFP conjugated beads. Alternatively, FLAG-tagged LKB1 was immunoprecipitated from HeLa cells expressing WT or KD-LKB1 (Section 2.15.1). Myelin basic protein (MBP) (200 µg/ml) or GST (2.5 µg) were also used as substrates in *in vitro* phosphorylation assays. Finally, commercially available recombinant proteins were denatured by heating at 95°C for 5 min and 2.5 µg used as a substrate for assays.

2.16.2   Lambda phosphatase treatment

Immunoprecipitated substrates were incubated with commercial lambda phosphatase (New England Biolabs cat. 0735) to limit endogenous phosphorylation. Briefly, magnetic beads were washed with water and volumes adjusted to 40 µl using water, 5 µl 10X NEB protein metalloPhosphatases buffer was added with 5 µl 10 mM $MnCl_2$ and 1 µl (400 U) lambda protein phosphatase. Reactions were incubated at 30°C for 1 h on a vibrating hot block. Beads were then separated and washed twice with PBS. Beads were either resuspended in 2xLSB, HEPES-Brij DTT or kinase assay buffer.

2.16.3   Phosphorylation reaction

In vitro phosphorylation reactions were set up as follows; 5 µl substrate (from 2.14.1); 5 µl kinase assay buffer (or HEPES-Brij DTT for assays using AMPK); 5 µl 1 mM ATP and 25 mM $MgCl_2$ containing 0.2 µCi/µl [γ^{32}P] ATP; 5 µl the appropriate active kinase; 5 µl the appropriate cofactors; 1 mM AMP for reactions using AMPK or 1 mM $CaCl_2$ and 10 µM calmodulin for reactions using CaMKKß. Reactions using aurora A, aurora B or PLK1 did not require cofactors so an additional 5 µl buffer was added.

Reactions were incubated for 30 min at 30°C on a vibrating platform. Reactions were terminated by either separating reaction mixture from magnetic beads followed by the addition of 15 µl 2X LSB or the addition of 8 µl 4X LSB directly to reaction. Samples were incubated at 70°C for 5 min.

2.16.4   SDS-PAGE and visualisation

Phosphorylation products were resolved by SDS-PAGE as described in Section 2.5. Gels were stained using Coomassie blue solution for 20 min. Gels were washed using destain solution until background staining cleared and dried onto 3 mm filter paper by heating at 85°C for 2 h under a vacuum. Radioactive ^{32}P incorporation was detected using a Fuji FLA 7000 Phosphor Imager.

2.17 Transformation of competent *E. coli*

Chemically competent *E. coli* (XL-1 blue or STBL3 depending on the required plasmid) were mixed with 1 µl plasmid DNA and incubated on ice for 20 min. *E. coli* were heat shocked at 42°C for 45 sec followed by incubation on ice for 2 min and the addition of 300 µl 2YT media. Cells were then incubated at 37°C for 1 h with shaking. Cells (200 µl) were spread onto solid 2YT media with the appropriate antibiotic and incubated overnight at 37°C.

2.18 Preparation of plasmid DNA

Plasmid DNA was purified using QIAGEN® plasmid Maxi kit. Briefly, *E. coli* cultures were grown overnight in 100 ml 2YT containing the appropriate antibiotic at 37°C with vigorous shaking. *E. coli* were harvested by sedimentation at 6000 x *g* for 1 h and resuspended in the supplied lysis buffer and incubated for 5 mins. Neutralisation solution was added and cell debris pelleted by centrifugation at 20000 x *g* for 1 h. Lysate was loaded onto a QIAGEN-tip and allowed to flow through. Columns were washed twice with supplied wash solution. Plasmid was eluted and resuspended in 500 µl water. DNA concentration was quantified using a nanodrop spectrophotometer.

2.19 PCR

PCR reactions were assembled in thin-walled PCR tubes as follows: 1X PCR master mix, 0.2 mM ATP, 0.2 mM CTP, 0.2 mM GTP, 0.2 mM TTP,1.5 mM $MgCl_2$, 0.5 µM primers, 2.5 U *Taq* DNA polymerase and template DNA. Reactions were carried out in a Biometra T-gradient thermocycler. Reactions were heated to 95°C for 3 min followed by 35 cycles of: 95°C 1 min, 55°C 1 min, 72°C 45 sec-2 mins and finally 10 min at 72°C.

2.20 Agarose gel electrophoresis and visualisation of PCR products

PCR products were separated on a 0.8-2 % (w/v) agarose gels containing 0.2 µg/ml ethidium bromide. DNA was combined 5:1 NEB 6X DNA loading dye and gel electrophoresed at 70 V. Gels were visualised on an AlphaImager™ 3400 UV-trans-illuminator

2.21 General *S.pombe* methods

The methods used were based on Rezig *et al.*, 2019 and Moreno *et al.*, 1991. *S. pombe* were allocated a "Glasgow" (GG) number and were Stored in 30% (v/v) glycerol at -70°C. Strains were resurrected from glycerol stocks by spreading onto solid YE medium and incubated at 25-30°C for 2-3 days prior to experimentation. Appendix 1 outlines the full genotypes for the *S. pombe* strains used in this Thesis.

2.22 Generating mutants by homologous recombination

2.22.1   Generating transforming DNA

The method used was adapted from Bähler *et al.*, (1998). Transforming DNA was generated by PCR using primers composed of an 80 base pair sections homologous to the untranslated region (UTR) regions 5' (forward primer) or 3' (reverse primer) of the gene to be deleted (*ssp2* in this case), and a 20 base pair section homologous to the kanMX6 sequence present on the pFA6a-kanMX6 plasmid (Table 2-6). This PCR generated the transforming DNA; a linear fragment containing the sequence of the kanMX6 cassette flanked by sequences homologous to sequences 5' and 3' of *ssp2* (Figure 2-1A).
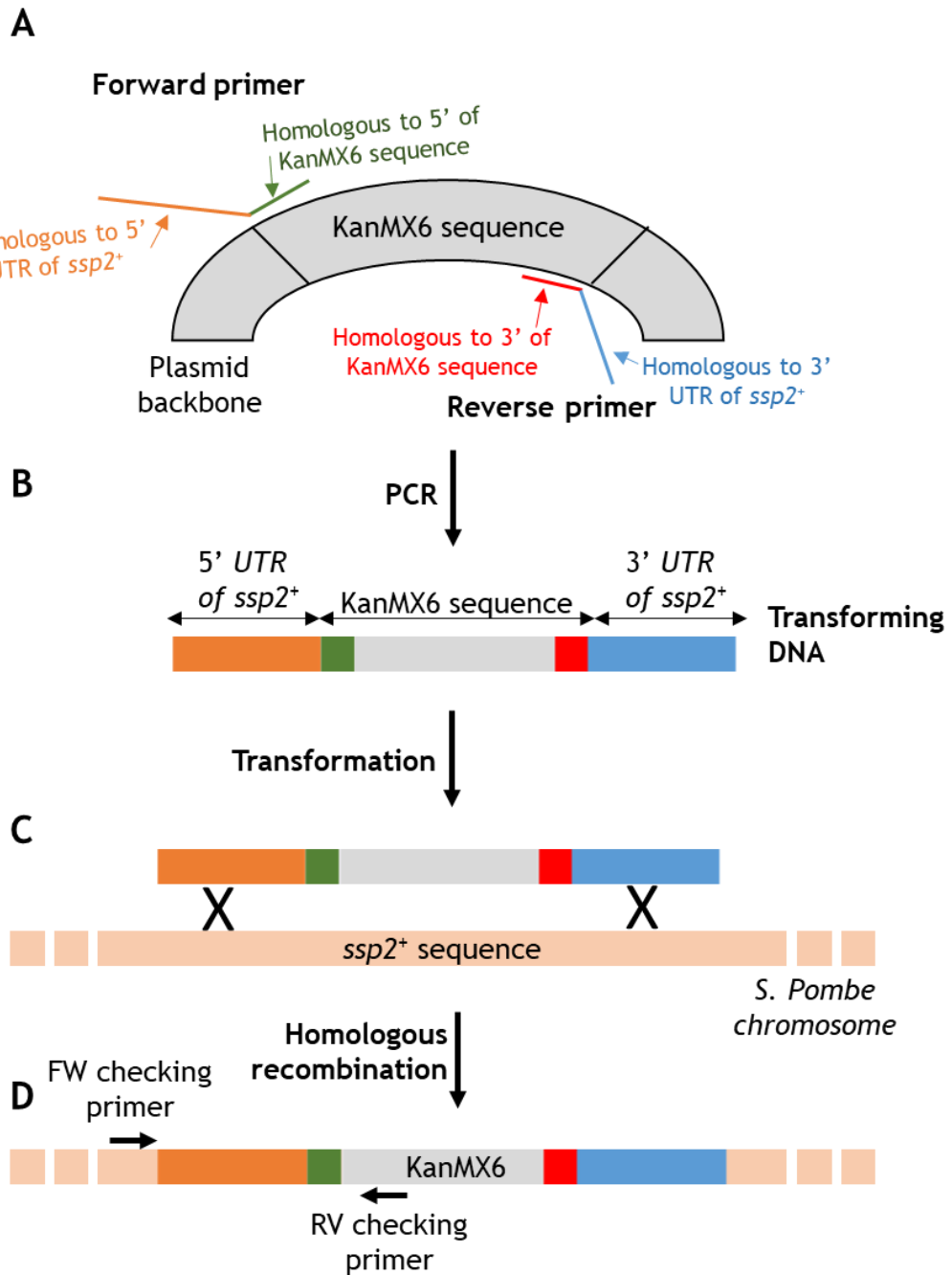
Figure 2-1: Schematic diagram showing the chromosomal deletion of *ssp2* based on homologous recombination.

(A and B) Transforming DNA was generated by PCR using a forward primer containing a region homologous to the 5' UTR of the gene of interest (*here ssp2+*) and a region homologous to the first 20 bases of the kanMX6 located on a plasmid. Similarly the reverse primer is composed of a region homologous to the 3' UTR of the *ssp2* and a region homologous to the kanMX6 sequence. **(C and D)** The linear DNA is transformed into *S. pombe* cells. Homologous recombination occurs between the transforming DNA and the yeast chromosome around the *ssp2* gene. This resulting in the replacement of *ssp2* gene with the kanMX6 sequence. The position of the "checking primers" is shown.

2.22.2   Transformation of *S. pombe*

S. pombe strains were grown in liquid YE medium to approximately 10^7 cells/ml. Cells were washed once with sterile water and resuspended in 1 ml of water in a microcentrifuge tube. Cells were sedimented at 350 x *g* for 3 mins and resuspended in 1 ml TE buffer containing 0.1 M lithium acetate (LiAc/TE buffer). Cells were washed once with LiAc/TE buffer and resuspended at $2x10^9$ cells/ml. Cells (100 µl) were mixed with 2 µl of 10 mg/ml sheared salmon sperm DNA and 15 µl transforming DNA. Reactions were incubated at room temperature for 10 mins followed by the addition of 260 µl 40% (w/v) polyethylene glycol in LiAc/TE and transferred to a shaking incubator at 30°C for 60 mins. DMSO (43 µl) was added and cells heat shocked at 42°C for 5 mins. Cells were washed once with water and resuspended in 500 µl water. The transformation reaction (250 µl) was spread onto solid YE medium and incubated overnight at 30°C. Cells were replica plated onto solid YE medium containing G418 (final concentration 100 mg/l) and incubated at 30°C until colonies formed.

2.22.3   Confirmation of homologous recombination

G418-resistant yeast colonies were grown to stationary phase in 5 ml liquid YE medium. Cells were washed twice with water and resuspended in 0.5 ml water in 1.5 ml microcentrifuge tubes. Cells were sedimented at 350 *g* for 3 mins and resuspended in 200 µl genome extraction buffer. Acid washed beads (0.3 g) were added with 200 µl phenol: chloroform: isoamyl alcohol (25:24:1) and vortex mixed for 5 mins. The aqueous layer was isolated by centrifugation at 21,910 x *g* for 5 mins and transferred to a fresh microcentrifuge tube. DNA was precipitated by the addition of 1 ml ethanol and pelleted (21,910 x *g* for 5 mins). DNA was air dried and resuspended in 50 µl TE buffer.

PCR reactions were preformed using 5 µl genomic DNA. The forward primer was homologous to a section 5' of the recombination event and the reverse primer was homologous to a sequence at the beginning of the KanMX6 cassette (Figure 2-1D). PCR products were resolved using a 2% agarose gel.

2.23 Generation of double mutants

2.23.1 Mating of *S. pombe* strains

Equal sized colonies of actively growing yeast strains were mixed with 100 μl sterile water on solid ME medium. Cultures were incubated at 25°C for 2-3 days.

2.23.2 Tetrad analysis

The methods used to generate fission yeast double mutants by tetrad analysis is described in detail in Rezig *et al.*, 2019, on which this section is based. The mating mixture from Section 2.23.1 was spread onto thinly poured (~1 mm thick) solid YE medium along one side of the Petri dish (Figure 2-2). The mating mixture was examined using a Singer MSM Ascus Dissector with a micro-manipulator needle. Tetrad asci containing four ascospores were isolated and moved to form a vertical line along the centre of the Petri dish (Figure 2-2). Plates were incubated at 37°C for 3-5 h to induce the breakdown of the ascus membrane releasing the four ascospores. Ascospores were then separated to form a horizontal line (Figure 2-2) and plates incubated between 25-30°C until colonies formed.
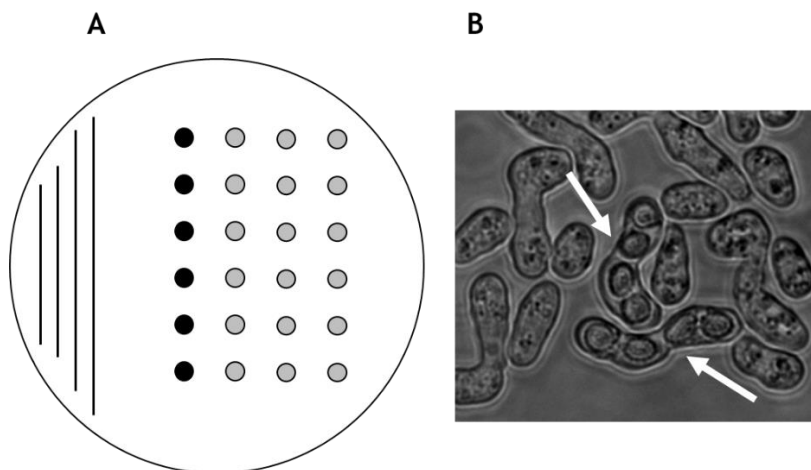
Figure 2-2: Schematic representation of tetrad analysis used to identify double mutants in fission yeast.
(A) Yeast mating mixture was spread onto solid YE medium along one side of a Petri dish, termed the *inoculum*. Tetrad ascospores were isolated and placed in a vertical line along the centre of the dish (black circles). Plates were incubated at 37°C until the ascus membrane degraded. The four ascospores were then separated to form a horizontal line (grey circles) **(B)** Representative picture of *S. pombe* tetrads (indicated by white arrows).

2.23.3   Random spore analysis

S. pombe strains were crossed as described in Section 2.23.1. Mating mixture was suspended in 1 ml sterile water containing 5% (v/v) β-glucuronidase from *Helix pomatia* (MERCK, cat G7017). Cell suspension was incubated at 25°C overnight on a shaking hot block. The following morning, a small amount of the mating mixture was placed on a glass slide and assessed using a light microscope to ensure that vegetative cells and asci membranes had been digested. Cell suspension was sedimented at 350 x g for 1 min and supernatant removed. Cell pellet was resuspended in 1 ml water. 3-10 μl was spread onto solid YE media and incubated between 25-30°C until colonies formed.

2.23.4   Genotype analysis/replica plating

To determine the genotype of the colonies generated by tetrad analysis or random spore analysis, replica plating onto selective media was carried out. Sterile velvet material mounted on a circular metal block was used to transfer yeast from the original plate onto selective media. To examine for the presence of auxotrophic markers, growth was tested on solid EMM where the appropriate nutrient was omitted which included; adenine (400 μl 375 mg/l), uracil (375 mg/l), leucine (187.5 mg/l leucine) and histidine (187.5 mg/l). For each case, 400 μl stock solutions was spread onto solid EMM media and allowed to dry. To select for the presence of the antibiotic resistance cassettes, 40 μl of 50 mg/ml G418 or 20 μl of100 mg/ml nourseothricin (clonNat) was spread onto solid YE media. Alternatively plates were incubated at different temperatures to examine temperature sensitivity.

2.24 Serial dilution analysis of *S. pombe*

Cells were suspended in sterile water and 100 μl of cell suspension mixed with 10 ml ISOTON® in plastic cuvettes and cell number counted using a Z2 Coulter counter. Cell suspensions were diluted to 1.5×10^6 cells/ml, 1.5×10^5 cells/ml, 1.5×10^4 cells/ml and 1.5×10^3 cells/ml and 10 μl of each dilution was pipetted onto solid YE media. Plates were incubated for 2-3 days at different temperatures. A wild type strain was diluted on each plate as a reference for cell growth.

2.25 Analysis of septation phenotypes

Analysis of septation phenotypes was undertaken as previously described (Bhutta *et al.*, 2014; Rezig *et al.*, 2019). Yeast strains were grown overnight in liquid YE media at 30°C in a shacking incubator. Culture (1 ml) was transferred to 1.5 ml microcentrifuge tubes and mixed with 30 μl 1 mM Calcofluor-White and incubated for 1 min in the dark. Cells were sedimented by centrifugation at 17,530 x *g* for 30 sec. Supernatant was removed and cells resuspended in 100 μl water. Cells (8 μl) were transferred onto a glass microscope slide, covered with a 22 X 22 mm cover slip and sealed using clear nail polish. Slides were visualised with a Zeiss Axiovert 135 fluorescent microscope with a Zeiss 63X Plan-APOCHROMAT oil-immersion objective lenses. Calcofluor-White excitation was examined at 370 nm and emission at 440 nm. Septation phenotype of 100 cells was analysed across the three technical replicates and repeated three times. Septation phenotype were classified based on the descriptions from Bhutta *et al.*, 2014.

2.26 Statistical analysis

Results are shown as mean ± standard error of the mean (SEM). Statistical significance was assessed by either two-tailed Students *t*-test, one-way or two-way analysis of variance (ANOVA) with $p<0.05$ being deemed significant.

3 Chapter 3-AMPK may have a role in mammalian mitosis

3.1 Introduction

Emerging evidence has suggested a role for AMPK in controlling the cell cycle and mitosis. Active phospho-T172 AMPK has been reported to localize to specific areas during mitosis; as cells enter mitosis phospho-T172 AMPK is located at the MTOC, and during telophase phospho-T172 AMPK localises to the midbody (Vazquez-Martin *et al.*,2009). One of the principal downstream targets of AMPK, phospho-S79 ACC, has also been reported to follow the same spatio-temporal localisation as phospho-T172 AMPK, indicating a functional effect of AMPK at these locations (Vazquez-Martin *et al.*, 2013). Furthermore, levels of phospho-Ser79 ACC increase during mitosis and treatment of cells with the poorly-selective AMPK inhibitor, compound C reduces mitotic accumulation (Thaiparambil *et al.*, 2012).

In the present study AMPK localisation during mitosis was assessed in primary human cells and in cell lines. Additionally, the effect of modulating AMPK activity by pharmacological or genetic means on the cell cycle was assessed. Initially HeLa cells were chosen for investigation as they have been widely used in the study of the cell cycle. However, as HeLa cells lack the AMPK kinase LKB1, experiments were also carried out on primary HUVECs as a more biologically relevant model.

3.2 Results

3.2.1 AMPK subcellular localisation during mitosis

3.2.1.1 Subcellular localisation of AMPKα subunits during mitosis

It has been reported that the AMPKα2 subunit localises to the midbody in HUVECs and that phospho-T172 AMPKα similarly localises to the midbody and MTOC in HeLa cells and the A431 cancer cell line (Vazquez-Martin *et al.*, 2009; Pinter *et al.*, 2012;). The localisation of AMPKα subunits during mitosis was therefore investigated in primary human cells (HUVECs) and HeLa cells. Using antibodies raised to amino acids 344-358 of AMPKα1, immunoreactivity was observed at the MTOCs in HeLa cells (Figure 3-1) and HUVECs (Figure 3-2), whereas no staining was observed at the midbody. Conversely, when stained with an antibodies raised to amino acids 351-356 of AMPKα2, immunoreactivity was observed at the midbody with no immunoreactivity at the MTOCs in HeLa cells (Figure 3-1) and HUVECs (Figure 3-2). In both cell lines, AMPKα2 localised to two discreet areas on either side of the midbody (highlighted in Figure 3-2D). AMPKα1 and AMPKα2 immunoreactivity was also observed in the cytoplasm of mitotic cells. Further immunofluorescence experiments were undertaken using antibodies raised to distinct epitopes (amino acids 357-524 of AMPKα1 or amino acids 29-510 of AMPKα2), however no immunoreactivity was observed in HUVECS (data not shown).

To avoid specificity issues of antibodies, HeLa cells were transfected with plasmids encoding genes for either AMPKα1-GFP, AMPKα2-GFP or GFP alone. Cells were fixed with PFA and GFP localisation assessed by fluorescence confocal microscopy. Despite successful induction of AMPKα1/2-GFP expression (Figure 3-3D), the majority of GFP-positive cells were senescent. Only three GFP positive cells were observed which were connected by an intracellular bridge, and in all three cases GFP was apparent at the midbody (Figure 3-3).
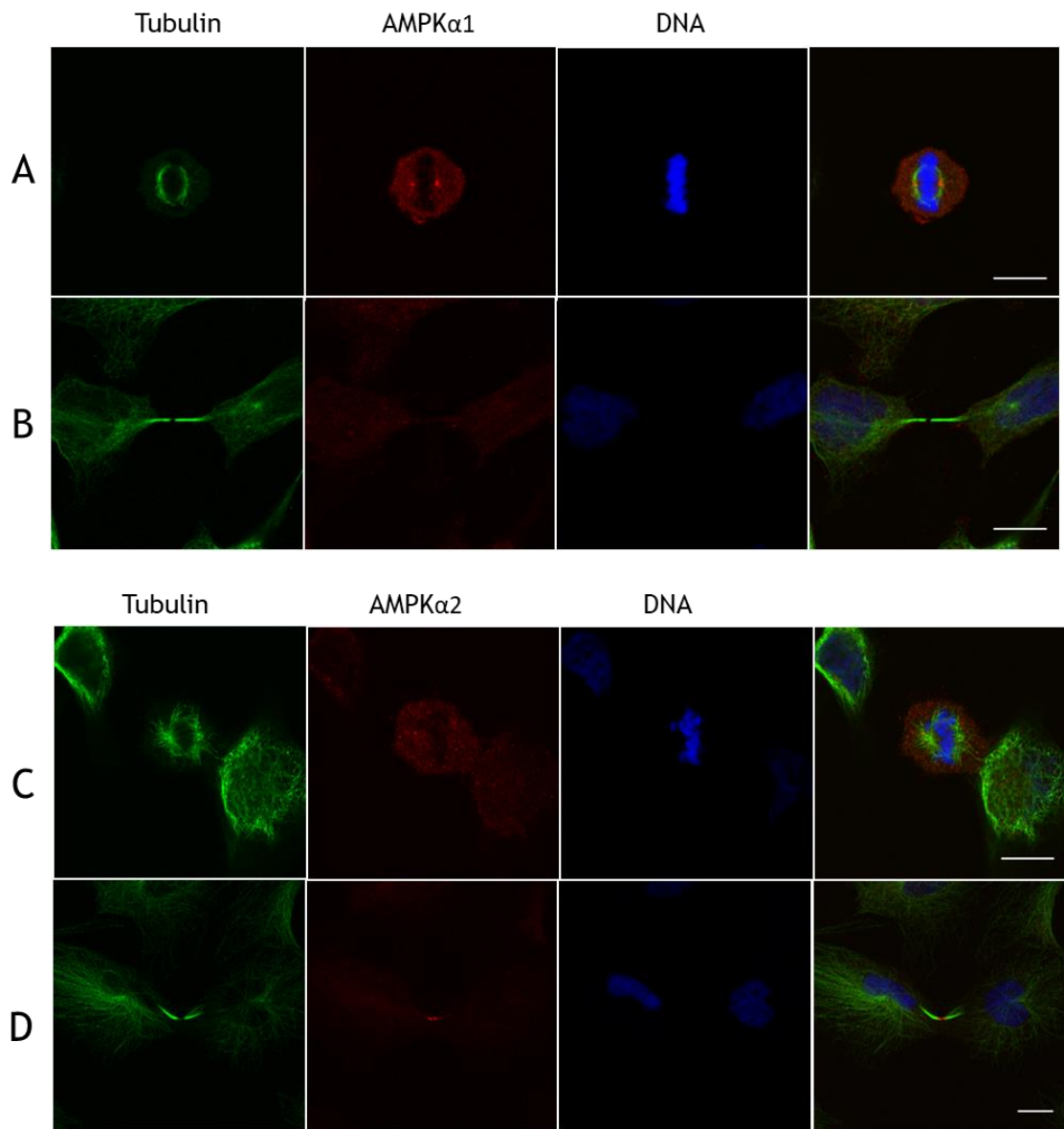
Figure 3-1. Subcellular localisation of AMPKα subunits during mitosis in HeLa cells
HeLa cells were fixed with 4% (w/v) PFA and stained with anti-tubulin (Abcam, ab6160), anti-AMPKα1 (epitope raised against amino acids 344-358 of AMPKα1) (A and B) or anti-AMPKα2 (epitope raised against 351-356 of AMPKα2) antibodies (C and D). DNA was stained with RedDot2. Cells undergoing metaphase are shown in A and C, cells undergoing telophase are shown in B and D. Scale bar 10 μm. Representative images are shown from three independent experiments in each case.
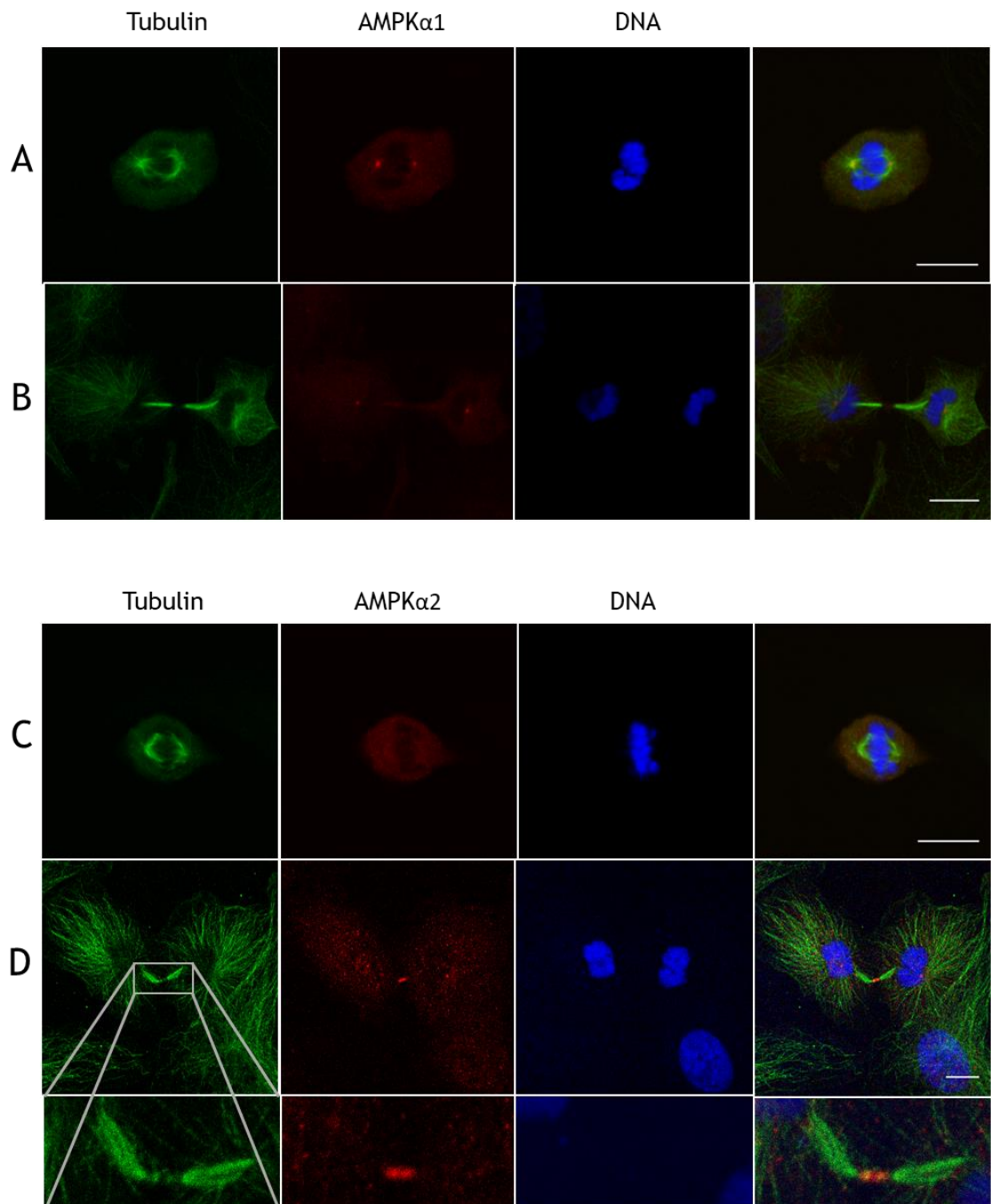
Figure 3-2. Subcellular localisation of AMPKα subunits during mitosis in HUVECs
HUVECs were fixed with 4% (w/v) PFA and stained with anti-tubulin (Abcam, ab6160), anti-AMPKα1 (epitope raised against amino acids 344-358 of AMPKα1) (A and B) or anti-AMPKα2 (epitope raised against 351-356 of AMPKα2) antibodies (C and D). DNA was stained with RedDot2. Cells undergoing metaphase are shown in A and C, cells undergoing telophase are shown in B and D. Scale bar 10 µm. Representative images are shown from three independent experiments in each case.
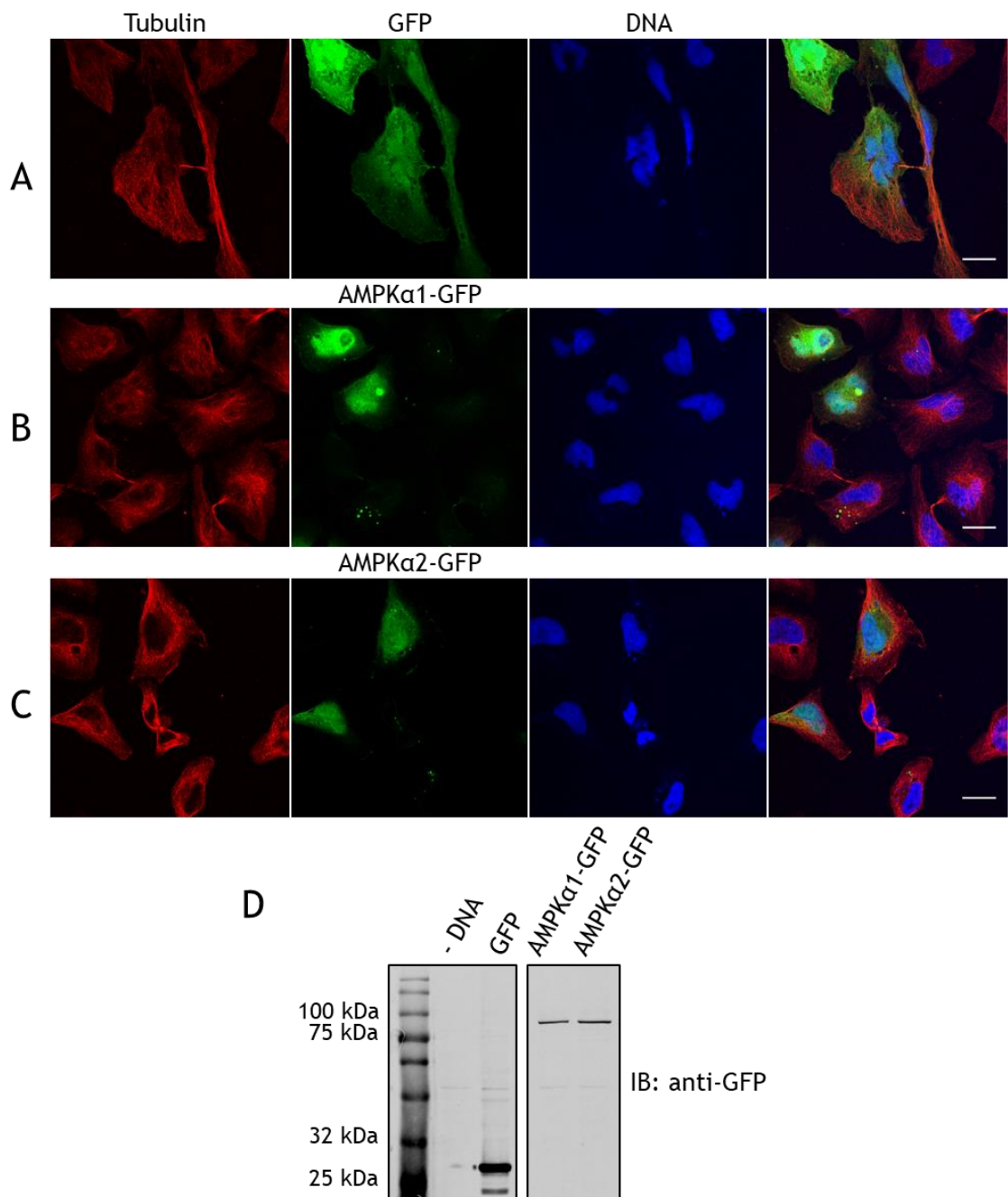
Figure 3-3. Subcellular localisation of AMPKα-GFP in HeLa cells
HeLa cells were transfected with plasmids containing the genes for GFP, AMPKα1-GFP or AMPKα2-GFP. **(A-C)** Representative images of transfected cells stained with anti-tubulin (Abcam, ab6160) antibodies and for DNA with RedDot2 from two independent experiments. Scale bar 10 μm. **(D)** HeLa cells were transfected with the plasmids described. Lysates were prepared 24 h following transfection and resolved by SDS-PAGE followed by immunoblotting using anti-GFP antibodies. N=1.

3.2.1.2 Subcellular localisation of phospho-T172 AMPK during mitosis

Using two different anti-phospho-T172 AMPK antibodies, immunoreactivity was observed at the MTOCs when cells were in metaphase and at the midbody during telophase in both HeLa cells (Figure 3-4) and HUVECs (Figure 3-5). Immunoreactivity of phospho-T172 AMPK was also observed in the cytoplasm of mitotic cells using both antibodies. Anti-phospho-T172 AMPK immunoreactivity was also detected at the spindle midzone of metaphase cells (Figure 3-4 and Figure 3-5).

To determine if the observed anti-phospho-T172 AMPK immunoreactivity was specific, immunoreactivity of the antibodies was examined in AMPK α1/α2 double knockout (AMPK -/-) MEFs. The wild type and AMPK -/- MEFs rapidly progress through the cell cycle, as a result M-phase cells were rarely observed when examined by microscopy (data not shown). To examine mitotic cells, MEFs were synchronised using a thymidine block followed by nocodazole arrest. Anti-phospho-T172 AMPK (sc-101630) immunoreactivity was observed at the midbody in both wild type and surprisingly in AMPK -/- MEFs (Figure 3-6). Comparative levels of cytosolic and nuclear immunoreactivity was observed between the cell types (Figure 3-6).
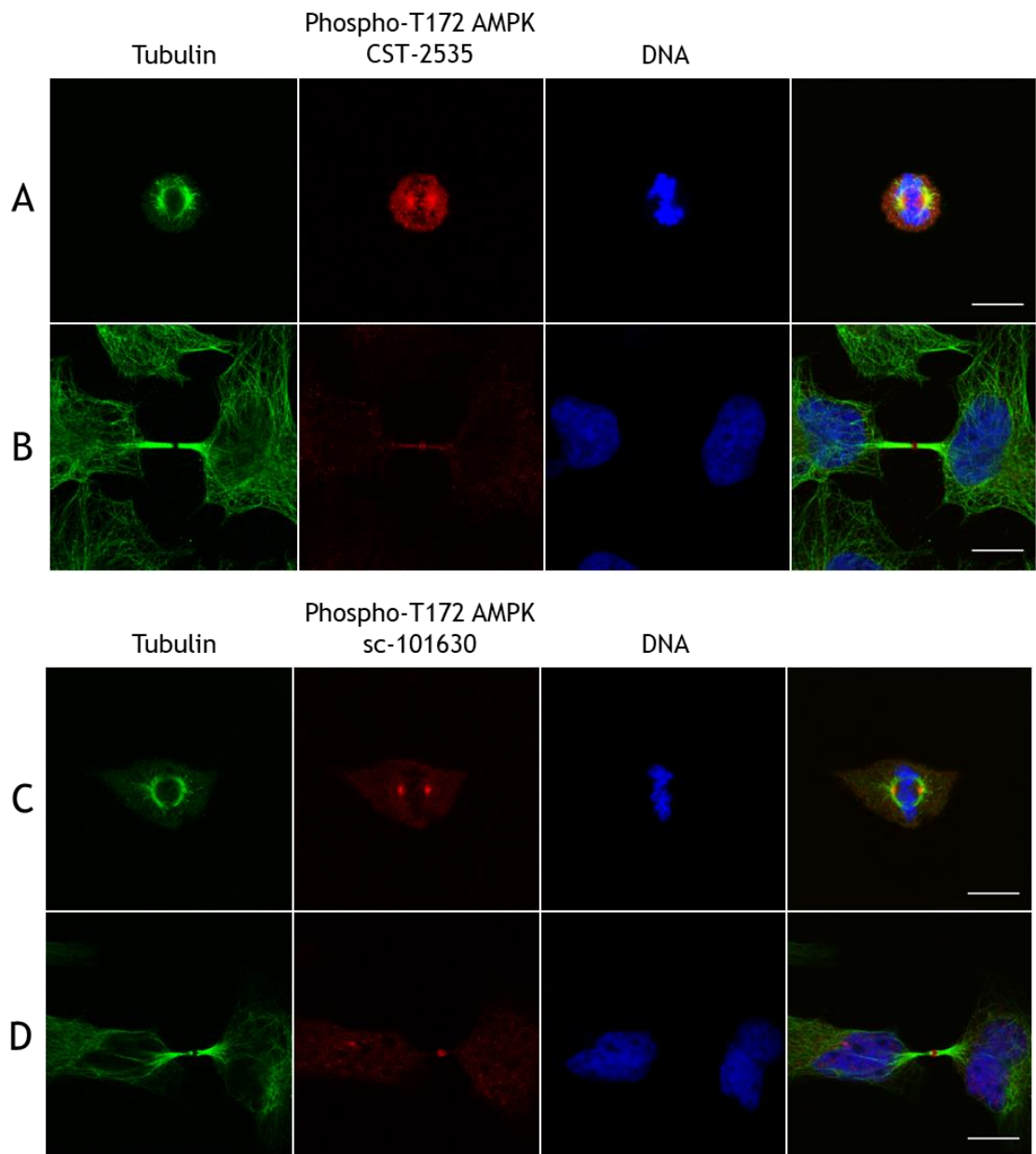
Figure 3-4. Subcellular localisation of phospho-T172 AMPK during mitosis in HeLa cells
HeLa cells were grown on glass cover slips, fixed with 4% (w/v) PFA and stained with anti-tubulin (Abcam ab6160), and either anti-phospho-T172 AMPK from Cell Signalling Technologies (CST) #2535 (A and B) or Santa Cruz Inc. sc-101630 (C and D). DNA was stained with RedDot2. Cells undergoing metaphase are shown in A and C. Cells undergoing telophase are shown in B and D. Scale bar 10 μm. Representative images from three independent experiments are shown.
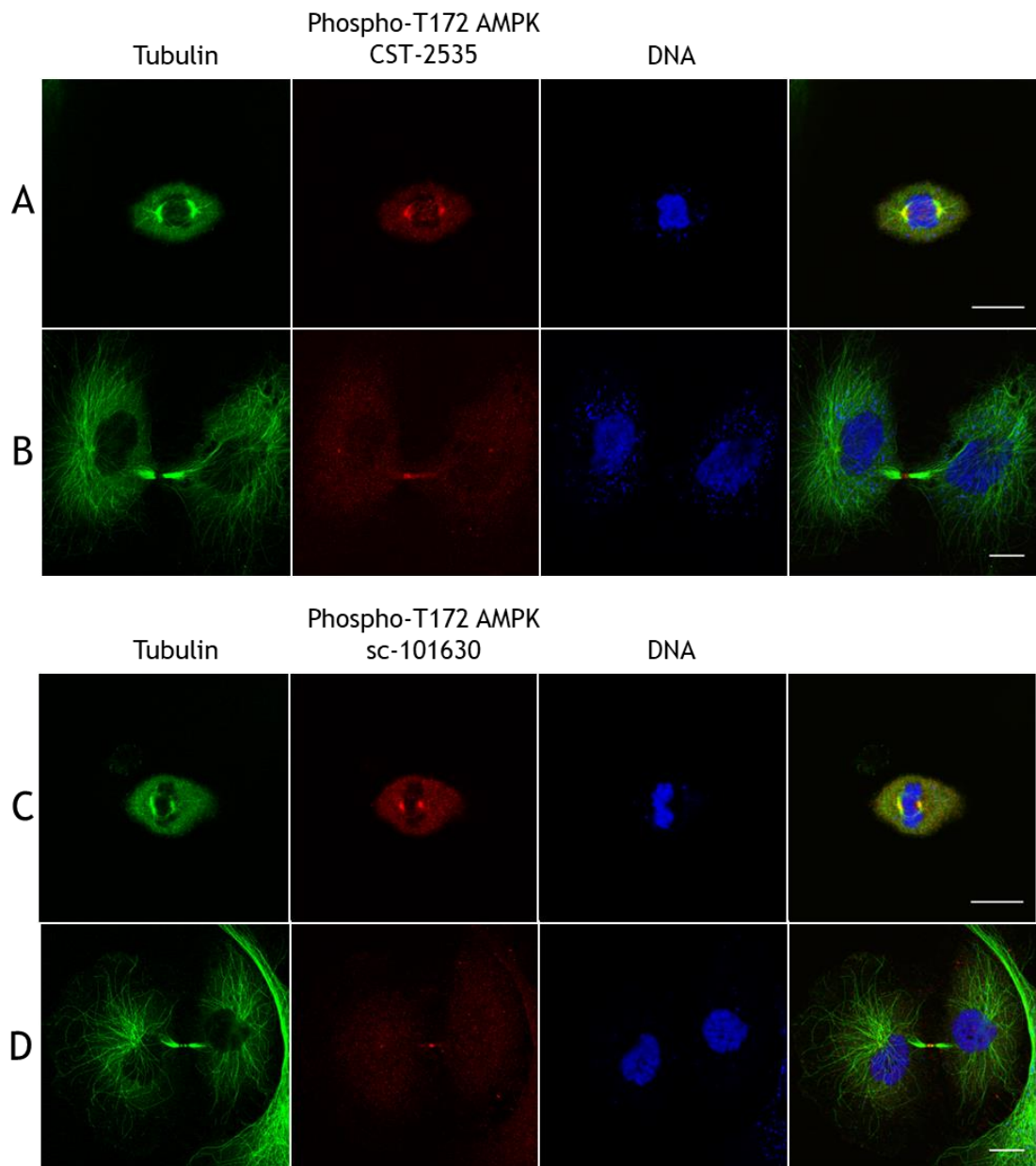
Figure 3-5. Subcellular localisation of phospho-T172 AMPK during mitosis in HUVECs
HUVECs were grown on glass cover slips, fixed with 4% (w/v) PFA and stained with anti-tubulin (Abcam ab6160) and either anti-phospho-T172 AMPK from Cell Signalling Technologies (CST) #2535 (A and B) or Santa Cruz Inc. sc-101630 (C and D). DNA was stained with RedDot2. Cells undergoing metaphase are shown in A and C. Cells undergoing telophase are shown in B and D. Scale bar 10 μm. Representative images from three independent experiments are shown.
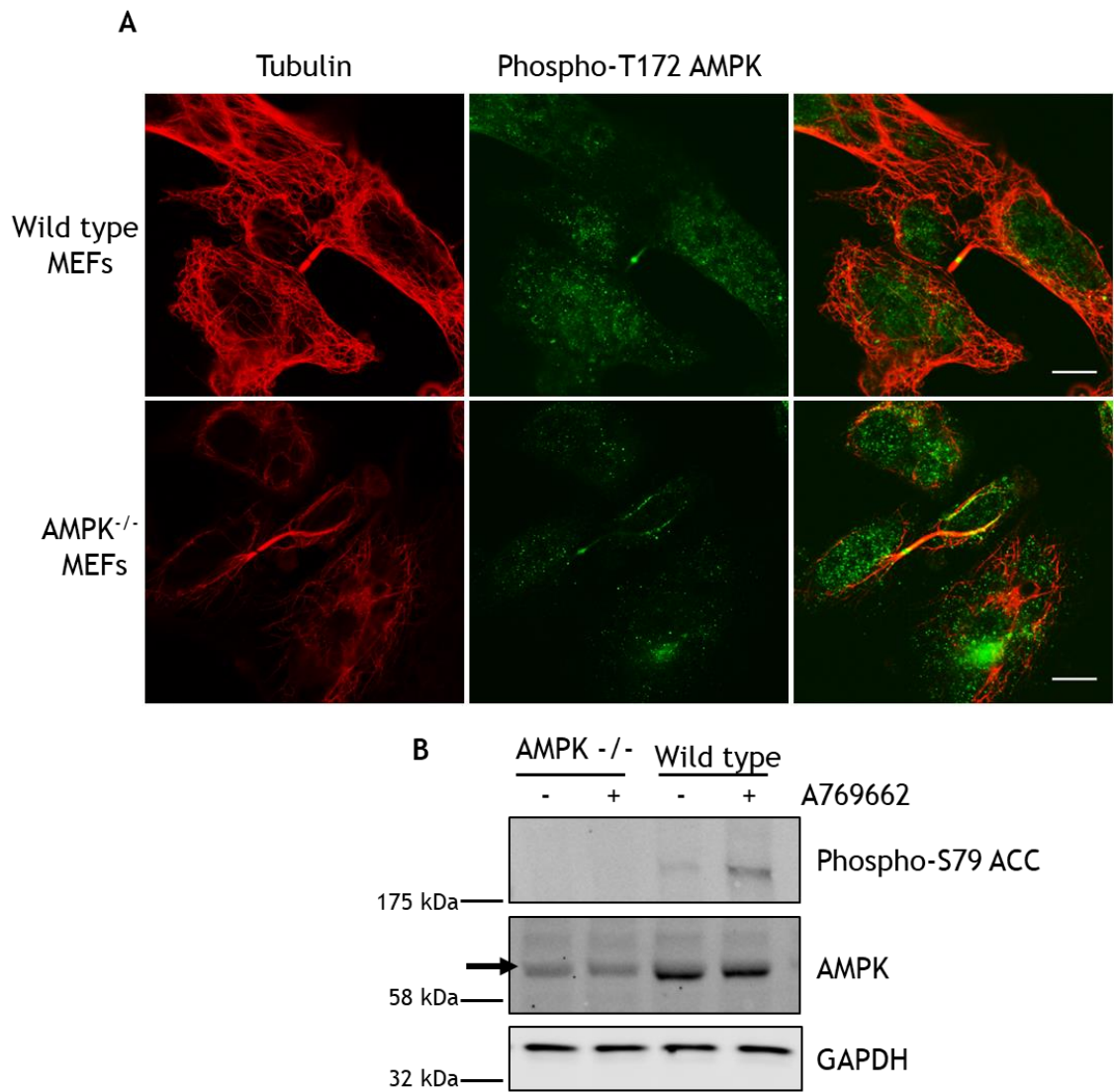
Figure 3-6 Subcellular localisation of phospho-T172 AMPK during mitosis in wild type and AMPK -/- MEFs

(A) Wild type and AMPK -/- MEFs were synchronised using a thymidine and nocodazole block. Synchronised MEFs were seeded onto 8-well Ibidi chambers and incubated until cells entered telophase. Cells were fixed using 4% (w/v) PFA and stained with anti-tubulin (Abcam, ab6160) and anti-phospho-T172 AMPK (Santa Cruz Inc. sc-101630) antibodies. Scale bar represents 10 µm. Representative images from two independent experiments are shown. **(B)** Unsynchronised wild type and AMPK -/- MEFs were incubated with 100 µM A769662 for 30 min before lysates were prepared. Lysates were resolved by SDS-PAGE followed by immunoblotting with the antibodies indicated. Arrow indicates a non-specific band of a higher molecular mass than AMPK. Representative immunoblots from three separate experiments.

3.2.1.3 Subcellular localisation of phospho-S79 ACC

It has been reported that phospho-S79 ACC, a site phosphorylated exclusively by AMPK, exhibits a subcellular localisation which mirrors that of phospho-T172 AMPK during mitosis in A431 cells. (Ha *et al.*, 1994; Vazquez-Martin *et al.*, 2013). However, during the course of this investigation, phospho-S79 ACC was not found to localise to the MTOC or the midbody in HUVECs (Figure 3-7). Immunoreactivity was observed in the cytoplasm of HUVECs. Additionally, phospho-S79 ACC immunoreactivity did not increase in response to A769662 (100 μM, 30 min) when examined by immunofluorescence microscopy, although A769662 stimulation caused a clear increase in phospho-S79 ACC signal intensity when assessed by immunoblotting (Figure 3-7).
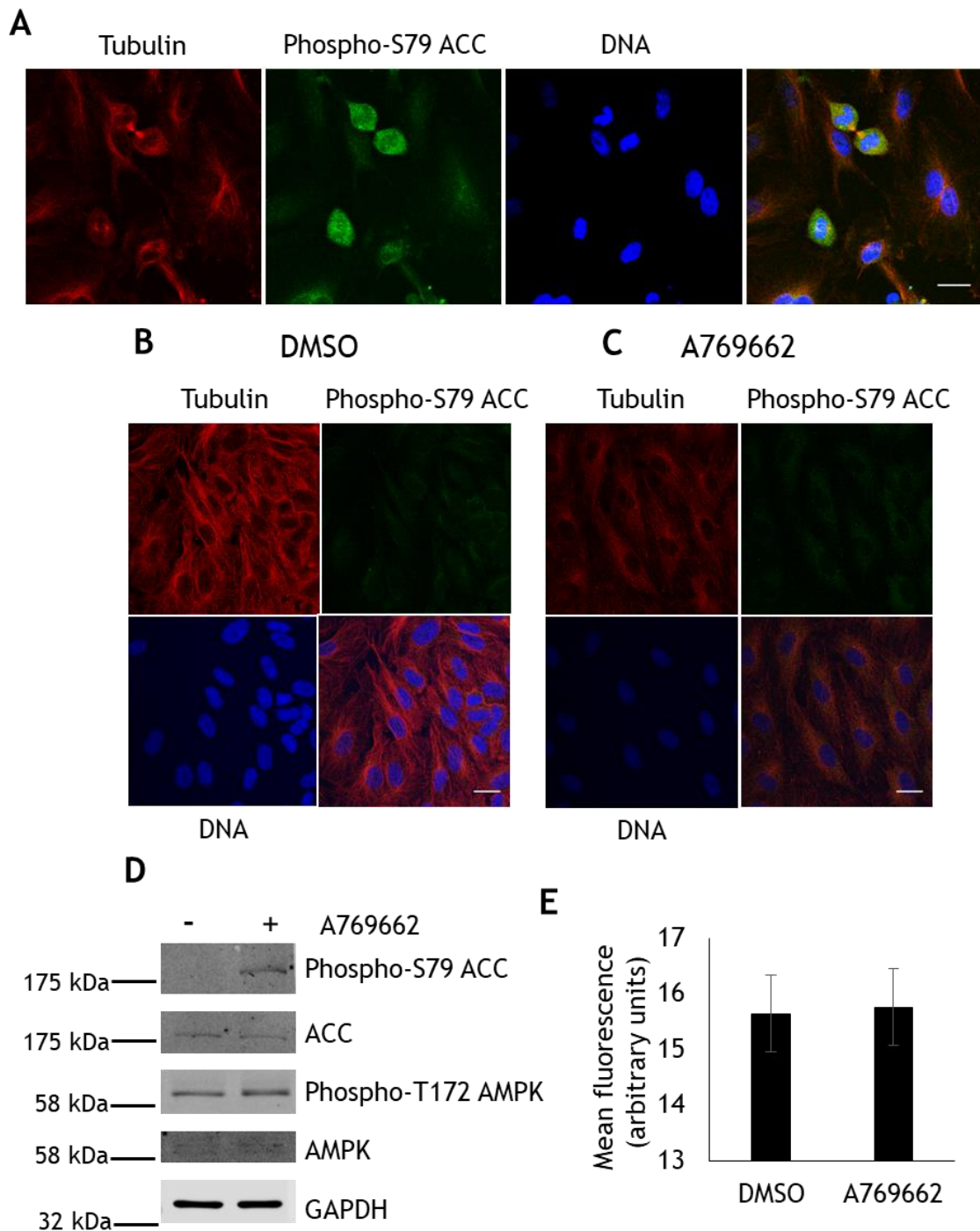
Figure 3-7. Subcellular localisation of Phospho-S79 ACC during mitosis in HUVECs
(A) HUVECs were seeded onto glass coverslips and stained with anti-tubulin (Abcam, ab6160) and anti-phospho-S79 ACC (Cell Signalling technology ®, #11818) antibodies and for DNA with RedDot2. Scale bar 10 μm. Representative images from three independent experiments are shown. **(B-E)** HUVECs were incubated with DMSO vehicle control or A769662 (100 μM, 30 min). **(B/C)** Cells were stained for anti-tubulin, anti-phospho-S79 ACC antibodies and DNA. **(D)** Cells were lysed and resolved by SDS-PAGE followed by immunoblotting with the antibodies indicated. **(E)** Mean fluorescence intensity of phospho-S79 ACC staining was measured in 20 cells using image J software. N=1.

3.2.2 AMPK activity may influence mitosis in mammalian cells

3.2.2.1 Pharmacological modulation of AMPK activity affects the fidelity of mitosis

Next the functional consequences of AMPK activity during the cell cycle was investigated. HeLa cells were treated with pharmacological compounds known to alter AMPK activity namely; STO-609 (CaMKK/AMPK inhibitor), compound C (a poorly selective AMPK inhibitor) or A769662 (AMPK activator) (Tokumitsu *et al.*, 2002; Göransson *et al.*, 2007; Isakovic *et al.*, 2007). Cells were fixed with PFA, stained and examined by confocal microscopy where binucleation was assessed as a read out of failed cytokinesis. HeLa cells incubated with DMSO had a binucleation rate of approximately 2% (Figure 3-8). Compound C (10 µM) caused a modest but significant increase in the proportion of binucleated cells compared to DMSO treated cells (Figure 3-8). STO-609 (5 µM or 10 µM) did not significantly alter the proportion of binucleated cells, but a trend towards increased binucleation was apparent at higher concentrations (Figure 3-8). Stimulation with A769662 (10 µM) did not alter the proportion of binucleated cells (Figure 3-8).

To assess binucleation/polyploidy in a greater number of cells, flow cytometry was undertaken using the DNA dye propidium iodide (PI). Quantification of PI incorporation into cells enabled the phase of the cell cycle to be identified; 2n DNA content represents cells in G_0 or G_1; 2-4n DNA content represents cells in S phase; 4n DNA content represents cells in G_2/M phase or binucleated cells; >4n DNA content is polyploid cells. HeLa cells were treated with AMPK inhibitors/activators as described for 18 h prior to staining. Compound C caused a significant increase in the proportion of HeLa cells with 4n DNA and reduced the proportion of cells with 2n DNA content although this did not achieve statistical significance ($p=0.1$) (Figure 3-9). Incubation of HeLa cells with STO-609 (5 µM or 10 µM) or A769662 (10 µM) did not alter DNA content (Figure 3-9).
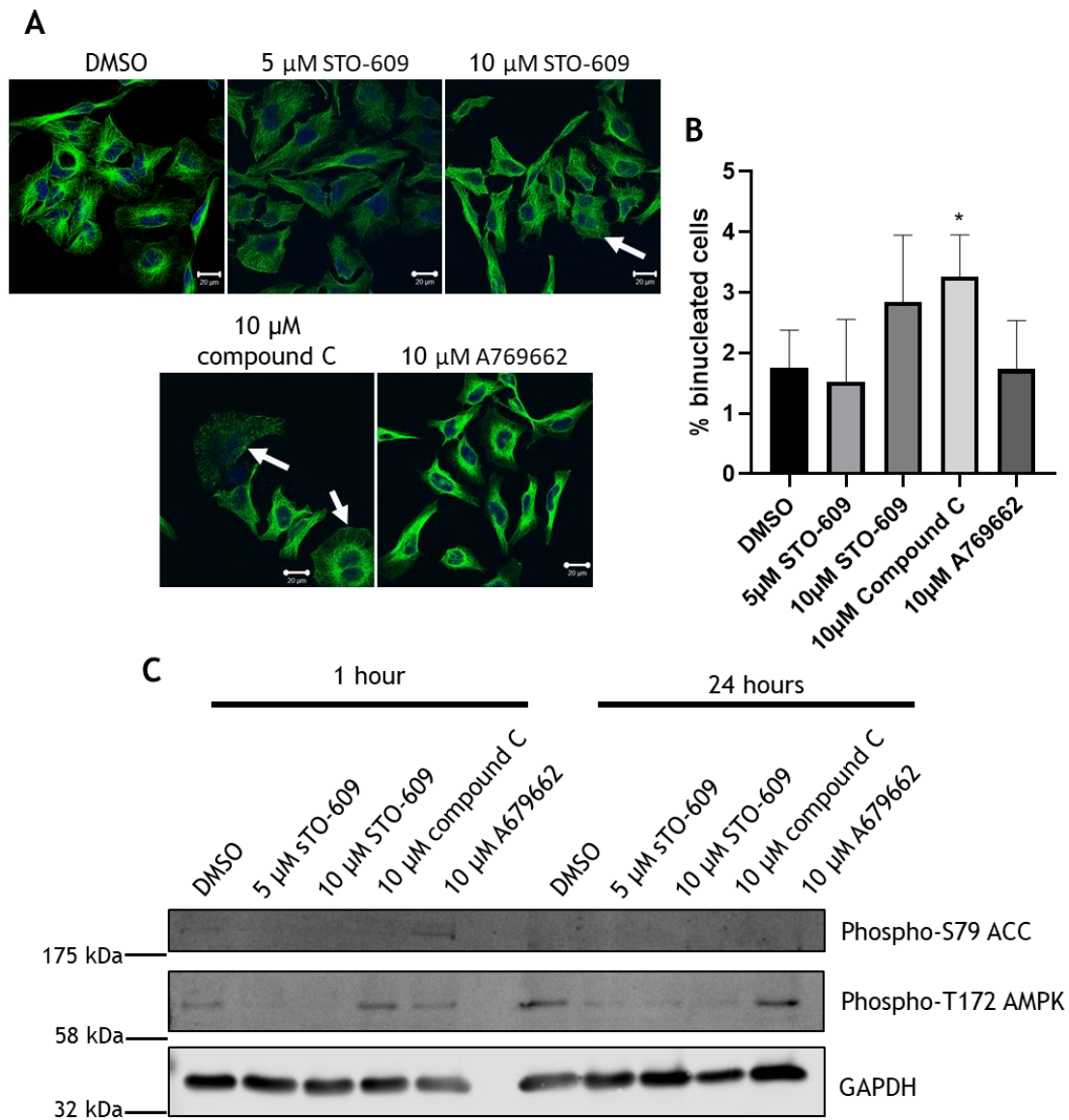
Figure 3-8. The effect of modulating AMPK activity on binucleation in HeLa cells
HeLa cells were treated with the indicated compound for 24 h. **(A)** Representative images of cells strained with anti-tubulin (Abcam, ab6160) antibodies and for DNA (DAPI). White arrows indicate binucleated cells, scale bar represents 10 μm. **(B)** Quantification of binucleated HeLa cells. **(C)** HeLa cells were treated as described prior to lysis. Cell lysates were resolved by SDS-PAGE and subjected to immunoblotting using the antibodies indicated. Representative images from three independent experiments are shown. * $p < 0.05$ relative to DMSO alone (Students *t*-test).
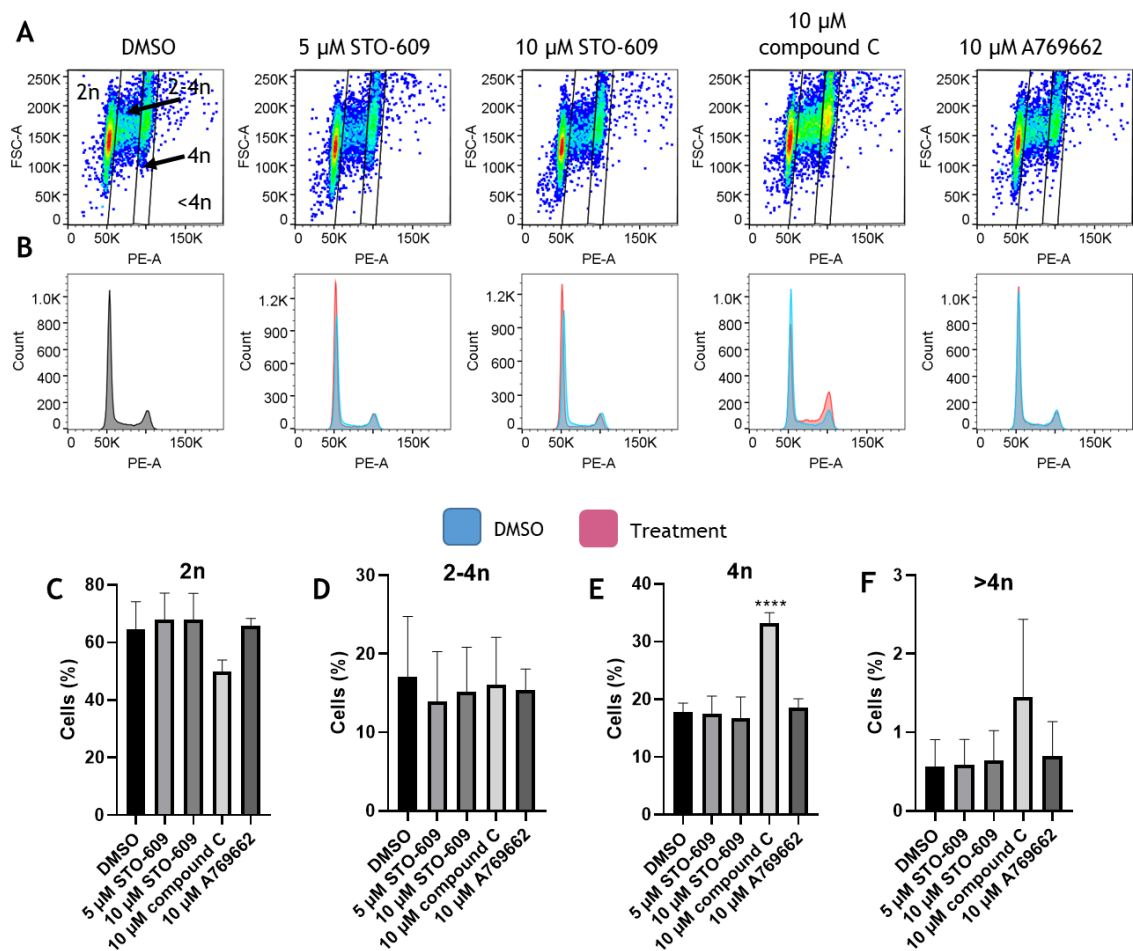
Figure 3-9. The effect of modulating AMPK activity on the DNA content of HeLa cells
HeLa cells were incubated with the compounds indicated for 24 h. Cells were harvested and fixed with ice cold 70% (v/v) ethanol. DNA was stained with PI and DNA content measured by flow cytometry. **(A)** Representative scatter plots showing the gating used. FSC-A (forward scatter by area), PE-A (Phycoerythrin by area, used as a pseudo measurement for PI staining). **(B)** Representative histograms, DMSO treated cells are shown in blue with the indicated treatment in pink. **(C-F)** Quantification of HeLa cell DNA content. Data shown as mean ± SEM. N=3-4. **** $p < 0.001$ relative to DMSO (one-way ANOVA).

To assess how pharmacological modulation of AMPK activity may affect HeLa cell viability, MTS assays were undertaken in which the conversion of a tetrazolium salt to a coloured product was measured. This reaction is catalysed by succinate dehydrogenase, a component of the mitochondrial electron transport chain (Wang *et al.,* 2010). Therefore, MTS assays measure mitochondrial activity as an indirect measure of cell viability. Compound C caused a dramatic reduction in HeLa cell viability (Figure 3-10A). Neither STO-609 nor A769662 altered HeLa cell viability (Figure 3-10A).

Additionally, BrdU assays were undertaken to measure proliferation. BrdU is an analogue of thymidine and is incorporated into DNA during S phase and can be readily detected. STO-609, compound C and A769662 all caused a significant reduction in HeLa cell proliferation with compound C having the largest effect (Figure 3-10B).
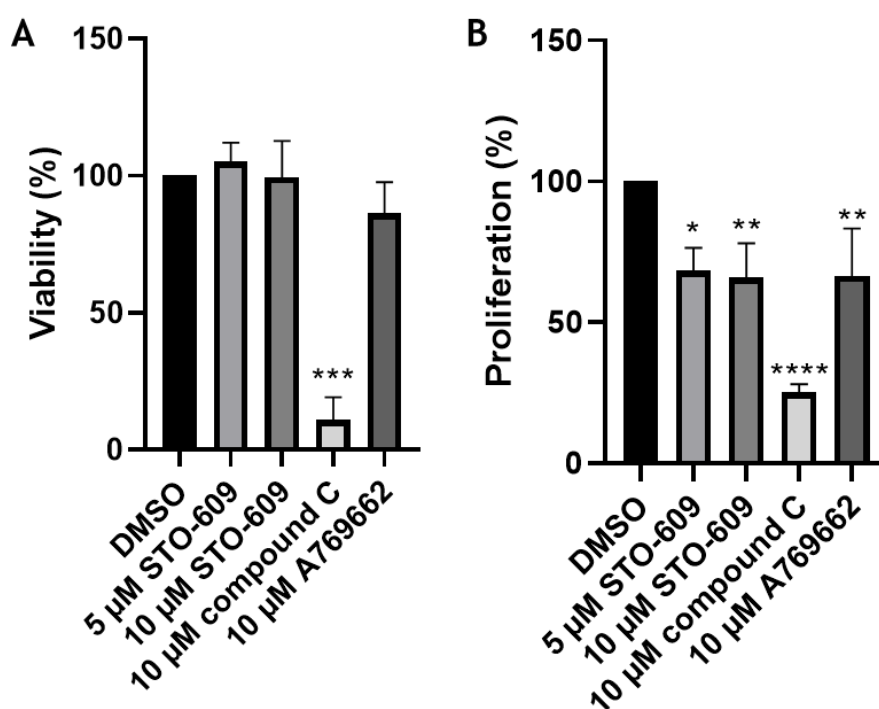
Figure 3-10. The effect of modulating AMPK activity on HeLa cell viability and proliferation
HeLa cells were seeded in a 96-well plate and incubated for 4 h prior to incubation as indicated for 18 h. **(A)** Cells were cultured in the presence of MTS reagent for 3 h to assess cell viability. **(B)** HeLa cells were cultured with BrdU reagent for 18 h to measure cell proliferation. Data shown as mean ± SEM % viability/proliferation relative to DMSO vehicle. N=3. * $p < 0.05$, ** $p < 0.01$ **** $p < 0.0001$ relative to DMSO vehicle (one-way ANOVA).

As HeLa cells lack LKB1, HUVECs were utilised as a more biologically relevant model to establish how AMPK activity may influence mitosis (Sapkota *et al.*,2002). A greater number of AMPK pharmacological modulators were also examined; namely; AICAR (AMP-mimetic), canagliflozin and metformin (increase intracellular AMP) and salicylate (direct AMPK activator) (Corton *et al.*, 1995; Zhou *et al.*, 2001; Hawley *et al.*, 2012, 2016). Metformin and salicylate (MetSal) were used in combination due to their synergistic mechanisms of AMPK activation (Hawley *et al.*, 2012). HUVECs were incubated with the drugs indicated for 18 h and DNA content assessed by flow cytometry. Compound C (5 μM and 10 μM) significantly increased the proportion of cells with 2n DNA content, dramatically reduced the proportion of cells with 2-4n DNA and increased the proportion of cells with >4n DNA (Figure 3-11). The 4n population was not affected by compound C (Figure 3-11). Activation of AMPK with MetSal caused a significant increase in the proportion of cells with 2n DNA content while reducing the proportion of cells with >4n DNA content (Figure 3-11). AICAR (0.1 mM and 1 mM) caused an increase in the proportion of cells with 2-4n DNA although there was considerable variation in the data set ($p=.0.21$ and $p=0.18$ respectively) (Figure 3-11). STO-609 (10 μM), A769662 (10 μM or 50 μM), metformin (3 mM) or salicylate (5 mM) did not alter the DNA content of HUVECs (Figure 3-11).

Selected pharmacological compounds were then investigated further, namely; 10 μM compound C, 50 μM A769662, 1 mM AICAR, 10 μM canagliflozin and MetSal. Cells were incubated with the compounds for 18 h, fixed with PFA and stained for tubulin and DNA. Cells were examined by confocal microscopy and the proportion of binucleated cells assessed. No treatments significantly altered the proportion of binucleated cells (Figure 3-12).
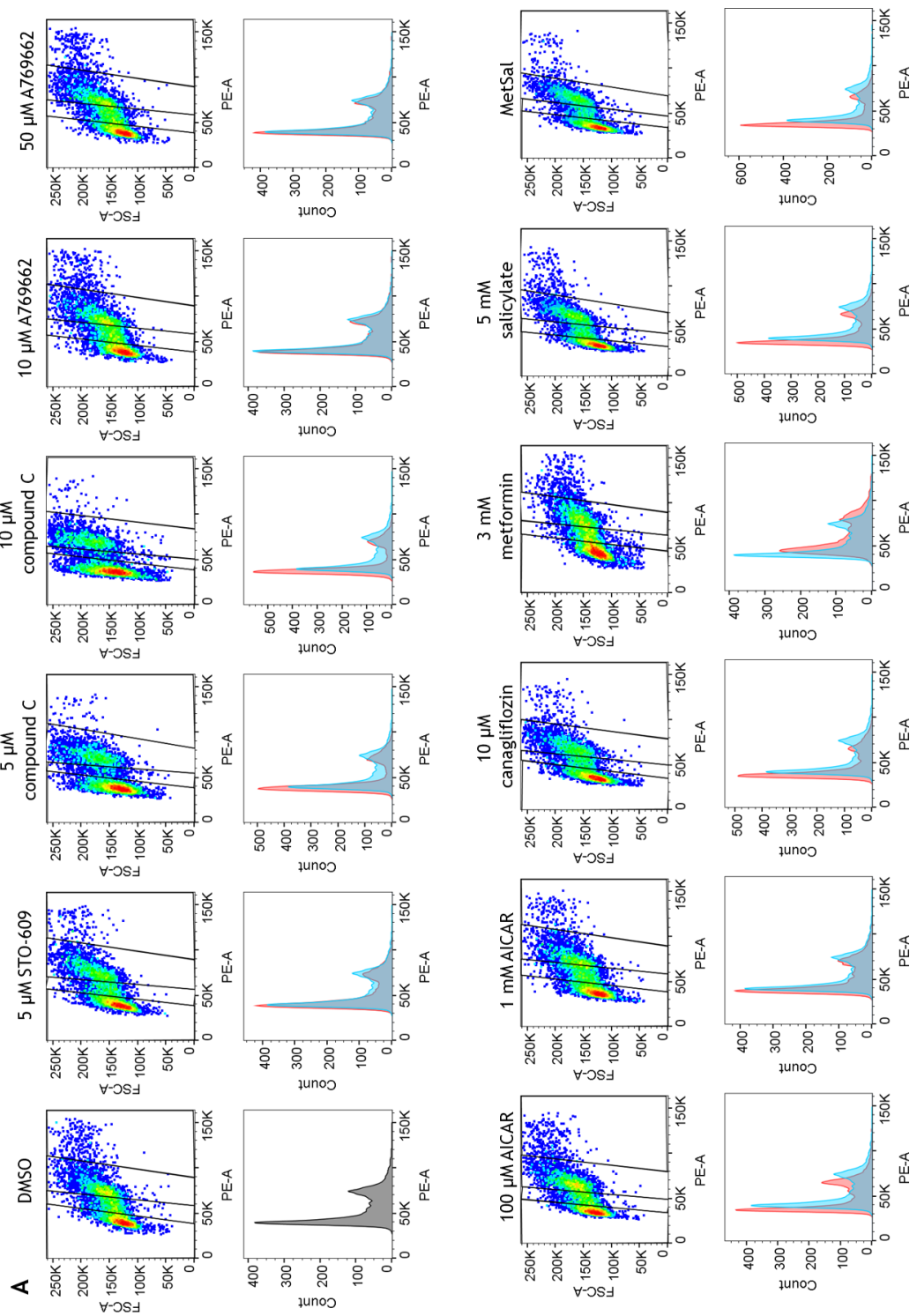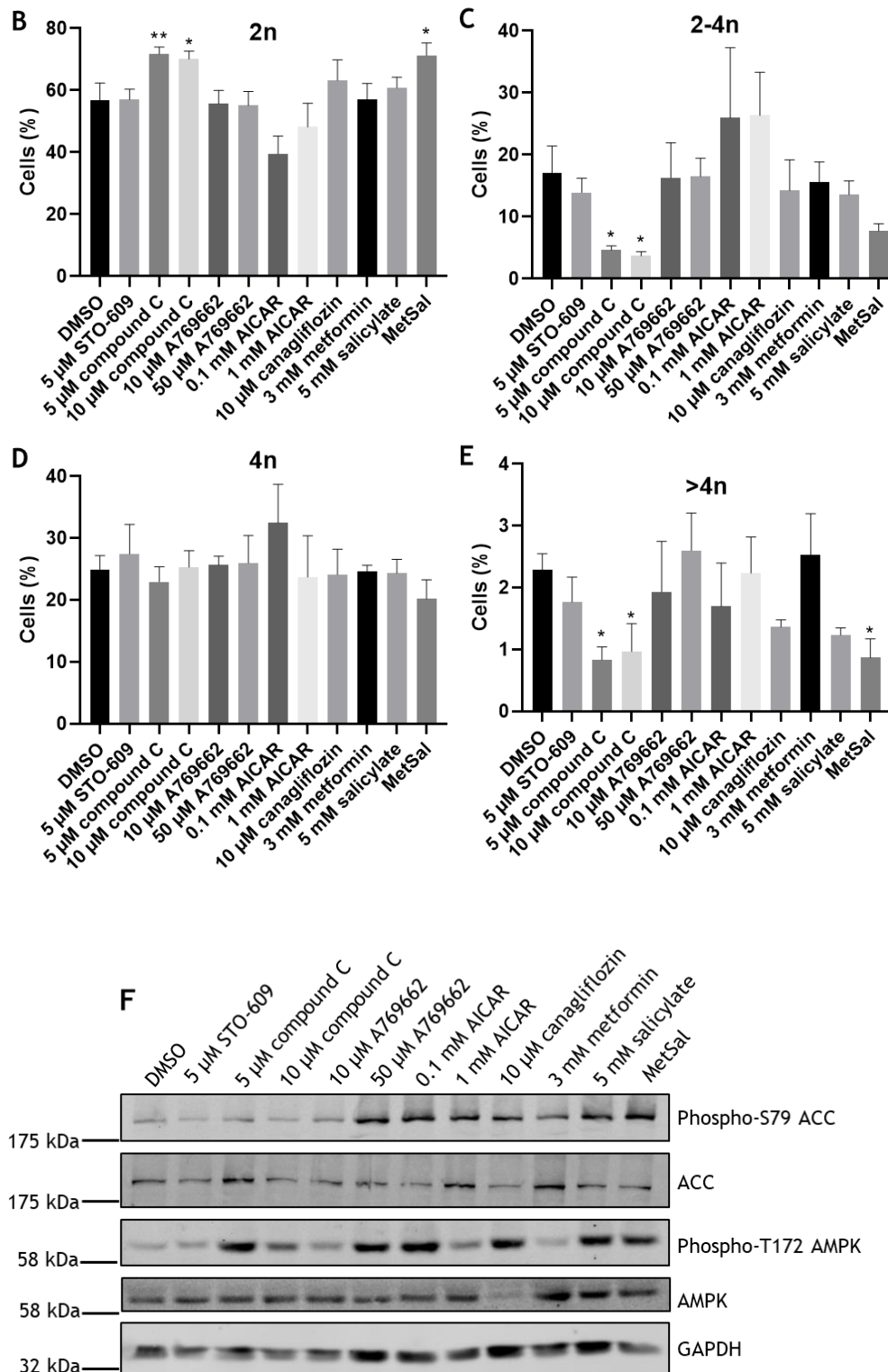
Figure 3-11. The effect of modulating AMPK activity on the DNA content of HUVECs
HUVECs were incubated with the indicated compounds for 18 h. Cells were harvested and fixed with ice cold 70% (v/v) ethanol. DNA was stained with PI and DNA content measured by flow cytometry. **(A)** Representative scatter plots showing the gating used. FSC-A (forward scatter by area), PE-A (Phycoerythrin by area, used as a pseudo measurement for PI staining). Gating was carried out individually for each treatment Representative histograms are shown below, DMSO treated cells are shown in blue with the indicated treatment in pink. **(B-E)** Quantification of HUVEC DNA content. **(F)** HUVECs were treated as described prior to lysis. Cell lysates were resolved by SDS-PAGE and subjected to immunoblotting using the antibodies indicated. Data shown as mean ± SEM % cells. * $p < 0.05$, ** $p < 0.01$ relative to DMSO vehicle (one way ANOVA). N=3.
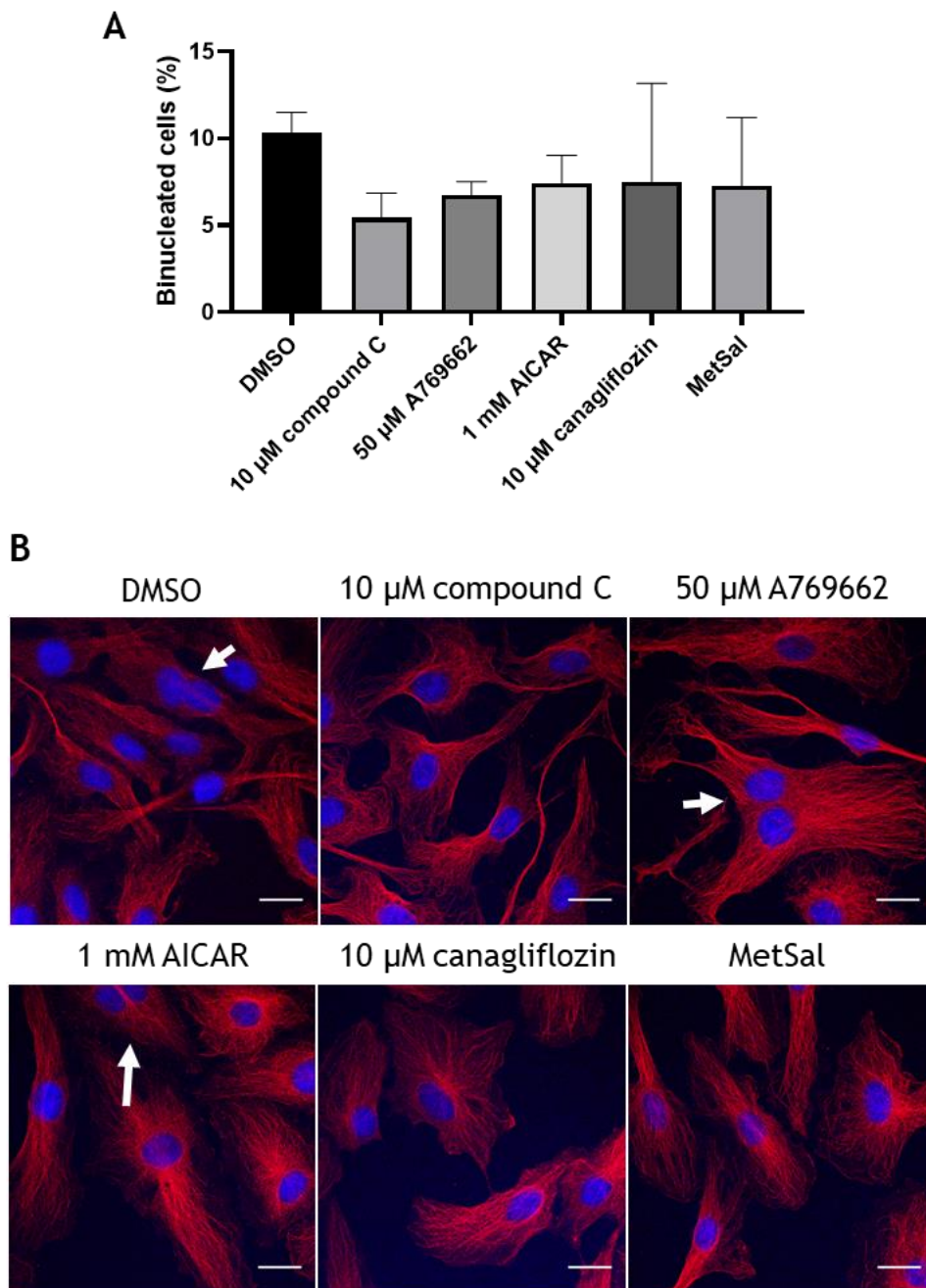
Figure 3-12. The effect of modulating AMPK activity on binucleation in HUVECs
HUVECs were incubated with the described compounds for 18 h. Cells were fixed with PFA and strained with anti-tubulin (Abcam, ab6160) antibodies and for DNA using RedDot2. **(A)** The mean ± SEM percentage of binucleated cells are shown. **(B)** Representative images of stained cells. White arrows indicate binucleated cells, scale bar represents 10 µm. N=3.

During the course of the investigation, an inhibitor of Unc-51-like kinase 1 (ULK1), SBI-0206965, was identified as a potent inhibitor of AMPK (Dite *et al.*, 2018). Concentrations of SBI-0206965 above 10 µM inhibited AICAR (1 mM, 1 h) stimulated phosphorylation of ACC S79 in HUVECs (Figure 3-13G). Therefore, SBI-0206965 was used as another pharmacological tool to investigate how modulating AMPK activity may influence polyploidy. HUVECs were incubated with SBI-0206965 for 18 h and DNA content assessed by flow cytometry. SBI-0206965 (10 µM) did not alter the DNA content of HUVECs, although 30 µM caused an apparent reduction in the proportion of cells with 2-4 DNA content (Figure 3-13).

To assess how manipulation of AMPK activity influenced cell viability and proliferation in HUVECs, MTS and BrdU assays were carried out. All tested pharmacological modulators of AMPK activity significantly reduced HUVEC viability (Figure 3-14A). Compound C (5 µM and 10 µM), canagliflozin (10 µM), MetSal and SBI-0206965 (10 µM and 30 µM) significantly reduced proliferation when assessed by BrdU incorporation (Figure 3-15B). Neither A769662 (50 µM) or AICAR (1 mM) affected BrdU incorporation (Figure 3-15B).
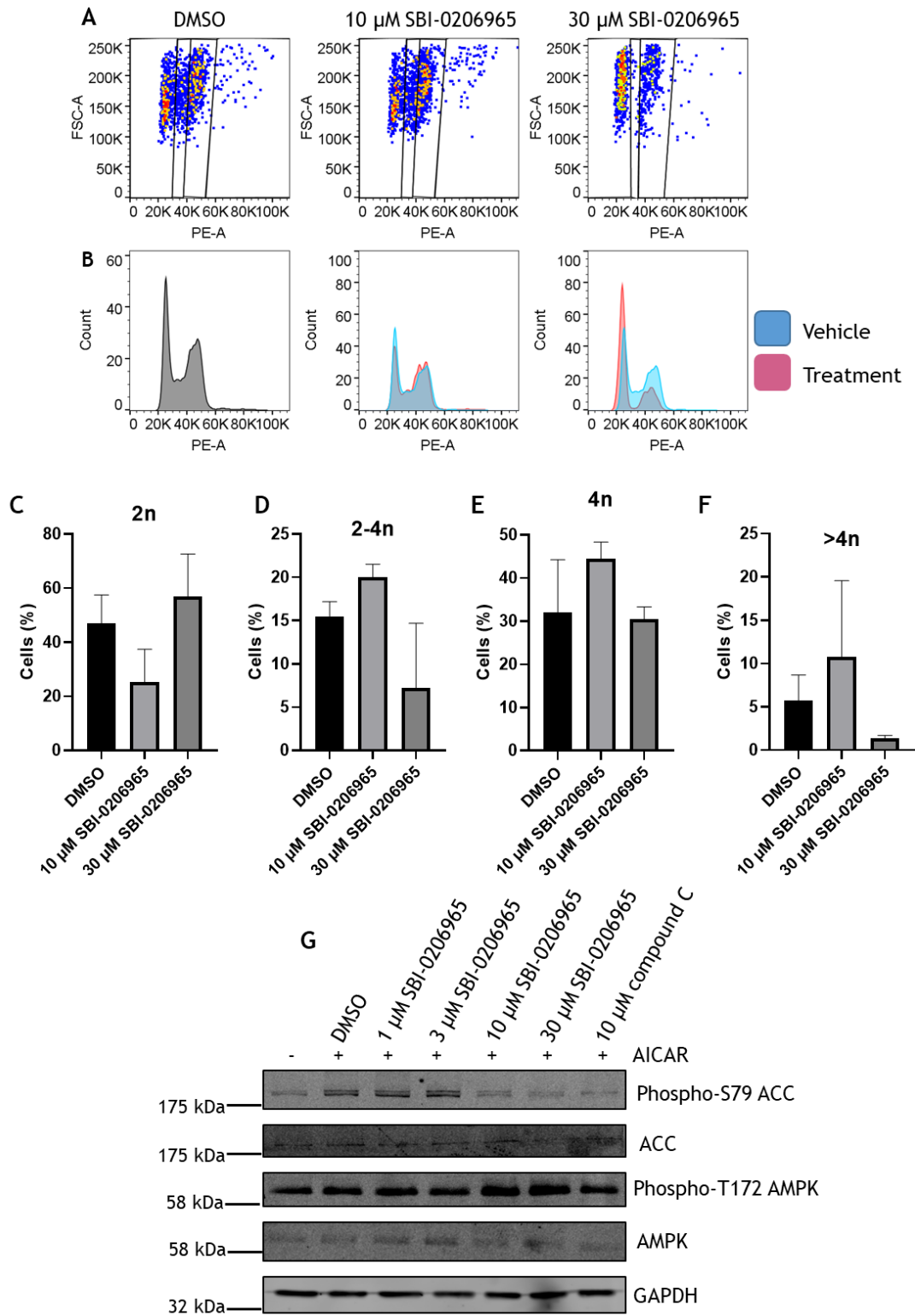
Figure 3-13. The effect of SBI-0206965 on the DNA content of HUVECs
HUVECs were treated as detailed for 18 h and DNA content measured by flow cytometry using PI staining. **(A)** Representative scatter plots showing the gating used. FSC-A (forward scatter by area), PE-A (Phycoerythrin by area, used as a pseudo measurement for PI staining). **(B)** Representative histograms from flow cytometry analysis comparing DMSO treated cells (pink histogram) and drug-treated (blue histogram). **(C-F)** Analysis of the proportion of cells with 2n, 2-4n, 4n or >4n DNA content. **(G)** HUVECs were pre-treated with AICAR (1 mM, 1 h) followed by the detailed treatments with SBI-0206965 for 30 min. Cells were lysed and resolved by SDS-PAGE and interrogated by immunoblotting using the antibodies indicated. Data shown ± SEM. Data shown from two independent experiments.
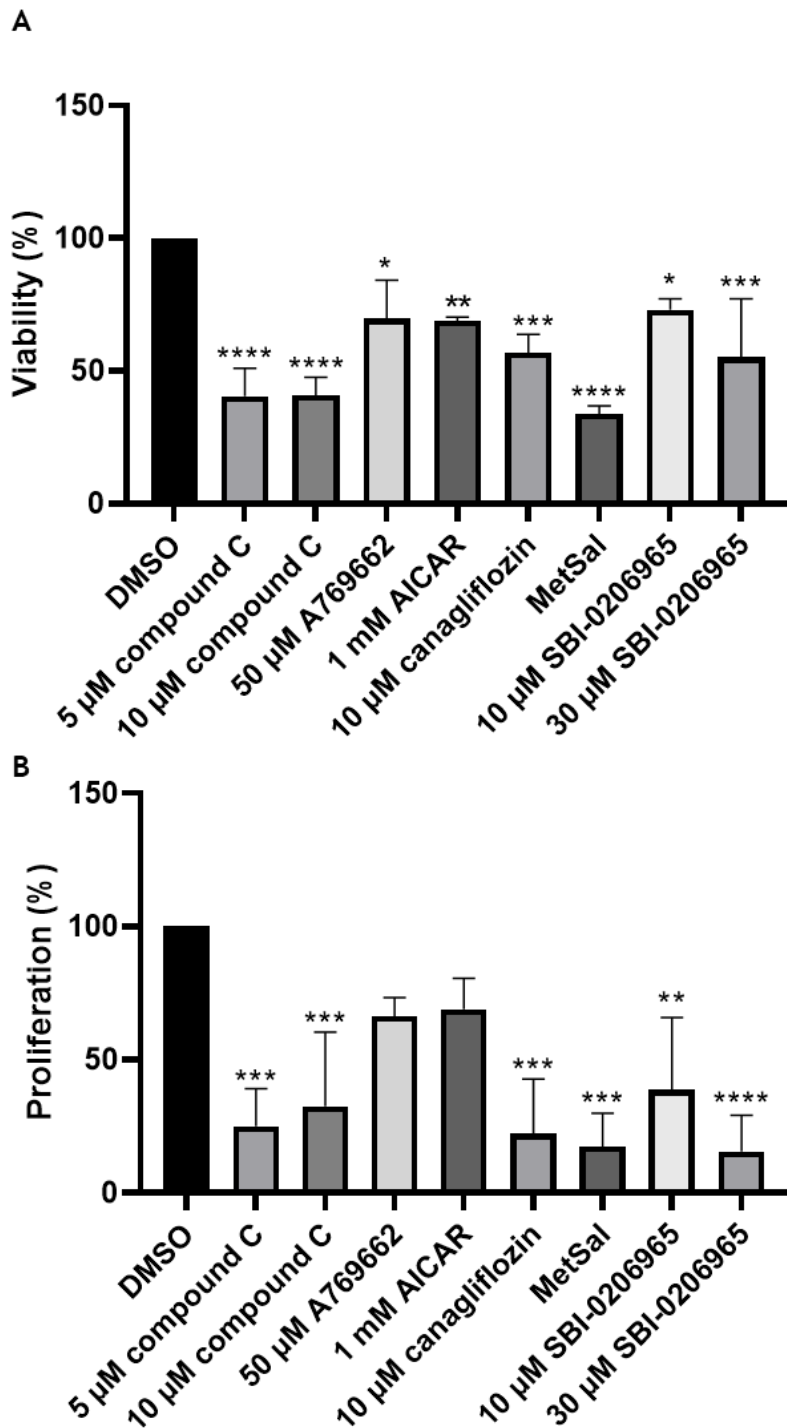
Figure 3-14. The effect of modulating AMPK activity on HUVEC viability and proliferation
HUVECs were seeded in a 96-well plates and incubated for 4 h. Cells were treated as indicated for 18 h. **(A)** Cells were cultured in the presence of MTS reagent for 2 h to assess cell viability. **(B)** HUVECs were cultured with BrdU reagent for 18 h to measure cell proliferation. Data shown as mean ± SEM % viability/proliferation relative to DMSO vehicle N=3. * $p<0.05$, ** $p<0.01$, *** $p<0.005$ and **** $p<0.0001$ relative to DMSO (one-way ANOVA).

To determine if the observed alterations in binucleation/DNA content in response to pharmacological compounds were AMPK-dependent, experiments were undertaken using wild type and AMPK -/- MEFs. Compound C (5 μM and 10 μM) markedly altered the DNA content of both MEF genotype. Scatter plots of compound C treated cells showed a broad spread of cell population that could not easily be separated. Comparing the histogram overlays of cells incubated with DMSO versus that of compound C treated cells indicated that in wild type MEFs compound C caused a dramatic reduction of cells with 4n DNA. AMPK -/- MEFs had cells correlating with 4n DNA but at a lower rate than DMSO treated cells (Figure 3-15). When the gating of DMSO treated cells was applied to compound C treated cells, the only statistically significant alteration was an increase in the proportion of 2-4n DNA in AMPK-/-MEFs (Figure 3-15). Neither A769662 (50 μM) nor canagliflozin (10 μM) significantly altered the DNA content of either wild type of AMPK -/- MEFs, although a substantial right shift was apparent for AMPK -/- MEFs incubated with A769662 (Figure 3-15). MetSal caused a left-shift in the AMPK -/- MEF histogram compared to both DMSO treated AMPK -/- cells and wild type MetSal treated MEFs (Figure 3-15).

Compound C (5 μM) markedly reduced wild type MEF viability, whereas this effect was lessened in AMPK -/- MEFS (Figure 3-16A). Higher concentrations of compound C (10 μM) affected wild type and AMPK -/- MEFs equally (Figure 3-17A). Low concentrations of SBI-0206965 (10 μM) reduced AMPK -/- MEF viability but did not affect wild type MEF viability (Figure 3-17A). At higher concentrations, SBI-0206965 (30 μM) reduced wild type and AMPK -/- MEF viability to a similar extent (Figure 3-16A). A769662 (50 μM), AICAR (1 mM), canagliflozin (10 μM) or MetSal did not significantly alter MEF viability (Figure 3-176A).

Compound C (5 μM and 10 μM), A769662 (50 μM), AICAR (1 mM), MetSal and SBI-0206965 (10 μM and 30 μM) reduced MEF proliferation of both genotypes to a comparable extent (Figure 3-16B). Canagliflozin (10 μM) was the only compound not to alter MEF proliferation (Figure 3-17B).

A

Wild type

Vehicle
Treatment

B

AMPK -/-

C

Wild type
AMPK -/-

MetSal
10 μM canagliflozin
50 μM A769662
10 μM compound C
5 μM compound C
DMSO

H

Wild type   AMPK -/-

DMSO
5 μM Compound C
10 μM Compound C
50 μM A769962
10 μM Canagliflozin
MetSal

DMSO
5 μM Compound C
10 μM Compound C
50 μM A769962
10 μM Canagliflozin
MetSal

175 kDa —   Phospho-S79 ACC

175 kDa —   ACC

58 kDa —   Phospho-T172 AMPK

32 kDa —   GAPDH

100

Figure 3-15. The effect of modulating AMPK activity on the DNA content of wild type and AMPK -/- MEFs

Wild type and AMPK -/- MEFs were incubated as indicated for 18 h and DNA content measured by flow cytometry using PI staining. **(A)** Representative scatter plots showing the gating used for wild type MEFs; FSC-A (forward scatter by area), PE-A (Phycoerythrin by area, used as a pseudo measurement for PI staining). Representative histogram overlays comparing DMSO treated cells blue) with drug treated cells (pink) of AMPK wild type MEFS. **(B)** Representative scatter plots and histogram overlays comparing DMSO treated cells (blue) with drug treated cells (pink) of AMPK -/- MEFS **(C)** Comparison of wild type (green) and AMPK -/- (blue) MEF DNA content histograms. **(D-G)** Analysis of the proportion of cells with 2n, 2-4n, 4n or >4n DNA content. **(H)** MEFs were treated with the indicated compounds for 18 h. Cells were lysed and resolved by SDS-PAGE and immunoblotting using the antibodies detailed. Data shown are mean ± SEM % cells. ** $p<0.01$ relative to DMSO (two-way ANOVA). N=3.
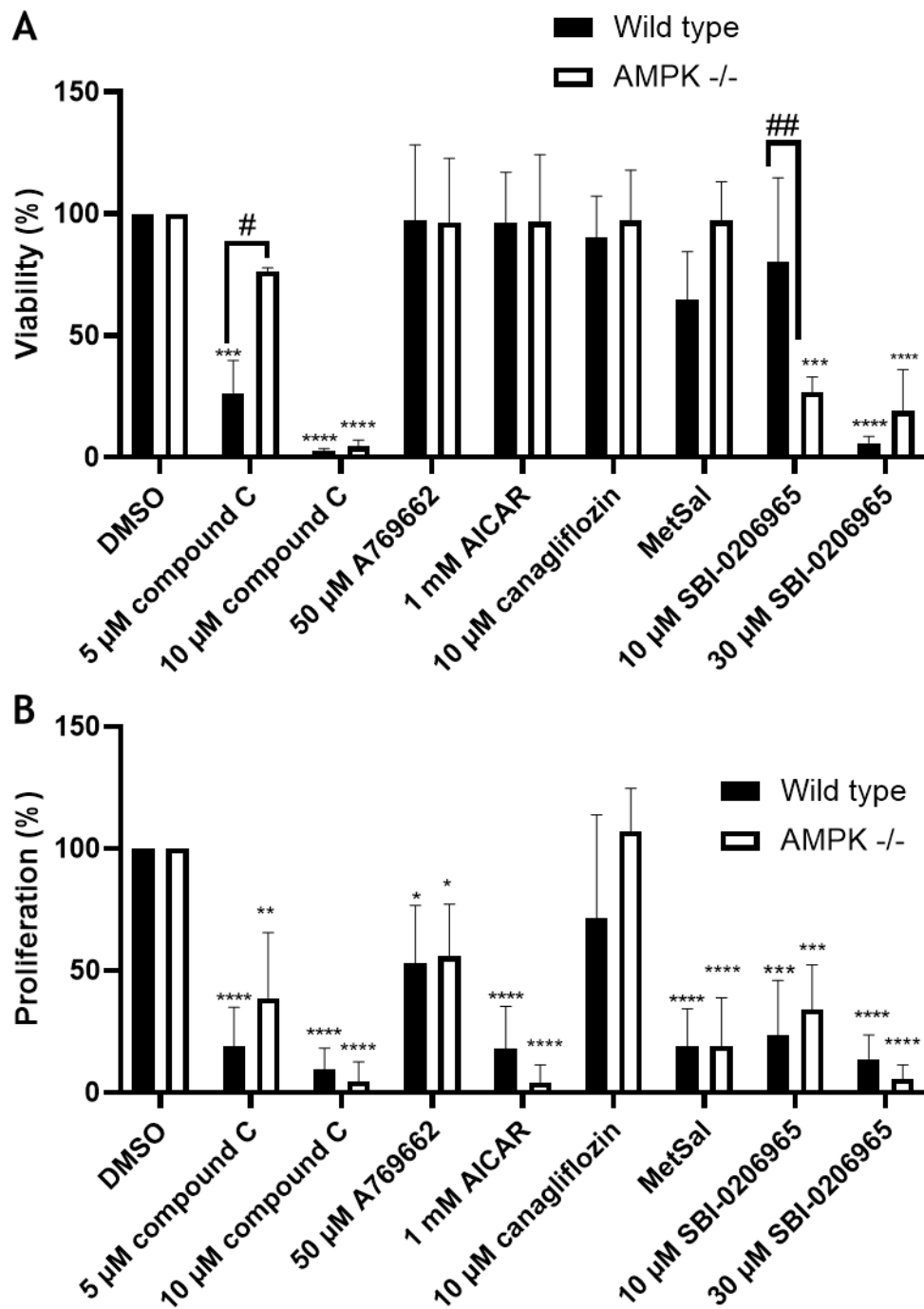
Figure 3-16. The effect of modulating AMPK activity on wild type and AMPK -/- MEF viability and proliferation
Wild type and AMPK -/- MEFs were seeded in 96-well plates and incubated for 6 h. Cells were treated as indicated for 18 h. **(A)** Cells were cultured in the presence of MTS reagent for 4 h to assess viability. **(B)** MEFs were cultured with BrdU reagent for 18 h to measure proliferation. Data shown as mean ± SEM % viability/proliferation relative to DMSO. *$p<0.05$, *** $p<0.005$, **** $p<0.0001$ relative to DMSO treated cells (two-way ANOVA). # $p<0.05$, #'# $p<0.001$ relative to wild type MEFs (two-way ANOVA). N=3.

3.2.2.2 Genetic alteration of AMPK activity can alter polyploidy in HUVECs

As many of the pharmacological modulators used during this investigation can have AMPK-independent effects, a genetic approach was employed to study polyploidy. HUVECs were infected with adenoviruses encoding either a dominant negative form of AMPK (Ad.AMPKα1-DN), constitutively active AMPK (Ad.AMPK-CA) or GFP (Ad.GFP) and binucleation assessed. Infected cells were identified by confocal microscopy by either GFP fluorescence or myc immunoreactivity (Ad.AMPK-CA co-expressed GFP from a distinct promoter and Ad.AMPKα1-DN is myc-tagged). Expression of constitutively active AMPK caused a 20% reduction in the proportion of binucleated cells relative to Ad.GFP infected cells (Figure 3-17). Expression of dominant negative AMPK appeared to reduce binucleation although this did not achieve statistical significance (p=0.11) (Figure 3-17).

AMPKα expression was downregulated using targeted siRNA and DNA content assessed by flow cytometry. AMPKα1 and AMPKα2 expression was downregulated by 46.4 ± 12% and 65.3 ± 24.5% respectively, from two independent experiments (Figure 3-18). Transfection of cells with siRNA caused the appearance of so-called "microcells" which contained 2n DNA but had a smaller size (Figure 3-18). AMPKα1 downregulation caused the greatest increase in microcells. Incubation of HUVECs with AMPKα1 siRNA caused a reduction in the proportion of cells with 4n DNA relative to scrambled (Sc) siRNA treated cells (Figure 3-18). Downregulation of AMPKα2 did not alter the DNA content of HUVECs (Figure 3-18).
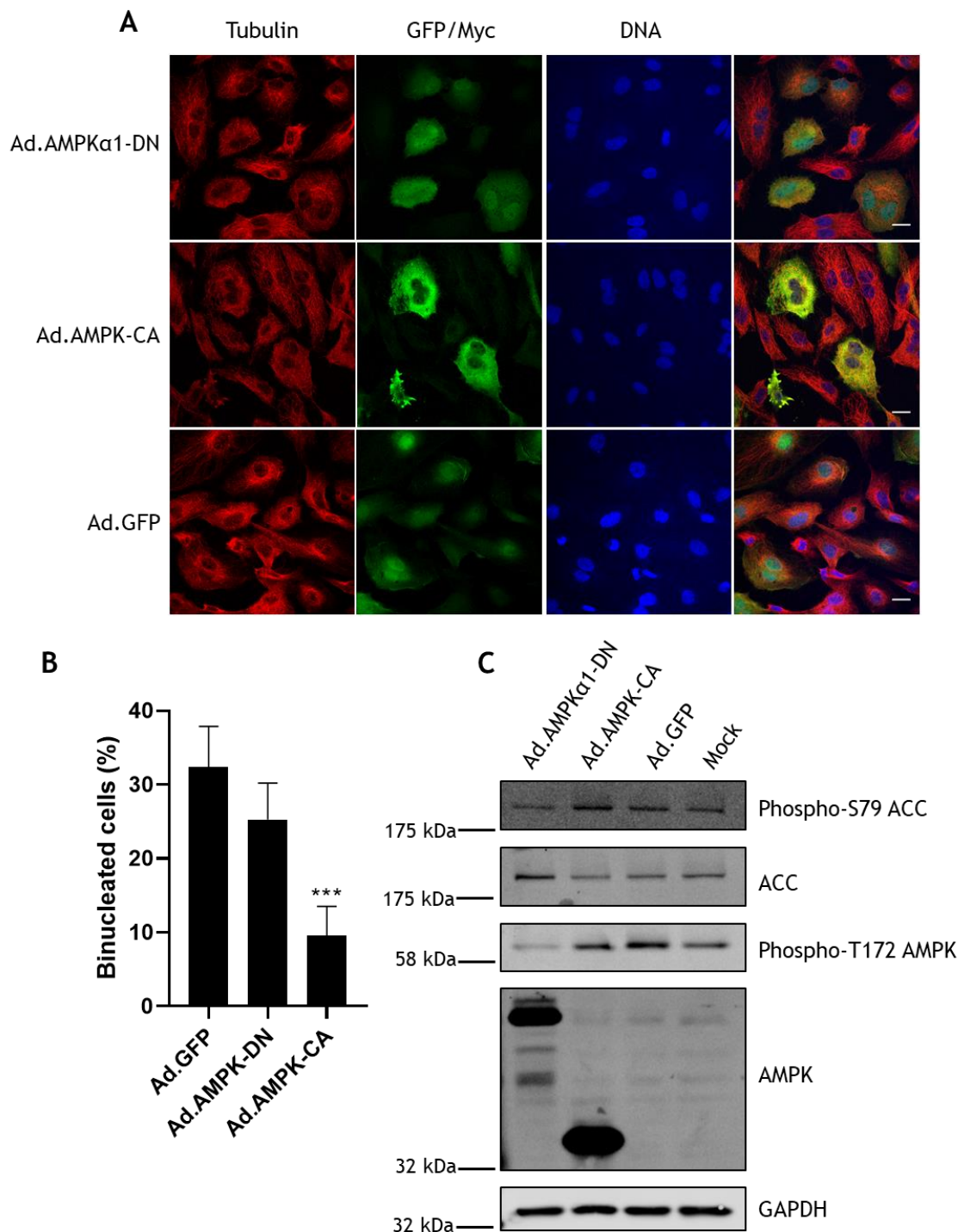
Figure 3-17. The effect of adenovirus infection on binucleation in HUVECs
HUVECs were infected with 30 PFU/cell adenoviruses expressing either constitutively active AMPK (Ad.AMPK-CA), dominant negative mutant AMPK (Ad.AMPK-DN) or GFP (Ad.GFP) for 24 h. **(A)** Representative images of infected HUVECs stained with anti-tubulin antibodies (Abcam, ab6160 for Ad.AMPK-DN and Ad.GFP infected cells, New England Biolabs, #2125 for Ad.AMPK-CA infected cells). DNA was stained with RedDot2. Ad.AMPKα1-DN infected cells were stained with anti-myc antibodies (Santa Cruz sc-40). GFP fluorescence is shown for Ad.GFP and Ad.AMPK-CA (which co-expresses GFP). **(B)** The proportion of binucleated cells was assessed in adenovirus infected cells. Data shown are the mean ± SEM % binucleated cells, *** $p<0.005$ relative to Ad.GFP-infected cells (one-way ANOVA), N=4. **(C)** Lysates were prepared from infected HUVECs and analysed by immunoblotting using the antibodies indicated. N=1.
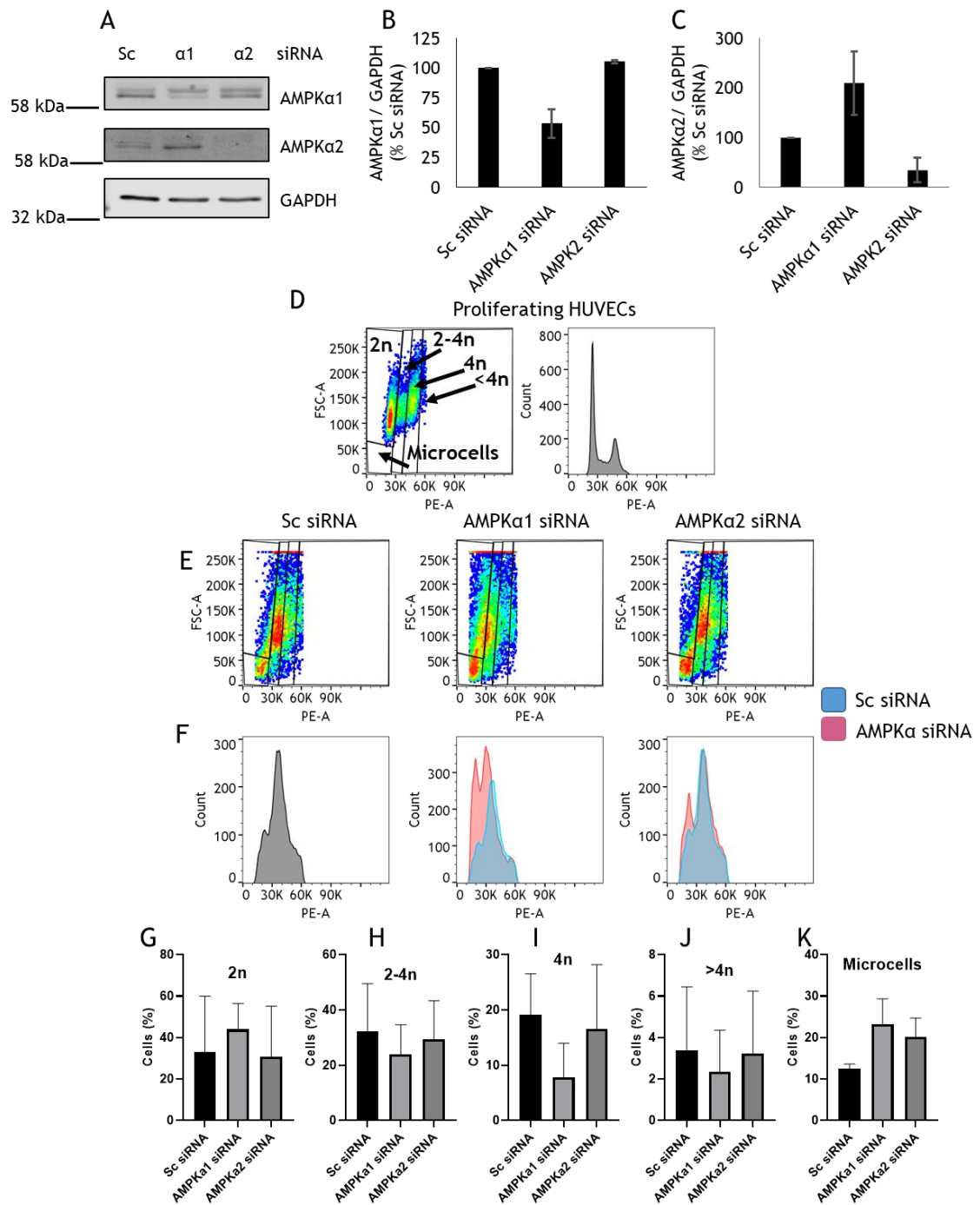
Figure 3-18. The effect of AMPKα knockdown on the DNA content of HUVECs
HUVEC cells were incubated with scrambled (Sc) siRNA or siRNA targeting AMPKα1 or AMPKα2 for 48 h. **(A)** HUVECs were lysed and resolved by SDS-PAGE followed by immunoblotting using the antibodies indicated. Representative Immunoblots are shown**. (B)** Quantification of AMPKα1 knockdown relative to GAPDH as mean ± SEM, N=2. **(C)** Quantification of AMPKα2 knockdown relative to GAPDH as mean ± SEM, N=2. **(D)** Representative flow cytometry scatter plot and histogram of proliferating HUVECs. Scatter plot showing FSC-A (forward scatter by area), PE-A (Phycoerythrin by area, used as a pseudo measurement for PI staining). Gating used is indicated. **(E)** HUVECs incubated with siRNA were stained with PI and DNA content assessed by flow cytometry. Representative scatter plots are shown. **(F)** Representative histograms of siRNA treated HUVECs with Sc siRNA (blue) overlaid on AMPKα1/2 downregulation (pink) **(G-K)** Analysis of the mean ± SEM % cells. Data from two independent experiments are shown.

3.2.2.3 AMPK activity is important for the timing of mitosis

To examine how AMPK function may regulate the timing of the cell cycle, HUVECs were synchronised using a double thymidine block to arrest in S phase. When cells were released from the block they were incubated with compound C (10 µM) and either lysed for immunoblotting or fixed with 4% (w/v) PFA for assessment by confocal microscopy. Cyclin B1 (a key mitotic regulator) (Pines and Hunter, 1989), expression peaked between 6-8 h post release (Figure 3-19. Compound C caused a delay in cyclin B1 expression until 13 h post-release (Figure 3-19). Examination of cells by confocal microscopy, revealed that cells which were incubated with DMSO were undergoing telophase 8 h post block, whereas compound C delayed mitotic entry, with cells undergoing metaphase after 12 h (Figure 3-19).

A

| | 0 | 2 | 4 | 6 | 8 | 10 | 13 | Hours after release |

Compound C: - + - + - + - + - + - + - +

58 kDa — Cyclin B1

58 kDa — Phospho-T172 AMPK

32 kDa — GAPDH

B

Cyclin B1 / GAPDH (as %control)

Hours after release

■ DMSO □ Compound c

C

DMSO   Compound C

Hours after release from block

8 hours

12 hours
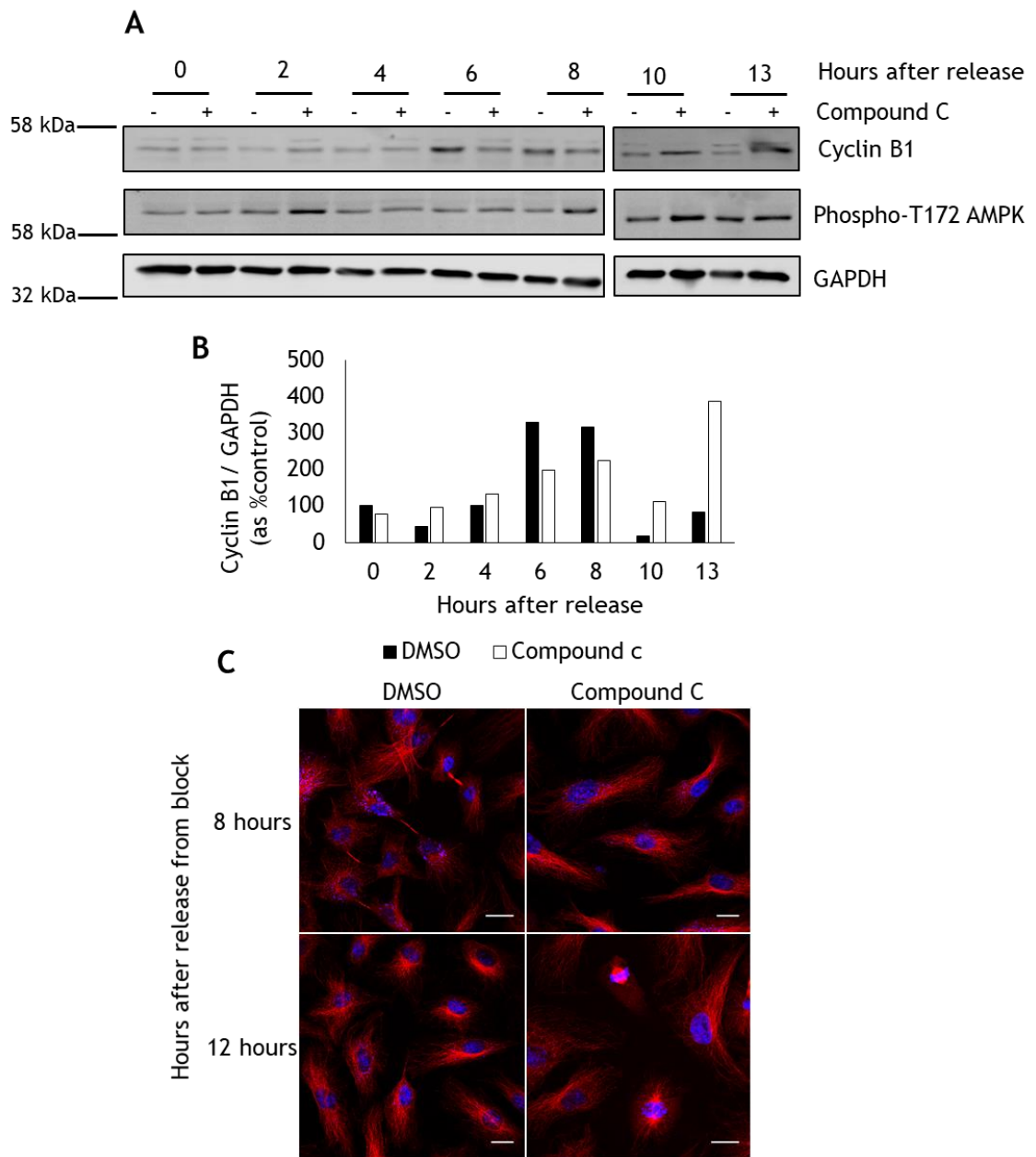
Figure 3-19. The effect of compound C on the timing of mitosis
HUVECs were synchronised using a double thymidine block. Cells were released from S-phase block and treated with DMSO or 10 µM compound C. Cells were incubated as required and either lysed for immunoblotting or fixed with PFA and examined by confocal microscopy. **(A)** Lysates were resolved by SDS-PAGE and immunoblotted with the antibodies detailed. **(B)** Analysis of cyclin B1 expression relative to GAPDH expression. **(C)** Cells were stained with anti-tubulin antibodies (Abcam, ab6160) and for DNA (RedDot2). Representative images of cells 8 or 12 h following block. N=1. Scale bar represents 20 µm.

3.3 Discussion

3.3.1 Principal findings

- A novel subcellular localisation for AMPKα1 was described; the subunit isoform was detected at the MTOC of HeLa cells and HUVECs

- AMPKα2 was confirmed to localise to the midbody in both primary cells (HUVECs) and shown to occur in HeLa cells for the first time

- Compound C causes increased rates of binucleation in HeLa cells but not in HUVECs

- Viral delivery of a constitutively active AMPK mutant reduced binucleation rates of HUVECs

3.3.2 Localisation of AMPK mitosis

A previously published study reported that during cytokinesis AMPKα2 localised to the midbody, cytoplasm, membrane and nucleus of HUVECs, whereas AMPKα1 localised to the cytoskeletal fraction (Pinter et al., 2012). The midbody localisation of AMPKα2 was confirmed in this Chapter, and a novel localisation for AMPKα1 (but not AMPKα2) was described at the MTOC. Despite AMPKα1 immunoreactivity being observed at the MTOC there was no obvious co-localisation with other microtubules instead appearing diffuse in the cytoplasm. Anti-AMPKα2 immunoreactivity at the midbody (but not the MTOC or the spindle midzone) was also observed in HeLa cells. Furthermore, AMPKα2 immunoreactivity was observed in the cytoplasm and the nuclei of telophase cells. The nuclear localisation of AMPKα2 is consistent with previous reports in HUVECs and the rat INS-1 cell line (Salt *et al.*, 1998; Pinter *et al.*, 2012).

To circumvent potential non-specific binding of anti-AMPKα antibodies, HeLa cells were transfected with plasmids encoding GFP-AMPKα fusion proteins, which would also enable live cell imaging to examine the spatio-temporal dynamics of AMPK in the cell cycle. Unfortunately, following plasmid DNA transfection the majority of cells became senescent with few GFP positive cells undergoing mitosis. These issues were further complicated when GFP itself was found to

localise to the midbody, whereas other studies have not reported GFP localisation to the midbody in HeLa cells (Neto *et al.*, 2013). In future the transfection protocol should be optimised and alternatives techniques such as electroporation examined.

Phospho-T172 AMPK has previously been described at the midbody in human epidermoid carcinoma A431 cells and at the MTOC in a number of cell lines including A431 cells, HeLa cells, human lung carcinoma H1299 cell line and marsupial PtK1 cells (Vazquez-Martin *et al.*, 2009; Thaiparambil *et al.*, 2012). In agreement, this study found phospho-T172 AMPK localisation at the MTOC and midbody of HeLa cells and in primary human cells (HUVECs) with two different antibodies. The selectivity of one of the anti-phospho-T172 AMPK (sc-101630) antibodies was investigated utilising wild type and AMPK -/- MEFs. Cytosolic and midbody immunoreactivity was observed at comparable level in both wild type and AMPK -/- MEFs (Figure 3-7). This suggests that the anti-phospho-T172 AMPK antibodies lack specificity. This therefore casts doubt on the authenticity of phospho-T172 AMPK localisation to the midbody. Phospho-T172 AMPK MTOC localisation couldn't be assessed in MEFs as cells in early phases of mitosis weakly adhered to the Ibidi chambers and were inadvertently washed off during staining. The immunoreactivity in AMPK -/- MEFs is therefore likely non-specific, although it may be possible that the anti-phospho-T172 AMPK antibodies could recognise the orthologous phosphorylated site on an AMPK-related kinase family member (Lizcano *et al.*, 2004).

The subcellular localisation of the AMPK substrate, phospho-S79 ACC has been reported to follow the same subcellular localisation as phospho-T172 AMPK (Vazquez-Martin *et al.*,2013; Vazquez-Martin *et al.*,2009). In the current study, anti-phospho-S79 ACC immunoreactivity was observed in the cytoplasm of HUVECs but no staining was observed at either the MTOC or midbody (Figure 3-8). Consistent with the observation of ACC in the cytoplasm, ACC1 (the predominant isoform in HUVECs) has been reported to be predominantly cytosolic whereas ACC2 is associates with mitochondria in primary neonatal rat cardiomyocytes, mouse skeletal muscle cells and cancer cell lines (HepG2 and T47D cells) (Abu-Elheiga *et al.*, 2000; Glatzel *et al.*, 2018).

The differences in phospho-S79 ACC localisation between A431 cells and HUVECs may in part be due to the cells having different AMPK regulation/activity. A431 cells have over activation of AMPK whereas HUVECs have a low basal AMPK activity, which might affect this localisation (Mizrachy-Schwartz *et al.*, 2011). It is proposed that in A431 cells, AMPK is recruited to the MTOC/midbody where ACC is phosphorylated, in HUVECs however, AMPK localises to the MTOC and midbody but may not phosphorylate ACC. Potentially this could either be due to limited AMPK activity, AMPK having a higher affinity for alternative substrates during mitosis or that ACC may not be recruited/be excluded from these structures. At the midbody, diffusion from the cytoplasm is restricted (Schmidt and Nichols, 2004), thus if ACC was not actively transported to the midbody, phospho-S79 ACC would not be observed. When assessed by immunoblotting, A769662 induced an increase in phospho-S79 ACC, yet no increase in immunofluorescence intensity was observed by confocal microscopy, which may cast doubt on the specificity of the antibody.

3.3.3 AMPK activity and the cell cycle

3.3.3.1 Down regulation of AMPK activity

Assessing binucleation as a readout of failed cytokinesis is an established way to discern how pharmacological and genetic manipulations influence mitosis (Vazquez-Martin *et al.*, 2011; Högnäs *et al.*, 2012; Neto *et al.*, 2013). In line with the results presented in this study, HeLa cells have been shown to have a basal binucleation rate of approximately 3% (Neto *et al.*, 2013). Incubation of HeLa cells with compound C caused a modest but significant increase in the proportion of binucleated cells. Furthermore, compound C caused an increase in the proportion of cells with 4n DNA content when assessed by flow cytometry. A 4n DNA content could represents either cells in G_2/M-phase or binucleated cells. Since flow cytometry cannot differentiate between cells in G_2/M-phase or binucleated cells, it is important to interpret flow cytometry results in tandem with microscopic assessment of cells. Taken together it is clear that compound C increased binucleation in HeLa cells. Similarly, in U2OS cells, an osteosarcoma cell line, compound C caused a 3-fold increase in multinucleated cells (Banko *et al.*, 2011).

However, in HUVECs compound C did not alter the proportion of cells with 4n DNA content or binucleation. Instead, compound C caused an increase in the proportion of HUVECS with 2n DNA content and a decrease in the proportion of 2-4n and >4n cells. In HUVECs, compound C has a documented anti-proliferative role, however this may be AMPK-independent (Esfahanian $et\ al.$, 2012; Liu $et\ al.$, 2014). Therefore, the reduction in HUVECs with 2-4n DNA may represent cell cycle arrest prior to S-phase with cells accumulating with 2n DNA in G_1 or G_0 phase. In both HeLa cells and HUVECs, compound C significantly reduced cell viability and proliferation when measured by MTS or BrdU assay respectively. In a different primary endothelial cell line, human aortic endothelial cells (HAECs), 5 µM compound C did not alter the cell viability (Reihill $et\ al.$, 2011), whereas in this Chapter 5 µM compound C caused a significant reduction in HUVEC viability. The sensitivity to compound C may reflect the different vascular origins of HUVECs and HAECs in addition to the juvenile/adult sources respectively.

Unexpectedly, wild type and AMPK -/- MEFs responded differently to PI staining. Wild type MEFs incubated with DMSO showed two peaks of PI staining at approximately 90K (2n DNA content) and 150K (4n DNA content), whereas in AMPK -/- cells, peaks were apparent at 70K and 130K, indicating an overall reduction in PI staining. Potentially AMPK -/- MEF DNA may be less accessible to PI resulting in less PI intercalation and thus less fluorescence.

Compound C drastically altered both wild type and AMPK -/- MEF DNA content which made the gating of distinct populations difficult. Rather than having two distinct peaks of PI staining, compound C caused a broad spread of cell staining. Furthermore, comparison of wild type and AMPK -/- MEFs treated with 5 µM compound C indicated that the cells responded differently. Wild type MEFs had a peak at approximately 130K for PI staining, a lower value than would be expected for a 4n population as discussed above. When the gating of DMSO control cells was applied to wild type cells it was apparent that there were almost no cells in the 4n DNA population. This may indicate that compound C caused cell cycle arrest during S-phase. Consistently, wild type cells had an increase in the proportion of cells with 2-4n DNA content after compound C incubation although this did not achieve statistical significance (p=0.12). Therefore wild type MEFs may initiate S-phase but arrest during the DNA replication process. In contrast, AMPK -/- MEFs treated with 5 µM compound C

had a broad spread of cell populations including cells with 4n DNA content, implying that the S-phase block induced by compound C was AMPK-dependent. As the individual populations could not be differentiated by gating following compound C treatment this may have introduced artefacts.

A higher concentration of compound C (10 μM) reduced both wild type and AMPK -/- MEF viability and proliferation (Figure 3-17). Interestingly, 5 μM compound C did not reduce AMPK -/- cell viability but significantly reduce wild type MEF viability (Figure 3-17). This indicated that the reduction in cell viability (or mitochondrial activity) induced by 5 μM compound C was AMPK-dependent. Both genotypes were effected equally with higher concentrations of compound C. In contrast, 5 μM and 10 μM compound C reduced proliferation in both genotypes indicating it was an AMPK-independent effect (Figure 3-17). Compound C is at best a poorly-selective AMPK inhibitor, having been reported to inhibit a number of kinases *in vitro* to a greater extent than the inhibition of AMPK (Bain *et al.*, 2007).

During the course of this investigation, the ULK1 inhibitor, SBI-0206965 was described to be a potent inhibitor of AMPK (Dite *et al.*, 2018), in HUVECs concentrations greater than 10 μM SBI-0206965 inhibited AMPK. At higher concentrations (30 μM) it appeared that SBI-0206965 reduced the proportion of cells with 2-4n DNA and may also reduce the proportion of cells with 4n DNA content, however more replicates would be necessary before statistical analysis could be carried out. Similarly to compound C, SBI-0206965 also reduced HUVEC viability and proliferation. As SBI-0206965 was originally described as an inhibitor of ULK1 the apparent anti-proliferative effects of SBI-0206965 (and potentially compound C) could be mediated through the inhibition of autophagy as AMPK and ULK1 are both central regulators of the autophagy pathway (Egan *et al.*, 2015).

During autophagy cellular component such as proteins and organelles are digested to generate nutrients and energy to maintain cellular homeostasis. When nutrients are available, AMPK is inhibited whereas mTOR is active promoting proliferation while also inhibiting autophagy through the phosphorylation of ULK1 (Chan, 2009; Egan *et al.*, 2011). However, when the energy state of the cell is low, AMPK is activated which phosphorylates and

activates ULK1 thereby promoting autophagy (Egan *et al.*, 2011). Furthermore, AMPK inhibits mTOR to relieve the inhibitory phosphorylation of ULK1 (Inoki *et al.*, 2003; Egan *et al.*, 2011). Interestingly, autophagy has recently been implicated to play a role in mitosis and cell cycle progression. During mitosis autophagy is inhibited in part through the phosphorylation of Vps34 by CDK1 (Eskelinen *et al.*, 2002; Furuya *et al.*, 2010). Mitotic inhibition of autophagy is thought to protect DNA from degradation following nuclear envelope breakdown and Golgi dispersion. Autophagy then recommences at the end of telophase and in G_1 when DNA is no longer vulnerable in the cytoplasm (Eskelinen *et al.*, 2002). Vps34, a phosphatidylinositol-3-phosphate (PtdIns3P) kinase class III (PI(3)K-III) and has a role in both autophagy and cytokinesis. Vps34 produces the phospholipid PtdIns3P at the midbody (at a time coinciding with increased autophagy), which recruits the centrosomal proteins FYVE-CENT and TTC19 which in turn recruit the ESCRT-III component CHMP4 to mediate abscission (Sagona *et al.*, 2010, 2011; You *et al.*, 2016). Downregulation of the PI(3)K-III machinery cause cells to arrest during cytokinesis resulting in binucleation (Sagona *et al.*, 2010). Thus, the inhibition of AMPK/ULK1 by compound C/SBI-0206965 may arrest the cell cycle or cause defective cytokines by altering autophagy.

As compound C is poorly-selective and SBI-0206965 inhibits both ULK1 and AMPK a genetic means of downregulating AMPK activity was employed (Egan *et al.*, 2015; Dite *et al.*, 2018). To this end, HUVECs were infected with adenoviruses which expressed a dominant negative form of AMPKα1 (Ad.AMPKα1-DN) (Woods *et al.*, 2000). The dominant negative AMPKα1 (α1DN) contained a D157A mutation rendering it catalytically inactive. α1DN is said to function in a dominant negative manner by competing with endogenous α subunits to bind with the regulatory β and γ subunits (Woods *et al.*, 2000). However, due to the presence of endogenous AMPKα subunits, expression of α1DN does not completely abolish AMPK activity (Woods *et al.*, 2000). Expression of α1DN in proliferating HUVECs caused a reduction in the proportion of binucleated cells compared to Ad.GFP infected cells but did not reach statistical significance (p=0.11). Cells infected with Ad.GFP appeared to have increased instances of binucleation, where approximate 30% of infected HUVECs were binucleated in contrast to ~10% binucleated HUVECs when incubated with DMSO. Ideally an

Ad.Null control would have been carried out to discern if the increase in binucleation was due to viral infection or the overexpression of viral proteins/GFP. Previously HeLa cells infected with Ad.Null viruses have not been reported to have increased instance of binucleation so it is unlikely that adenovirus infection is always associated with binucleation (Neto *et al.*, 2013). As HUVECs are a primary cell line, they may be more sensitive viral infection and the hijacking of the transcription/translation machinery which may in turn cause mitotic failure.

Although infection of cells with Ad.AMPK-DN downregulated AMPK activity, there was overexpression of α1DN which may influence signalling pathways mediated through protein-protein interactions. Therefore, AMPKα subunits were downregulated by incubation of HUVECs with targeted siRNA. AMPKα1 protein expression was reduced by 46.4 ± 12% and AMPKα2 by 65.3 ± 24.5% relative to cells incubated with Sc siRNA. Unexpectedly, downregulation of AMPKα1 caused an increase in AMPKα2 expression by 110% ± 64% (Figure 3-19). This is a novel observation and may reflect an adaptive mechanism of HUVECs to compensate for the loss of AMPKα1, the predominant α-subunit in these cells.

Assessment of siRNA treated cells by flow cytometry indicated that there was a sub-population of cells which had a small size and fit into the 2n DNA population gate, termed "microcells". As microcells were produced following incubation with Sc siRNA but not pharmacological tools, it is likely that they formed as a consequence of the transfection protocol. When cells were assessed by immunofluorescence, no unusual cell morphology was apparent (data not shown). To determine if the cells were apoptotic, co-staining for annexin could be carried out.

Downregulation of AMPKα1 caused a decrease in the proportion of cells with 4n DNA whereas knockdown of AMPKα2 did not alter the DNA content of HUVECs. However, accurate gating of cell populations was difficult due to the unusual spread of cell populations, therefore the quantification may be skewed by the gating applied. Examination of the histogram overlay of Sc siRNA versus AMPKα1 siRNA-treated cells showed that the number of cells at approximately 50K PE-A appeared identical in both cases. This region correlated to 4n DNA so it is likely that AMPKα1 knockdown does not influence HUVEC DNA content. This is

consistent with a previous report in U2OS cells where expression of shRNA to both AMPKα1 and AMPKα2 did not increase in the proportion of multinucleated cells (Banko *et al.*, 2011).

To investigate how AMPK inhibition by compound C may influence mitosis, HUVECs were synchronised to S-phase using a double thymidine block. When cells were released from the block they were incubated with either compound C or DMSO vehicle control. Cells which were incubated with DMSO entered telophase 8 h post release whereas compound C appeared to delay mitotic entry/progress, cells were observed to undergo metaphase 12 h after the block. Ideally this preliminary work would be replicated a number of times and evaluation of DNA content by flow cytometry following synchronisation and incubation with compound C treatment.

As both the AMPKα subunits are genetically deleted in the AMPK -/- MEFs, they are a model where there was complete downregulation of AMPK. As such AMPK must not be essential for the cell cycle otherwise the cell line would not be viable. Assessment of the MEFs by flow cytometry revealed no difference in the proportion of cells with 2n, 2-4n, 4n or <4n DNA content between the two genotypes. In AMPK -/- MEFs the mitotic role of AMPK could instead be carried out by an AMPK-related kinase (ARK) enabling the cells to divide normally. Alternatively AMPK may play a more subtle role in MEF mitosis which does not severely influence the cell cycle when AMPK is absent.

3.3.3.2 Up regulation of AMPK activity

As HeLa cells and HUVECs have low basal AMPK activity, down regulation of AMPK may have limited effects. Therefore, upregulation of AMPK activity may be more informative to determine how AMPK can regulate the cell cycle. Incubation of HeLa cells with A769662 did not alter binucleation, DNA content or cell viability but reduced proliferation. As A769662 reduced proliferation, it was surprising there was not an associated reduction of cells with 2-4n DNA. Conversely, synchronised U2OS cells have been reported to exhibit a significant increase in multinucleated cells following incubation with A769662 (Banko *et al.*, 2011). This may be due to the cells being synchronised at metaphase prior to acute incubation with A769662. It is possible that during metaphase over

activation of AMPK may cause mitotic failure, whereas chronic incubation (18-24 h) of unsynchronised cells may not produce the same effect.

In HUVECs A769662 did not alter the DNA content of cells or proliferation although a reduction in viability was apparent. Additionally in MEFs, A769662 did not alter the DNA content in cells of either genotype. A769662 reduced both wild type and AMPK -/- MEF proliferation to a comparable extent, indicating that the reduction in MEF proliferation was AMPK-independent. A769662 also likely has cell-type specific effects, reducing proliferation in HeLa cells and MEFs without altering HUVEC proliferation. Conversely A769662 did not lower the viability of HeLa cells or MEFs but reduced HUVEC viability/mitochondrial activity. These cells likely have different metabolisms; HeLa cells (like most cancer cells) exhibit Warburg metabolism where cells generate the majority of their ATP by glycolysis (Warburg, 1925; Amemiya *et al.*, 2017). Thus, HeLa cells are less dependent on mitochondrial respiration so the results obtained from MTS assays may not be the same observed in primary cells.

When assessed by flow cytometry, A769662 caused a substantive right-shift (towards higher PI staining) in AMPK -/- MEFs, whereas wild type MEFs and HUVECs were unaffected. This right shift aligned the histogram of AMPK -/- cells with that of wild type cells. When cells were manually gated, the percentage of cells in each population was comparable with both AMPK -/- cells incubated with DMSO and wild type MEFs incubated with A769662. This could indicate that functionally A769662 did not affect the cell cycle but altered how cells respond to PI staining rather than causing a partial increase in the DNA complement.

MetSal drastically altered AMPK -/- MEF DNA content, whereby there was a large left shift compared to DMSO control MEFs. This shift was not observed in wild type MEFs. A left shift/a population of cells with <2n DNA could potentially represent cells undergoing apoptosis/necrosis or "microcell" formation. Metformin is a mild mitochondrial toxin causing an increase in intracellular AMP (Zhou *et al.*, 2001). It is possible that AMPK -/- MEF were unable to withstand the metabolic stress induced by metformin and became apoptotic. However, canagliflozin activates AMPK in a similar manner as metformin, and left shift was not observed (Zhou *et al.*, 2001; Hawley *et al.*, 2016). Furthermore, neither canagliflozin nor MetSal affected cell viability/mitochondrial activity of MEFs

when assessed by MTS assay. Apoptosis was not apparent when HUVECs when assessed by microscopy, so this may be a facet of AMPK -/- MEFs.

Consistent with observations made in HUVECs, canagliflozin has previously been reported to reduce cell viability but not proliferation (Mancini *et al.*, 2018). AICAR (2 mM) and A79662(10 µM) has also been reported to reduce HAEC viability (Reihill *et al.*, 2011). The present study showed that both compounds reduced HUVEC proliferation albeit at different concentrations (1 mM AICAR and 50 µM A769662). AICAR has also been shown to inhibit HUVEC proliferation between 50-500 µM (Peyton *et al.*, 2012). Additionally, A769662 (300 µM) and metformin (2 mM) were reported to reduce HUVEC proliferation and DNA synthesis arresting cells in G_0/G_1 by increasing expression of the CDKIs p21 and p27, and increasing p53 protein levels and its phosphorylation while decreasing cyclin A and Rb phosphorylation (Peyton *et al.*, 2012). In the present study, neither AICAR (1 mM) nor A769662 (50 µM) reduced HUVEC proliferation, however, different concentrations of each drug was used in the present study. It is unlikely that the differences in concentration would make a substantial difference as the higher AICAR concentration used in the current study would still be expected to activate AMPK and the lower concentration of A76962 (50 µM) used in this study was sufficient to increase AMPK activity.

HUVECs were infected with adenoviruses containing a gene for a constitutively active form of AMPK (Ad.AMPK-CA), which is composed of the first 312 amino acids of AMPKα1 with a T172D mutation and an N-terminal myc tag (Woods *et al.*, 2000). Expression of constitutively active AMPK caused a significant reduction in the proportion of binucleated cells compared to Ad.GFP infected cells. Ad.AMPK-CA infection reduced binucleation to approximately 10%, in line with basal HUVEC binucleation rates. Thus constitutively active AMPK was able to prevent adenovirus induced binucleation demonstrating a role of AMPK to control the fidelity of cytokinesis.

3.3.4 Summary

While there is evidence supporting AMPKα subunit localization during mitosis, there are caveats that require resolution. MTOC/midbody localisation has been observed using anti-AMPKα1, anti-AMPKα2 and two different anti-phospho-T172

AMPK in HeLa cells and HUVECs. However midbody immunoreactivity of phospho-T172 AMPK was observed in AMPK -/- MEFs suggesting that the anti-phospho-T172 AMPK antibody lacks specificity. Collectively, the experiments outlined in this Chapter suggest that AMPK activity is important for the timing of the cell cycle and mitosis. Alterations in AMPK activity affected cell cycle progression and the fidelity of cytokinesis. Interestingly, the subcellular localisation of AMPK shows a considerable overlap with a number of mitotic proteins including PLK1 (Vazquez-Martin *et al.*, 2011). Additionally, the PLK1 inhibitor GW843682X, abolishes AMPK recruitment to the MTOC and midbody and causes binucleation in A431 cells (Vazquez-Martin *et al.*, 2011).The signalling pathways AMPK may regulate during mitosis remain unclear and in the following Chapters the interaction between AMPK and well-established mitotic regulators will be investigated.

4 Chapter 4-Using fission yeast to investigate the role of AMPK in mitosis

4.1 Introduction

S. pombe is a popular model organism in the study the cell cycle due to the high degree of conservation between S. *pombe* and humans as well as the relative ease of study of this organism in the lab. Importantly, the genome of *S. pombe* has been sequenced making it a useful model for genetic screens such as the one outlined in this Chapter (Wood *et al.,* 2002). A number of proteins are known to have crucial roles in regulating mitosis and cytokinesis in all eukaryotic organisms, these include the aurora kinase family (Ark1p in *S pombe*), anillin (Mid1p), polo-like kinase (Plo1p), and the ESCRT proteins (Bähler *et al.,* 1998; Wu *et al.,* 2003; Musab S Bhutta *et al.,* 2014). Human and *S. pombe* orthologues are summarised in Table 4-1, an outline of ESCRT orthologues can be found in Table-4-3.

Human protein	*S. pombe* protein
AMPKα	Ssp2p
AMPKβ	Amk2p
AMPKγ	Cbs2p
Aurora kinase	Ark1p
Anillin	Mid1p
Polo-like kinase	Plo1p

Table 4-1. Comparison of mammalian and *S. pombe* orthologues.

Accumulating evidence has indicated a role for AMPK during the cell cycle, such as the alterations in polyploidy in response to AMPK activity modulation and the localisation of AMPK in mitosis (detailed in Chapter 3). However, the mechanism by which AMPK signalling regulates mitosis is unknown. To address this, a yeast genetic approach was used to identify novel interactions between AMPK and a

number of key regulators of mitosis and cytokinesis. Fission yeast with chromosomal deletions of either the AMPK subunits; *ssp2* (α subunit orthologue), *amk2* (ß subunit), *cbs2* (γ subunit) or *ssp1* (CaMKK orthologue), were individually crossed with yeast strains containing mutations in genes encoding proteins known to have significant roles in the cell cycle, namely *ark1, plo1, mid1* and various ESCRT genes. Double mutant strains were isolated by tetrad analysis or random spore analysis and examined for the presence of so-called "synthetic phenotypes". Such synthetic phenotypes are apparent in double mutant strains, but absent in single mutant strains. The appearance of a synthetic phenotype provides evidence of a genetic interaction between the two genes, suggesting a functional interaction between the encoded proteins. Thus this genetic approach was used to identify novel interactions between AMPK and other proteins required for cytokinesis.

Results

4.1.1 AMPK has a role in cytokinesis in *S. pombe*

To examine how AMPK may influence *S. pombe* cytokinesis, septation was assessed using Calcofluor-White staining in *ssp1Δ*, ssp2Δ, a*mk2Δ* and *cbs2Δ* strains (Rezig *et al.*, 2019). The relative frequency of previously described "septation phenotypes" were classified as follows (Class A-F as described in Bhutta *et al.*, 2014, Class G noted in this study):

- Class A-centrally positioned septa

- Class B-non-central septa

- Class C-misaligned septa

- Class D-multiple septa

- Class E-absent septa

- Class F-delayed separation after septation

- Class G-ectopic deposition of septa material

Wild type cells predominantly displayed the Class A phenotype (~80% of cells), the next most frequent phenotype was Class F (~20% cells) with very few cells having any other septation phenotypes (Figure 4-1). Wild type cells had a Class A:F ratio of 4.61 (Figure 4-1). In contrast, chromosomal deletion of *ssp2*, *cbs2*, or *ssp1* caused a significant increase in the proportion of cells with the Class F phenotype coinciding with a reduction in the proportion with the Class A phenotype (Figure 4-1). Although alterations in the septation phenotype of a*mk2Δ* cells did not achieve statistical significance, there was a trend to increased Class F phenotype (p=0.16) and reduced Class A phenotype respectively (p=0.17), as well as a shift in the ratio of Class A:F phenotype (Figure 4-1). Overall, these observations demonstrate that AMPK is involved in efficient septation and thus cytokinesis in *S. pombe*.
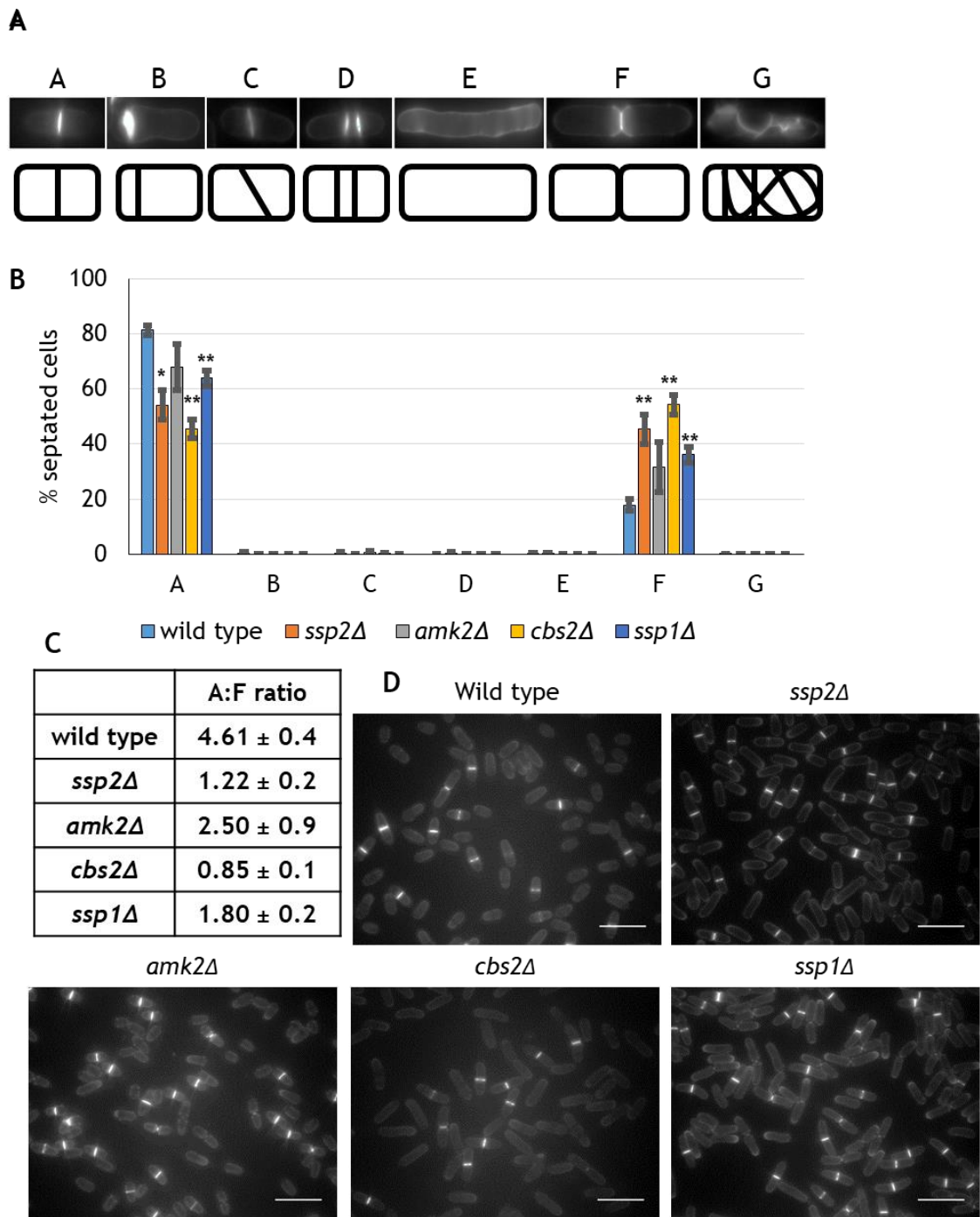
Figure 4-1. Chromosomal deletions of genes encoding AMPK subunits or *ssp1* alter septation in *S. pombe*.
(A) Representation of the different septation phenotypes, showing either Calcofluor-White staining (upper) or illustration (lower). **(B)** Wild type (GG1278), *ssp2Δ* (GG3033), *amk2Δ* (GG2981), *cbs2Δ* (GG2981) and *ssp1Δ* (GG3080) strains were cultured in liquid YE media at 30°C for 18 h. Division septa were visualised using Calcofluor-White staining followed by fluorescence microscopy where the frequency of each phenotype was recorded. At least 300 cells were counted over three technical replicates which was performed on three independent occasions for each genotype. **(C)** Quantification of Class A:F phenotypes ± SEM. **(D)** Representative images of Calcofluor-White stained cells. Scale bar represents 20 μm. * $p < 0.05$, ** $p < 0.01$ relative to wild type (Students *t* test).

4.1.2 Generation of double mutant strains

To identify novel interaction between AMPK and proteins involved in mitosis, a synthetic phenotype screen was undertaken. Yeast strains with individual chromosomal deletions of either *ssp2*, *amk2*, *cbs2* or *ssp1* were crossed with strains containing mutations in genes with established roles in cytokinesis. Such strains included: temperature sensitive mutation in the aurora kinase *ark1* (*ark1-T8* (Koch *et al.*, 2011)); a temperature sensitive mutations in polo-like kinase *plk1* (either the *plo1-ts18* or *plo1-ts35* allele (Anderson *et al.*, 2002)); chromosomal deletion of the anillin *mid1* (*mid1Δ* (Sohrmann *et al.*, 1996)); or chromosomal deletion of selected ESCRT proteins (*sst4Δ, sst6Δ, vps28Δ, vps36Δ, vps35Δ, vps20Δ, vps32Δ, vps2Δ* or *vps4Δ* (Iwaki *et al.*, 2007)). Double mutant strains were either generated by tetrad analysis or random spore analysis (detailed in Section 2.25).

During tetrad analysis, two yeast strains of opposite mating type were mixed and incubated on solid ME media to induce mating and tetrad formation (Rezig *et al.*, 2019). Mating mixture was transferred to solid YE media and tetrads isolated using a micro-manipulator. Ascus wall breakdown was induced by incubation at 37°C and individual spores were separated. Cells were incubated until colonies formed and genotype interrogated by replica-plating onto selection media. Representative tetrad crosses are shown in Figure 4-2. Once double mutants were identified, they were allocated a "Glasgow" (GG) number and stored in the laboratory collection at -80°C. Table 4-2 outlines the double mutant strains generated through the course of this investigation. A full list of strain list can be found in Appendix 1.

As the chromosomal deletion of *ssp2*, *amk2*, *cbs2 and ssp1* have been reported to reduce *S. pombe* mating efficiency (Valbuena and Moreno, 2012), random spore analysis was utilised as a way to generate double mutant cells more efficiently. In random spore analysis, the mating mixture is incubated with β-glucuronidase to digest vegetative cells and the ascus membrane without affecting ascospores. Ascospores were incubated until colonies formed, isolated and the genotype analysed by replica plating to identify double mutant cells (Figure 4-3). However, if both parental strains were tagged with the same auxotrophic marker/antibiotic resistance cassette, tetrad analysis was necessary.
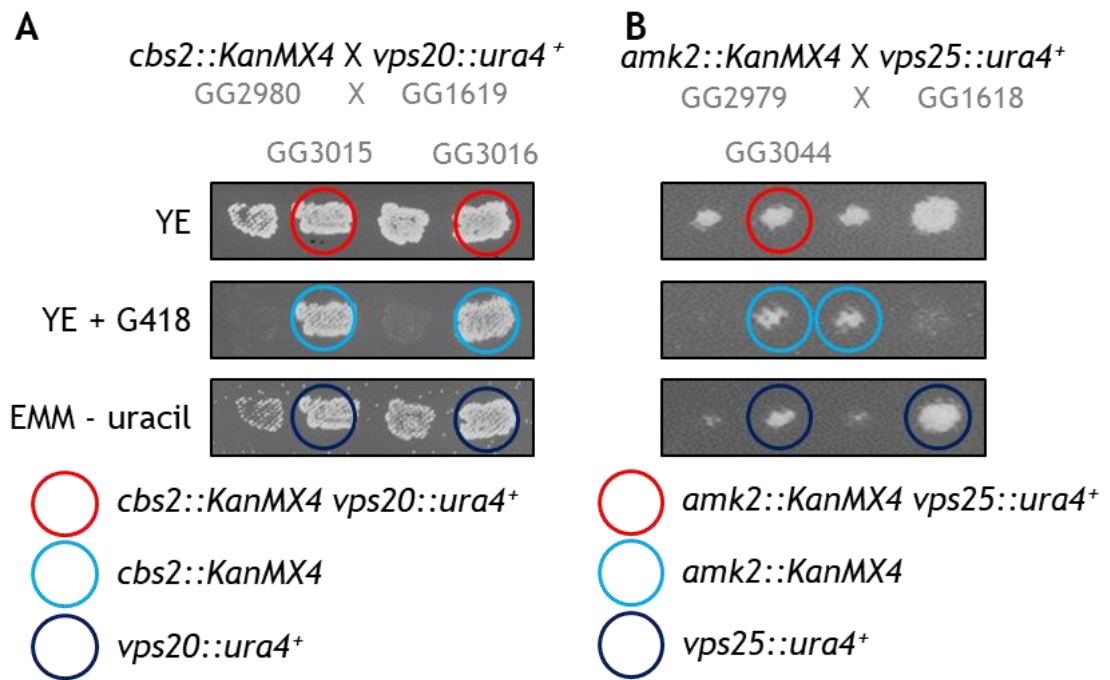
Figure 4-2. Representative examples of *S. pombe* double mutant isolation by tetrad analysis
(A) Cells containing a chromosomal deletion of *cbs2Δ* tagged with a kanamycin resistance cassette
(*cbs2::KanMX4,* GG2980) were crossed with cells containing a deletion of the ESCRT gene
vps20Δ tagged with an auxotrophic uracil marker (*vps20::ura4+,* GG1619*)*. Resulting tetrads were
isolated and incubated until colonies formed. Plates were replica-plated onto selective media; solid
YE media containing the antibiotic G418 or minimal media (EMM) lacking uracil. Double mutant
cells could then be identified and were allocated the "Glasgow" reference numbers (GG3015 or
GG3016). **(B)** Tetrad analysis of a cross between strains *amk2::KanMX4 (*GG2981) and
*vps25::ura4+ (*GG1618). A double mutant strain is indicated with a red circle and allocated the
reference GG3044.
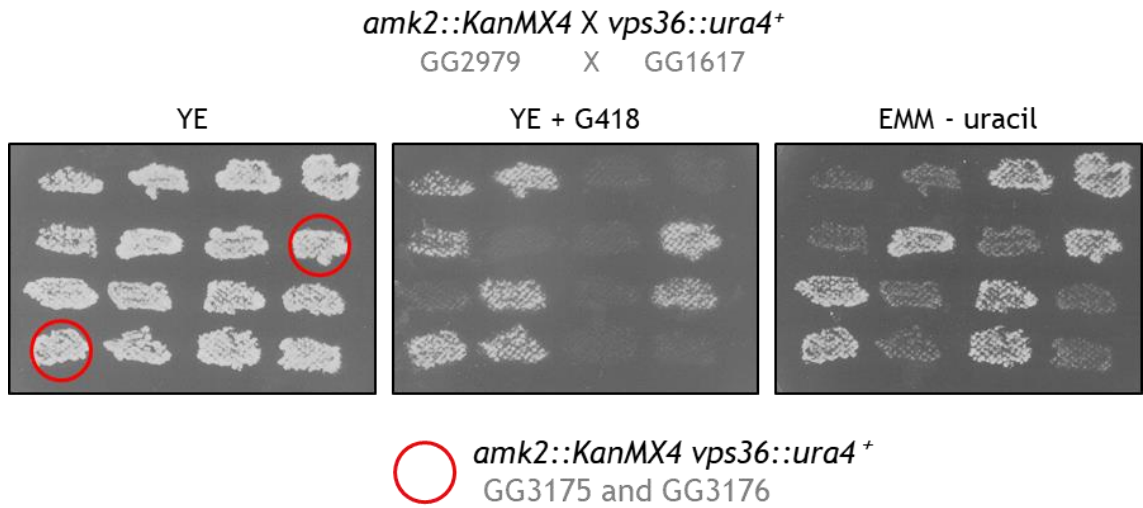
Figure 4-3. Representative example *S. pombe* double mutant isolation by random spore analysis

A strain containing a chromosomal deletion of *amk2* tagged with a kanamycin resistance cassette *(amk2::KanMX4*, GG2979) was crossed with a strain containing a chromosomal deletion of the ESCRT protein *vps36* tagged with an auxotrophic uracil marker *(vps36::ura4+,* GG1617*)*. The mating mixture was incubated with β-glucuronidase to digest ascus membranes and vegetative cells. The resulting mixture was incubated on solid YE media until colonies formed. Colonies were transferred to solid YE media followed by replica-plating onto selective media in order to identify double mutant strains, indicated with red circles.

Genotype	ssp2Δ	amk2Δ	cbs2Δ	ssp1Δ
sst4Δ		GG2995	GG3012	GG3128
		GG2996	GG3013	GG3129
		GG2997	GG3014	GG3130
sst6Δ		GG3006	GG3108	GG3090
		GG3007	GG3109	GG3121
		GG3075	GG3110	GG3122
vps28Δ		GG3008	GG3084	GG3087
		GG3055	GG3085	GG3088
		GG3076	GG3086	GG3089
vps36Δ		GG3175	GG3029	GG3137
		GG3176	GG3030	GG3138
		GG3177	GG3031	GG3139
vps25Δ	GG3064	GG3044	GG3068	
	GG3065	GG3045	GG3069	
		GG3046	GG3083	
vps20Δ		GG2998	GG3015	GG3116
		GG2999	GG3016	GG3123
		GG3000	GG3017	GG3124
vps32Δ		GG3009		GG3131
		GG3010		GG3132
		GG3058		GG3133
vps2Δ		GG3002	GG3052	GG3117
		GG3003	GG3053	GG3163
		GG3004	GG3054	GG3164
vps4Δ		GG3050	GG3056	GG3125
		GG3051	GG3131	GG3126
		GG3071	GG3135	GG3127
plo1-ts35	GG3092			GG2987
	GG3093			GG2988
				GG2993
plo1-ts18	GG3169	GG3144	GG3148	GG3152
	GG3170	GG3145	GG3149	GG3153
		GG1346	GG3150	GG3154
ark1-T8	GG3057	GG3081	GG3077	GG2983
	GG3073	GG3082	GG3078	GG2989
	GG3074			GG2990
midΔ	GG3099	GG3097	GG3094	GG3166
	GG3160	GG3098	GG3095	GG3167
	GG3161	GG3113	GG3096	GG3168

Table 4-2. Double mutant *S. pombe* strains generated in this study.
Double mutant strains were allocated a Glasgow "GG" collection number and stored at -80ºC in 30% (v/v) glycerol. A full list of genotypes is shown in Appendix 1.

4.1.3 Attempted generation of *ssp2::KanMX6* strain

As the *ssp2Δ* strain in the lab collection (GG3033, original sourced from Dr. Petersen, Flinders University, Australia (Davie *et al.*, 2015)) was tagged with a uracil auxotrophic marker (*ssp2::ura4⁺*), random spore analysis was not feasible to generate double mutant strains with many of the ESCRT deletion strains as most of the strains were also tagged with uracil auxotrophic markers. Therefore, attempts were made to generate a *ssp2* chromosomal deletion strain tagged with a kanamycin resistance cassette (*ssp2::kanMX6*) based on a homologous recombination method (Bähler *et al.*, 1998).

Transforming DNA was generated by PCR using a plasmid encoding the kanMX6 cassette and 100mer primers containing 20 bases homologous to the kanMX6 module and 80 bases homologous to either the 5' UTR (forward primer) or 3' UTR (reverse primer) of the ssp2 gene (schematically shown in Figure 2-1, Section 2.22). Transforming DNA was generated using different combinations of forward and reverse primers each with different regions of homology to the 5' or 3' UTR (Figure 4-4A). The combination of FW2 and RV2 did not generate a PCR product (data not shown).

Transformation reactions were carried out as described (Section 2.22) and cells grown on solid YE media containing G418 until colonies formed. G418-resistant colonies were isolated and cultured in liquid YE media overnight at 30°C with shaking. Genomic DNA was isolated and PCR performed to determine if the correct recombination event occurred. PCR was performed using the "*ssp2Δ* primers" consisting of a forward primer that would recognise a sequences 5' of the initial deletion primer and a reverse primer homologous to an area in the kanMX6 sequence (Figure 4.4B). To ensure that isolated DNA was of good quality, a PCR was carried out simultaneously using primers for the *fkh2* gene that would generate a product similar in size to the *ssp2Δ* primers. A number of transformation reactions were performed and unfortunately it was not possible to generate the *ssp2::KanMX6* strain (Figure 4-4B).
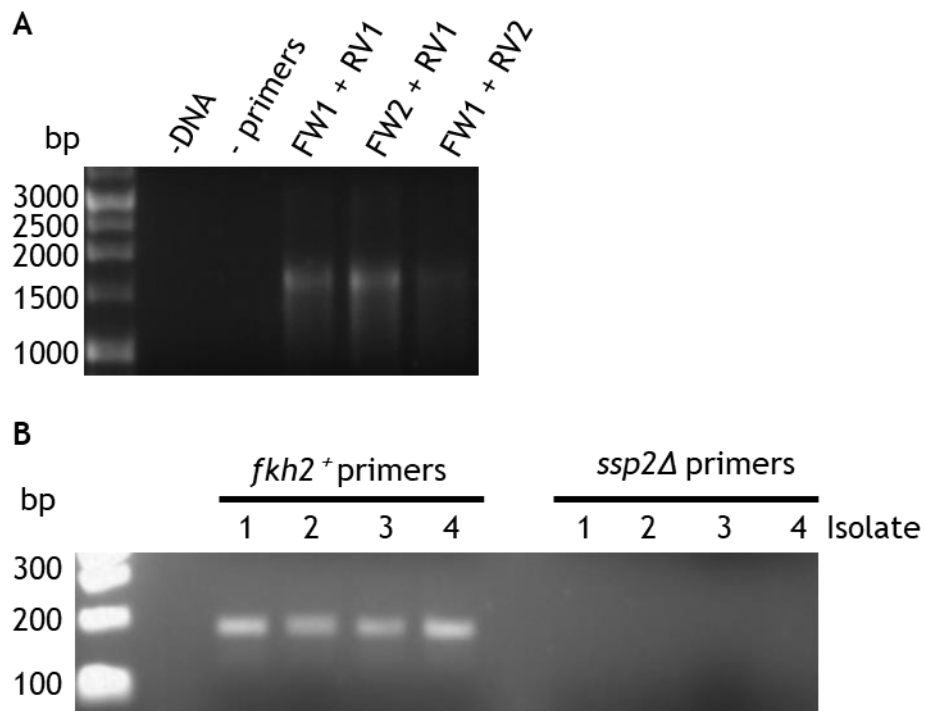
Figure 4-4. Attempted generation of *ssp2::KanMX6 S. pombe* **strain based on the homologous recombination method**
(A) Generation of linear transforming DNA by PCR using the kanMX6 plasmid backbone and a combination of different forward (FW) and reverse (RV) primers. A 1.6 kbp product was generated as expected. **(B)** PCR of genomic DNA from G418 resistant colonies (numbered 1-4) revealed no PCR product from the *ssp2Δ* checking primers. *fkh2+* primers successfully produced a product of approximately 200 bp.

4.1.4 *ark1* interacts genetically with *ssp1*, *ssp2* and *amk2*

Double mutant S. *pombe* strains were generated to contain a chromosomal deletion of either the *ssp1, ssp2, amk2* or *cbs2* gene and a temperature sensitive mutation in *ark1* (*ark1-T8*). Double mutant strains were investigated for synthetic growth phenotypes by serial dilution onto solid YE media and incubation at different temperatures. s*sp1Δ ark1-T8* double mutant strains showed less growth at 28ºC and 30ºC than either parental strain (Figure 4.5). This synthetic phenotype is indicative of a genetic interaction between the *ssp1⁺* and *ark1⁺* genes.

To further analyse the synthetic phenotype of the *ssp1Δ ark1-T8* cells, septation was analysed using Calcofluor-White staining. Double mutant cells showed a significant reduction in cells with the Class A phenotype compared to both parental strains (Figure 4-6). The double mutant cells also had a significant increase in the Class E (absent septa) phenotype compared to the parental strains. A significant increase in Class B, D and G phenotypes was found compared to *ssp1Δ* but were at a comparable frequency to that of *ark1-T8* (Figure 4-6). Interestingly, *ssp1Δ ark1-T8* cells had similar levels of the Class F (reduced separation after septation) phenotype as wild type and *ark1-T8* cells but approximately 20% less than *ssp1Δ* cells (Figure 4-6).
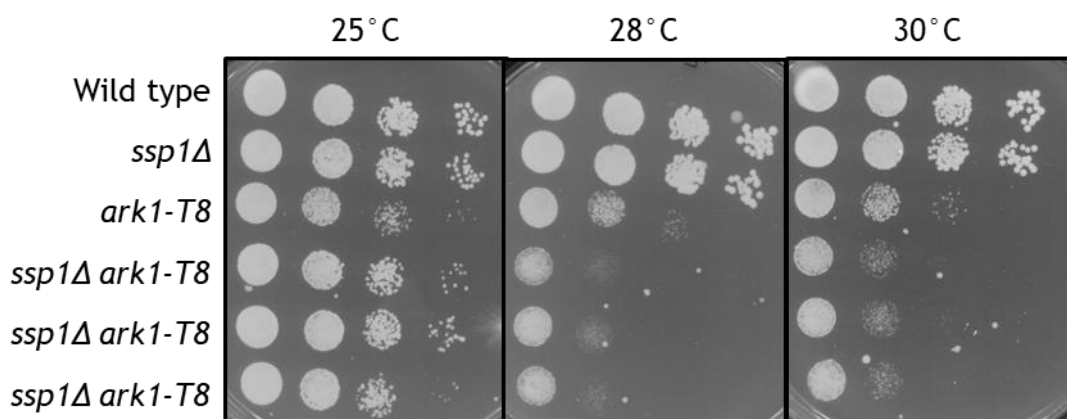
Figure 4-5. Growth defects in *ssp1Δ ark1-T8* double mutant cells.
Wild type (GG1278), *ssp1Δ* (GG3080), *ark1-T8* (GG2426) and three separate isolates of *ssp1Δ ark1-T8* (GG2983, GG2989, GG2990) strains were suspended at 1.5x10⁶ cell/ml and subjected to 10-fold serial dilution. Cell suspension was pipetted onto solid YE media and incubated at the indicated temperatures for 3 days.
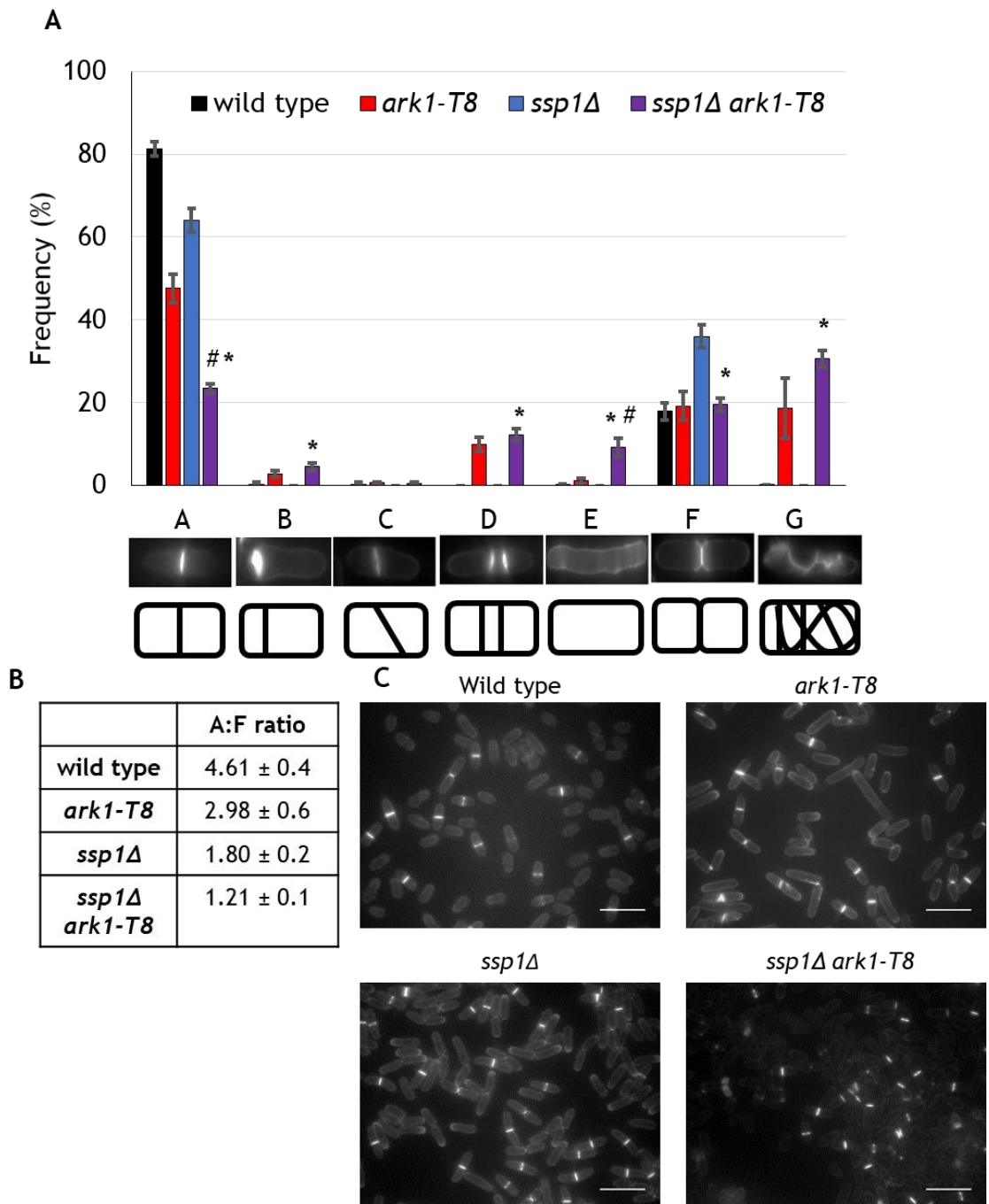
Figure 4-6. Septation defects in _ssp1Δ ark1T8_ double mutant cells.
Wild type (GG1278), _ark1-T8_ (GG2426), _ssp1Δ_ (GG3080) and three separate isolates of _ssp1Δ ark1-T8_ (GG2983, GG2989, GG2990) strains were grown in liquid YE media for 18 h. Division septa were visualised using Calcofluor-White, examined by fluorescence microscopy and the frequency of each phenotype recorded. 300 cells in total were counted over three technical replicates, performed on three independent occasions for each genotype. **(B)** Quantification of Class A:F phenotypes ± SEM. **(C)** Representative images of Calcofluor-White stained cells. Scale bar represents 20 μm. * $p < 0.05$ relative to _ssp1Δ_, # $p < 0.05$ relative to _ark1-T8_, (Students _t_ test).

Potential genetic interactions were next examined between *ark1* and the AMPK subunit orthologues. *ssp2Δ ark1-T8* cells exhibited increased growth compared to *ark1-T8* cells at 25ºC and 28ºC, indicating a partial rescue of the *ark1-T8* phenotype, however, the cells had reduced growth compared to *ssp2Δ* cells (Figure 4.7A). *amk2Δ ark1-T8* cells had reduced growth rates compared to the parental strains thereby demonstrating a synthetic phenotype (Figure 4-7B). In contrast, c*bs2Δ ark1-T8* double mutant strains did not exhibit any apparent synthetic growth phenotypes and had a similar growth rate to *ark1-T8* cells (Figure 4-7C). A table collating these results will be presented in the Discussion section (Table 4-3)
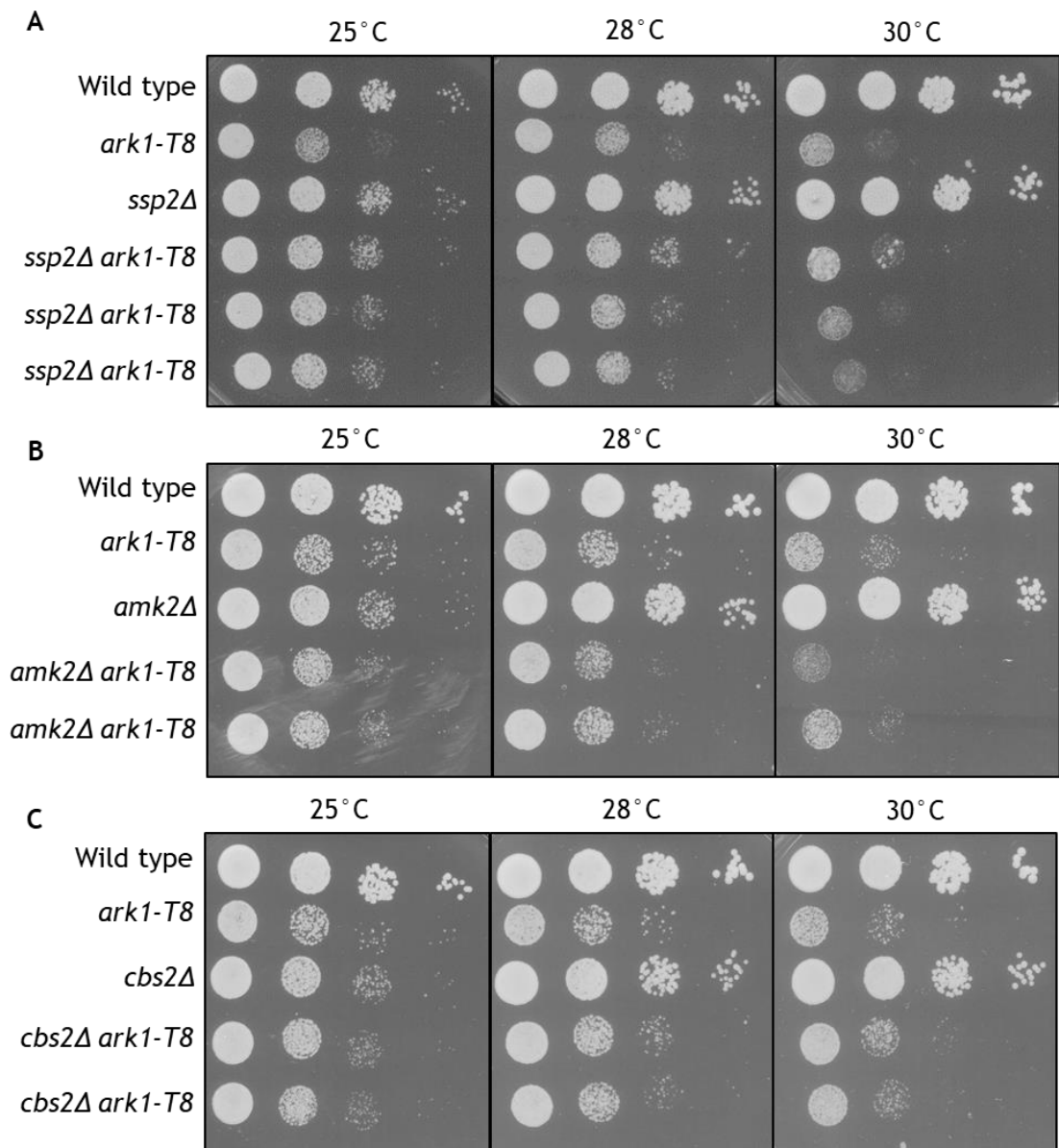
Figure 4-7. Growth defects in *ssp2Δ ark1-T8*, *amk2Δ ark1-T8*, and *cbs2Δ ark1-T8* double mutant cells.
(A) Wild type (GG1278), *ark1-T8* (GG2426), *ssp2Δ* (GG3033) and three separate isolates of *ssp2Δ ark1-T8* (GG3057, GG3073, GG3074). **(B)** Wild type (GG1278), *ark1-T8* (GG2426), *amk2Δ* (GG2979) and two separate isolates of *amk2Δ ark1-T8* (GG3081, GG3082). **(C)** Wild type (GG1278), *ark1-T8* (GG2426), *cbs2Δ* (GG2981) and two separate isolates of *cbs2Δ ark1-T8* (GG3077, GG3078). Strains were suspended at 1.5x10^6 cell/ml and subjected to 10-fold serial dilution. Cell suspension was pipetted onto solid YE media and incubated at the indicated temperatures for 3 days.

4.1.5 *plo1* interacts genetically with *ssp1, amk2* and *cbs2*

To investigate if the *ssp1* and *plo1* genes interacted, double mutant strains were generated containing a chromosomal deletion of *ssp1* and a temperature sensitive mutation in *plo1*, either the *plo1-ts35* or *plo1-ts18* allele. s*sp1Δ plo1-ts35* cells displayed a synthetic growth phenotype where double mutant strains were more heat tolerant than *plo1-ts35* cells, yet were not able to grow to the same extent as s*sp1Δ* cells (Figure 4-8A). A synthetic phenotype was also apparent in s*sp1Δ plo1-ts18* cells; at 25°C *ssp1Δ plo1-ts18* cells exhibited increased growth compared to both s*sp1Δ* cells and *plo1-ts18* cells (Figure 4-8B). Double mutant cell growth appeared to be faster than that of *plo1-ts18* but less than *ssp1Δ* at 35°C (Figure 4-8B).

As *ssp1Δ plo1-ts35* cells showed growth intermediate of the parental strains, the growth rate was analysed further in liquid media. Cells were seeded at 5 x10^5 cells/ml in liquid YE media and cell number assessed over a 36 h period. This confirmed that *ssp1Δ plo1-ts35* cells grew faster than *plo1-ts35* cells but slower than *ssp1Δ* cells (Figure 4-9). Septation analysis of s*sp1Δ plo1-ts* mutants did not reveal any synthetic phenotypes (Figure 4-10). Notably, *plo1-ts35* and s*sp1Δ plo1-ts35* strains only exhibited Class G phenotype, with ectopic deposition of new cell wall.

A synthetic growth phenotype was also apparent in *amk2Δ plo1-ts18* and *cbs2Δ plo1-ts18* strains (Figure 4-11). These double mutants showed increased growth at 25°C compared to the respective parental strains. However, ssp2Δ *plo1-ts18* strains had comparable growth to *ssp2Δ* parental strain (Figure 4-11). Calcofluor-White staining and analysis of septation of *amk2Δ plo1-ts18* cells did not reveal any obvious synthetic phenotype, instead these cells closely resembled the *plo1-ts18* parental strain (Figure 4-12A). Similarly, *cbs2Δ plo1-ts18* cells showed a closer resemblance to *plo1-ts18* cells than *cbs2Δ* cells (Figure 4-12B).
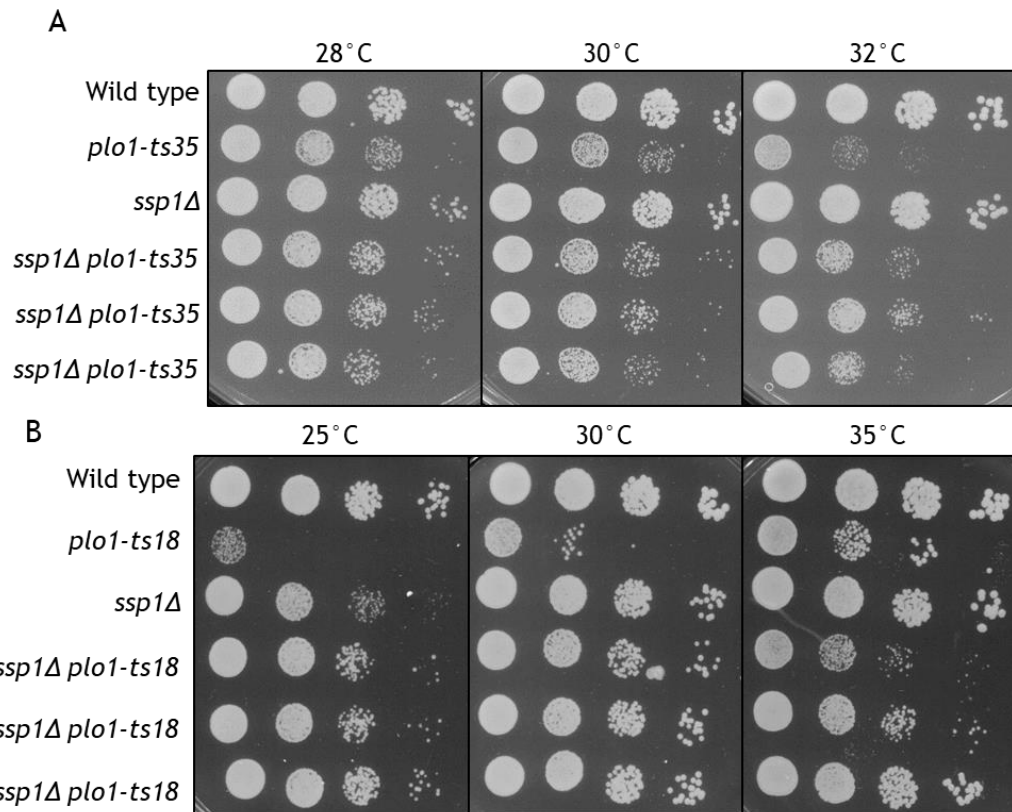
Figure 4-8. Synthetic growth defects in *ssp1Δ plo1-ts* double mutant cells.
(A) Wild type (GG1278), *plo1-ts35* (GG1167), *ssp1Δ* (GG2966) and three separate isolates of *ssp1Δ plo1-ts35* (GG2989, GG2988, GG2993) **(B)** Wild type (GG1278), *plo1-ts18* (GG380), *ssp1Δ* (GG3080) and three separate isolates of *ssp1Δ plo1-ts18* (GG3152, GG3153, GG3154). Strains were suspended at 1.5×10^6 cell/ml and subjected to 10-fold serial dilution. Cell suspension was pipetted onto solid YE media and incubated at the indicated temperatures for 3 days.
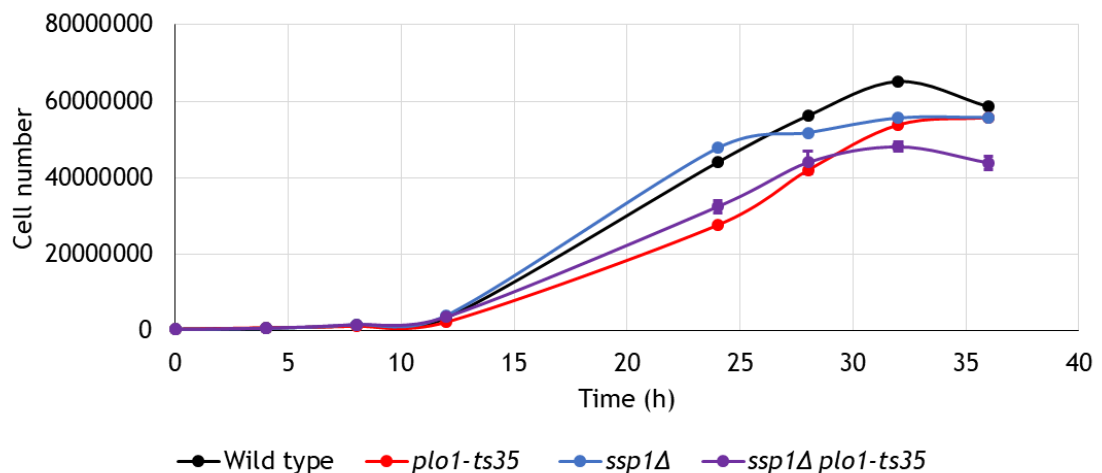
Figure 4-9. Growth defects in *ssp1Δ plo1-ts35* cells grown in liquid YE media.
Wild type (GG1278), *plo1-ts35* (GG1167), *ssp1Δ* (GG2966) and three separate isolates of *ssp1Δ plo1-ts35* (GG2989, GG2988, GG2993) were culture in liquid YE media in a shacking water bath at 28°C for 36 h. Cell number was analysed using a Coulter Z2 cell counter.
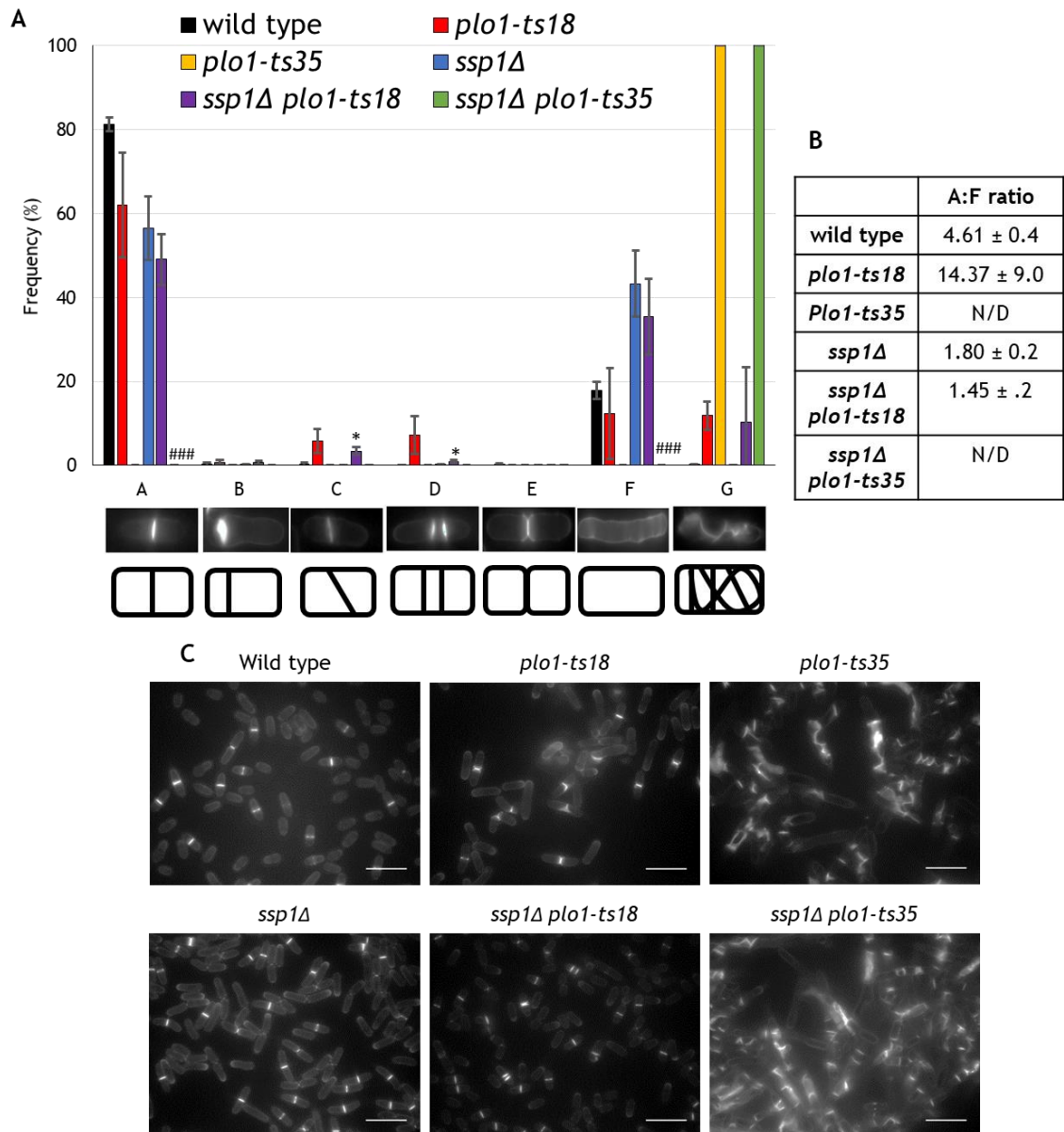
Figure 4-10. Synthetic septation defects in *ssp1Δ plo1-ts* double mutant cells.
(A) Wild type (GG1278), *plo1-ts18* (GG380), *plo1-ts35* (GG1167), *ssp1Δ* (GG2966 and GG3080), three separate isolates of *ssp1Δ plo1-ts18* (GG3152, GG3153, GG3154) and three separate isolates of *ssp1Δ plo1-ts35* (GG2989, GG2988, GG2993). Strains were cultured in liquid YE media at 30°C for 18 h. Division septa were visualised using Calcofluor-White, examined by fluorescence microscopy and the frequency of each phenotype recorded. 300 cells in total were counted over three technical replicates, performed on three independent occasions for each genotype. **(B)** Quantification of Class A:F phenotypes ± SEM. **(C)** Representative images of Calcofluor-White stained cells. Scale bar represents 20 μm. * *p*< 0.05 when comparing *ssp1Δ* to *ssp1Δ plo1-ts18*, ### *p*< 0.005 when comparing *ssp1Δ* to *ssp1Δ plo1-ts35* (Students *t* test).
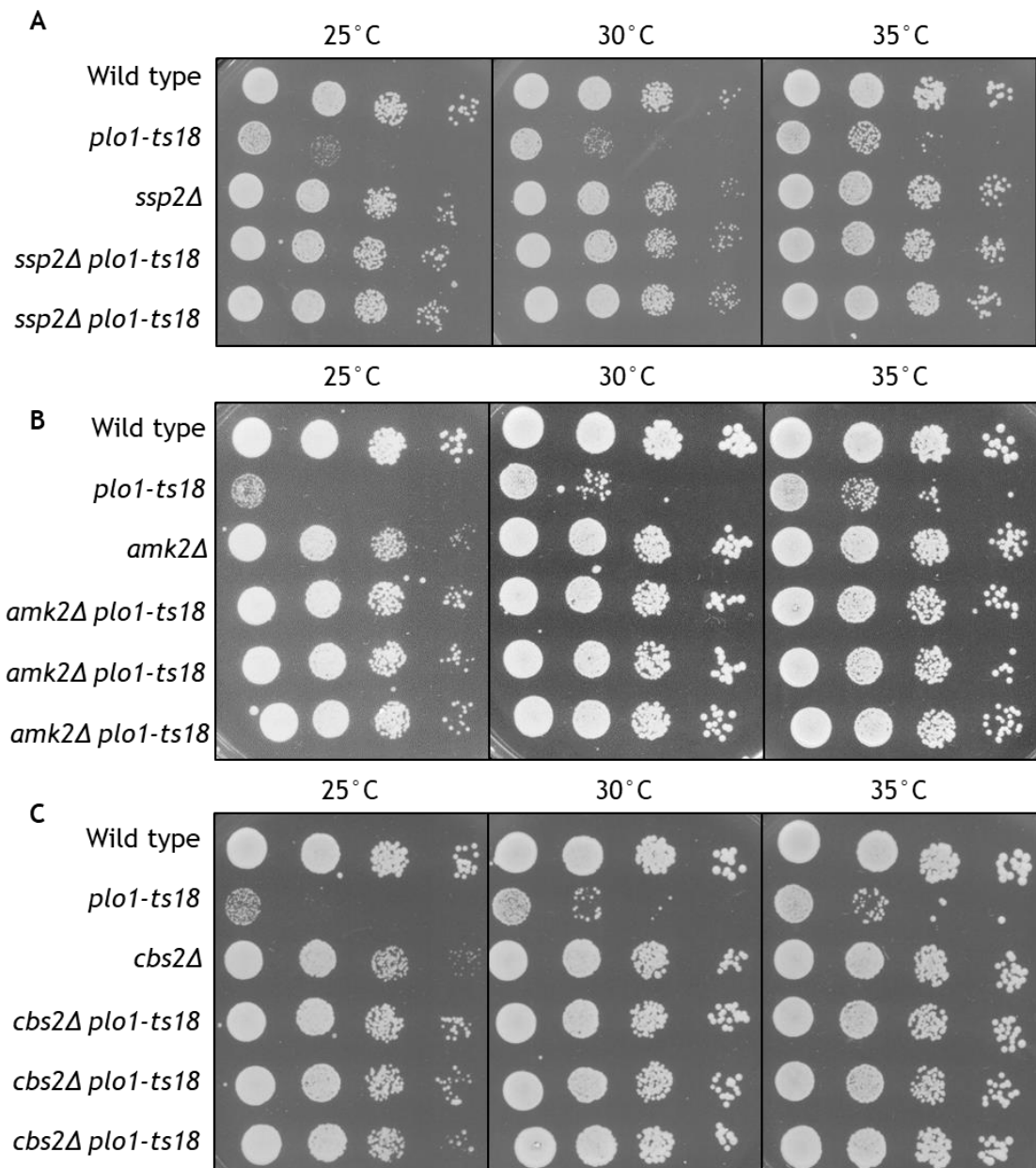
Figure 4-11. Analysis of synthetic growth defects in *ssp2Δ plo1-ts18*, *amk2Δ-plo1-ts18* and *cbs2Δ-plo1-ts18* mutant strains.
(A) Wild type (GG1278), *ssp2Δ* (GG3033), *plo1-ts18* (GG380) and two separate isolates of *ssp2Δ plo1-ts18* (GG3169, GG3170). **(B)** Wild type (GG1278), *amk2Δ* (GG2979), *plo1-ts18* (GG380) and three separate isolates of *amk2Δ plo1-ts18* (GG3144, GG3145, GG3146). **(C)** Wild type (GG1278), *cbs2Δ* (GG2981), *plo1-ts18* (GG380) and three separate isolates of *cbs2Δ plo1-ts18* (GG3148, GG3149, GG3150). Strains were suspended at 1.5×10^6 cell/ml and subjected to 10-fold serial dilution. Cell suspension was pipetted onto solid YE media and incubated at the indicated temperatures for 3 days.

C

	A:F ratio
wild type	4.61 ± 0.4
plo1-ts18	14.37 ± 9.0
amk2Δ	2.50 ± 0.9
amk2Δ plo1-ts18	4.62 ± 1.8
cbs2Δ	0.85 ± 0.1
cbs2Δ plo1-ts18	2.37 ± 0.2

Figure 4-12. Synthetic septation defects in *amk2Δ plo1-ts18* and *cbs2Δ plo1-ts18* double mutant cells.

Division septa were visualised using Calcofluor-White, examined by fluorescence microscopy and the frequency of each phenotype recorded. 300 cells in total were counted over three technical replicates, performed on three independent occasions for each genotype. **(A)** Wild type (GG1278), *plo1-ts18* (GG380), *amk2Δ* (GG2979) and three separate isolates of *amk2Δ plo1-ts18* (GG3144, GG3145, GG3146) **(B)** Wild type (GG1278), *plo1-ts18* (GG380), cbs2Δ (GG2981) and three separate isolates of *cbs2Δ plo1-ts18* (GG3148, GG3149, GG3150). Strains were cultured in liquid YE media at 30°C for 18 h. **(C)** Quantification of Class A:F phenotypes ± SEM. **(D)** Representative images of Calcofluor-White stained cells. Scale bar represents 20 μm. * $p < 0.05$ comparing *amk2Δ* to *amk2Δ plo1-ts18,* # $p < 0.05$ comparing *plo1-ts18Δ* to *ssp1Δ plo1-ts18*, $ $p < 0.05$ comparing *cbs2Δ* to *cbs2Δ plo1-ts18* (Students *t* test).

To further understand the genetic interactions noted between the AMPK pathway and *ark1/plo1, ark1-GFP* and *plo1-GFP* strains were acquired from the Japanese National BioResource Project. These stains which expressed GFP-fusion proteins were acquired with the aim of studying the subcellular localisation of Ark1p/Plo1p and to examine if localisation was altered upon the chromosomal deletion of AMPK subunits/*ssp1*. Strains were lysed and resolved by SDS-PAGE to determine the presence of a GFP-fusion protein by immunoblotting. No GFP or GFP-fusion proteins was detected from *plo1-GFP* cells at the expected molecular weight (27 kDa for GFP and ~110 kDa for Plo1p) (Figure 4-13). An immunoreactivite band was detected at ~75 kDa from *ark1-GFP* cells, corresponding to the expected molecular weight of the fusion protein (Figure 4-13). Unfortunately, GFP fluorescence from *ark1-GFP* cells was very faint and could not be detected by confocal microscopy (data not shown).
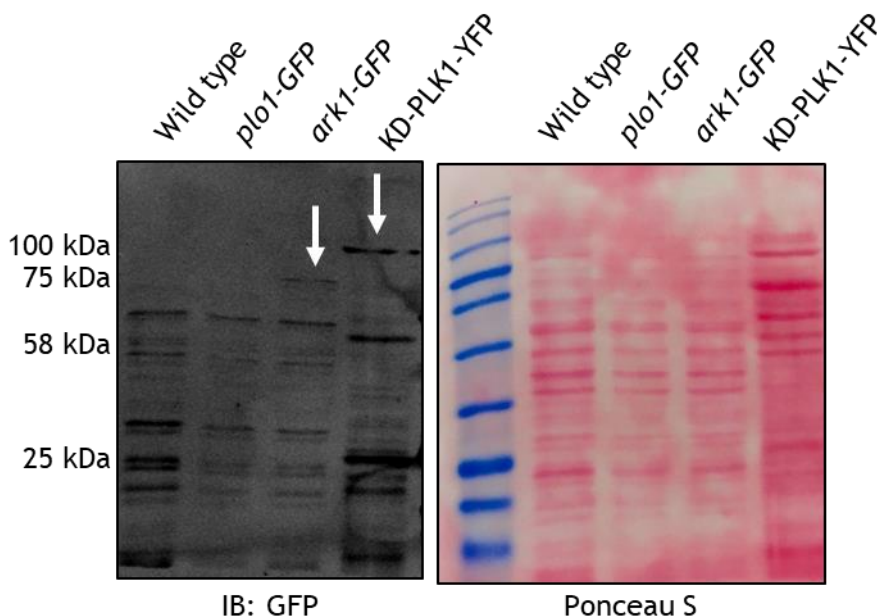
Figure 4-13. *Plo1-GFP* cells did not express GFP fusion protein.
Wild type (GG1278), *plo1-GFP* (GG3226) and *ark1-GFP* (GG3227) strains were cultured overnight in liquid YE media at 30°C with shaking. Cells were lysed by incubation with 1% (v/v) Triton X-100 solution containing phosphatase inhibitors followed by vortex mixing with HCl-washed glass beads. Resulting lysates were resolved by SDS-PAGE and immunoblotted with anti-GFP antibodies. In parallel, cell lysates prepared from HEK 293 cells transfected with a plasmid encoding kinase dead (KD)-PLK1-YFP was assessed as a positive control (anti-GFP antibodies also recognise YFP isoforms). Total protein was stained with Ponceau S. GFP-fusion protein bands are indicated with a white arrow.

4.1.6 *mid1* interacts genetically with *ssp1, ssp2, amk2* and *cbs2*

Mid1⁺is important for *S. pombe* cytokinesis as its chromosomal deletion results in random positioning of the contractile ring and division septa (Sohrmann *et al.*, 1996b; Wu *et al.*, 2006). Additionally Mid1p is also a downstream target of Plo1p (Almonacid *et al.*, 2011). Therefore, it was investigated if the *mid1* gene interacted with *ssp1* or the AMPK subunits. Serial dilution of such double mutant strains on solid YE media indicated that synthetic phenotypes were present for each of the double mutant strains. In all cases the double mutant was more heat tolerant than *mid1Δ* cells but less tolerant that the associated deletion of *ssp1, ssp2, amk2* or *cbs2* at both 30ºC and 35ºC (Figure 4-14).
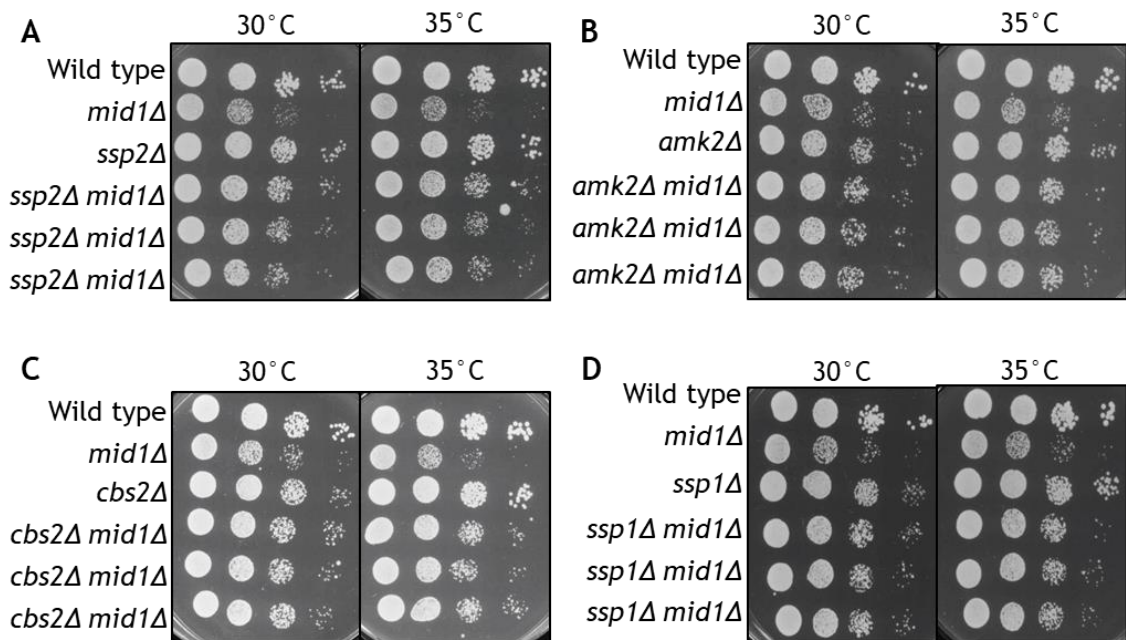
Figure 4-14. Growth defects in *mid1Δ* and *ssp1Δ/ssp2Δ/amk2Δ/cbs2Δ* double mutant cells. **(A)** Wild type (GG1278), *mid1* (GG1554), *ssp2Δ* (GG3033) and three separate isolates of *ssp2Δ mid1Δ* (GG3099, GG3160, GG3161). **(B)** Wild type (GG1278), *mid1Δ* (GG1125), *amk2Δ* (GG2979) and three separate isolates of *amk2Δ mid1Δ* (GG3097, GG3098, GG3113). **(C)** Wild type (GG1278), *mid1Δ* (GG1125), *cbs2Δ* (GG2981) and three separate isolates of *cbs2Δ mid1Δ* (GG3094, GG3095, GG3096). **(D)** Wild type (GG1278), *mid1Δ* (GG1554), *ssp1Δ* (GG2966) and three separate isolates of *ssp1Δ mid1Δ* (GG3166, GG3167, GG3168) Strains were suspended at 1.5x10⁶ cell/ml and subjected to 10-fold serial dilution. Cell suspension was pipetted onto solid YE media and incubated at the indicated temperatures for 3 days.

4.1.7 *ssp1* interacts genetically with components of the ESCRT pathway

The ESCRT proteins form a series of multi-protein complexes divided into four functional classes; ESCRT-0, ESCRT-I, ESCRT-II and ESCRT-III which function with many accessory proteins such as Vps4p (Wollert and Hurley, 2010). The ESCRT machinery facilitate the curving of the cell membrane and abscission during cytokinesis, and are important regulators of cel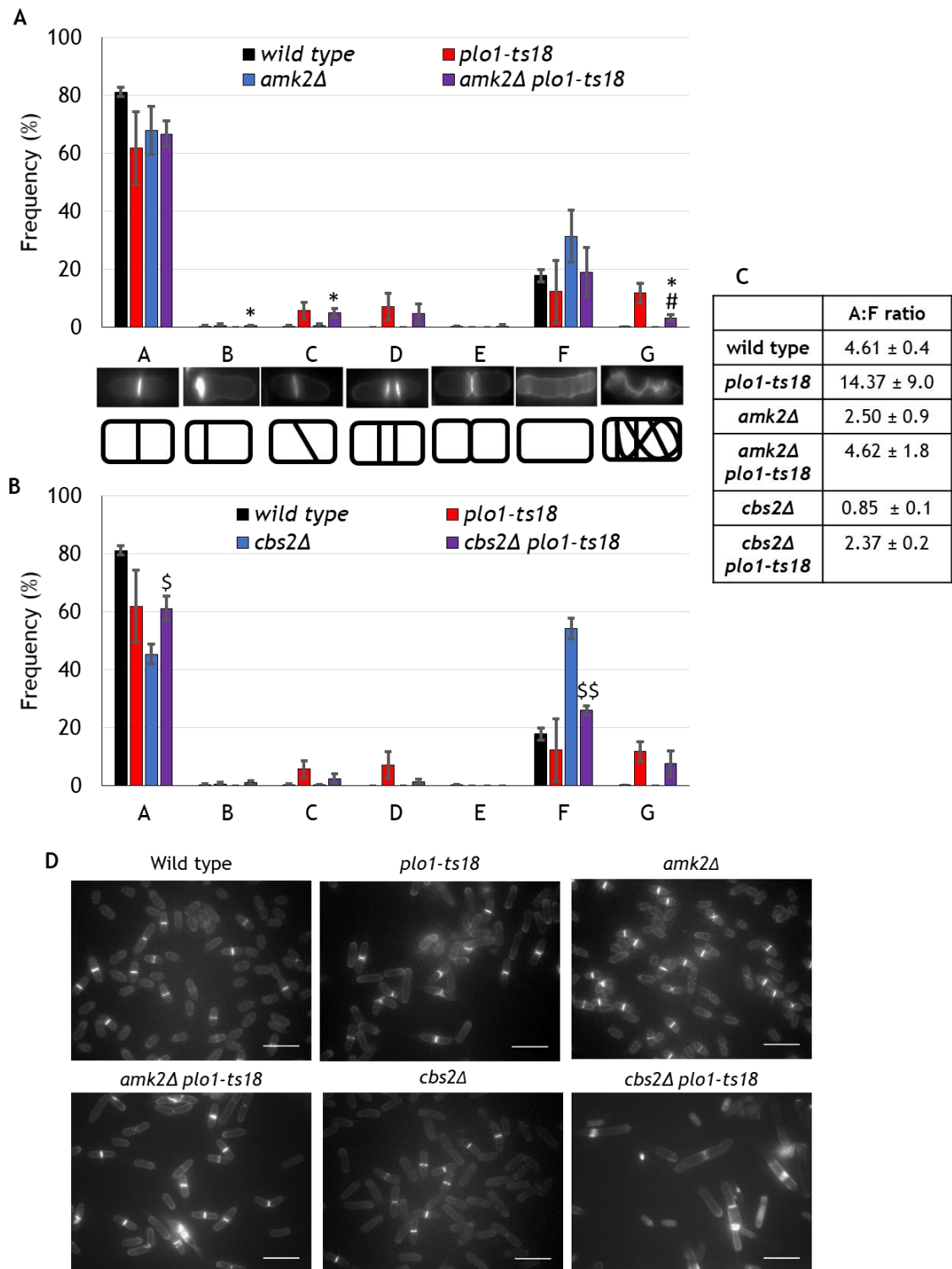l separation and cytokinesis in *S. pombe* (Bhutta *et al.*, 2014). In the present study, a number of *S. pombe* strains containing single chromosomal deletions of ESCRT genes were used, namely; *sst4Δ, sst6Δ, vps28Δ, vps36Δ, vps35Δ, vps20Δ, vps32Δ, vps2Δ* and *vps4Δ* (Table 4-2).

GG number	Genotype	Human orthologue	ESCRT Class
GG1623	*sst4Δ*	HRS	ESCRT-0
GG1615	*sst6Δ*	TSG101	ESCRT-I
GG1616	*vps28Δ*	Vps28	ESCRT-I
GG1617	*vps36Δ*	EAP45	ESCRT-II
GG1618	*vps25Δ*	EAP20	ESCRT-II
GG1619	*vps20Δ*	CHMP6	ESCRT-III
GG2540	*vps32Δ*	CHMP4	ESCRT-III
GG1621	*vps2Δ*	CHMP2A/B	ESCRT-III
GG1622	*vps4Δ*	VPS4A/B	Accessory protein

Table 4-3. Summary of ESCRT deletion strains used in the present study.

A striking genetic interactions was apparent between *vps2Δ* and *ssp1Δ*. The double mutant strain had dramatically reduced growth at both 30°C and 35°C compared to the parental strains (Figure 4-15). Although a synthetic septation phenotype was not apparent in *ssp1Δ vps2Δ* cells, a significant increase in the proportion of Class F phenotype compared to *vps2Δ* was detected (Figure 4-16). Additionally, *ssp1Δvps2Δ* cells had a decrease in the Class A:F ratio compared to the parental strains (Figure 4-16). Single mutant parental strains both had very similar septation phenotypes, approximately 55% Class A and 45% Class F (Figure 4-16).
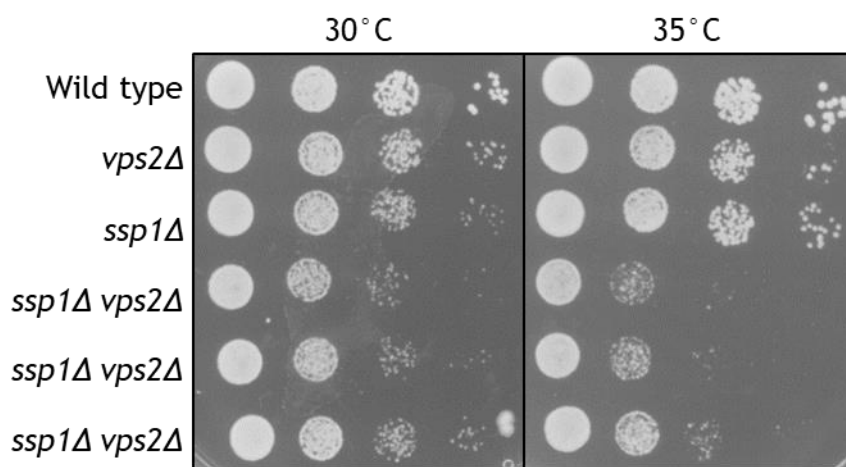
Figure 4-15. Analysis of synthetic growth defects in *ssp1Δ vps2Δ* double mutant ells.
Wild type (GG1278), *vps2Δ* (GG1621), *ssp1Δ* (GG3080) and three separate isolates of *ssp1Δ vps2Δ* (GG3117, GG3163, GG3164). Strains were suspended at 1.5×10^6 cell/ml and subjected to 10-fold serial dilution. Cell suspension was pipetted onto solid YE media and incubated at the indicated temperatures for 3 days.

A

B

	A:F ratio
wild type	4.61 ± 0.4
vps2Δ	1.22 ± .01
ssp1Δ	1.80 ± 0.2
ssp1Δ vps2Δ	0.82 ± 0.1

C

Wild type   *vps2Δ*
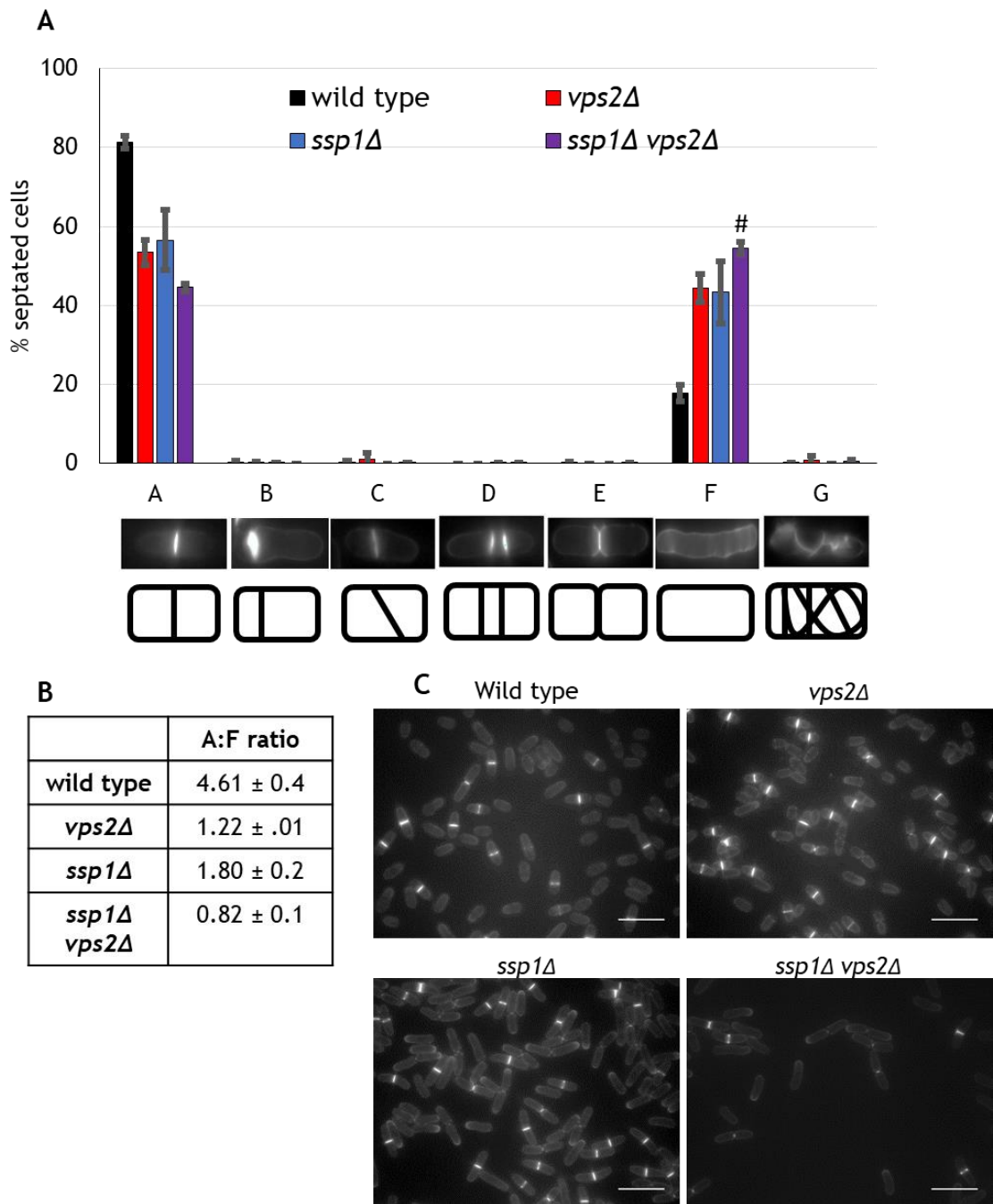
ssp1Δ   *ssp1Δ vps2Δ*

Figure 4-16. Analysis of synthetic septation defects in *ssp1Δ vps2Δ* double mutant cells. Wild type (GG1278), *vps2Δ* (GG1621), *ssp1Δ* (GG3080) and three separate isolates of *ssp1Δ vps2Δ* (GG3117, GG3163, GG3164). Division septa were visualised using Calcofluor-White, examined by fluorescence microscopy and the frequency of each phenotype recorded. 300 cells in total were counted over three technical replicates, performed on three independent occasions for each genotype. **(B)** Quantification of Class A:F phenotypes ± SEM. **(C)** Representative images of Calcofluor-White stained cells. Scale bar represents 20 μm. # $p < 0.05$ comparing *vps2Δ* to ssp1Δ *vps2Δ* (Students *t* test).

A genetic interaction was also detected between *ssp1* and *vps4*. The *ssp1Δ vps4Δ* cells were more temperature sensitive than parental strains at 35°C (Figure 4-17). Analysis of the septation phenotype of *ssp1Δ vps4* cells revealed a significant increase in the proportion of Class F cells relative to vps4Δ cells, however there was no significant alteration compared to ssp1Δ cells (Figure 4-18).

Analysis of growth by serial dilution of other combinations of AMPK/ESCRT deletion strains did not reveal any synthetic phenotypes and are displayed in Appendix 2.
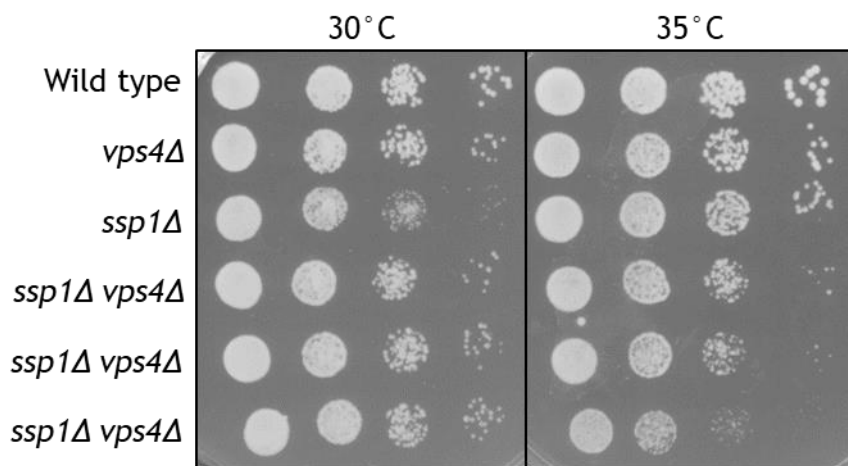
Figure 4-17. Analysis of synthetic growth defects in *ssp1 vps4* double mutant cells.
Wild type (GG1278), *vps4Δ* (GG1622), *ssp1Δ* (GG3080) and three separate isolates of *ssp1Δ vps4Δ* (GG3125, GG3126, GG3127). Strains were suspended at 1.5×10^6 cell/ml and subjected to 10-fold serial dilution. Cell suspension was pipetted onto solid YE media and incubated at the indicated temperatures for 3 days.
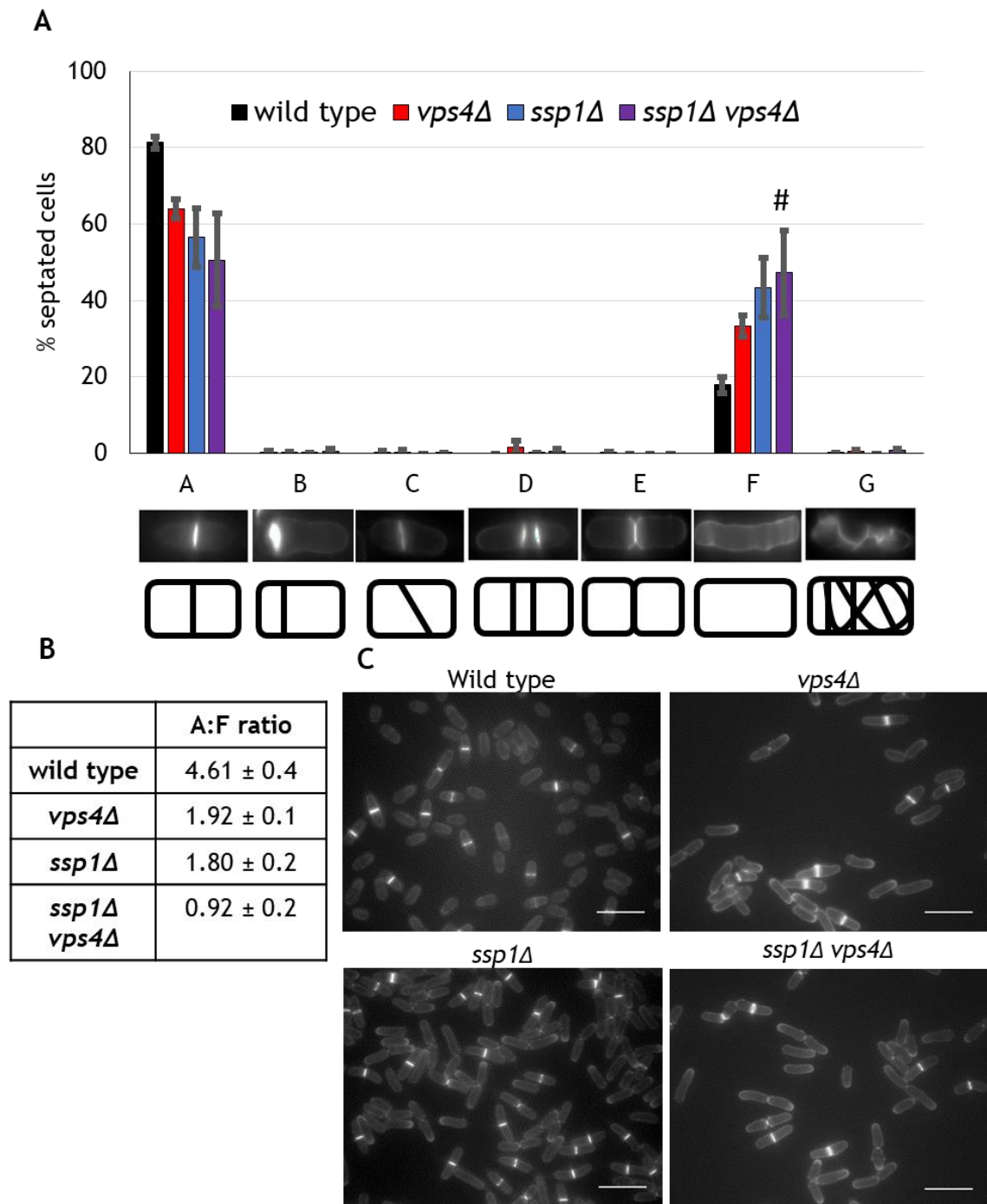
Figure 4-18. Analysis of synthetic septation defects in *ssp1Δ vps4Δ* double mutant cells.
(A) Wild type (GG1278), *vps4Δ* (GG1622), *ssp1Δ* (GG3080) and three separate isolates of *ssp1Δ vps4Δ* (GG3125, GG3126, GG3127). Division septa were visualised using Calcofluor-White, examined by fluorescence microscopy and the frequency of each phenotype recorded. 300 cells in total were counted over three technical replicates, performed on three independent occasions for each genotype. **(B)** Quantification of Class A:F phenotypes ± SEM. **(C)** Representative images of Calcofluor-White stained cells. Scale bar represents 20 μm. # $p< 0.05$ comparing *vps4Δ* to ssp1Δ *vps4Δ* (Students *t* test).

4.2 Discussion

4.2.1 Principal findings

- *S. pombe* AMPK has a role in the efficient septation/cytokinesis of daughter cells

- The genes encoding components of the AMPK heterotrimer/*ssp1* were described to interact with *ark1-T8*, *mid1* and *plo1-ts18*/*plo1-ts35*

- *ssp2* interacted with components of the ESCRT machinery; *vps2* and *vps4*

4.2.2 AMPK has a role in controlling *S. pombe* cytokinesis

The data presented in this Chapter demonstrated that the AMPK pathway has a role in mitosis and specifically cytokinesis in *S. pombe*. Chromosomal deletion of each of *ssp2, cbs2* or *ssp1* caused an alteration in the septation phenotype of dividing cells. Class F phenotypes (delayed separation after septation) were increased by approximately 20% compared to wild type strains. Such increased frequency of Class F phenotype could reflect delayed cytokinesis, mis-timed cytokinesis or defective septum degradation. In future, real time fluorescence microscopy could be employed to examine the length of time taken to resolve the septa in these mutants.

Previously, the septation phenotype of wild type cells was described as approximately 90% Class A and 10% Class F (inferred A:F ratio of 9) (Bhutta *et al.*, 2014). In this study, wild type cells were described as 80% class A and 20% Class F (A:F of 4.61). The over representation of Class F in this study may reflect different culturing methods of yeast strains. Alternatively, as phenotype classification is a subjective process, how an individual records either Class A or Class F may differ. Importantly, in this study yeast strains were cultured in the same manner prior to Calcofluor-White staining; 18 h in liquid YE media at 30°C with shaking. Secondly, elements of the experiments were double blinded; in doing so the genotype was not known when septation phenotype was assessed. Blinded and non-blinded experiments produced comparable results.

4.2.3 The AMPK pathway genetically interacts with a number of mitotic regulators in *S. pombe*

Synthetic phenotypes were observed in a number of double mutant *S. pombe* strains generated in this study (Table 4-3). The nature of the synthetic phenotypes varied; a number of double mutant strains were less viable than the parental strains whereas some strains had a phenotype intermediate of the parental strains or finally a synthetic phenotype that was "fitter" than parental strains. Genetic interactions studied in this Chapter are shown in Table 4-3.

	ssp2Δ	*amk2Δ*	*cbs2Δ*	*ssp1Δ*
ark1-T8	#	-	X	-
plo1-ts18	X	+	+	+
plo1-ts35				#
midΔ	#	#	#	#
sst4Δ		X	X	X
sst6Δ		X	X	X
vps28Δ		X	X	X
vps36Δ		X	X	X
vps25Δ	X	X	X	
vps20Δ		X	X	X
vps32Δ		X		X
vps2Δ		X	X	-
vps4Δ		X	X	-

Table 4-4. Summary of the genetic interactions detected in *S. pombe*
Double mutant strains where genetic interactions were detected are shaded green. Combinations which resulted in a synthetic phenotype which grew less that the respective parents are denoted by "-". In cases where double mutant strains had a phenotype between the parental strains are noted by "#". Where double mutant stains displayed a phenotype "fitter" than parental strains are noted by "+". Lack of a synthetic phenotype is noted by "X". Grey boxes represent combinations where double mutant strains were not generated.

4.2.3.1 *ark1* double mutants

Intriguingly, the nature of synthetic growth phenotypes varied depending on the associated deletion of AMPK genes; *ssp1Δ ark1-T8* and *amk2Δ ark1-T8* strains had reduced growth compared to both parental strains, whereas *ssp2Δ ark1-T8* cells had a partial rescue of *ark1-T8* temperature sensitivity and grew at an

intermediate rate between the respective parental strains. From this growth phenotype, it can be inferred that *ssp2* is epistatic to *ark1*, suggesting that Ssp2p likely acts downstream of Ark1p.

Analysis of the septation phenotype of *ssp1Δ ark1-T8* revealed an overall similar pattern to that of *ark1-T8* cells, with both genotypes having similar proportions of Class B, D and G phenotypes although double mutants had elevated instances of Class E relative to both parental strains. Previously the *ark1-T8* septation phenotype was characterised as approximately 50% Class A, 5% Class C, 15% Class E and 30% Class F (Bhutta *et al.*, 2014) bearing a similarity to the phenotype described in this Chapter. The most notable difference was the description of a new septation phenotype in this study representing ectopic deposition of the septa material (Class G phenotype). Due to differences in culturing techniques (25°C opposed to 30°C, or shaking speed of the incubator) ectopic deposition may not have been observed in the previous study. Alternatively, Class G cells may have been discounted from the analysis. Surprisingly, 20% of *ssp1Δ ark1-T8* cells displayed the Class F phenotype, the same proportion as wild type and *ark1-T8* cells, compared to 35-40% in *ssp1Δ* cells. This "rescue" of double mutant cells from the *ssp1Δ*/delayed separation phenotype may indicate a functional relationship between the encoded proteins and is further evidence of an interaction between Ssp1p and Ark1p.

Despite evidence of a genetic interaction between *ark1* and *ssp1, ssp2* or *amk2*, there was no interaction between *ark1* and *cbs2*. This may indicate that the interaction between *S. pombe* AMPK and Ark1p is independent of AMP or the Cbs2p subunit. Structural analysis of the *S. pombe* AMPK heterotrimer (Ssp1p-Amk2p-Cbs2p) indicated that the interactions between Amk2p and Cbs2p are mediated through hydrogen bonding and ionic interactions (Townley and Shapiro, 2007). This led the authors to suggest that the Amk2p-Cbs2p interaction may not be obligatory for Ssp2p function (Townley and Shapiro, 2007). If the interaction between aurora kinase and AMPK was conserved in human cells, it is likely that the redundancy of the regulatory subunits would not be conserved as canonically it is believed that AMPK is only active as a heterotrimer.

4.2.3.2 *plo1* double mutants

Two different temperature sensitive mutant alleles of *plo1* were utilised in this investigation, *plo1-ts18* and *plo1-ts35* (Anderson *et al.*, 2002). These mutant alleles produced drastically different phenotypes; *plo1-ts35* cells grew efficiently between 28-30°C, although not to the same extent as wild type cells, and showed reduced growth at 32°C. In contrast, *plo1-ts18* cells had limited growth between 25-30°C but had considerable growth at 35°C although at a lower rate than wild type cells. Septation also occurs differently between the mutation types; 100% of *plo1-ts35* cells had the Class G phenotype whereas *plo1-ts18* had a spread of septation phenotypes (approximately 60% Class A, 10% Class C, 10% Class D, 10% Class F and 10% Class G). Septation of *plo1-ts35* was previously quantified as approximately; 45% Class A, 5% Class C, 5% Class D, 20% Class E and 15% Class F (Bhutta *et al.*, 2014). Unusually, the results of Bhutta *et al.* do not align with the results presented in this Chapter. In previous studies, *plo1-ts35* was cultured at 25°C (30°C in this investigation) therefore the observed shift of *plo1-ts35* cells to a Class G phenotype may reflect strains being cultured at or beyond the restrictive temperature of the particulate mutation. *plo1-ts18*, has a single mutation in the kinase domain causing a arginine to glycine at position 216 (MacIver *et al.*, 2003). *plo1-ts35* also has a mutation in the kinase domain but the exact identity is not known (C. McInerny, personal communications). Identifying the precise *plo1-ts35* mutation may help understand the synthetic phenotypes observed between the AMPK pathway.

ssp1Δ plo1-ts35 strains had a partial rescue of *plo1-ts35* temperature sensitivity at 32°C but had reduced growth rate compared to *ssp1Δ*. Consistently, when *ssp1Δ plo1-ts35* strains were grown in liquid culture at 28°C, double mutant cells were able to grow more than *plo1-ts35* cells but less than *ssp1Δ* cells. Double mutant cells growth plateaued at a lower cell concentration than both *ssp1Δ* and *plo1-ts35* cells. In contrast, the synthetic growth phenotype of *ssp1Δ plo1-ts18* cells presented as increased growth at 25°C than both parental strains. At 35°C *ssp1Δ plo1-ts18* cells had increased growth compared to *plo1-ts18* cells but slower growth compared to *ssp1Δ* cells (Figure 4-8B).

Analysis of septation in *ssp1Δ plo1-ts18* cells also indicated synthetic phenotypes. As discussed, *plo1-ts18* cells displayed an array of septation

phenotypes (approximately 62% Class A, 6% Class C, 7% Class D, 12% Class F and 12% Class G). However, the combination of *ssp1Δ* and *plo1-ts18* masked the *plo1-ts18* phenotype; double mutant cells had approximately 50% Class A, 3% class C, 35% Class F and 10% Class G bearing a closer resemblance to *ssp1Δ* cells (55% Class A and 45% Class F). This combined evidence indicates a genetic interaction between the *ssp1* and *plo1* genes, however epistasis and the order of interaction remains difficult to discern at this point.

A synthetic phenotype was not present in *ssp2Δ plo1-ts18* cells as double mutant cells grew at a comparable rate to *ssp2Δ* cells at all tested temperatures. However, ssp2 may be a negative regulator of *plo1*, chromosomal deletion of *ssp2* in *plo1-ts18* mutant cells negated the *plo1-ts18* phenotype of limited growth at 25°C. The deletion of *amk2* or *cbs2* in *plo1-ts18* cells caused an interesting synthetic phenotype where double mutant cells exhibited increased growth at 25°C in comparison to the respective parental strains. Interestingly, a second AMPKα orthologue has been described in *S. pombe*, termed *ppk9* (Hanyu *et al.*, 2009; Matsusaka *et al.*, 1995). As interactions were present between *plo1* and *amk2* and *cbs2*, it is possible that Plo1p interacts with *S. pombe* AMPK but only in the context of the Ppk9p-Amk2p-Cbs2p heterotrimer and not the Ssp1p-Amk2p-Cbs2p complex.

4.2.3.3 *mid1* double mutants

Genetic interactions were detected between *mid1* and *ssp1, ssp2, amk2* and cbs2; in each case double mutant strains showed a partial recovery of the *mid1Δ* temperature sensitivity between 30-35°C, whereby double mutant cells were able to grow faster than *mid1Δ* cells but not as well as the respective *ssp1Δ* or AMPK deletion parental strain (Figure 4-14). Although the synthetic phenotypes appeared subtle, as *mid1* was described to interact with *ssp1, ssp2, amk2* and *cbs2*, it is likely that the genetic interactions reflect a functional interaction between the encoded proteins.

Ssp1p has been shown to regulate mitotic entry by phosphorylating Cdr2p (Deng *et al.*, 2014). Cdr2p localises to the cortical nodes with a number of proteins including Mid1p, with which Cdr2p co-immunoprecipitates (Moseley *et al.*, 2009). Cdr2p is the *S. pombe* orthologue of human brain-specific kinase 1/2 (BRSK1/2),

an AMPK-related kinase (ARK). ARKs are characterised by sequence similarity around T172 of AMPKα and require T172 (or orthologous residue) to be phosphorylated for activation. (Lizcano *et al.*, 2004). In human cells LKB1 can phosphorylate all 12 ARKs (Lizcano *et al.*, 2004). Therefore the observed genetic interaction between *ssp1* and *mid1* may indicate a number of outcomes which are not mutually exclusive; a direct interaction between Ssp1p and Mid1p (A in Figure 4-19); Ssp1p may influence Mid1p through the Ssp2p heterotrimer (B in Figure 4-19); Ssp1p may influence Midp1 through the ARK Cdr2p as previously indicated (C in Figure 4-19) (Moseley *et al.*, 2009); Ssp1p may influence Mid1p by an unidentified pathway (D in Figure 4-19). As a genetic interaction was noted between each of the genes encoding the AMPK subunits with *mid1*, it would be expected that the Ssp2p heterotrimer would have a role in the regulation of Mid1p along with Ssp1p.
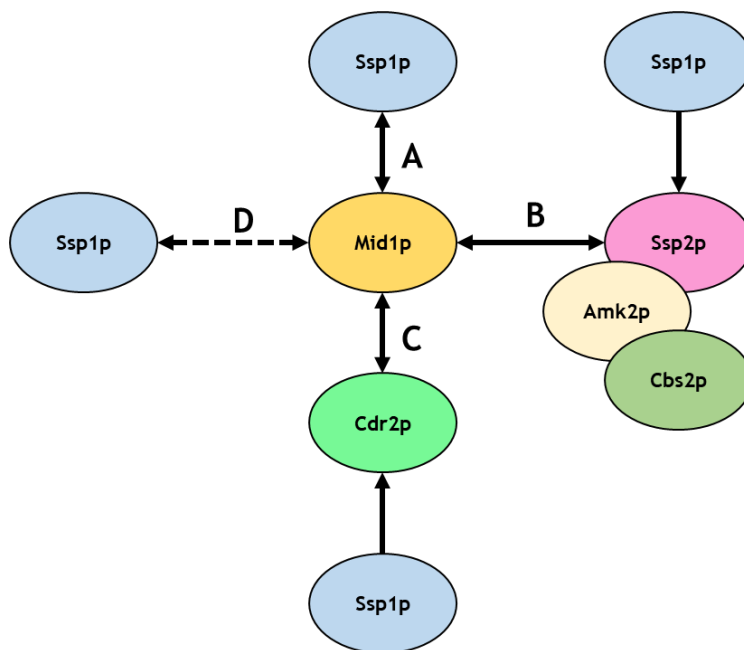
Figure 4-19. Ssp1p may regulate Mid1p in a number of ways
Ssp1p may interact with Mid1p directly (scenario A). Ssp1p may influence Mid1p by activating the Ssp2p heterotrimer, scenario B. Ssp1p may regulate Mid1p through activation of Cdr2p, scenario C. Alternatively, Ssp1p may influence Mid1p by an unidentified mechanism, scenario D. These scenarios are not mutually exclusive.

4.2.3.4 ESCRT double mutants

A number of double mutant strains were generated utilising chromosomal deletions of selected components of the ESCRT pathway and either *ssp1Δ, ssp2Δ, amk2Δ* or *cbs2Δ*. The majority of these double mutant strains did not display any synthetic growth phenotypes when assessed by serial dilution (Appendix 2).

However, synthetic phenotypes were detected in *ssp1Δ vps2Δ* and *ssp1Δ vps4Δ* strains. Interestingly, *ssp1Δ, vps2Δ* and *vps4Δ* all had similar septation defects, with a comparable reduction in Class A phenotypes and increased prevalence of Class F phenotype. As genetic interactions were observed between *vps2/vps4* and *ssp1* but not *amk2* or *cbs2*, this may indicate that Ssp1p regulation of the ESCRT-III pathways is mediated by an AMPK-independent pathway although *ssp2Δ vps2Δ* and *ssp2Δ vps4Δ* strains were not generated so a role for AMPK should not be ruled out. Both *vps2* and *vps4* encode proteins which function at the end of the ESCRT cascade and are involved in catalysing abscission. This could indicate that *ssp1* may function in regulating the final stages of ESCRT recruitment to the midbody or by regulating Vps4p ATPase activity, rather than having a role earlier in the ESCRT pathway.

4.2.4 Summary

The results presented in this Chapter are the first to link the AMPK pathway to *ark1, plo1, mid1* and the ESCRT pathways in *S. pombe*. This further supports the hypothesis that the AMPK pathway has a role in mitosis and cytokinesis. In the following Chapter, the yeast genetic interactions will be investigated further in a mammalian system. *In vitro* protein phosphorylation assays will be utilised to demonstrate a functional link between the interacting proteins.

5 Chapter 5–Phosphorylation of mammalian mitotic proteins by AMPK and CaMKKβ

5.1 Introduction

In Chapter 3 a role for AMPK was described in the control and fidelity of the cell cycle in mammalian cells. Additionally, in Chapter 4 the fission yeast AMPK pathway was suggested to interact genetically with a number of key mitotic proteins as follows;

- *ssp2, amk2* and *ssp1* interacted with *ark1*

- *amk2, cbs2* and *ssp1* interacted with *plo1*

- *ssp2, amk2, cbs2* and *ssp1* interacted with *mid1*

- *ssp1* interacted with *vps2*

- *ssp1* interacted with *vps4*

The AMPK heterotrimer is well conserved between humans and *S. pombe* with the fission yeast AMPK being composed of Ssp2p (AMPKα subunit), Amk2p (ß) and Cbs2p (γ) (Hanyu *et al.*, 2009). *S. pombe ssp1* is orthologous to CaMKKß but functionally is more similar to LKB1 (Hanyu *et al.*, 2009). The human orthologues of the mitotic proteins are also well conserved from fission yeast, Ark1p is orthologous to the aurora kinase family in human cells which have diverged to form 3 paralogues termed aurora A-C which have distinct functions (Bischoff *et al.*, 1998; Giet and Prigent, 1999). Plo1p has also been conserved as the PLK family in human cells, PLK1 is more conserved in terms of sequence and function to *plo1* whereas PLK2-5 have diverged further (Kothe *et al.*, 2007). Mid1p is orthologous to human anillin which acts as a scaffold protein and is an integral component of the actomyosin ring which mediates early stages of cytokinesis (Piekny and Glotzer, 2008). Vps2p and Vps4p function as part of the ESCRT machinery; Vps2p (CHMP2A/B in mammalian cells) forms part of the ESCRT-III machinery involved in abscission and Vps4p (also Vps4 in human cells) is an AAA-ATPase crucial to the recycling of ESCRT subunits and abscission (Carlton and Martin-Serrano, 2007; Su *et al.*, 2017).

In this Chapter, many of the genetic interactions identified in Chapter 4 were investigated further in a mammalian system. First, a functional link between LKB1 and aurora A, aurora B and PLK1 was assessed in transgenic HeLa cells. Secondly, a series of *in vitro* phosphorylation assays were performed using mammalian proteins.

5.2 Results

5.2.1 LKB1 function does not influence mitosis in HeLa cells

HeLa cells do not express LKB1 (LKB1 -/-), so genetically modified HeLa cells were utilised to examine how LKB1 expression/activity could influence the cell cycle. These cells either expressed FLAG-tagged wild type-LKB1 (WT-LKB1) or kinase dead-LKB1 (KD-LKB1) under the control of a tetracycline inducible promoter (Sapkota *et al.*,2002). Both constructs could be induced by the incubation with tetracycline although expression of KD-LKB1 was lower than that of WT-LKB1 (Figure 5-1). As anticipated in LKB1 -/- HeLa cells, AICAR (1 mM, 1 h) caused an increase in phospho-S79 ACC but did not alter phospho-T172 AMPK indicating the allosteric effect of AICAR/ZMP on AMPK activity (Figure 5-1). Similarly, in KD-LKB1 expressing cells, AICAR stimulated phosphorylation of ACC but not AMPK (Figure 5-1). WT-LKB1 HeLa cells had higher basal and AICAR-stimulated phosphorylation of ACC, an increase in phospho-T172 AMPK was also apparent following stimulation with AICAR as expected (Figure 5-1).

Next the subcellular localisation of LKB1 in these cells was investigated by immunofluorescence microscopy. Staining of LKB1 -/- HeLa cells with anti-LKB1 antibodies produced low levels of non-specific immunoreactivity (Figure 5-1). Higher levels of LKB1 immunoreactivity were detectable in both LKB1-WT and LKB1-KD HeLa cells, which localised to the cytoplasm and nucleus (Figure 5-1). LKB1 also localised to the intracellular bridge but not to the midbody.
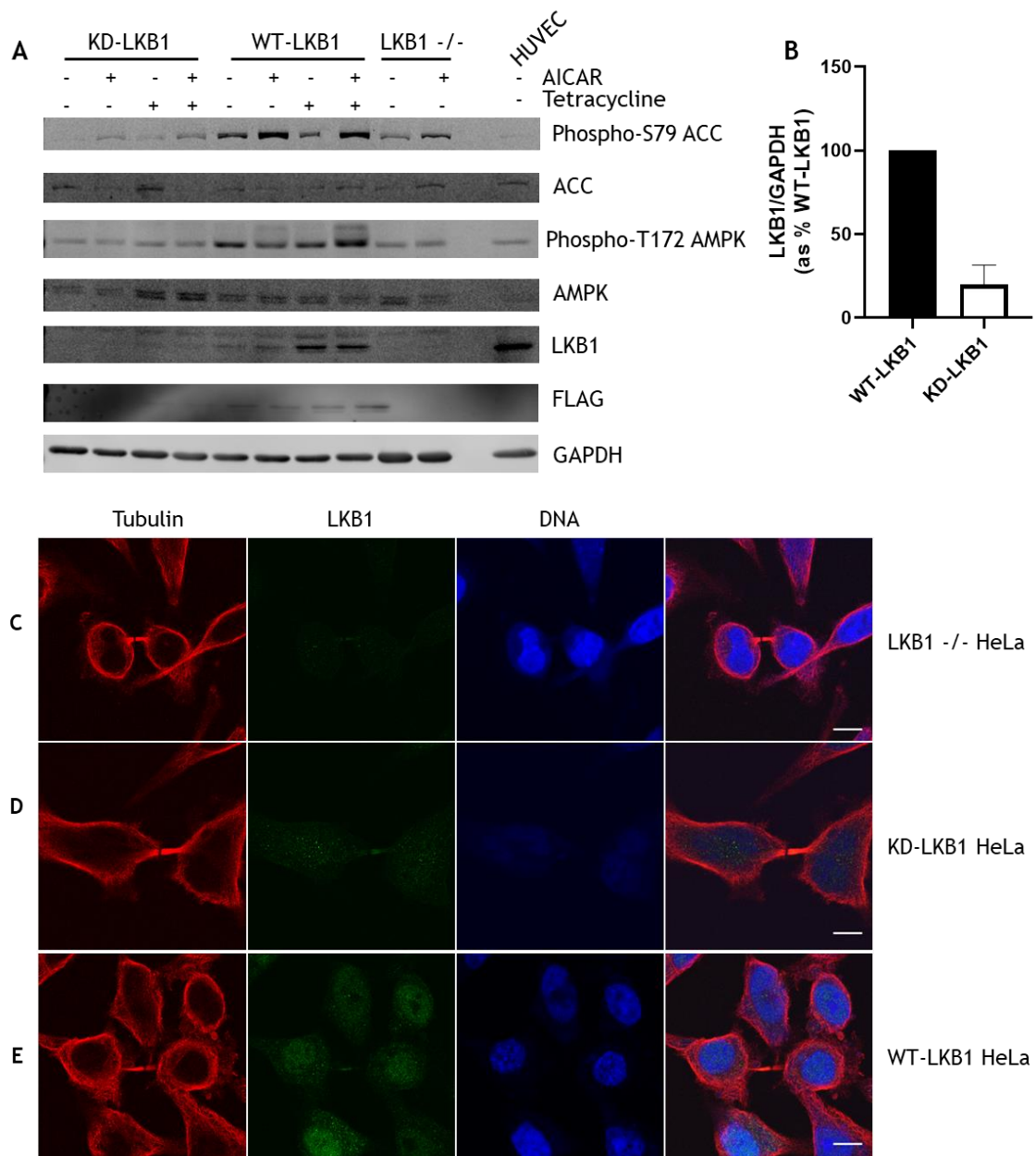
Figure 5-1. Subcellular localisation of LKB1 during telophase
(A) KD-LKB1 or WT-LKB1 HeLa cells were incubated in the presence or absence of tetracycline (1 µg/ml) for 24 h to induce expression of FLAG-tagged mutant LKB1. KD-LKB1, WT-LKB1 and LKB1 -/- HeLa cells were subsequently incubated in the presence or absence of AICAR (1 mM, 1 h) and lysates prepared. Lysates were resolved by SDS-PAGE and subjected to immunoblotting with the antibodies indicated, a HUVEC lysate was included as a positive control. N=1. **(B)** Quantification of tetracycline-induced LKB1 expression relative to GAPDH. Presented as %WT-LKB1 expression. N=4. **(C-E)** KD-LKB or WT-LKB1 HeLa cells were incubated with tetracycline (1 µg/ml) for 24 h. LKB1 -/-, KD-LKB1 or WT-LKB1 HeLa cells were fixed with 4% (w/v) PFA and stained with anti-tubulin (Abcam, ab6160) and anti-LKB1 (New England Biolabs, #3050) antibodies. DNA was stained with RedDot2. Scale bar=10 µm. Representative images are shown from three independent experiments in each case.

As a genetic interactions were described between the AMPK kinase *ssp1* and both *ark1* and *plo1* in Chapter 4, the localisation of their mammalian orthologues (aurora A/aurora B and PLK1) was assessed in WT-LKB1, KD-LKB1 HeLa cells, LKB1 -/- Hela cells and HUVECs. Aurora A immunoreactivity was observed in the cytoplasm and nuclei of all tested cell lines (Figure 5-2). Midbody localisation of aurora A was only observed in HUVECs (Figure 5-2). In HeLa cells, there was enrichment of aurora A at the intracellular bridge but not at the midbody proper (Figure 5-2). Similarly, aurora B immunoreactivity was detected in the cytoplasm and nuclei of LKB1 -/- HeLa cells, LKB1-KD HeLa cells, LKB1-WT HeLa cells and HUVECs (Figure 5-3). Midbody localisation of aurora B was only observed in HUVECs (Figure 5-3). Finally, PLK1 immunoreactivity was detected in the cytoplasm and nuclei of all tested cells and at the midbody in HUVECs (Figure 5-4).
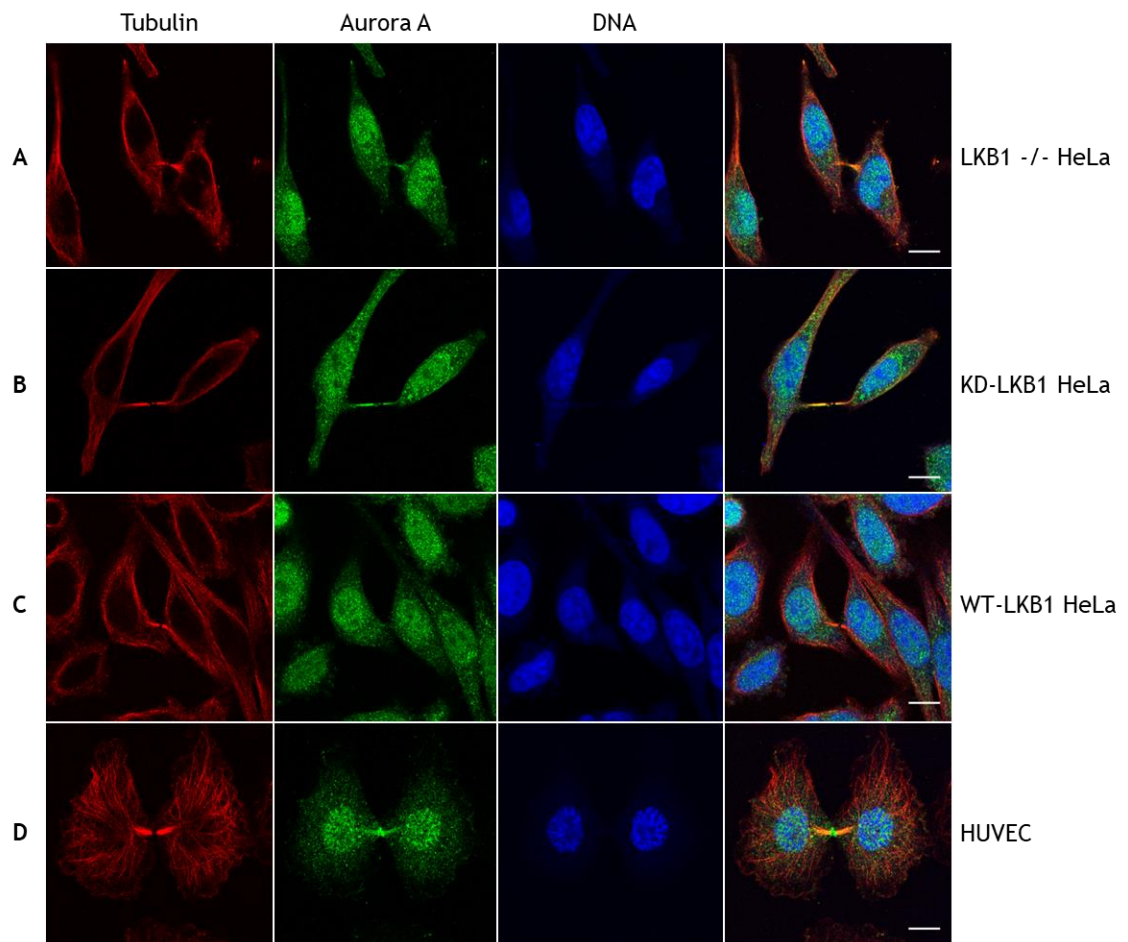
Figure 5-2. Subcellular localisation of aurora A during telophase
(A) LKB1 -/- HeLa cells, **(B)** KD-LKB1 HeLa cells, **(C)** WT-LKB1 HeLa cells and **(D)** HUVECs were fixed with 4% (w/v) PFA. Cells were stained with anti-tubulin (Abcam, ab6160) and anti-aurora A (Abcam, ab1287) antibodies. DNA was stained with RedDot2. KD-LKB1 and WT-LKB1 HeLa cells were pre-treated with tetracycline (1 µg/ml) for 24 h. Scale bar=10 µm. Representative images are shown from three independent experiments in each case.
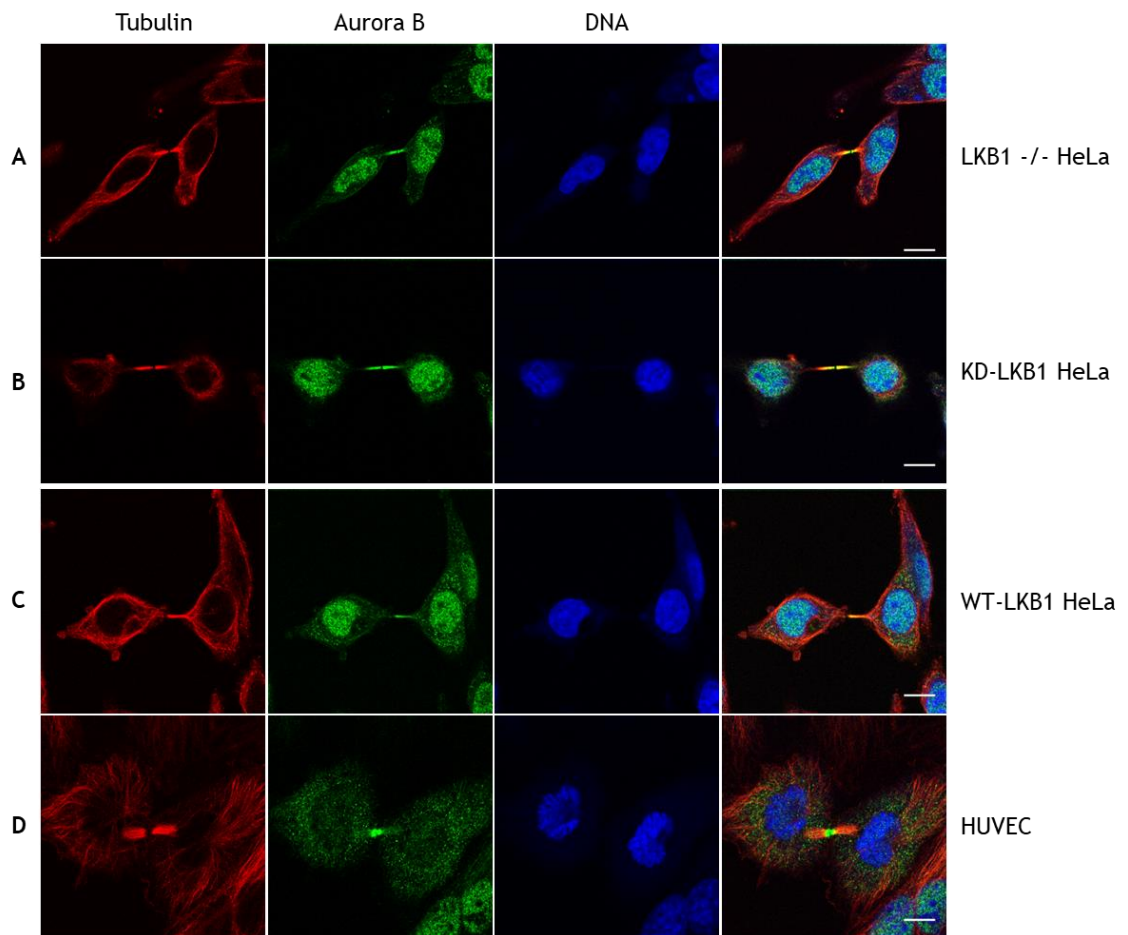
Figure 5-3. Subcellular localisation of aurora B during telophase
(A) LKB1 -/- HeLa cells, **(B)** KD-LKB1 HeLa cells, **(C)** WT-LKB1 HeLa cells and **(D)** HUVECs were fixed with 4% (w/v) PFA. Cells were stained with anti-tubulin (Abcam, ab6160) and anti-aurora B (Abcam, ab2254) antibodies. DNA was stained with RedDot2. KD-LKB1 and WT-LKB1 HeLa cells were pre-treated with tetracycline (1 µg/ml) for 24 h. Scale bar 10=µm. Representative images are shown from three independent experiments in each case.

	Tubulin	PLK1	DNA	
A				LKB1 -/- HeLa
B				KD-LKB1 HeLa
C				WT-LKB1 HeLa
D				HUVEC
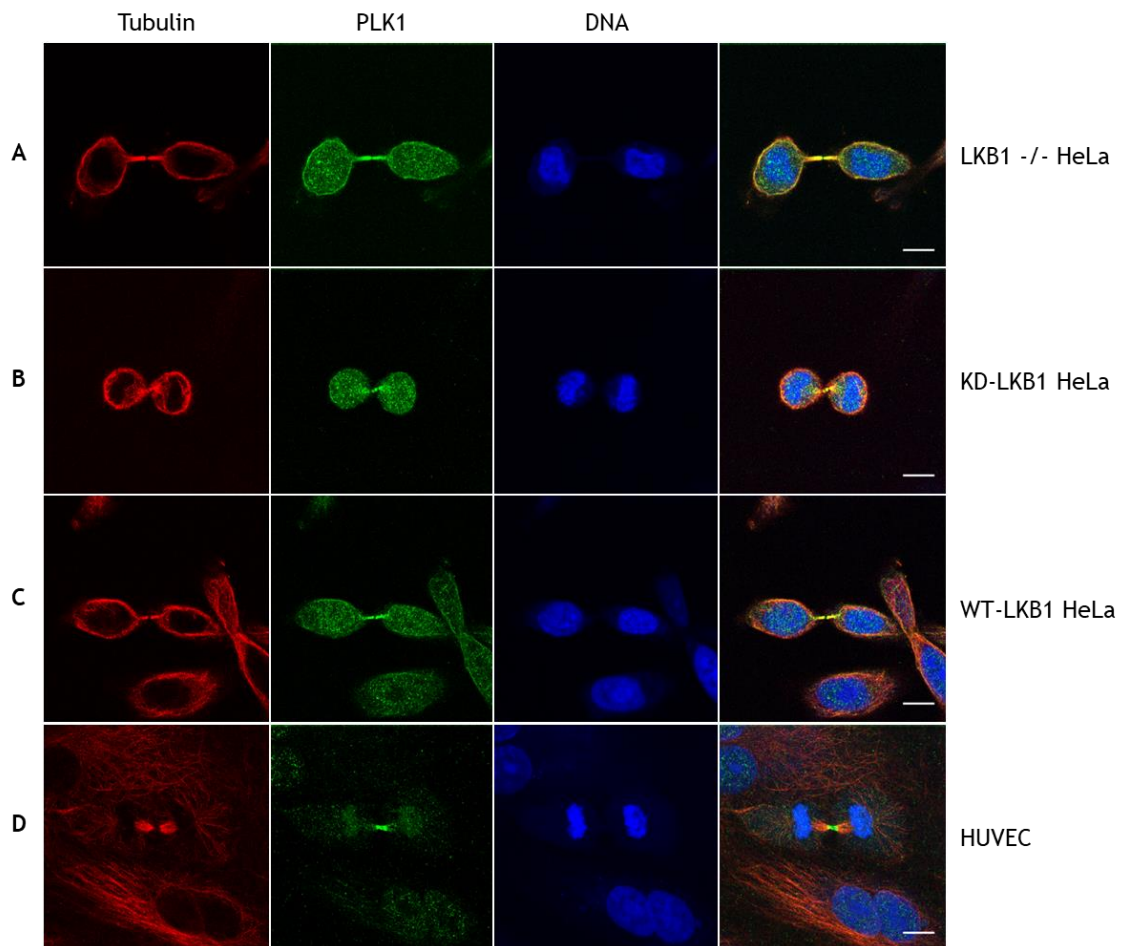
Figure 5-4. Subcellular localisation of PLK1 during telophase
(A) LKB1 -/- HeLa cells, **(B)** KD-LKB1 HeLa cells, **(C)** WT-LKB1 HeLa cells and **(D)** HUVECs were fixed with 4% (w/v) PFA. Cells were stained with anti-tubulin (Abcam, ab6160) and anti-PLK1 (Novus Biologicals, NB-100-547) antibodies. DNA was stained with RedDot2. KD-LKB1 and WT-LKB1 HeLa cells were pre-treated with tetracycline (1 µg/ml) for 24 h. Scale bar 10=µm. Representative images are shown from three independent experiments in each case.

Next, the expression of WT-LKB1 or KD-LKB1 on HeLa cell polyploidy was assessed. Cells were incubated with AMPK activators or inhibitors for 18 h prior to staining with PI and assessment of DNA content by flow cytometry. Expression of either WT-LKB1 or KD-LKB1 did not influence HeLa cell DNA content (Figure 5-5). Compound C (10 µM) caused a significant reduction in the proportion of KD-LKB1 cells with 2n DNA coinciding with an increase in the proportion of cells with 4n DNA (Figure 5-5). In contrast, compound C did not significantly alter DNA content of WT-LKB1 HeLa cells (Figure 5-5). Incubation with STO-609, A769662, AICAR or canagliflozin did not alter the DNA content of either KD-LKB1 or WT-LKB1 HeLa cells.

HeLa cells which expressed KD-LKB1 had low basal levels of phospho-S79 ACC which did not increase in response to either AICAR, A769662 or canagliflozin (Figure 5-5I). A769662 and AICAR significantly increased phospho-S79 ACC in WT-LKB1 HeLa cells, however, canagliflozin did not stimulate AMPK activity. Neither STO-609 nor compound C reduced basal phospho-S79 ACC levels in either cell type (Figure 5-5I). Expression of LKB1 was markedly lower in KD-LKB1 expressing cells. Surprisingly, both compound C and AICAR significantly increased levels of WT-LKB1 relative to GAPDH (Figure 5-6). AICAR stimulated an increase in phospho-T172 AMPK in WT-LKB1 HeLa cells but not in KD-LKB1 HeLa cells, no other treatments altered phospho-T172 AMPK (Figure 5-6).
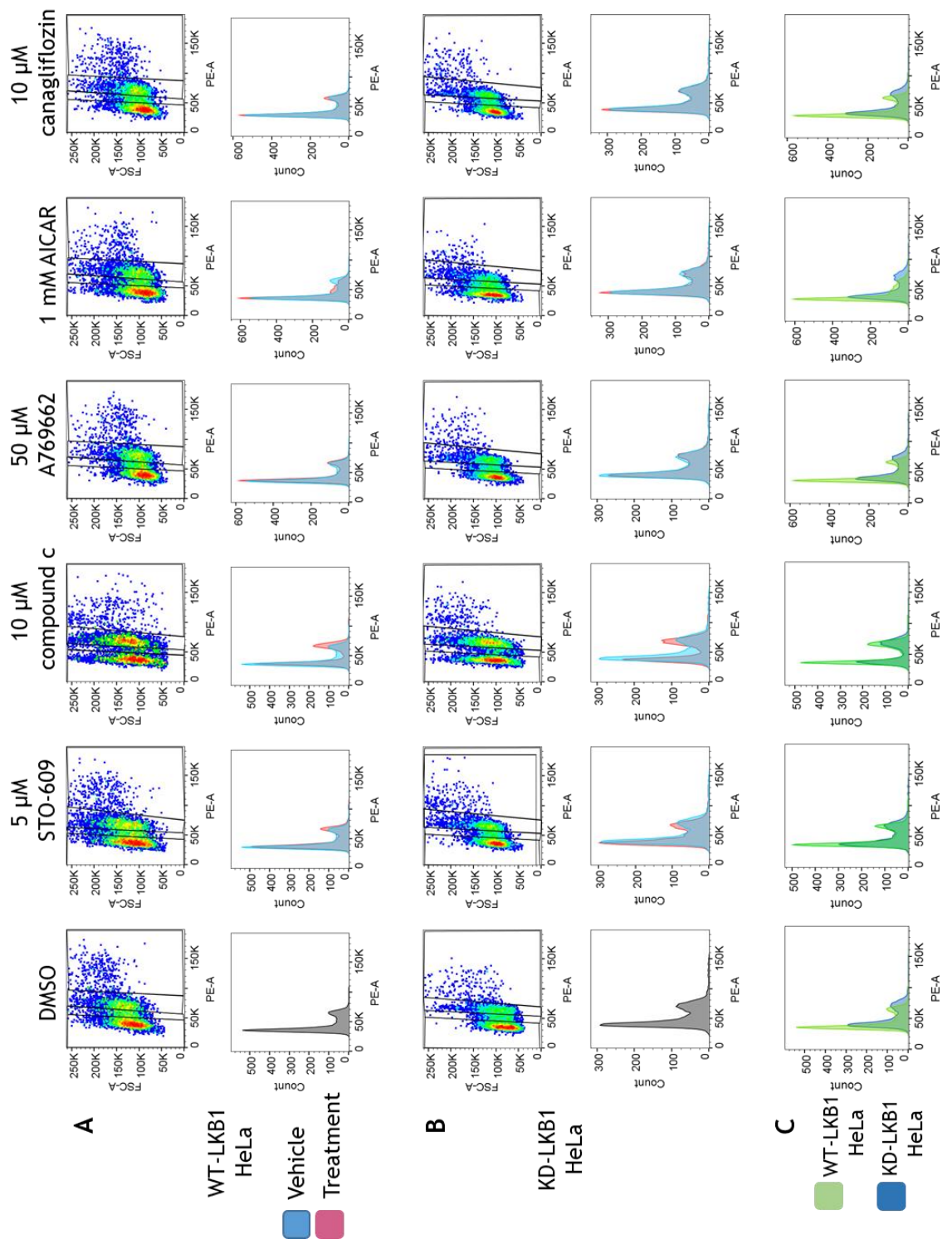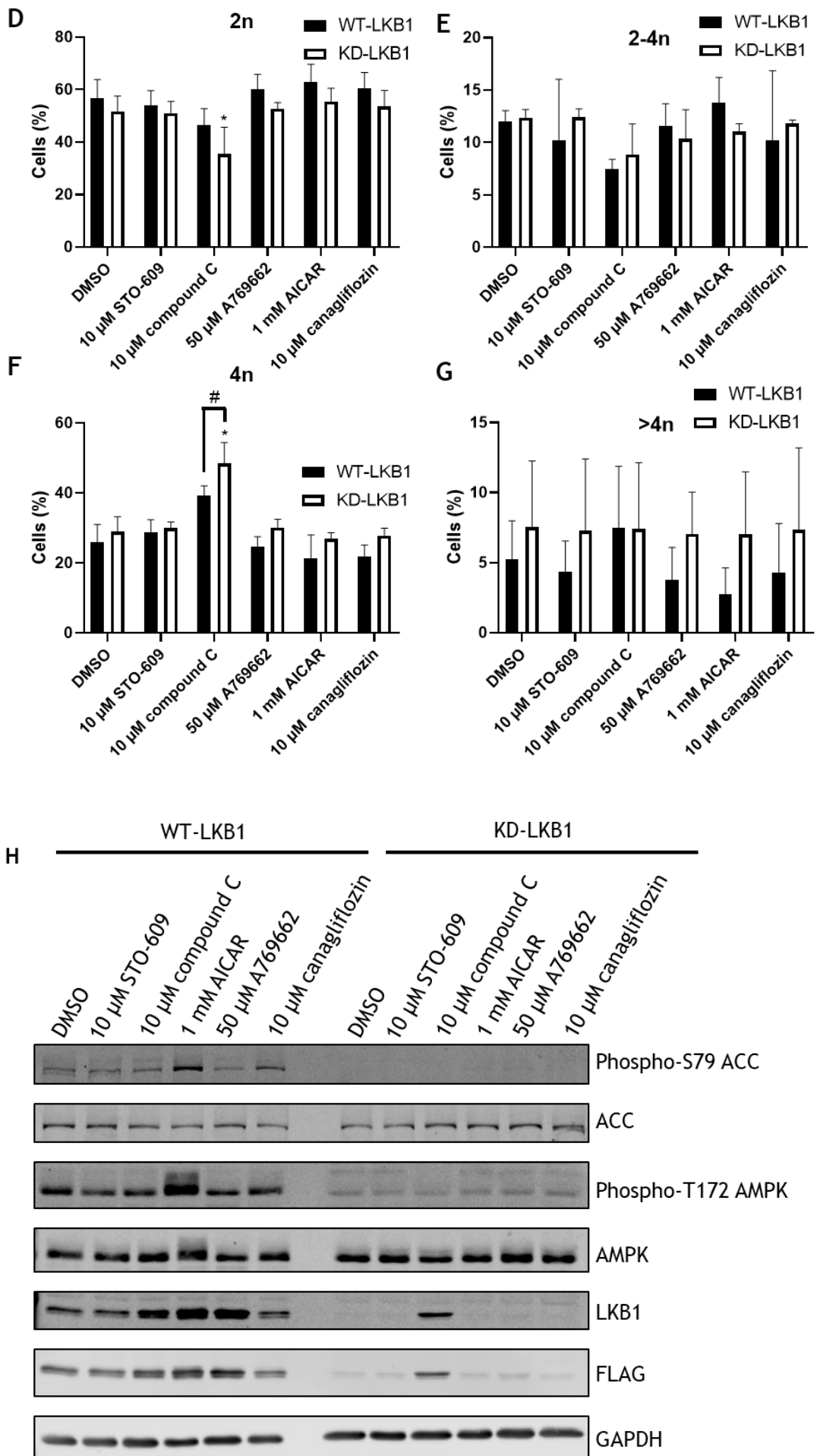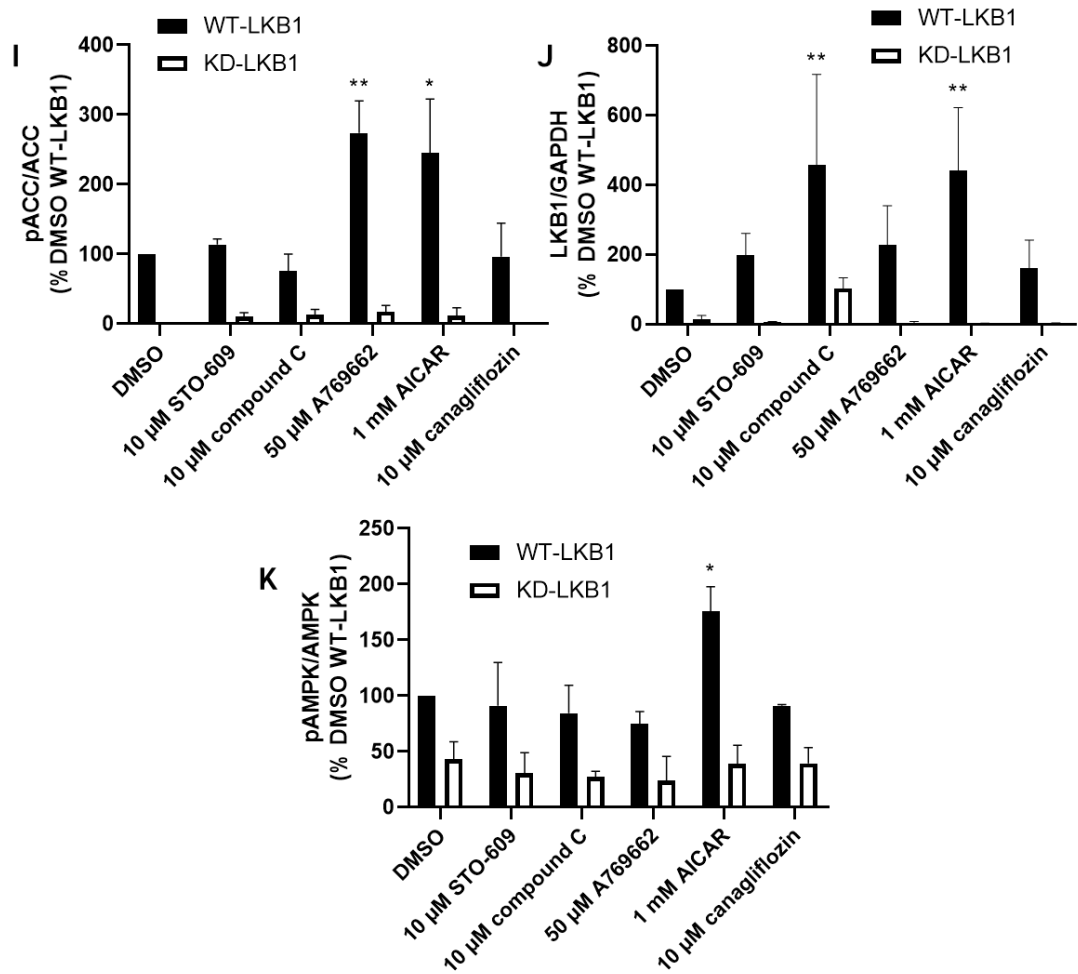
Figure 5-5. The effect of modulating AMPK activity on the DNA content of WT- and KD-LKB1 expressing HeLa cells

KD-LKB1 and WT-LKB1 inducible HeLa cells were pre-treated with tetracycline (1 μg/ml) for 24 h. HeLa cells were then seeded into 6-well plate and incubated for 4 h until cells adhered. Cells were subsequently treated as indicated for 18 h with tetracycline (1 μg/ml). **(A)** Representative scatter plots and histogram overlays comparing DMSO (blue) with activator/inhibitor treated cells (pink) of WT-LKB1 HeLa cells. **(B)** Representative scatter plots and histogram overlays comparing DMSO (blue) with activator/inhibitor treated cells (pink) of KD-LKB1 HeLa cells. **(C)** Comparison of WT-LKB1 (green) and KD-LKB1 (blue) HeLa histograms. **(D-G)** Analysis of the proportion of cells with 2n, 2-4n, 4n or >4n DNA content presented as % cells ± SEM from 3 independent experiments. **(H)** HeLa cells were treated with the indicated compounds for 18 h and lysates prepared. Lysates were resolved by SDS-PAGE and immunoblotted using the antibodies indicated. Representative images are shown. **(I)** Quantification of phospho-S79 ACC relative to total ACC, presented as % DMSO of WT-LKB1 ± SEM. **(J)** Quantification of LKB1 relative to GAPDH, presented as % DMSO of WT-LKB1. **(K)** Quantification of phospho-T172 AMPK relative to total AMPK, presented as % DMSO of WT-LKB1. * $p < 0.05$, ** $p < 0.01$ relative to cells incubated with DMSO and # $p < 0.05$ as indicated (two-way ANOVA). N=3.

5.2.2 Development of *in vitro* phosphorylation assays

To examine the genetic interactions outlined in Chapter 4 further, *in vitro* phosphorylation assays were undertaken using mammalian protein orthologues. As many of the described genetic interactions were between kinases, "kinase dead" (KD) mutant proteins were utilised as substrates to limit autophosphorylation and to ensure *in vitro* phosphorylation occurred only from the active kinase in question to the substrate and not the reverse. A number of experiments were first undertaken to optimise the *in vitro* phosphorylation assays and generation of substrate proteins, which will be outlined in this Section.

HEK 293 cells were transfected with plasmids encoding genes for substrates (KD-aurora A-mCherry, KD-aurora B-GFP, KD-PLK1-YFP, CHMP2A-GFP, CHMP2B-GFP, GFP or mCherry) and harvested after 48 h. Lysates were resolved by SDS-PAGE and interrogated by immunoblotting. Successful expression of KD-aurora A-mCherry was confirmed by probing with anti-aurora A and anti-mCherry antibodies (Figure 5-6A). KD-aurora A-mCherry appeared as a two distinct species when probed with either of the antibodies (Figure 5-6A). The higher molecular mass species represented the molecular mass expected for the fusion protein (~72 kDa). Expression of KD-PLK1-YFP was confirmed by probing with anti-PLK1 and anti-GFP (which also recognises YFP isoforms) antibodies (Figure 5-6B/E). mCherry expression was confirmed by probing with anti-mCherry antibodies (Figure 5-6D). Finally the expression of GFP, CHMP2A-GFP and KD-aurora B-GFP was confirmed by probing with anti-GFP antibodies (Figure 5-6C/E). No obvious GFP immunoreactivity was observed in HEK 293 cells transfected with plasmids encoding CHMP2B-GFP.
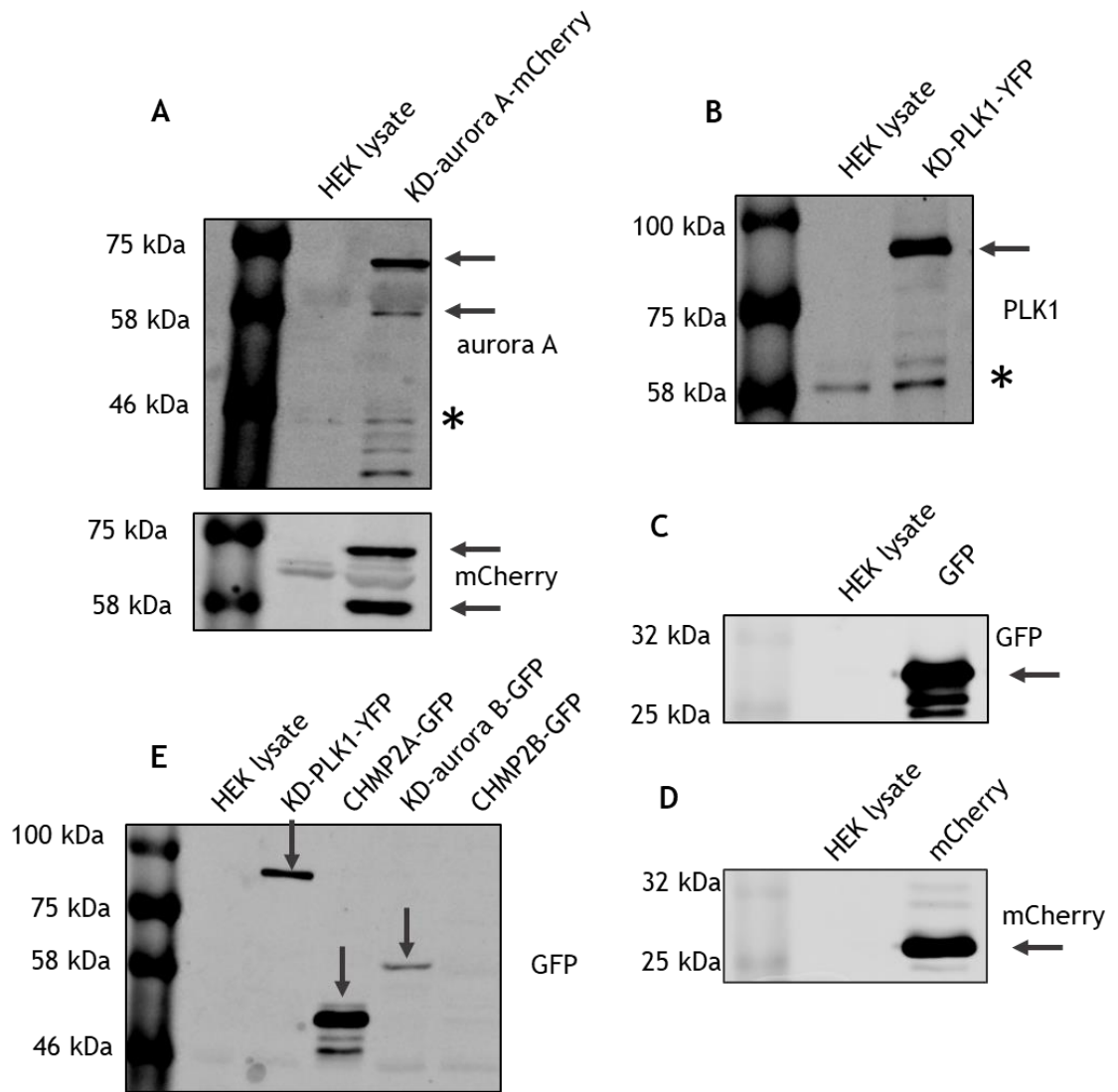
Figure 5-6. Expression of substrates for *in vitro* phosphorylation assays in HEK 293 cells
HEK 293 cells were transfected with the indicated plasmids and incubated for 48 h and lysates prepared. Lysates were resolved by SDS-PAGE and immunoblotted with the antibodies indicated. HEK 293 cells were transfected with **(A)** A plasmid expressing KD-aurora A-mCherry. **(B)** A plasmid expressing KD-PLK1-YFP. **(C)** A plasmid expressing GFP. **(D)** A plasmid expressing mCherry. **(E)** Plasmids expressing either KD-PLK1, CHMP2A-GFP, KD-aurora B-GFP or CHMP2B-GFP. Note that anti-GFP antibodies also bind YFP isoforms. Arrows indicate the proteins at the expected molecular masses. * Endogenous aurora A or PLK1.

To generate a kinase dead AMPK, HEK 293 cells were infected with adenoviruses encoding a dominant negative AMPKα1 mutant (Ad.AMPKα1-DN). This mutant AMPK contained a myc tag and a D157A mutation to render it inactive (KD-AMPKα1-myc) (Woods *et al.*, 2000). Cells were lysed after 24 h and KD-AMPKα1 immunoprecipitated with anti-myc nanobodies conjugated to magnetic beads. The resultant immunoprecipitate (IP) and immunodepleted lysate (ID) were subjected to immunoblotting for AMPK subunits and myc. AMPKα1 and AMPKβ1 were successfully detected in the immunoprecipitate (Figure 5-7).
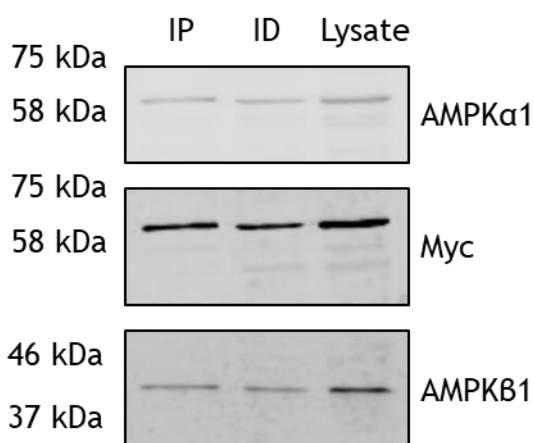
Figure 5-7. Immunoprecipitation of KD-AMPKα1-myc from adenovirus infected HEK 293 cells

HEK 293 cells were infected with Ad.AMPKα1-DN for 24 h. Lysates were prepared and incubated with anti-myc conjugated magnetic beads for 1 h with rotation at 4°C. Supernatant was removed and retained as the immunodeplete (ID). Samples were resolved by SDS-PAGE and subjected to immunoblotting with the indicated antibodies. N=1.

The final substrate for *in vitro* phosphorylation assays to be generated was KD-LKB1 which was immunoprecipated from KD-LKB1 HeLa cells using anti-FLAG antibodies (Sapkota *et al.*, 2002). KD-LKB1 was successfully immunoprecipated and 5 µl of the IP was sufficient to provide a detectable signal when probed with anti-LKB1 antibodies (Figure 5-8).
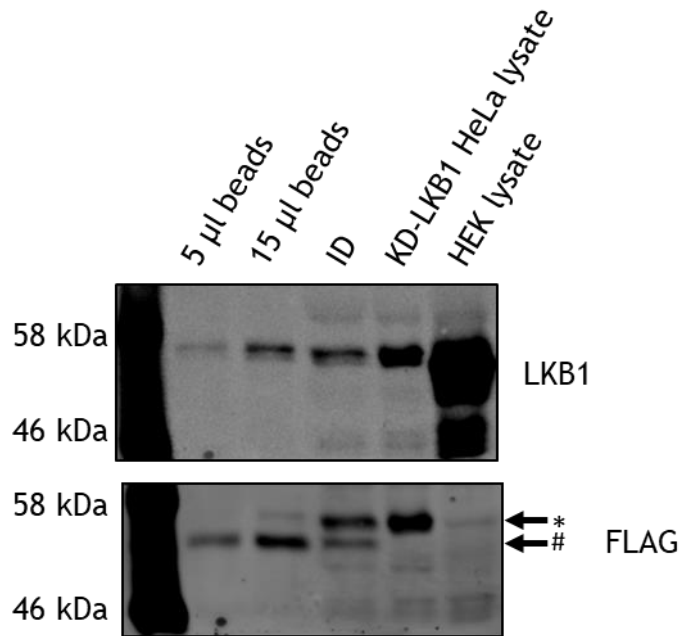
Figure 5-8. Immunoprecipitation of KD-LKB1-FLAG from transgenic HeLa cells
KD-LKB1 HeLa cells were incubated with tetracycline (1 µg/ml) for 24 h to induce expression of FLAG-tagged KD-LKB1 and lysates prepared. Anti-FLAG antibodies were bound to magnetic beads and incubated with lysates overnight with rotation at 4°C. Supernatant was removed and retained as the immunodeplete (ID). Beads were resuspended in 20 µl LSB. Samples were resolved by SDS-PAGE and subjected to immunoblotting with the antibodies indicated. * LKB1-FLAG, # IgG heavy chain. N=1.

To reduce any endogenous phosphorylation of immunoprecipitated proteins, dephosphorylation assays were performed. To track dephosphorylation, AMPK T172 was examined due to the ease of immunoprecipitation and phospho-antibody availability. AMPK was immunoprecipitated from a 2-6.5% PEG isolate of rat liver and incubated with λ-phosphatase as described in Section 2.16.2. IP pellet was resolved by SDS-PAGE and immunoblotted for phospho-T172 AMPK. Incubation with 400 U λ-phosphatase substantially dephosphorylated AMPK T172 (Figure 5-9).
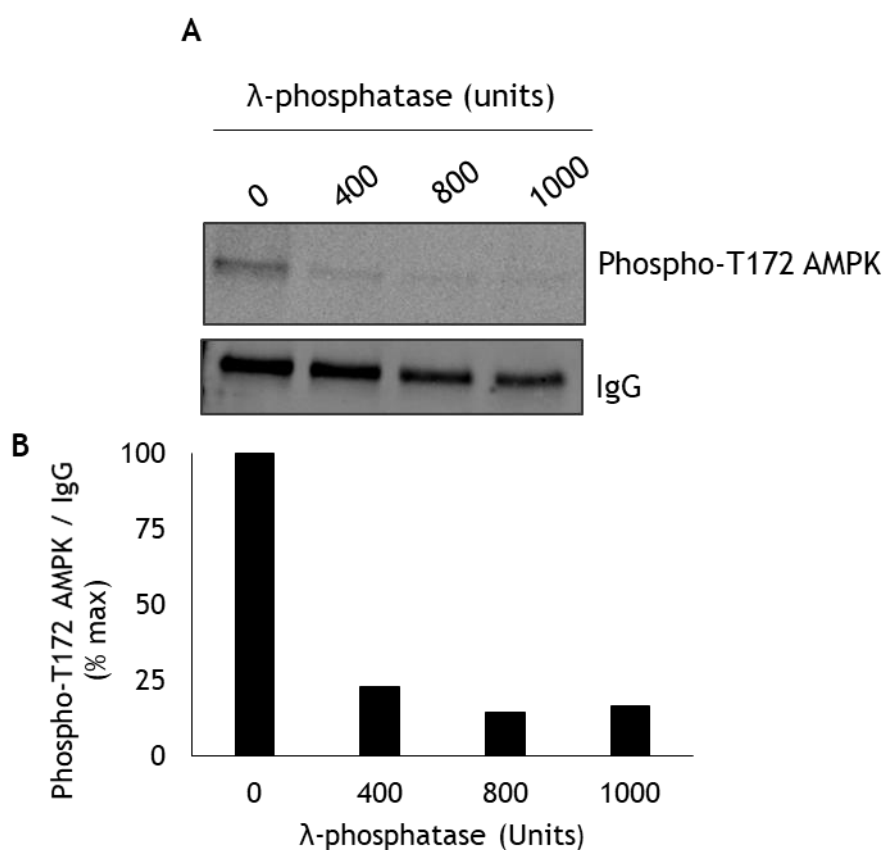
Figure 5-9. Dephosphorylation of rat liver AMPK by lambda phosphatase
(A) AMPK was immunoprecipitated from a 2-6.5% PEG precipitate of rat liver. Beads (5 μl/ reaction) were incubated with lambda phosphatase at 30°C for 1 h on a shaking platform. Beads were washed and resuspended in 2x LSB. Reactions were resolved by SDS-PAGE and immunoblotted with anti-phospho-T172 AMPK antibodies and IgG examined as a loading control. **(B)** Densitometric analysis of phospho-T172 AMPK relative to IgG. N=1.

The activity of the recombinant protein kinases used to phosphorylate substrate proteins (aurora A-GST, aurora B-GST, PLK1-His, CaMKKß-GST, AMPKα1ß1γ1 or AMPKα2ß2γ1) were assayed using myelin basic protein (MBP) as a substrate. *In vitro* phosphorylation was performed as detailed in Section 2.16.3 and samples resolved by SDS-PAGE and phosphorylation of MBP was determined by phosphorimaging. All recombinant kinases phosphorylated MBP, demonstrating kinase activity (Figure 5-10).
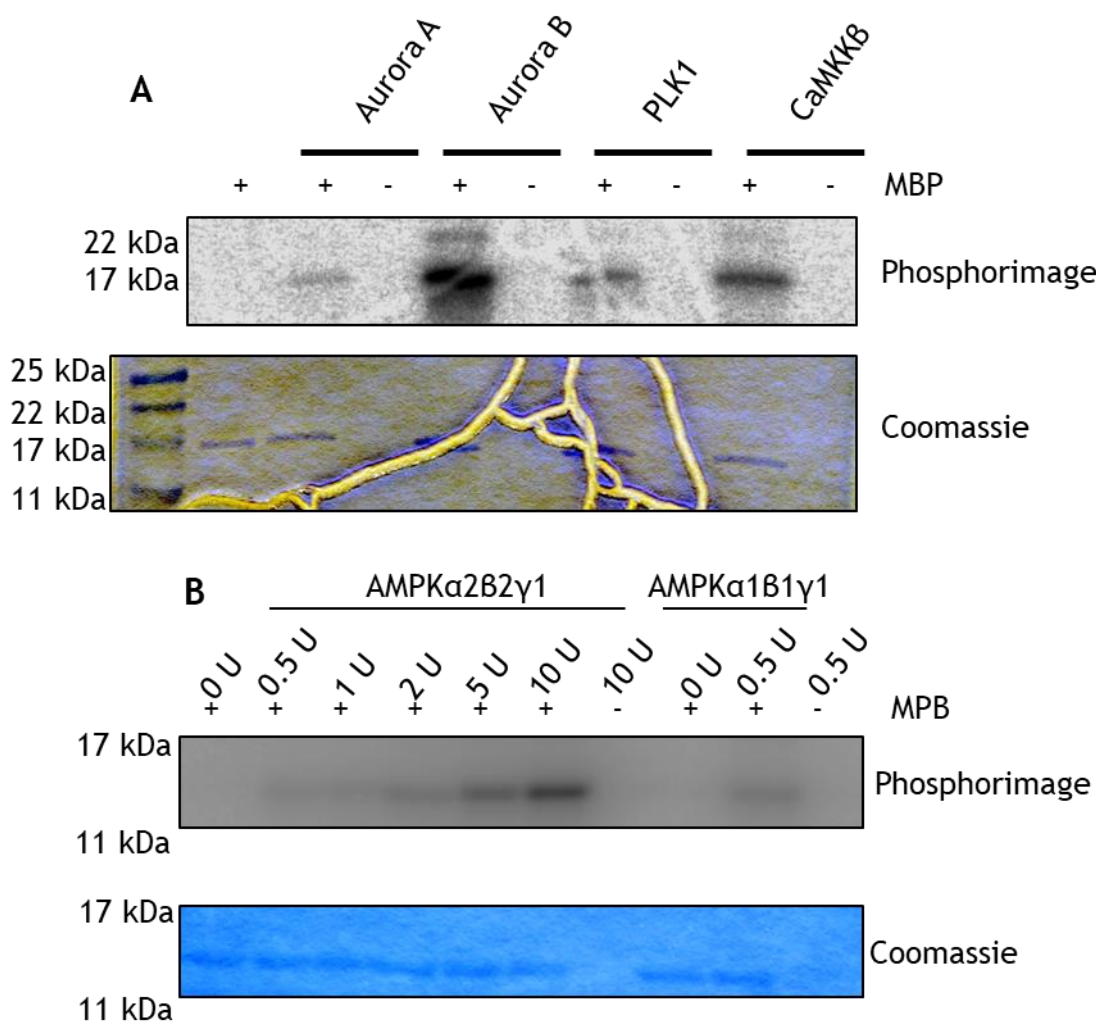
Figure 5-10. *In vitro* phosphorylation of MBP by recombinant proteins
(A) *In vitro* phosphorylation of MBP (5 µg) by aurora A-GST, aurora B-GST, PLK1-His or CaMKKβ-GST (50 ng each). **(B)** *In vitro* phosphorylation of MBP by either AMPKα1β1γ1 or AMPKα2β2γ1 (units of activity indicated, where 1 U is 1 nmol ^{32}P incorporated/min into SAMS peptide). Reactions were terminated by the addition of 2x LSB and resolved by SDS-PAGE. Gels were stained with Coomassie and dried. ^{32}P incorporation was assessed by phosphorimaging.

5.2.3 Analysis of *In vitro* phosphorylation

5.2.3.1 Aurora A phosphorylates KD-LKB1-FLAG but not DN-AMPK or CaMKKß-GST *in vitro*

KD-LKB1-FLAG was immunoprecipitated from transgenic KD-LKB1 HeLa cells using anti-FLAG antibodies as described in Figure 5-8. As a suitable control, an anti-FLAG immunoprecipitation was carried out in parallel on HeLa cell lysates (which lack LKB1). Alternatively, kinase dead AMPK (KD-AMPKα1-myc) was immunoprecipitated from HEK 293 cells infected with Ad.AMPKα1-DN using anti-myc conjugated beads as described in Figure 5-7. Additionally, an immunoprecipitation using anti-myc conjugated beads was performed on lysates prepared from Ad.Null infected HEK 293 cells. Immunoprecipitation products were incubated with active aurora A (Aurora A-GST, 50 ng) in the presence of [γ-^{32}P]ATP. Reactions were also performed using MBP (5 µg) as a positive control to demonstrate kinase activity. Products were resolved by SDS-PAGE and ^{32}P incorporation assessed using a phosphorimager.

KD-LKB1 was phosphorylated to an extent when aurora A was omitted from the reaction (figure 5-11). This could indicate the construct was not entirely kinase dead or the anti-FLAG immunoprecipitation pulled down additional kinases. Densitometric analysis of two independent experiments indicated that KD-LKB1 band intensity increased approximately 40% ± 8% when KD-LKB1 was incubated with aurora A (Figure 5-11). No incorporation of [γ-^{32}P]ATP was observed in anti-FLAG immunoprecipitates from LKB1 -/- HeLa cell lysates (Figure 5-11). No bands of the correct molecular mass could be attributed to AMPK subunits in KD-AMPKα1-myc immunoprecipitates when visualised on a phosphorimager (Figure 5-11). Anti-myc immunoprecipitation of Ad.Null infected HEK 293 cell lysates, had an identical phosphorylation pattern to immunoprecipitation of Ad.AMPKα1-DN infected HEK 293 lysates demonstrating that anti-myc immunoprecipitation lacked specificity and that aurora A did not phosphorylate KD-AMPKα1 (Figure 5-11).

Next, to determine if aurora A could phosphorylate CaMKKß-GST *in vitro*, CaMKKß-GST or GST were denatured by heating at 95°C for 5 min to abolish kinase activity. Aurora A did not phosphorylate denatured CaMKKß-GST or GST (Figure 5-12).

Figure 5-11. Analysis of *in vitro* phosphorylation of KD-LKB1 and DN-AMPK-myc by aurora A

KD-LKB1-FLAG was immunoprecipitated from KD-LKB1 HeLa cells stimulated with tetracycline (1 µg/ml, 24 h) using anti-FLAG antibodies. In parallel, an IP was performed on cell lysates prepared from LKB1 -/- HeLa cells. KD-AMPKα1-myc was immunoprecipitated from Ad.AMPKα1-DN infected HEK 293 cell lysates using anti-myc conjugated beads. Simultaneously an IP was performed using anti-myc conjugated beads on cell lysates from Ad.Null infected HEK 293 cells. MBP (5 µg) was also used as a substrate for aurora A. Substrate were incubated in the presence or absence of 50 ng aurora A-GST and [γ-^{32}P]ATP for 30 min at 30°C. Reactions were terminated by the removal of the supernatant and addition of 2x LSB. Alternatively, Alternatively 4x LSB was added to reactions using MBP as a substrate or reactions when substrate was omitted. Reactions were resolved by SDS-PAGE and resulting gels stained with Coomassie, dried and ^{32}P incorporation assessed using a phosphorimager **(A)** Representative phosphorimage and coomassie stained gel. **(B)** Densitometric analysis of KD-LKB1-FLAG phosphorylation by aurora A. Data shown as ± SEM. N=2.

Figure 5-12. Analysis of *in vitro* phosphorylation of CaMKKβ-GST by aurora A
CaMKKβ-GST or GST (500 ng) were heated at 95°C for 5 min. *In vitro* phosphorylation reactions were carried out using aurora A (50 ng). Reactions were incubated with [γ-^{32}P]ATP for 30 min at 30°C. Boiled CaMKKβ-GST and aurora A were also incubated with MBP (5 µg). *In vitro* phosphorylation reactions were terminated by the addition of 4x LSB. Reactions were resolved by SDS-PAGE and resulting gel stained with Coomassie, dried and ^{32}P incorporation assessed using a phosphorimager. N=1.

5.2.3.2 Aurora B may phosphorylate KD-LKB1-FLAG but not DN-AMPK or CaMKKß-GST *in vitro*

As described in Section 5.2.3.1, KD-LKB1 and DN-AMPK were immunoprecipitated from cell lysates with the appropriate controls. Immunoprecipitation products were incubated with aurora B-GST and [γ-^{32}P]ATP to assess *in vitro* phosphorylation. Phosphorylation of KD-LKB1 by aurora B was inconsistent, densitometric analysis of KD-LKB1 phosphorylation from two independent experiments had considerable variability (Figure 5-13B). A strong ^{32}P-labelled band was observed in the KD-AMPKα1-myc immunoprecipitates at approximately 50 kDa, which may represent AMPKγ3 (which has a predicted mass of approximately 54 kDa). Band intensity was not altered by aurora B (Figure 5-13). Furthermore, aurora B did not phosphorylate denatured CaMKKß-GST or GST (Figure 5-14).

5.2.3.3 PLK1 may phosphorylate CaMKKβ but not KD-LKB1-FLAG or DN-AMPK *in vitro*

PLK1 did not phosphorylate KD-LKB1 *in vitro* (Figure 5-15). Incubation of DN-AMPK with PLK1 did not alter band intensity (Figure 5-15). Heat denatured CaMKKß-GST (~82 kDa) and GST (~27 kDa) could both be phosphorylated by PLK1 to a similar extent (Figure 5-16).
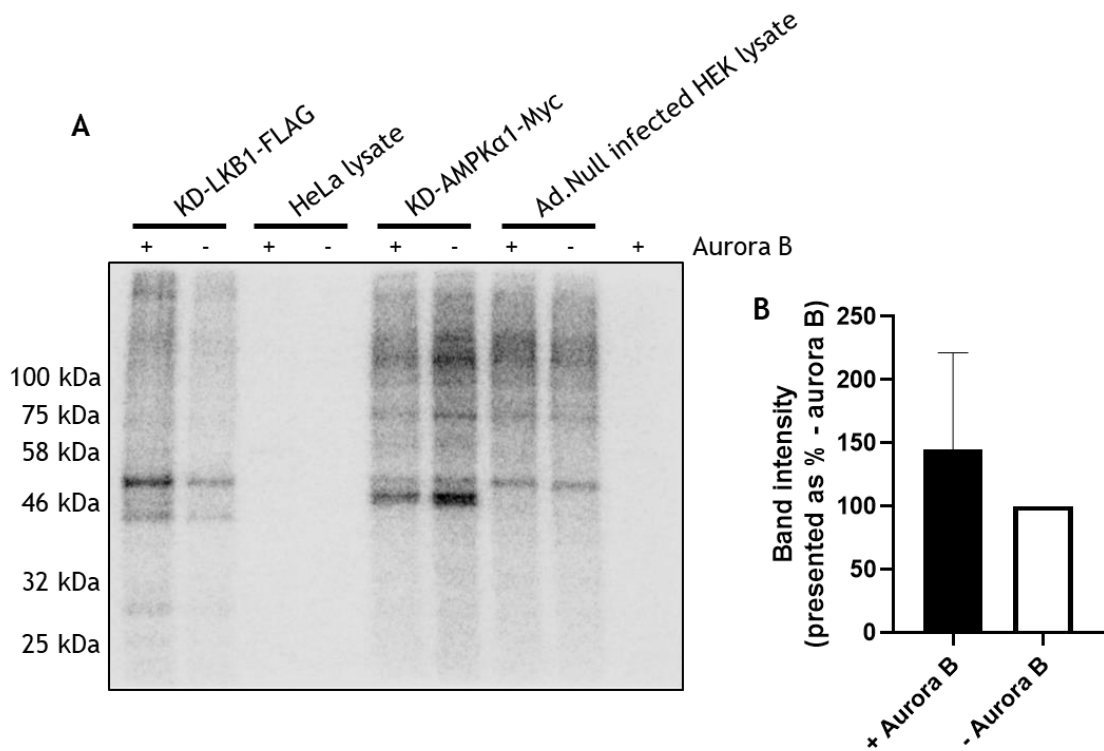
Figure 5-13. Analysis of *in vitro* phosphorylation of KD-LKB1 and DN-AMPK-myc by aurora B

KD-LKB1-FLAG was immunoprecipitated from KD-LKB1 HeLa cells stimulated with tetracycline (1 µg/ml, 24 h) using anti-FLAG antibodies. In parallel, an IP was performed on cell lysates prepared from LKB1 -/- HeLa cells. KD-AMPKα1-myc was immunoprecipitated from Ad.AMPKα1-DN infected HEK 293 cell lysates using anti-myc conjugated beads. Simultaneously an IP was performed using anti-myc conjugated beads on cell lysates from Ad.Null infected HEK 293 cells. MBP (5 µg) was also used as a substrate for aurora B. Substrate were incubated in the presence or absence of 50 ng aurora A-GST and [γ-^{32}P]ATP for 30 min at 30°C. Reactions were terminated by the removal of the supernatant and addition of 2x LSB. Alternatively 4x LSB was added to reactions where substrate was omitted. Reactions were resolved by SDS-PAGE and resulting gels dried and ^{32}P incorporation assessed using a phosphorimager **(A)** Representative phosphorimage and coomassie stained gel. **(B)** Densitometric analysis of KD-LKB1-FLAG phosphorylation by aurora A. Data shown as ± SEM. N=2.
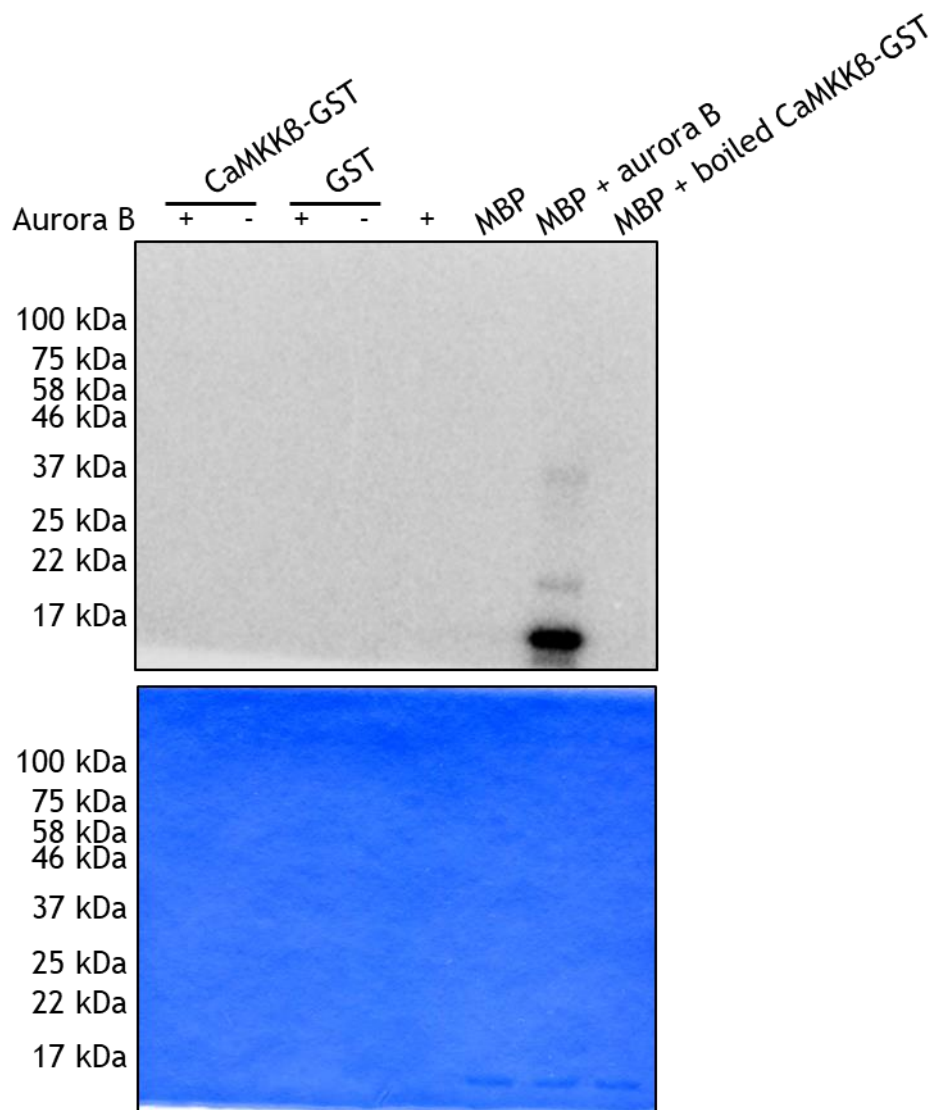
Figure 5-14. Analysis of *in vitro* phosphorylation of CaMKKβ-GST by aurora B
CaMKKβ-GST or GST (500 ng) were heated at 95°C for 5 min. *In vitro* phosphorylation reactions were carried out using aurora B (50 ng). Reactions were incubated with [γ-^{32}P]ATP for 30 min at 30°C. Boiled CaMKKβ-GST and aurora A were also incubated with MBP (5 µg). *In vitro* phosphorylation reactions were terminated by the addition of 4x LSB. Reactions were resolved by SDS-PAGE and resulting gel stained with Coomassie, dried and ^{32}P incorporation assessed using a phosphorimager. N=1.
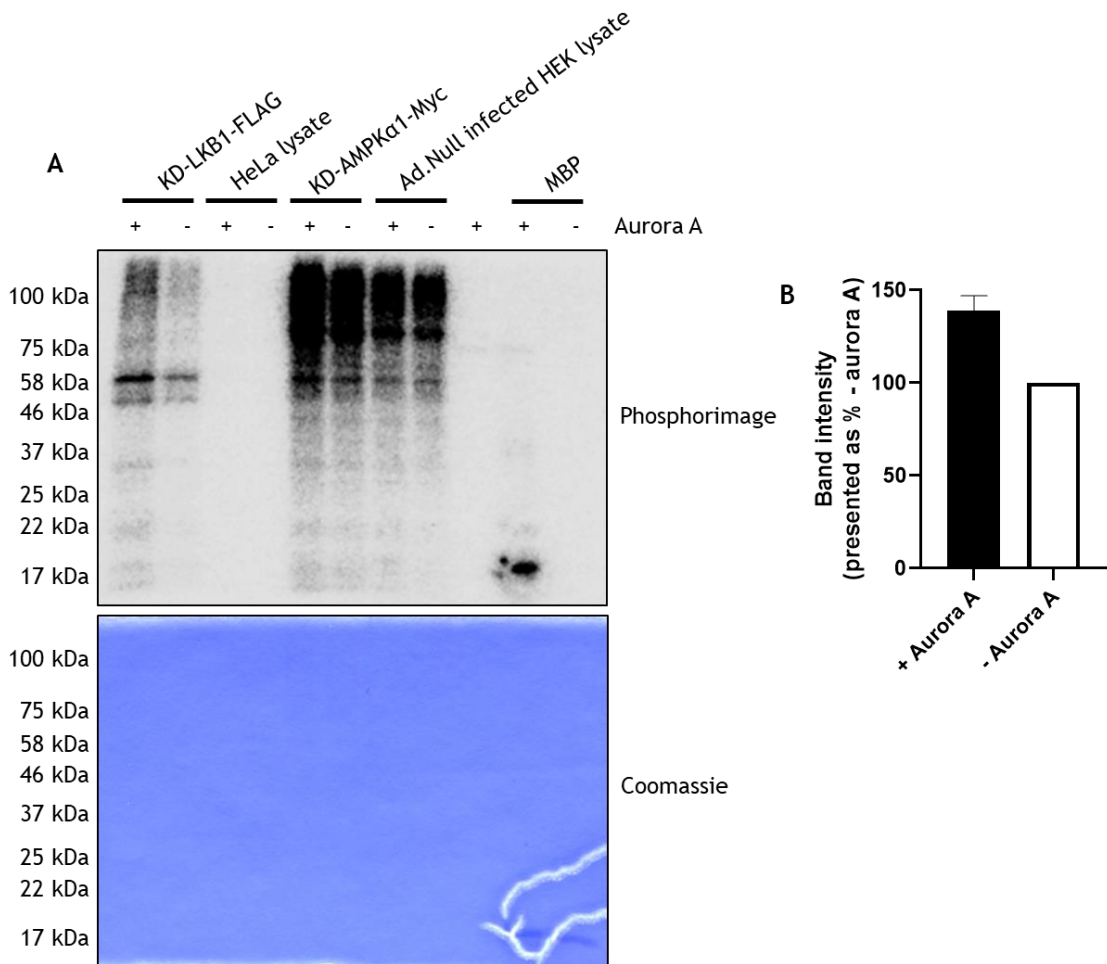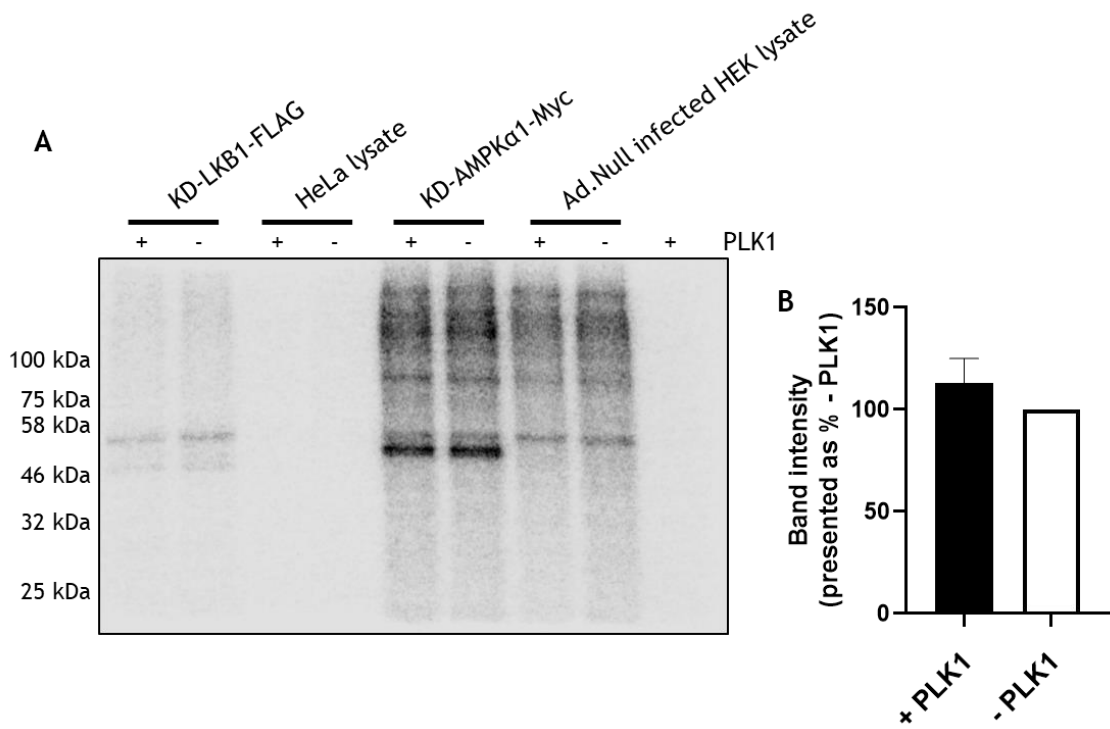
Figure 5-15. Analysis of *in vitro* phosphorylation of KD-LKB1 and DN-AMPK-myc by PLK1
KD-LKB1-FLAG was immunoprecipitated from KD-LKB1 HeLa cells stimulated with tetracycline (1 µg/ml, 24 h) using anti-FLAG antibodies. In parallel, an IP was performed on cell lysates prepared from LKB1 -/- HeLa cells. KD-AMPKα1-myc was immunoprecipitated from Ad.AMPKα1-DN infected HEK 293 cell lysates using anti-myc conjugated beads. Simultaneously an IP was performed using anti-myc conjugated beads on cell lysates from Ad.Null infected HEK 293 cells. MBP (5 µg) was also used as a substrate for PLK1. Substrate were incubated in the presence or absence of 50 ng aurora A-GST and [γ-^{32}P]ATP for 30 min at 30°C. Reactions were terminated by the removal of the supernatant and addition of 2x LSB. Alternatively 4x LSB was added to reactions where substrate was omitted. Reactions were resolved by SDS-PAGE and resulting gels stained with Coomassie, dried and ^{32}P incorporation assessed using a phosphorimager **(A)** Representative phosphorimage and coomassie stained gel. **(B)** Densitometric analysis of KD-LKB1-FLAG phosphorylation by aurora A. Data shown as ± SEM. N=2.
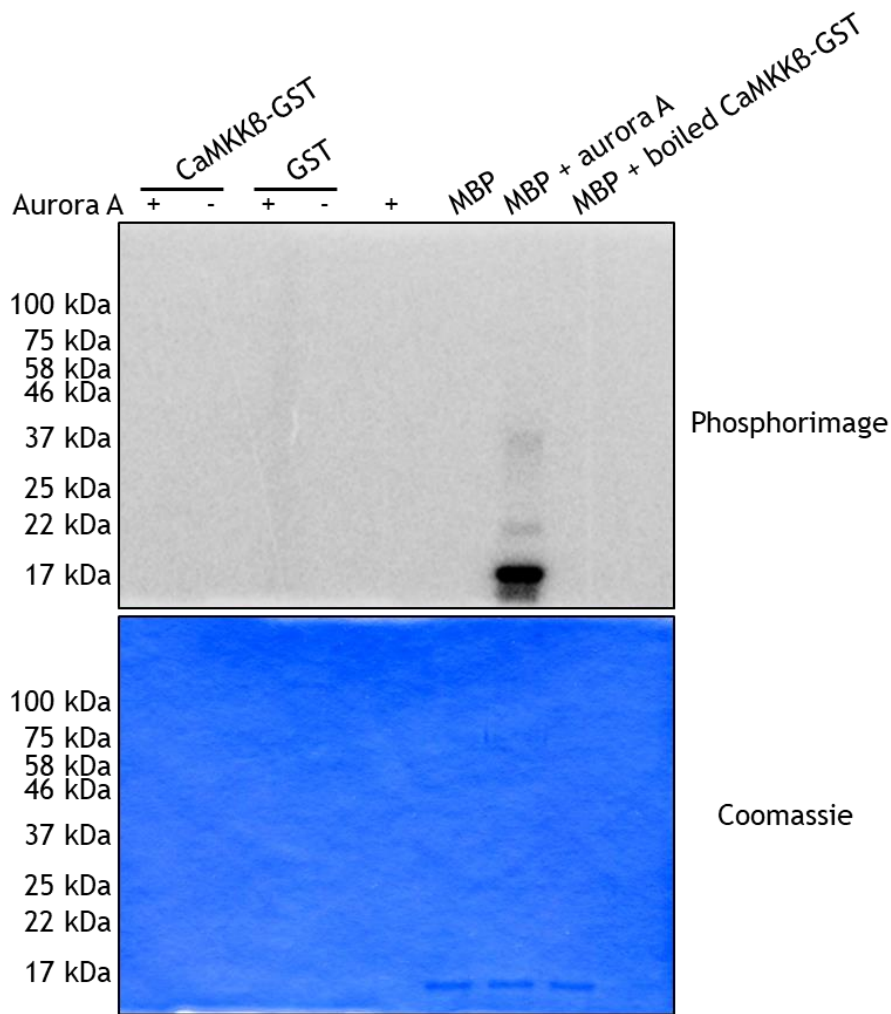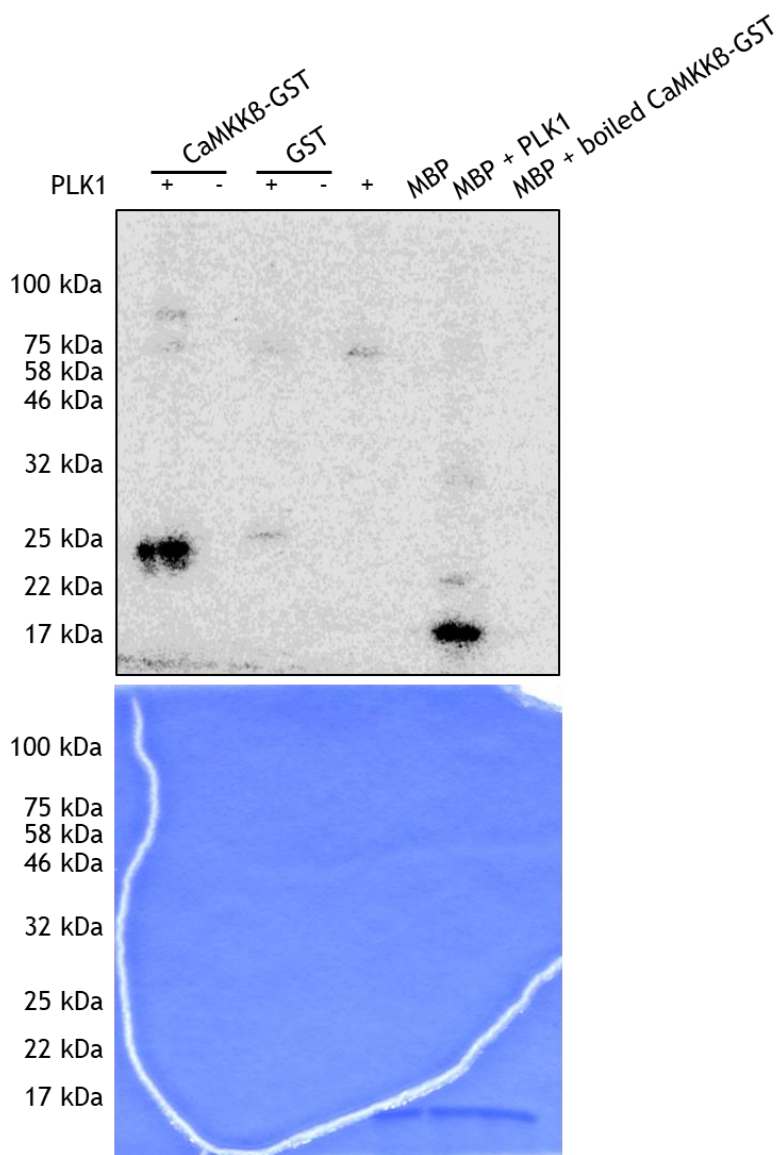
Figure 5-16. Analysis of *in vitro* phosphorylation of CaMKKβ-GST by PLK1
CaMKKβ-GST or GST (500 ng) were heated at 95°C for 5 min. *In vitro* phosphorylation reactions were carried out using aurora A (50 ng). Reactions were incubated with [γ-^{32}P]ATP for 30 min at 30°C. Boiled CaMKKβ-GST and PLK1 were also incubated with MBP (5 μg). *In vitro* phosphorylation reactions were terminated by the addition of 4x LSB. Reactions were resolved by SDS-PAGE and resulting gel stained with Coomassie, dried and ^{32}P incorporation assessed using a phosphorimager. N=1.

5.2.3.4 CaMKKβ phosphorylates KD-Aurora A-mCherry, KD-Aurora B-GFP and may phosphorylate KD-PLK1-YFP *in vitro*

HEK 293 cells were transfected with plasmids encoding either; KD-Aurora A-mCherry, KD-Aurora B-GFP, KD-PLK1-YFP, CHMP2A, GFP or mCherry and incubated for 48 h. Cells were lysed and immunoprecipitated using either anti-mCherry or anti-GFP nanobodies (which recognise YFP isoforms) conjugated to magnetic beads as appropriate. Substrate-bound beads were incubated with CaMKKβ-GST in the presence of [γ-^{32}P]ATP. Reactions were resolved by SDS-PAGE and examined using a phosphorimager.

Bands were visible on the coomassie stained gel for KD-Aurora A-mCherry (~72 kDa and ~60 kDa), KD-Aurora B-GFP (~66 kDa), KD-PLK1-YFP (~95 kDa), GFP (~27 kDa) and mCherry (~24 kDa) at the expected molecular mass (Figure 5-17). No band could be attributed to CHMP2A-GFP (expected molecular weight of ~50 kDa) (Figure 5-17).

Incubation of KD-Aurora A-mCherry with CaMKKβ-GST produced two bands on the phosphorimage at the appropriate molecular masses for the fusion protein (Figure 5-17). Bands were not apparent when CaMKKβ was omitted from the reaction, indicating *in vitro* phosphorylation by CaMKKβ (Figure 5-17). *In vitro* phosphorylation of KD-aurora B-GFP was also evident as band intensity was reduced or absent when CaMKKβ was omitted from the reaction (Figure 5-17). CaMKKβ-mediated phosphorylation of KD-PLK1-YFP was inconsistent between replicates (Figure 5-17). A faint band was produced when GFP was incubated with CaMKKβ (Figure 5-17). No phosphorylation of mCherry was observed (Figure 5-17).

Figure 5-17. Analysis of *in vitro* phosphorylation of DN-Aurora A-mCherry, DN-Aurora B-GFP, DN-PLK1-YFP and CHMP2A-GFP by CaMKKβ

HEK 293 cells were transfected with plasmids encoding DN-Aurora A-mCherry, DN-Aurora B-GFP, DN-PLK1-YFP or CHMP2A-GFP. Cells were lysed and immunoprecipitated with either anti-mCherry or anti-GFP (recognised YFP isoforms) conjugated magnetic beads as appropriate. Substrate bound beads or MBP (5 μg) were incubated with CaMKKβ-GST with 250 μM $CaCl_2$ and 2 μM calmodulin and [γ-^{32}P]ATP for 30 min at 30°C. *In vitro* phosphorylation reactions were terminated by the removal of the supernatant and addition of 2x LSB. Alternatively 4x LSB was added to reactions using MBP as a substrate or reactions when substrate was omitted. Reactions were resolved by SDS-PAGE and resulting gels stained with Coomassie, dried and ^{32}P incorporation assessed using a phosphorimager Representative phosphorimage and coomassie stained gel. **(B)** Densitometric analysis of CaMKKβ mediated phosphorylation of substrates. Data shown as ± SEM. N=2.

5.2.3.5 **AMPKα1ß1γ1 phosphorylates KD-Aurora A-mCherry, KD-Aurora B-GFP and KD-PLK1-YFP** *in vitro*

Substrates were prepared as described previously, and incubated with active recombinant AMPKα1ß1γ1 (a kind gift from Dr. S. Hawley, University of Dundee, UK). Incubation of KD-aurora A-mCherry or KD-aurora B-GFP with AMPKα1ß1γ1 caused a significant increase in band intensity (Figure 5-18). AMPKα1ß1γ1 also phosphorylated KD-PLK1-YFP, however, statistical analysis could not be undertake due to lack of replicates. Omission of AMP from the assay buffer reduced AMPKα1ß1γ1-mediated phosphorylation of both KD-aurora A-mCherry and KD-aurora B-GFP (Figure 5-19). AMPKα1ß1γ1 could phosphorylate GFP to an extent (Figure 5-18).

5.2.3.6 AMPKα2 does not phosphorylate KD-PLK1-YFP or KD-Aurora B-GFP but may phosphorylate KD-Aurora A-mCherry *in vitro*

To determine whether the AMPK heterotrimer composition altered phosphorylation, substrates were prepared as described previously, and incubated with active recombinant AMPKα2ß2γ1 (a kind gift from Dr. S. Hawley, University of Dundee, UK). Incubation of KD-aurora A-mCherry with AMPKα2ß2γ1 produced a band correlating to the higher molecular mass (~72 kDa) species. The lower molecular mass (~58 kDa) species was not further phosphorylated by AMPKα2ß2γ1 (Figure 5-20). AMPKα2ß2γ1 did not phosphorylated KD-PLK1-YFP or KD-Aurora B-GFP (Figure 3-20). GFP was not efficiently pulled down to examine phosphorylation by AMPKα2ß2γ1 (Figure 5-20). There was no phosphorylation of mCherry by AMPKα2ß2γ1 (Figure 5-20).
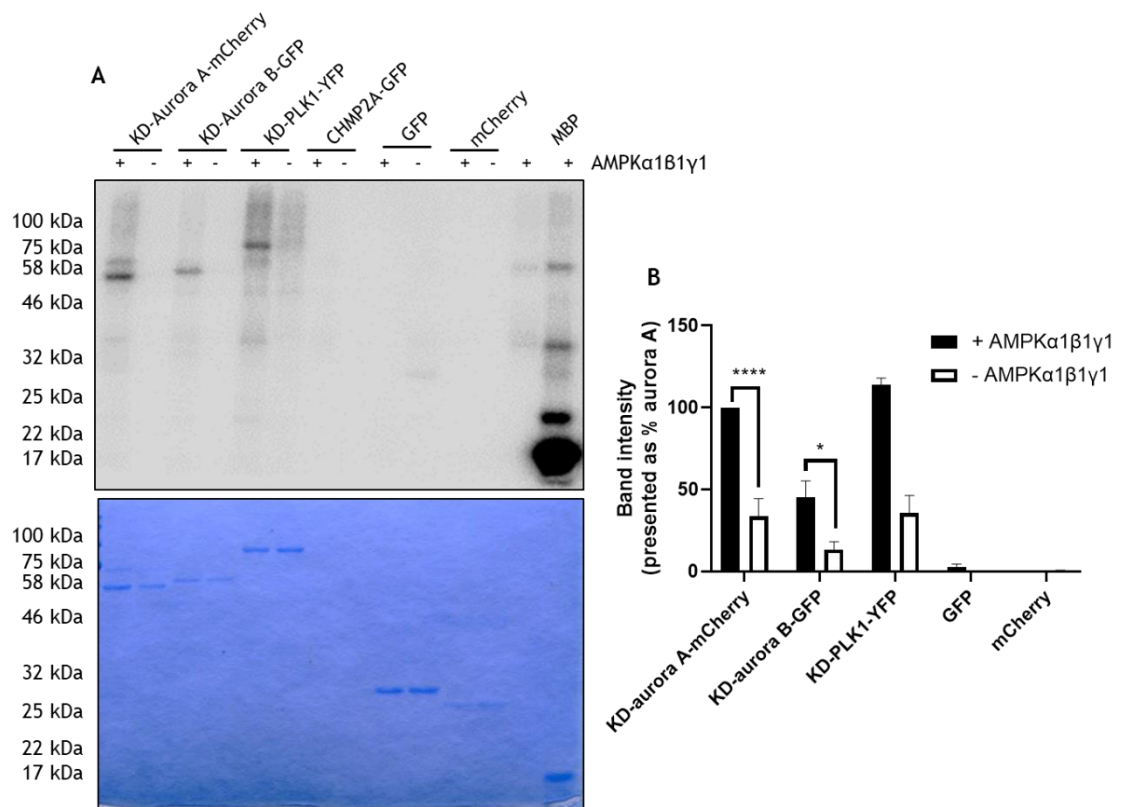
Figure 5-18. Analysis of *in vitro* phosphorylation of DN-Aurora A-mCherry, DN-Aurora B-GFP, DN-PLK1-YFP and CHMP2A-GFP by AMPKα1β1γ1

HEK 293 cells were transfected with plasmids encoding DN-Aurora A-mCherry, DN-Aurora B-GFP, DN-PLK1-YFP or CHMP2A-GFP. Cells were lysed and immunoprecipitated with either anti-mCherry or anti-GFP (recognised YFP isoforms) conjugated magnetic beads as appropriate. Substrate bound beads or MBP (5 µg) were incubated with 0.5 U AMPKα1β1γ1 (where 1 U is 1 nmol ^{32}P incorporated/min into SAMS peptide), 0.2 mM AMP and [γ-^{32}P]ATP for 30 min at 30°C. *In vitro* phosphorylation reactions were terminated by the removal of the supernatant and addition of 2x LSB. Alternatively 4x LSB was added to reactions using MBP as a substrate or reactions when substrate was omitted. Reactions were resolved by SDS-PAGE and resulting gels stained with Coomassie, dried and ^{32}P incorporation assessed using a phosphorimager Representative phosphorimage and coomassie stained gel. **(B)** Densitometric analysis of AMPKα1β1γ1 mediated phosphorylation of substrates. Data shown as ± SEM. N=3 phosphorylation of KD-aurora A-mCherry and KD-aurora B-GFP. N=2 phosphorylation of KD-PLK1-YFP, GFP and mCherry. * $p<0.05$ **** $p<0.001$ two-way ANOVA.
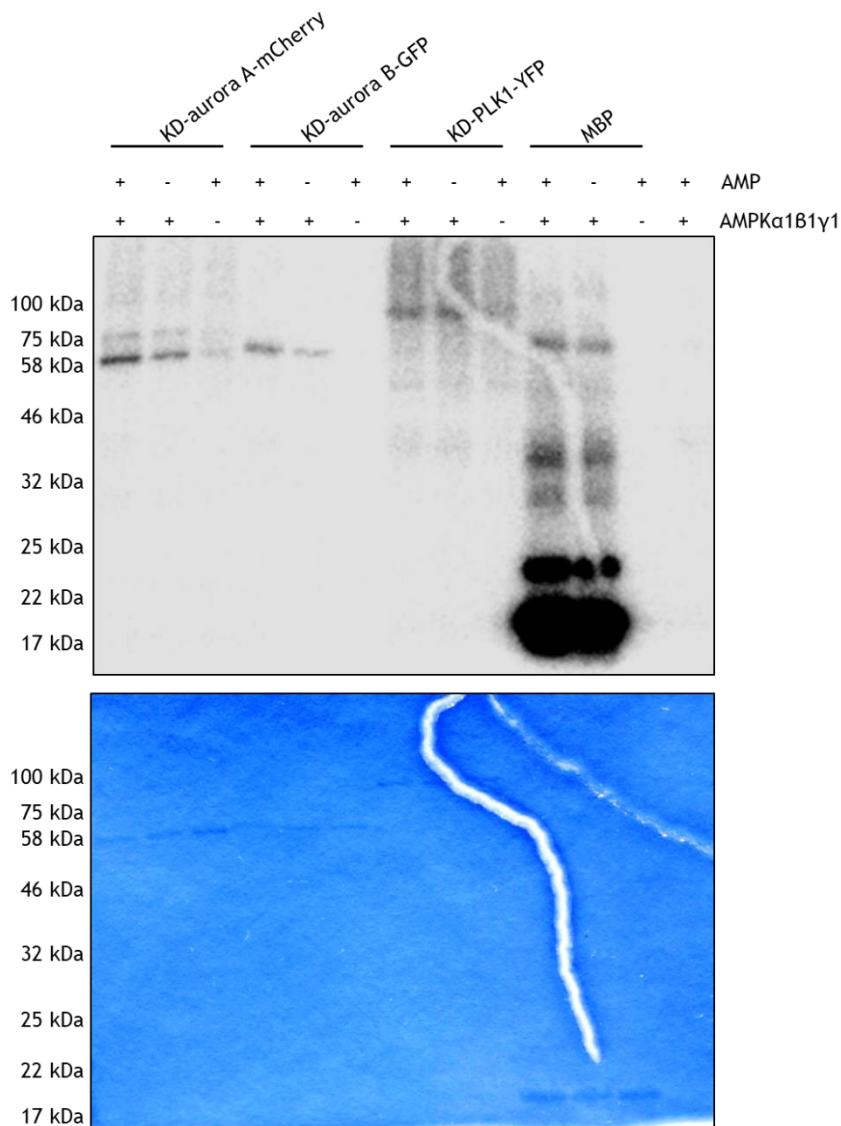
Figure 5-19. Analysis of AMP-dependence of the *in vitro* phosphorylation of DN-Aurora A-mCherry, DN-Aurora B-GFP or DN-PLK1-YFP by AMPKα2β2γ1

HEK 293 cells were transfected with plasmids encoding DN-Aurora A-mCherry, DN-Aurora B-GFP or DN-PLK1-YFP. Cells were lysed and immunoprecipitated with either anti-mCherry or anti-GFP (recognises YFP isoforms) conjugated magnetic beads as appropriate. Substrate-bound beads or MBP (5 µg) were incubated with 0.5 U AMPKα1β1γ1 (where 1 U is 1 nmol ^{32}P incorporated/min into SAMS peptide) and [γ-^{32}P]ATP with or without 0.2 mM AMP for 30 min at 30°C. *In vitro* phosphorylation reactions were terminated by the removal of the supernatant and addition of 2x LSB. Alternatively 4x LSB was added to reactions using MBP as a substrate. Reactions were resolved by SDS-PAGE and the resulting gels stained with Coomassie, dried and ^{32}P incorporation assessed using a phosphorimager. N=1.
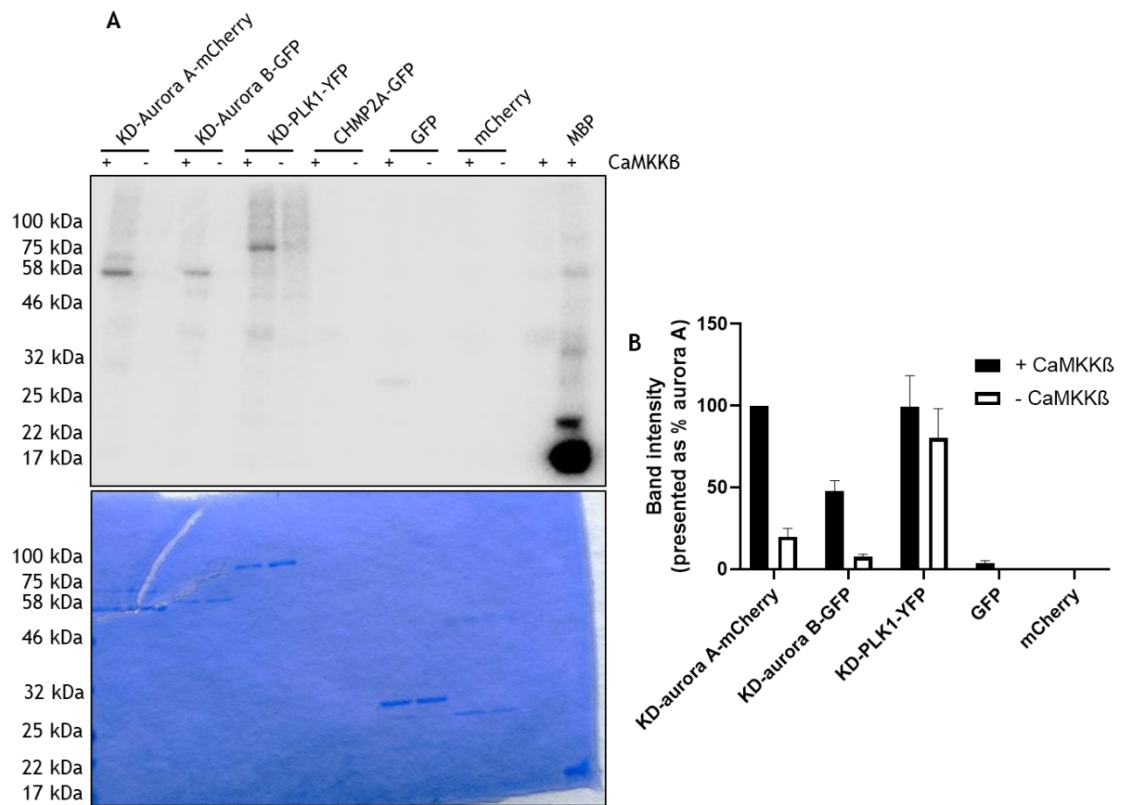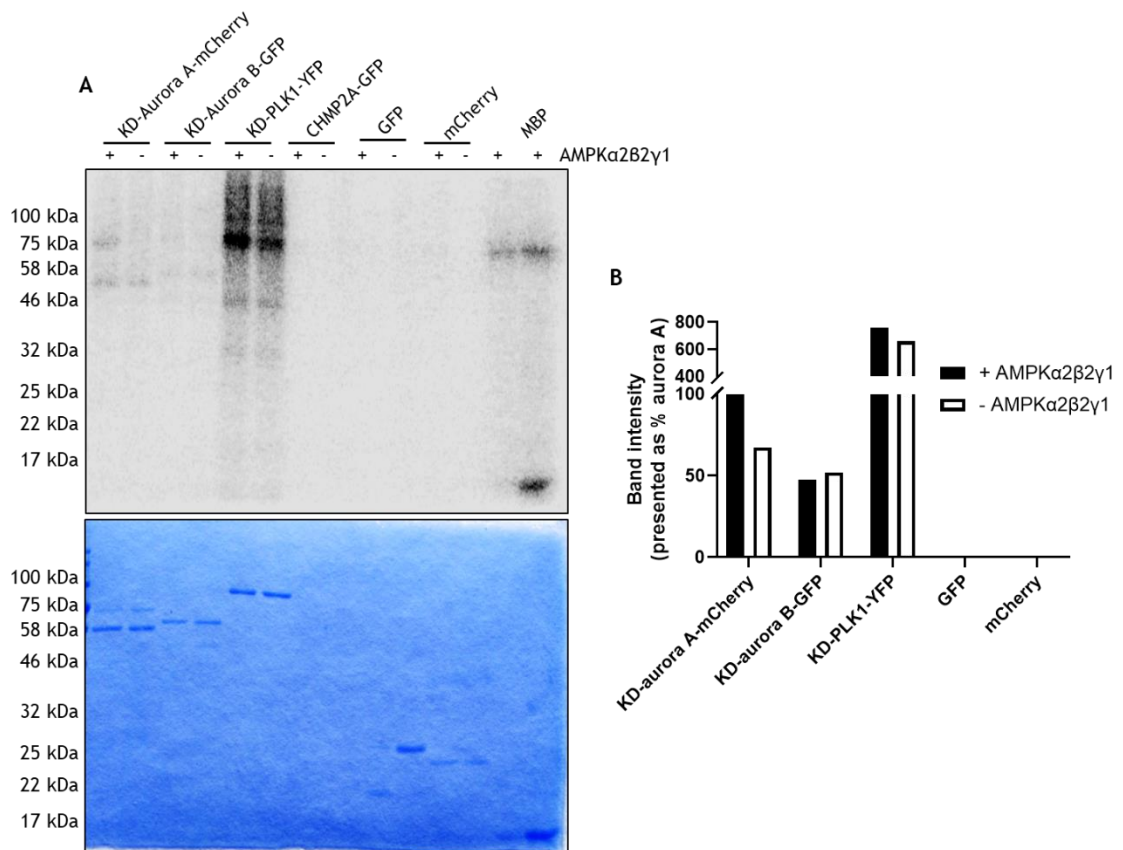
Figure 5-20. Analysis of *in vitro* phosphorylation of DN-Aurora A-mCherry, DN-Aurora B-GFP, DN-PLK1-YFP and CHMP2A-GFP by AMPKα2β2γ1

HEK 293 cells were transfected with plasmids encoding DN-Aurora A-mCherry, DN-Aurora B-GFP, DN-PLK1-YFP or CHMP2A-GFP. Cells were lysed and immunoprecipitated with either anti-mCherry or anti-GFP (recognised YFP isoforms) conjugated magnetic beads as appropriate. Substrate bound beads or MBP (5 μg) were incubated with 0.5 U AMPKα2β2γ1 (where 1 U is 1 nmol ^{32}P incorporated/min into SAMS peptide), 0.2 mM AMP and [γ-^{32}P]ATP for 30 min at 30°C. *In vitro* phosphorylation reactions were terminated by the removal of the supernatant and addition of 2x LSB. Alternatively 4x LSB was added to reactions using MBP as a substrate or reactions when substrate was omitted. Reactions were resolved by SDS-PAGE and resulting gels stained with Coomassie, dried and ^{32}P incorporation assessed using a phosphorimager. **(B)** Densitometric analysis of AMPKα2β2γ1 mediated phosphorylation of substrates. N=1.

5.3 Discussion

5.3.1 Principal findings

- LKB1 expression or function does not influence binucleation in transgenic HeLa cells

- LKB1 activity prevents compound C induced polyploidy in transgenic HeLa cells

- CaMKKß phosphorylates aurora A, aurora B and potentially PLK1 *in vitro*

- AMPKα1ß1γ1 phosphorylates aurora A, aurora B and PLK1 *in vitro*

5.3.2 LKB1 activity may influence HeLa cell mitosis

LKB1 was found to localise to the cytoplasm, nuclei and the intracellular bridge but not the midbody in transgenic HeLa cells. Localisation was consistent for both WT- and KD-LKB1. The specificity of anti-LKB1 antibodies were also demonstrated due to the lack of immunoreactivity observed in LKB1 -/- HeLa cells. Consistent with the subcellular localisation described in this work, in the human osteosarcoma epithelial cell line U2OS cells, LKB1 has been described to localise to the cytoplasm and nucleus but also the MTOC (Werle *et al.*, 2014). In U2OS cells LKB1 regulates the centrosome function and depletion of LKB1 causes an increase in the number of centrosomes in an AMPK-independent manner which is potentially mediated by altered regulation of PLK1 (Werle *et al.*, 2014). Transgenic HeLa cells undergoing early phases of mitosis weakly adhered to coverslips meaning that LKB1 localisation could not be assessed during metaphases.

During telophase, aurora A has been described to localise to the MTOC and to the intracellular bridge in HeLa cells without an enrichment at the midbody (Marumoto *et al.*, 2003). Consistently, in this study, aurora A was detected at the intracellular bridge and in the cytoplasm and nuclei. Localisation of aurora A was not influenced upon the expression of WT-LKB1 or KD-LKB1. In HUVECs (which have intact LKB1) aurora A was detected at the midbody, cytoplasm and

nucleus. Aurora A subcellular localisation during mitosis in HUVECs has not been described before.

Similarly, aurora B and PLK1 were detected in the nucleus, cytoplasm and the intracellular bridge but not the midbody of HeLa cells. In contrast, previous studies have reported aurora B localisation to the midbody as well as the nucleus and cytoplasm of HeLa cells in telophase (Crosio *et al.*, 2002; He *et al.*, 2013; Capalbo *et al.*, 2019). Additionally, PLK1 has also been described at the midbody and in the cytoplasm of HeLa cells (Pal *et al.*, 2010; He *et al.*, 2013; An *et al.*, 2018). Therefore, there was a clear discrepancy between the localisation of PLK1 and aurora B described in this Chapter and previous studies. These differences could be a result of different staining protocols, different antibodies or the source of HeLa cells. There has been a growing concern on the variation of HeLa cell stocks between different research institutes. HeLa cells collected from a number of different research institutes had genetic heterogeneity and phenotypic variation. Furthermore, these differences were amplified after successive passaging (Liu *et al.*, 2019). Regardless, replacing LKB1 expression/function did not influence aurora A, aurora B or PLK1 Localisation in HeLa cells.

Expression of either WT- or KD-LKB1 also did not influence the DNA content of HeLa cells. However, it was previously reported that expression of WT but not KD-LKB1 in LKB1-null squamous cell carcinoma (SSC) cells induced senescence and binucleation (Gurumurthy *et al.*, 2008). This effect was not due to AMPK/mTOR pathways so the downstream target(s) of LKB1 are unknown but likely would be an AMPK-related kinase (ARK).

Compound C caused a significant decrease in the proportion of cells with 2n DNA in KD-LKB1 HeLa cells and increased the proportion of cells with 4n DNA. Whereas the DNA content of WT-LKB1 HeLa cells was not significantly altered by compound C. This suggests that LKB1 activity can prevent compound C-induced cell cycle arrest/binucleation. As flow cytometry cannot differentiate between cells in G_2/M-phase prior to karyokinesis or cells which contained two nuclei, is not possible to determine if compound C caused an increase in binucleation or caused cells to accumulate at the G_2/M phase boundary. However, as STO-609 did not influence the DNA content of KD-LKB1 HeLa cells, it is likely that the

effects of compound C was mediated by an AMPK-independent mechanism. Alternatively, overexpression of WT-LKB1 may overcome the capacity of compound C to inhibition of AMPK.

5.3.3 A network of phosphorylation exists between AMPK, CaMKKß, LKB1 and mitotic proteins

During the course of this investigation, a number of phosphorylation events were described *in vitro* (Figure 5-21). These phosphorylation events have largely not been described before and are summarised as follows;

- CaMKKß phosphorylated aurora A, aurora B and may phosphorylate PLK1.

- AMPKα1ß1γ1 phosphorylated aurora A, aurora B and PLK1.

- AMPKα2ß2γ1 phosphorylated aurora A and PLK1.

- Aurora A phosphorylated LKB1, also described by Zheng *et al.*, 2018.

- Aurora B may phosphorylate LKB1.

- PLK1 may phosphorylate CaMKKß.
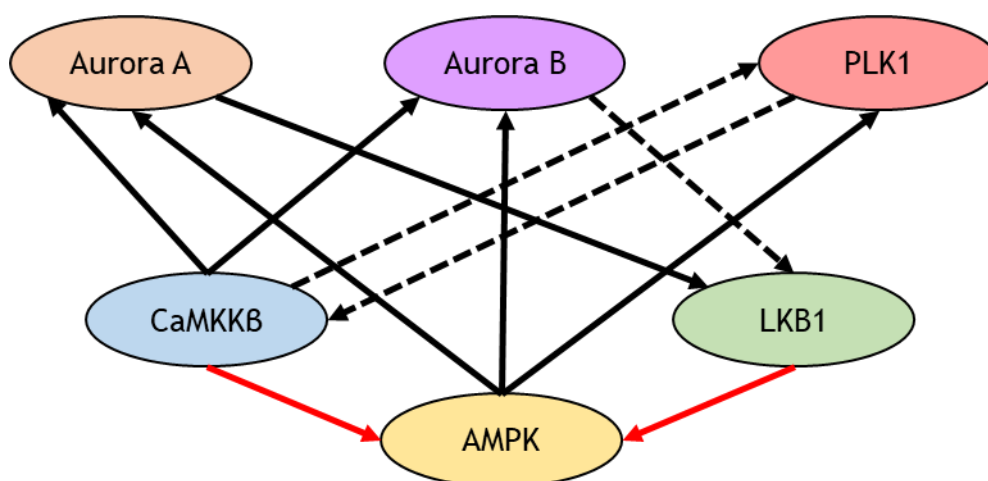
Figure 5-21. A number of phosphorylation events link the AMPK pathway to aurora A, aurora B and PLK1

In vitro phosphorylation events discovered in this Chapter are indicated with a black arrow. *In vitro* phosphorylation of LKB1 by aurora B and phosphorylation of CaMKKβ by PLK1 were unclear (dashed arrows). CaMKKß and LKB1 have well established roles in the phosphorylation of AMPK (red arrows).

Expression of a plasmid encoding KD-aurora A-mCherry in HEK 293 cells produced two distinct bands when assessed by SDS-PAGE and immunoblotting with anti-mCherry or anti-aurora A antibodies. The aurora A fusion protein contained I57V and K162R mutations to render it kinase dead and an N-terminal mCherry tag. The higher molecular mass species (~72 kDa) represented the expected molecular mass of the fusion protein whereas the lower molecular mass species was approximately 60 kDa. As both species were detected with anti-mCherry antibodies, it is most likely that a C-terminal truncation occurred. Expression of KD-aurora B-GFP and KF-PLK1-YFP generated products of the expected molecular mass, ~65 kDa and ~90 kDa respectively.

CaMKKβ and AMPK heterotrimers phosphorylated aurora A *in vitro*. AMPKα1β1γ1 mediated-phosphorylated of aurora A was reduced when AMP was omitted from the assay, demonstrating that phosphorylation was likely AMPK-dependent rather than due to contamination with a different protein kinase. AMPKα2β2γ1-mediated phosphorylation of aurora A occurred exclusively to the higher molecular mass species. The low molecular mass species was phosphorylated to a similar extent as when AMPK was omitted from the reaction. Potentially, the site which was phosphorylated by AMPKα2β2γ1 may not be present in the lower molecular mass species due to a C-terminal truncation. However, AMPKα2β2γ-mediated phosphorylation of aurora A was only assessed once, thus more replicates would be necessary.

AMPKα1β1γ1 also phosphorylated KD-aurora B-GFP in an AMP-dependent manner whereas AMPKα2β2γ1 did not phosphorylate aurora B. The AMPKα subunit isoforms have been described to have a subtly different substrate specificity *in vitro*, with different preferences for the bulky hydrophobic residues and basic residues that form the consensus sequence either side of the phosphorylated S/T (Woods *et al.*, 1996). Therefore it is possible that aurora B contained a sequence which fits the phosphorylation motif of AMPKα1 but not that of AMPKα2. Both AMPKα1β1γ1 and AMPKα2β2γ could phosphorylate KD-PLK1-YFP, however the AMP-dependence could not be determined.

The AMPK phosphorylation consensus has been well characterised as β-Ø-β-X-X-X-S/T-X-X-X-Ø, where β represents basic amino acids and Ø represents hydrophobic residues (Figure 5-22) (Hardie, 2011; Marin *et al.*, 2015). As such

S342 of aurora A may be a potential site for AMPK-mediated phosphorylation. Prior to S342 there is enrichment of basic residues and hydrophobic residues downstream of this site (Figure 5-22). The orthologous site in *Xenopus* (S349) is phosphorylated in M-phase although the kinase which phosphorylates this site is not known (Littlepage *et al.*, 2002). Phosphorylation of this site does not influence aurora A activity but is thought to regulate the protein structure or its regulation (Littlepage *et al.*, 2002). If this site was confirmed to be phosphorylated by AMPK (or perhaps CaMKKß) it could help inform how the protein structure of aurora A influences function in mitosis.

```
ØXXβØβXXXSXXXØ        AMPK phosphorylation motif
  QETYKRISRVEFTFP     Aurora A (S342)
  LELCRRRSLLELHKR     PLK1 (S137)

X-any amino acid
β-basic amino acids
Ø-hydrophobic amino acids
S-phospho-serine site
```

Figure 5-22. Sequence analysis of aurora A and PLK1 indicated the presence of an AMPK phosphorylation motif
The amino acids around S341 or aurora A and S137 of PLK1 aligned with the phosphorylation motif of AMPK. AMPK can phosphorylate both serine and threonine residues, but for clarity only serine is shown in the phosphorylation motif.

S137 of PLK1 could also fit the AMPK phosphorylation consensus (Figure 5-22). S137 is phosphorylated by PLK2 to promote cell survival during mitochondrial dysfunction (Matsumoto *et al.*, 2009). Additionally S137 is phosphorylated late in mitosis and its phosphorylation is integral to the proper timing of mitosis (van de Weerdt *et al.*, 2005). If these sites were validated to be phosphorylated by AMPK, it could indicate the role in which AMPK played in the timing of mitosis.

Incubation of KD-LKB1 with active aurora A-GST increased band intensity by 40% ± 8% when assessed by phosphorimaging, demonstrating that aurora A phosphorylated KD-LKB1 *in vitro*. This is consistent with a previous study in which aurora A phosphorylated LKB1 on S299 in non-small cell lung cancers (NSCLC). Aurora A mediated phosphorylation of LKB1 inhibited the interaction between LKB1 and AMPK thereby reducing AMPK phosphorylation and activity (Zheng *et al.*, 2018).

Immunoprecipitation and *in vitro* phosphorylation of KD-AMPKα1-myc produced a number of bands on the phosphorimage demonstrating a degree of non-specificity. This may have been expected due to immunoprecipitation of endogenous myc and potential interacting proteins. In some instances, a band of approximately 54 kDa was apparent which may represent AMPKγ3. Band intensity was not influenced by incubation with any of the kinases tested. If this band did represent AMPKγ3, it may be the first indication that this subunit is phosphorylated.

As a kinase dead form of CaMKKß could not be acquired, so to remove kinase activity commercial CaMKKß-GST was heated at 95°C for 5 minutes to cause denaturation. Heat denatured CaMKKß could not phosphorylate MBP. Neither aurora A nor aurora B phosphorylated denatured CaMKKß. PLK1 may phosphorylate CaMKKß-GST *in vitro* as a band of the appropriate molecular mass (~80 kDa) was detected, however, PLK1 phosphorylated GST to a comparable extent. Therefore it is more likely that PLK1 phosphorylated the GST tag rather than CaMKKß, although more replicates would be necessary before ruling our PLK1 mediated phosphorylation of CaMKKß. Conversely, CaMKKß appeared to phosphorylate KD-PLK1-YFP but results were inconsistent between replicates. Therefore, it is possible that PLK1 and CaMKKß may cross-regulate their function in a reciprocal manner, however, this would need to be assessed further.

As discussed, AMPK was demonstrated to phosphorylate PLK1 *in vitro*. Demonstrating a link between PLK1 and the AMPK pathway which could represent a novel regulatory pathway as previous reports have indicated a role for LKB1 in the regulation of PLK1 independent of AMPK. LKB1 activates the ARK NUAK1 which inhibits myosin phosphatase targeting-1 (MYPT1), a subunit of protein phosphatase 1ß (PP1ß) (Zagorska *et al.*, 2010; Werle *et al.*, 2014). Inactivation of PP1ß promotes accumulation of active phospho-T210 PLK1 (Werle *et al.*, 2014). Furthermore, NUAK1 is phosphorylated by PLK1 on S476 and S480 to promote polyubiquitination and degradation (Banerjee *et al.*, 2014). Consistent with this, when PLK1 activity is low in S-phase, NUAK1 levels are elevated, and when PLK1 activity is high in G_2/M-phase NUAK1 levels are low (Banerjee *et al.*, 2014). Additionally, A431 cells treated with the PLK1 inhibitor GW843682X have no mitotic accumulation of phospho-T172 AMPK and have an increased rated of binucleation (Vazquez-Martin *et al.*, 2011). GW843682X was

also reported to prevent phospho-S79 ACC localisation at the MTOC but not the midbody (Vazquez-Martin *et al.*, 2013). However, it should be noted that GW843682X can inhibit AMPK *in vitro*; 10 µM GW843682X reduced AMPK activity by over 50% (Protein Phosphorylation and Ubiquitination unit, University of Dundee, MRC, n.d.). Thus the identification of PLK1 as a substrate for both AMPK and CaMKK *in vitro* could have interesting implications on how PLK1 regulates mitosis and cytokinesis.

A limitation of the current study was that AMPKα1ß1γ1 and CaMKKß both phosphorylated GFP to an extent. As GFP was used as a tag for aurora B and a GFP isoform (YFP) used to tag PLK1, there was concern these results may represent AMPKα1ß1γ1 or CaMKKß phosphorylating the associated tag rather than aurora B/PLK1 directly. Phosphorylation of GFP was considerably less than that of AMPKα1ß1γ1/CaMKKß mediated-phosphorylation of KD-aurora B-GFP or KD-PLK1-YFP. Therefore it is proposed that AMPKα1ß1γ1 and CaMKKß could phosphorylate aurora B and PLK1 *in vitro* and to a considerably lesser extent also phosphorylated GFP. There was insufficient pull down of GFP for AMPKα2ß2γ1-mediated phosphorylation to be assessed. There was no phosphorylation of mCherry *in vitro* so there is not the same concern for AMPK and CaMKKß mediated phosphorylation of KD-aurora A.

5.3.4 Future work

5.3.4.1 CHMP2 isoforms as a substrate for phosphorylation

As a genetic interaction was described between *ssp1* and *vps2* in *S. pombe*, the human orthologues (CHMP2A and CHMP2B) were investigated as a substrate of AMPK/CaMKKß. Initially, transfection of HEK 293 cells with a plasmid containing a gene for CHMP2A-GFP produced a product of the expected molecular mass (~50 kDa). However, when transfections were repeated to generate substrates for *in vitro* phosphorylation reactions, there was no product viable on Coomassie stained gels. This could indicate that CHMP2A-GFP was not produced in HEK 293 cells or that the immunoprecipitation with anti-GFP conjugated beads was not sufficient in this instance. Transfection of HEK 293 cells with a plasmid encoding CHMP2B-GFP did not successfully generate a product.

Interestingly, the amino acid sequence surrounding T10 of CHMP2A and T9 of CHMP2B closely resemble the AMPK phosphorylation consensus (Figure 5-23). In both CHMP2 isoforms there is enrichment of basic residues prior to a threonine, and hydrophobic residues in the +4 and +5 positions relative to a threonine. While the sequences are not an exact match for the AMPK phosphorylation motif, it may indicate that CHMP2A and CHMP2B could be AMPK substrates and merits further research. Sequence alignment of Vps2 and CHMP2a indicates a serine residue at position 13 (aligns with T10 of CHMP2A) this may suggest that phosphorylation of the N-terminus is a conserved regulatory mechanism of ESCRT function between mammalian cells and fission yeast.

```
ØXXβØβXXXTXXXØ          AMPK phosphorylation motif
MDLLFGRRKTPEELLRQNQR    CHMP2A
 MASLFKKKTVDDVIKEQNRE   CHMP2B

X-any amino acid
β-basic amino acids
Ø-hydrophobic amino acids
T-phospho-threonine site
```

Figure 5-23. Sequence analysis of CHMP2A and CHMP2B indicated the presence of an AMPK phosphorylation motif
The first 20 amino acids of CHMP2A and CHMP2B aligned with the phosphorylation motif of AMPK. AMPK can phosphorylate both serine and threonine residues, but for clarity only threonine is shown in the phosphorylation motif.

5.3.4.2 Anillin and Vps4 as substrates for phosphorylation

While many of the genetic interactions identified in Chapter 4 were explored further in this Chapter, some of the interactions were not examined. This includes the interaction between ssp1/*ssp2*/*amk2*/*cbs2* with *mid1* or the interaction between *ssp1* and *vps4*. Unfortunately, due to time constraints it was not possible to examine if either anillin (mammalian orthologue of *S. pombe* Mid1p) or Vps4 were substrates for AMPK, CaMKKß or LKB1 but could be interesting to examine further.

5.3.4.3 Investigation into LKB1 ability to phosphorylate mitotic proteins

In Chapter 4, a number of genetic interactions were noted between the AMPK T172 kinase *ssp1* and mitotic proteins. In this Chapter, LKB1 was only examined

as a substrate for *in vitro* phosphorylation rather than as the active kinase. Therefor it would be interesting to examine if LKB1 could phosphorylate mitotic proteins. This could be achieved by immunoprecipitation of WT-LKB1 from inducible HeLa cells using an anti-FLAG antibody in a similar manner to how KD-LKB1 was isolated. It is unknown if an *in vitro* phosphorylation reaction would occur efficiently if both the substrate and the active kinase were bound to beads, therefore it would be suggested that WT-LKB1 be immunoprecipitated and incubated with heat denatured recombinant aurora A-GST, aurora B-GST or PLK1-His.

5.3.4.4 Investigating the significance of *in vitro* phosphorylation

To confirm phosphorylation *in* vivo, kinases could be mutated to utilise ATP analogues such as ATPγS as demonstrated by Hertz *et al.,* 2010. Thiophphorylated substrates could then be isolated and identified by mass spectrometry. This technique could also identify the residue which is phosphorylated. Next, the biological importance of the phosphorylation could be assessed in a number of way; plasmids could be generated containing phosphomimetic (Ser/Thr mutated to Asp) or phosphonull (Ser/Thr to Ala) mutations. Plasmids could be transfected into cells and the functional effects assessed by measuring binucleation, proliferation, cell morphology or how these mutations influenced kinase activity.

5.3.5 Summary

A number of phosphorylation events between the AMPK pathway and aurora A, aurora B and PLK1 were identified. Most of these phosphorylation events are novel with the only phosphorylation event that had been described previously being the phosphorylation of LKB1 by aurora A. While there have previously been links reported between LKB1and PLK1 in a number of studies, this is the first account of direct phosphorylation. Unfortunately due to time constraints the functional effects of the phosphorylation could not be examined but could represent a novel aspect of AMPK function.

6 Chapter 6–Discussion

6.1 Background

At the start of these studies, a number of publication had suggested a role for AMPK in the regulation of mitosis but the precise role AMPK plays was not fully understood. The AMPKα2 subunit had been described to localise to the midbody during telophase (Pinter *et al.*, 2012). Additionally phospho-T172 AMPK and phospho-S79 ACC were both reported to localise to the MTOC and to the midbody (Vazquez-Martin *et al.*, 2009; Vazquez-Martin *et al.*, 2013). These data indicated that AMPK localised to key compartments concerned with mitosis and cytokinesis. Furthermore, in a chemical genetic screen PPP1R12C and PAK2 were identified as substrates of AMPKα2 which implicated AMPK in the regulation of MRLC in mitosis (Banko *et al.*, 2011).

6.2 Final discussion

6.2.1 AMPK localisation in mitosis

The data described in this Thesis builds on these previous observations, demonstrating that in HUVECs and HeLa cells AMPKα1 localised to the MTOC (Figure 3-1 and 3-2). Additionally, previously described midbody localisation of AMPKα2 was confirmed in HUVECs (Pinter *et al.*, 2012) and also shown to occur in HeLa cells(Figure 3-1 and 3-2), suggesting AMPKα subunit localisation during mitosis is conserved within human cells. Localisation to these mitotic structures was mutually exclusive; AMPKα1 was never observed at the midbody and AMPKα2 was never detected at the MTOCs. This suggests that the AMPK heterotrimers have independent targeting mechanisms and most likely independent functions in mitosis. At the midbody, AMPK has been described in the context of a AMPKα2β2γ2 heterotrimer in HUVECs (Pinter *et al.*, 2012) but given the differential expression of AMPK subunit isoforms, it is unclear if the regulatory subunits play a role in AMPK function at the midbody. The regulatory subunits which associate with AMPKα1 at the MTOC remain unknown.

Active phospho-T172 AMPK has been reported to localise to the MTOC and midbody in a number of cancer cell lines and in primary marsupial cells

(Vazquez-Martin *et al.*, 2009; Thaiparambil *et al.*, 2012). This localisation was replicated in HeLa cells and demonstrated in HUVECs for the first time (figure 3-4 and 3-5). Anti-phospho-T172 AMPK antibodies recognised both phospho-AMPKα1 and phospho-AMPKα2 and is therefore consistent with the reported localisation of the individual subunit isoforms. However, the data presented here questions the specificity of phospho-T172 AMPK antibodies as immunoreactivity was detected in AMPK -/- MEFs with one commercial antibody (Figure 3-6).

It remains unclear if AMPK is phosphorylated at the MTOC/midbody or if phospho-T172 AMPK is recruited to these sites. In transgenic HeLa cells, LKB1 was found to localise to the cytoplasm, nuclei, the intracellular bridge but not the midbody when cells were in telophase. Interestingly, in U2OS cells, LKB1 has been reported to localise to the MTOC (Werle *et al.*, 2014). Therefore, it is possible that LKB1 is recruited to the MTOC where it phosphorylates AMPK. As LKB1 is also enriched in the intracellular bridge, LKB1 may phosphorylate AMPK as it is recruited to the midbody. Unfortunately, due to poor antibody selectivity, it was not possible to examine CaMKKß subcellular localisation.

The MTOC acts as a site for the non-dynamic end of microtubules to anchor to and nucleate from, thereby enabling chromatid separation. The MTOC also acts as a scaffolding site to integrate multiple signalling pathways central to the regulation of mitosis, including CDK1/cyclin B, aurora A and PLK1 (Jackman *et al.*, 2003). The localisation of AMPKα1 to the MTOC could therefore suggest a function for AMPK in the maturation of centrioles, microtubule nucleation, chromatid separation or in the regulation of aurora kinases or PLK1. AMPKα2 localisation to the midbody could suggest a role in vesicle transport or the regulation of ESCRT subunits.

6.2.2 AMPK activity during mitosis

AMPK activity is not absolutely required for mitotic progression as AMPKα1/AMPKα2 double homozygous knockout cell lines are viable. However, evidence suggests that AMPK activity may be important for the fidelity or timing of cytokinesis in mammalian cells and fission yeast.

In fission yeast, after contraction of the actomyosin ring the division septum is deposited between the newly formed daughter cells. Enzymatic digestion of the division septa then enables the daughter cells to separate (Sipiczki and Bozsik, 2000; Dekker *et al.*, 2004). Staining of the division septa with Calcofluor-White allowed for the classification of yeast septation phenotype to determine how genetic alterations influenced septation. Deletion of *ssp2, cbs2* or *ssp1* caused a significant increase in the frequency of the Class F septation phenotype, representing delayed separation after septation compared to wild type cells (Figure 4-1). This suggests that AMPK has a role in the timely coordination of fission yeast cytokinesis, however the precise mechanism by which downregulation of AMPK delayed separation is unknown. A similar phenotype was also observed in *vps2Δ* and *vps4Δ* strains (Figure 4-16 and 4-18) which may indicate a link between the AMPK pathway and the ESCRT machinery during fission yeast cytokinesis.

AMPK has well characterised anti-proliferative effects in mammalian cells, which is in part mediated by inducing cell cycle arrest at the G_1/S-phase boundary though the stabilisation of p53 (Jones *et al.*, 2005). Pharmacological stimulation of AMPK activity was demonstrated to reduced cell proliferation although an effect on cytokinesis was not observed as activation of AMPK with small molecule activators did not influence polyploidy. However, the expression of constitutively active AMPK prevented binucleation of HUVECs (Figure 3-17).

Compound C caused HUVECs to arrest prior to S-phase (Figure 3-12). Furthermore, compound C reduced BrdU incorporation into DNA (Figure 3-14), demonstrating reduced proliferation. However, the anti-proliferative effect of compound C is likely AMPK-independent as both wild type and AMPK -/- MEFs had similarly reduced BrdU incorporation. In both LKB1 -/- HeLa cells and in KD-LKB1 HeLa cells compound C caused a significant increase in the proportion of cells with 4n DNA (Figure 5-5). Interestingly, the expression of WT-LKB1 prevented the accumulation of polyploid cells in response to compound C. However, in other cells, such as HUVECs and MEFs compound C did not cause an increase in the proportion of cells with 4n DNA. Therefore, this may represent a cell type specific effect of compound C in HeLa cells. As, STO-609 did not influence polyploidy in HeLa cells it is believed that compound C induced polyploidy by an AMPK-independent manner which may be regulated by LKB1.

6.2.3 Signalling pathways AMPK may regulate in mitosis

To understand which signalling pathways AMPK may regulate during mitosis, a genetic screen was undertaken in *S. pombe*. In doing so, novel genetic interactions were identified between the genes for AMPK subunits/*ssp1* and *ark1, plo1* and *mid1*. Additionally, *ssp1* but not *amk2* or *cbs2* was found to interact with the ESCRT components *vps2* and *vps4* (Table 4-4). Many of these interactions were then further characterised by *in vitro* phosphorylation assays using the mammalian protein orthologues.

Aurora A and PLK1 have been described to localise to the MTOC where they regulate centrosome function and maturation in the early stages of mitosis (Arnaud *et al.,* 1998; Sugimoto *et al.*, 2002). It has also been reported that AMPK has a role in spindle orientation through MRLC and that pharmacological inhibition of PLK1 suppressed recruitment of phospho-T172 AMPK to the MTOC (Vazquez-Martin *et al.*, 2011; Thaiparambil, *et al.,* 2012). In this study, AMPK was found to phosphorylate both PLK1 and aurora A *in vitro* (Figure 5-18). Additionally CaMKKß phosphorylated aurora A and may phosphorylate PLK1 (Figure 5-17) which may indicate that a feedback loop exists between aurora A/PLK1 and CaMKKß/AMPK. Aurora A phosphorylated LKB1, consistent with previous publications (Zheng *et al.*, 2018). Together this could indicate a novel role for AMPK in the regulation of centrosomes. The integration of the AMPK pathway with aurora A and PLK1 at the MTOC during the early stages of mitosis may be a mechanism for cells to perform an energetic check point to ensure there was sufficient ATP for the timely completion of mitosis.

Aurora B has been described to localise to the midbody in a number of cell types (Crosio *et al.*, 2002; Fuller *et al.*, 2008; He *et al.*, 2013; Capalbo *et al.*, 2019) and was detected at the midbody of HUVECs in this study. *In vitro* both AMPKα1 and AMPKα2 phosphorylated KD-aurora A-GFP whereas only AMPKα1 phosphorylated aurora B. Although AMPKα1 was excluded from the midbody, it may phosphorylate aurora B in the cytoplasm/intracellular bridge where the two proteins were both detected. Additionally, AMPK may phosphorylate the aurora kinases/PLK1 during interphase to regulate their function.

Both *vps2* and *vps4* were described to interact with *ssp1* which may indicate that either LKB1 or CaMKKß could regulated ESCRT function in human cells. Vps2p (CHMP2A/CHMP2B human orthologue), an ESCRT-III component which oligomerize to deform the cell membrane to catalyse abscission (Elia *et al.*, 2012). Vps4p (also Vps4 in human cells) is an AAA-ATPase which remodels ESCRT-III polymers to regulate oligomerization, abscission and recycling of ESCRT subunits (Elia *et al.*, 2012). Interestingly, An AMPK consensus sequence is apparent at the N-terminus of both CHMP2 isoforms (T10 of CHMP2A and T9 of CHMP2B). Neither sites have been described to be phosphorylated previously and therefore could represent a novel means of regulation of the ESCRT pathway. Unfortunately, *ssp2Δ vps2Δ* and *ssp2Δ vps4Δ* strains were not generated in this study so a genetic interaction could not be assessed with the AMPKα subunit in *S. pombe*. Therefore the genetic interaction observed between *ssp1* and *vps2/vps4* may in fact represent a physical interaction with AMPK rather than CaMKKß or LKB1 directly, this will be discussed further in Section 6.6.

6.3 Proposed model for AMPK in mitosis

During the early phases of mitosis AMPKα1 localises to the MTOC where it may be phosphorylated by LKB1. AMPK regulates spindle orientation and MRLC through PPP1R12C and PAK2 (Banko *et al.*, 2011; Thaiparambil *et al.*, 2012). The AMPK pathway may also regulate centrosome function/maturation through the phosphorylation of aurora A or PLK1. Mitotic activation of AMPK may be negatively regulated by aurora A which phosphorylates LKB1 to limit T172 phosphorylation (Figure 6-1). AMPK activity may therefore be tightly regulated by antagonising signals which may explain why clear results were not obtained following pharmacological over activation or inhibition of AMPK.

As mitosis progresses AMPK may regulate the formation or contraction of the actomyosin ring through interactions with anillin, although this has not been fully characterised. During telophase AMPKα2 localises to the midbody and AMPKα1 is localised to the cytoplasm/ intracellular bridge. AMPK may then phosphorylate aurora B to enable cytokinesis to occur in a timely fashion (Figure 6-1). AMPK may also phosphorylate CHMP2 to regulate ESCRT-III polymerisation or transport to the midbody. AMPK may then phosphorylate Vps4 to regulate its ATPase activity enabling abscission or ESCRT recycling.
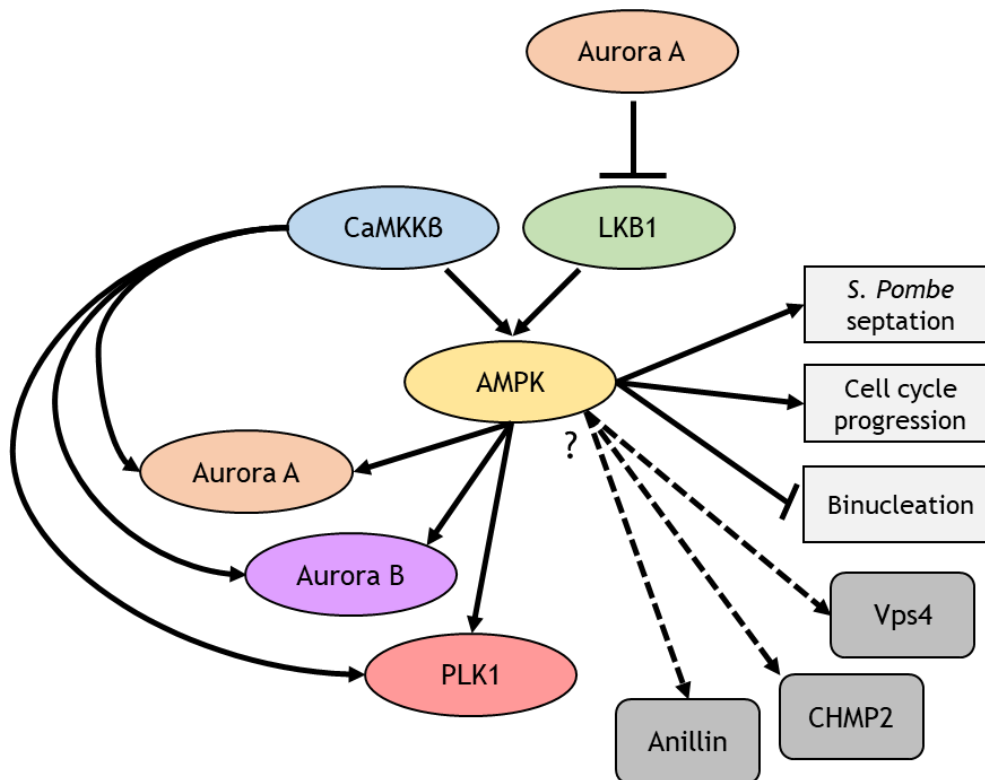
Figure 6-1. Proposed role for AMPK in mitosis and cytokinesis.
AMPK may regulate *S. pombe* septation, cell cycle progression and binucleation of mammalian cells. Both AMPK and CaMKKβ phosphorylated aurora A, aurora B and PLK1. Aurora A was described to phosphorylate LKB1, which has previously been described to inhibit the interaction between LKB1 and AMPK. Genetic interactions were described between the AMPK pathway and anillin (*mid1*), CHMP2 (*vps2)* and Vps4 (*vps4*) but *in vitro* phosphorylation was not assessed.

6.4 Summary

AMPK has a well-documented anti-proliferative effect to limit ATP consumption when nutrients are limiting. This is achieved through the regulation of a number of pathways including the stabilisation of p53 to cause cell cycle arrest (Jones *et al.*, 2005). Additionally AMPK downregulates mTOR to limit proliferation, protein synthesis and lipid synthesis (Inoki *et al.*, 2002; Gwinn *et al.*, 2008). With the localisation of AMPK to mitotic structures, the numerous genetic interactions described in *S. pombe* and network of cross-phosphorylation events detected *in vitro*, it is highly likely that AMPK plays a role in the regulation of mitosis. The precise role AMPK plays remains difficult to discern but it is most likely exerting an anti-proliferative cytostatic effect.

6.5 Limitations of the present study

The use of cancer cell lines which have undergone a number of genetic alterations should be considered as this could cause unforeseen effects on the

cell cycle. As HeLa cells lack LKB1, they are a useful tool in the study of how altered LKB1 signalling may affect AMPK and in particular the effects on proliferation. However, due to altered AMPK phosphorylation, the cell line may not be the best model to study the role of AMPK in physiological circumstances. This was addressed by the use of HUVECs to represent human primary cells but other cell types could also be assessed such as human fibroblasts. Another important consideration is the specificity of the pharmacological compounds used to investigate the influence of AMPK activity modulation on polyploidy. Many of the compound used have well documented AMPK-independent affects, such as compound C which can inhibit a number of kinases (Bain *et al.*, 2007).

A number of the key results of this work were generated by *in vitro* phosphorylation assays. These *in vitro* assays represent a simple experimental design to investigate protein phosphorylation but the results obtained *in vitro* may not be mirrored *in vivo*. Therefore, it would be important to confirm these results with observations *in vivo*.

6.6 Future work

The current study presents a number of avenues which warrant further investigation;

- What are the real-time spatio-temporal dynamics of AMPK and the upstream kinases during mitosis? And what functions does AMPK play at these locations?

Transfection of cells with plasmids encoding AMPK-GFP fusion proteins was attempted in HeLa cells to examine AMPK localisation without the need for antibodies. However, this proved to be unsuccessful for a number of reasons; low transfection rate; senescence of transfected cells; GFP localisation to the midbody. It would therefore be beneficial to optimise the transfection protocol and use alterative fluorophores. This approach would also enable real time visualisation of how pharmacological manipulation of AMPK activity influenced mitotic dynamics.

- How is septation altered in mutant *S. pombe* cells?

Deletion of AMPK subunits or *ssp1* caused in increase in the Class F septation phenotype but it is not known how abrogation of *S. pombe* AMPK altered septation. A number of possibilities may underlie this, including altered septum/membrane composition as a result of abrogated carbohydrate/lipid metabolism. Alternatively, there may be ineffective septum degradation due to altered expression or post-translational modification of hydrolytic enzymes. Altered septation may also be a result of delayed contraction of the actomyosin ring.

Real time analysis of septation using Calcofluor-White staining could help determine at which point septation is delayed. Additionally, the composition and dynamics of the actomyosin ring could be examined. Metabolomic analysis could also determine if AMPK subunit deletion influenced whole cell carbohydrate and lipid metabolism. Finally, expression/PTM of hydrolytic enzymes could be assessed.

- Do the genetic interactions between AMPK and mitotic proteins reflect physical interactions *in vivo*?

In this study when genetic interactions were identified *in vitro* phosphorylation assays were undertaken to determine if the gene products could phosphorylate each other. However a number of other genetic and biochemical approaches could be employed to examine protein interactions which would further validate the results. This could include carrying out yeast two-hybrid experiments in *S. pombe* where a transcription factor is split into two fragments, each of which is fused to theorised interacting proteins. If the proteins interacted *in vivo*, the transcription factor would be reconstituted and mediate the production of a measurable reported gene. This is an ideal technique to be carried out in *S. pombe* due to the relative ease of genetic manipulation. Further analysis could be carried out in mammalian cells by assessing co-immunoprecipitation or fluorescent in situ-hybridisation. Binding sequences could also be characterised using peptide arrays and alanine screens to determine the binding sequence.

- How are other cell cycle modulators influenced by AMPK?

It would also be interesting to evaluate how AMPK interacted with other cell cycle regulators such as MRLC, cyclins, CDK, CKIs or the anaphase-promoting complex. Genetic interactions could be assessed using *S. pombe* followed by performing *in vitro* phosphorylation assays.

- On which residues are the identified proteins phosphorylated? And what are the functional implications of phosphorylation?

The most striking results in this study was the discovery of a network of cross-phosphorylation which existed between AMPK/LKB1/CaMKKß and aurora A/aurora B/PLK1. After confirming *in vitro* phosphorylation of proteins, mass spectrometry could be undertaken to identify which residues were phosphorylated. This could be followed by the generation of phosphomimetic or phosphonull mutants. Then the activity of mutant proteins could be assessed to determine how phosphorylation influenced activity. Importantly the stoichiometry of the phosphorylation could also be assessed.

7 Appendix 1-*S. pombe* strain list

The following is the full genotype of *S. pombe* strains used and generated during the course of this investigation.

Lab number	Genotype	Source
GG380	*h⁺ plo1-ts18::ura4⁺ ura4-D18 his2 leu1-32 ade6-M210*	(MacIver, Glover and Hagan, 2003)
GG400	*h⁻ ade6-216 leu1-31 ura4-D18*	Laboratory stock
GG1125	*h⁻ mid1::ura4⁺ ura4-D18 leu1-32 ade6-M210*	A kind gift from A Paoletti, Centre de recherché de l'Institut Curie. (AP245). (Sohrmann *et al.*, 1996)
GG1167	*h⁺ plo1-ts35 ura4-D18 leu1-32*	(Anderson *et al.*, 2002)
GG1554	*h⁺ dmf1::kanMX4 ura4-D18 leu1-32 ade6-216*	A kind gift from A Paoletti, Centre de recherché de l'Institut Curie. (AP245). (Sohrmann *et al.*, 1996)
GG1615	*h⁹⁰ sst6::ura4⁺ ura4-D18 leu1-32 ade6-6-M210*	(Iwaki *et al.*, 2007)
GG1616	*h⁹⁰ vps28::ura4⁺ ura4-D18 leu1-32 ade6-M210*	(Iwaki *et al.*, 2007)
GG1617	*h⁻ vps36::ura4⁺ ura4-D18 leu1-32 ade6-M210*	(Iwaki *et al.*, 2007)
GG1618	*h⁻ vps25::ura4⁺ ura4-D18 leu1-32*	(Iwaki *et al.*, 2007)
GG1619	*h⁹⁰ vps20::ura4⁺ ura4-D18 leu1-32 ade6-M210*	(Iwaki *et al.*, 2007)

GG1621	h^- vps2::LEU2 ura4-C190T leu1-32	(Iwaki *et al.*, 2007)
GG1622	h^- vps4::ura4$^+$ ura4-D18 leu1-32	(Iwaki *et al.*, 2007)
GG2426	h^+ ark1-T8-GFP-flag-His<<kanR ura4-D18 leu1-32 ade6-210	(Koch *et al.*, 2011)
GG2540	h^{90} vps32::ura4$^+$ leu1-31 ura4-D18 ade6-M210	(Iwaki *et al.*, 2007)
GG2979	h^+ amk2::KanMX4 ade- leu- ura-	(Valbuena and Moreno, 2012)
GG2981	h^+ cbs2::KanMX4 ade- leu- ura-	(Valbuena and Moreno, 2012)
GG2966	h^- ssp1::ura4$^+$ ura4-D18	(Valbuena and Moreno, 2012)
GG2986	$h^?$ ssp1::ura4$^+$ ark1-T8-GFP-flag<<kanR ura4-D18	This study
GG2987	$h^?$ ssp1::ura4$^+$ plo1-ts35 ura4-D18	This study
GG2988	$h^?$ ssp1::ura4$^+$ plo1-ts35 ura4-D18 leu1-32	This study
GG2989	$h^?$ ssp1::ura4$^+$ ark1-T8-GFP-flag-His<<kanR ura4-D18 leu1-31	This study
GG2990	$h^?$ ssp1::ura4$^+$ ark1-T8-GFP-flag-His<<kanR ura4-D18 leu1-31 ade6-210	This study
GG2991	$h^?$ ssp1::ura4$^+$ ark1-T8-GFP-flag-His<<kanR ura4-D18 leu1-31 ade6-210	This study
GG2992	$h^?$ ssp1::ura4$^+$ ark1-T8-GFP-flag-His<<kanR ura4-D18 leu1-31 ade6-210	This study
GG2993	$h^?$ ssp1::ura4$^+$ plo-ts35 ura4-D18leu1-31	This study
GG2995	$h^?$ amk2::kanMX4 sst4::ura4$^+$ ura- leu-	This study
GG2996	$h^?$ amk2::kanMX4 sst4::ura4$^+$ ura- leu-ade-	This study
GG2997	$h^?$ amk2::kanMX4 sst4::ura4$^+$ ura- leu-	This study

GG2998	*h? amk2::kanMX4 vps20::ura4⁺ ura- leu-ade-*	This study
GG2999	*h? amk2::kanMX4 vps20::ura4⁺ ura- leu-ade-*	This study
GG3000	*h? amk2::kanMX4 vps20::ura4⁺ ura- leu-ade-*	This study
GG3001	*h? amk2::kanMX4 vps20::ura4⁺ ura- leu-ade-*	This study
GG3002	*h? amk2::kanMX4 vps2::LEU2 ura- leu- ade-*	This study
GG3003	*h? amk2::kanMX4 vps2::LEU2 ura- leu- ade-*	This study
GG3004	*h? amk2::kanMX4 vps2::LEU2 ura- leu- ade-*	This study
GG3005	*h? amk2::kanMX4 vps2::LEU2 ura- leu*	This study
GG3006	*h? amk2::kanMX4 sst6::ura4⁺ ura- leu- ade-*	This study
GG3007	*h? amk2::kanMX4 sst6::ura4⁺ ura- leu- ade-*	This study
GG3008	*h? amk2::kanMX4 vps28::ura4⁺ ura- leu- ade-*	This study
GG3009	*h? amk2::kanMX4 vps32::ura4⁺ ura- leu- ade-*	This study
GG3010	*h? amk2::kanMX4 vps32::ura4⁺ ura- leu- ade-*	This study
GG3012	*h? cbs2::kanMX4 sst4::ura4⁺ ura- leu-*	This study
GG3013	*h? cbs2::kanMX4 sst4::ura4⁺ ura- leu-*	This study
GG3014	*h? cbs2::kanMX4 sst4::ura4⁺ ura- leu-ade-*	This study
GG3015	*h? cbs2::kanMX4 vps20::ura4⁺ ura- leu- ade-*	This study
GG3016	*h? cbs2::kanMX4 vps20::ura4⁺ ura- leu- ade-*	This study

GG3017	*h? cbs2::kanMX4 vps20::ura4+ ura- leu- ade-*	This study
GG3029	*h? cbs2::kanMX4 vps36::ura4+ ura- leu- ade-*	This study
GG3030	*h? cbs2::kanMX4 vps36::ura4+ ura- leu-*	This study
GG3031	*h? cbs2::kanMX4 vps36::ura4+ ura- leu-*	This study
GG3032	*h? cbs2::kanMX4 vps36::ura4+ ura- leu- ade-*	This study
GG3033	*h- ssp2::ura4+ ura4-D18 leu1-32*	(Davie *et al.*, 2015)
GG3041	*h? ssp1::kanMX4*	(Davie *et al.*, 2015)
GG3044	*h? amk2::kanMX4 vps25::ura4+ ura- leu- ade-*	This study
GG3045	*h? amk2::kanMX4 vps25::ura4+ ura- leu- ade-*	This study
GG3046	*h? amk2::kanMX4 vps25::ura4+ ura- leu- ade-*	This study
GG3047	*h? amk2::kanMX4 vps36::ura4+ ura- leu- ade-*	This study
GG3048	*h? amk2::kanMX4 vps36::ura4+ ura- leu- ade-*	This study
GG3049	*h? cbs2::kanMX4 vps32::ura4+ ura- leu- ade-*	This study
GG3050	*h? amk2::kanMX4 vps4::ura4+ ura- leu- ade-*	This study
GG3051	*h? amk2::kanMX4 vps4::ura4+ ura- leu- ade-*	This study
GG3052	*h? cbs2::kanMX4 vps2::LEU2 ura- leu- ade-*	This study
GG3053	*h? cbs2::kanMX4 vps2::LEU2 ura- leu- ade-*	This study
GG3054	*h? cbs2::kanMX4 vps2::LEU2 ura- leu- ade-*	This study

GG3055	*h? amk2::kanMX4 vps28::ura4+ ura- leu-*	This study
GG3056	*h? cbs2::kanMX4 vps4::ura4+ ura- leu-*	This study
GG3057	*h? ssp2::ura4+ ark1-T8-GFP-flag-His<<kanR ura4-D18 leu1-32 ade6-210*	This study
GG3058	*h? amk2::kanMX4 vps32::ura4+ ura- leu- ade-*	This study
GG3059	*h? amk2::kanMX4 vps32::ura4+ ura- leu- ade-*	This study
GG3060	*h? amk2::kanMX4 vps32::ura4+ ura- leu- ade-*	This study
GG3061	*h+ ssp2::ura4+ leu1-32 ura4-D18*	This study
GG3062	*h- amk2::kanMX4+ ade- leu- ura-*	This study
GG3063	*h- cbs22::kanMX4+ ade- leu- ura-*	This study
GG3064	*h? ssp2::ura4+ vps25::ura4+ leu1-32 ura4-D18 ade-*	This study
GG3065	*h? ssp2::ura4+ vps25::ura4+ leu1-32 ura4-D18 ade-*	This study
GG3066	*h+ ssp2::ura4+ leu1-32 ura4-D18*	This study
GG3067	*h? amk2::kanMX4 vps32::ura4+ ura- leu- ade*	This study
GG3068	*h? cbs2::kanMX4 vps25::ura4+ ura- leu- ade*	This study
GG3069	*h? cbs2::kanMX4 vps25::ura4+ ura- leu-*	This study
GG3070	*h? cbs2::kanMX4 vps36::ura4+ ura- leu- ade*	This study
GG3071	*h? amk2::kanMX4+ vps4::ura4+ ura- leu-*	This study
GG3072	*h? amk2::kanMX4+ vps4::ura4+ ura- leu- ade-*	This study

GG3073	*h? ssp2::ura4+ ark1-T8-GFP-flag-His<<KanR ura-leu-*	This study
GG3074	*h? ssp2::ura4+ ark1-T8-GFP-flag-His<<KanR ura-leu-*	This study
GG3075	*h? amk2::kanMX4 sst6::ura6+ ura- leu- ade-*	This study
GG3076	*h? amk2::kanMX4 vps28::ura6+ ura- leu- ade-*	This study
GG3077	*h? cbs2::kanMX4 ark1-T8-GFP-flag-His<<KanR ura- leu- ade-*	This study
GG3078	*h? cbs2::kanMX4 ark1-T8-GFP-flag-His<<KanR ura- leu- ade-*	This study
GG3079	*h- ssp1::kanMX4 ura- leu-*	This study
GG3080	*h+ ssp1::kanMX4 ura- leu-*	This study
GG3081	*h? cbs2::kanMX4 ark1-T8-GFP-flag-His<<KanR ura- leu- ade-*	This study
GG3082	*h? cbs2::kanMX4 ark1-T8-GFP-flag-His<<KanR ura- leu- ade-*	This study
GG3083	*h? cbs2::kanMX4 vps25::ura4+ ura- leu- ade-*	This study
GG3084	*h? cbs2::kanMX4 vps28::ura4+ ura- leu- ade-*	This study
GG3085	*h? cbs2::kanMX4 vps25::ura4+ ura- leu- ade-*	This study
GG3086	*h? cbs2::kanMX4 vps25::ura4+ ura- leu- ade-*	This study
GG3087	*h? ssp1::kanMX4 vps28::ura4+ ura- leu- ade-*	This study
GG3088	*h? ssp1::kanMX4 vps28::ura4+ ura- leu- ade-*	This study
GG3088	*h? ssp1::kanMX4 vps28::ura4+ ura- leu- ade-*	This study
GG3090	*h? ssp1::kanMX4+ sst6::ura4+ ura- leu- ade-*	This study

GG3091	*h? cbs2::kanMX4 vps32::ura4+ ura- leu- ade-*	This study
GG3092	*h? ssp2::kanMX4 plo1-ts18::ura4+ ura- leu- ade-his2-*	This study
GG3093	*h? ssp2::kanMX4 plo1-ts18::ura4+ ura- leu- ade-his2-*	This study
GG3094	*h? cbs2::kanMX4 mid1::ura4+ ura- leu-*	This study
GG3095	*h? cbs2::kanMX4 mid1::ura4+ ura- leu-*	This study
GG3096	*h? cbs2::kanMX4 mid1::ura4+ ura- leu-*	This study
GG3097	*h? amk2::kanMX4 mid1::ura4+ ura- leu-*	This study
GG3098	*h? amk2::kanMX4 mid1::ura4+ ura- leu-*	This study
GG3099	*h? ssp2::ura4+ dmf1::kanMX4 ura- leu- ade-*	This study
GG3108	*h? cbs2::kanMX4 sst6::ura4+ ura- leu-ade-*	This study
GG3109	*h? cbs2::kanMX4 sst6::ura4+ ura- leu-ade-*	This study
GG3110	*h? cbs2::kanMX4 sst6::ura4+ ura- leu-ade-*	This study
GG3111	*h? cbs2::kanMX4 sst6::ura4+ ura- leu-ade-*	This study
GG3112	*h? amk2::kanMX4 mid1::ura4+ ura- leu-ade-*	This study
GG3113	*h? amk2::kanMX4 mid1::ura4+ ura- leu-ade-*	This study
GG3114	*h? amk2::kanMX4 mid1::ura4+ ura- leu-ade-*	This study
GG3115	*h? amk2::kanMX4 plo1-ts18::ura4+ ura- leu-ade-*	This study
GG3116	*h? ssp1::kanMX4 vps20::ura4+ ura- leu-ade-*	This study

GG3117	*h? ssp1::kanMX4 vps2::LEU2 ura- leu-ade-*	This study
GG3119	*h? cdr2::natMX6 ark1-T8-GFP-flag-His<<kanR ura- leu-*	This study
GG3120	*h? cdr2::natMX6 ark1-T8-GFP-flag-His<<kanR ura- leu-*	This study
GG3121	*h? ssp1::kanMX4 sst6::ura4$^+$ ura- leu- ade-*	This study
GG3122	*h? ssp1::kanMX4 sst6::ura4$^+$ ura- leu- ade-*	This study
GG3123	*h? ssp1::kanMX4 vps20::ura4$^+$ ura- leu-*	This study
GG3124	*h? ssp1::kanMX4 vps20::ura4$^+$ ura- leu-*	This study
GG3125	*h? ssp1::kanMX4 vps4::ura4$^+$ ura- leu-*	This study
GG3126	*h? ssp1::kanMX4 vps4::ura4$^+$ ura- leu-*	This study
GG3127	*h? ssp1::kanMX4 vps4::ura4$^+$ ura- leu-*	This study
GG3128	*h? ssp1::kanMX4 sst4::ura4$^+$ ura- leu-*	This study
GG3129	*h? ssp1::kanMX4 sst4::ura4$^+$ ura- leu-*	This study
GG3130	*h? ssp1::kanMX4 sst4::ura4$^+$ ura- leu-*	This study
GG3131	*h? ssp1::kanMX4 vps32::ura4$^+$ ura- leu-*	This study
GG3132	*h? ssp1::kanMX4 vps32::ura4$^+$ ura- leu- ade-*	This study
GG3233	*h? ssp1::kanMX4 vps32::ura4$^+$ ura- leu-*	This study
GG3134	*h? cbs2::kanMX4 vps4::ura4$^+$ ura- leu-*	This study
GG3135	*h? cbs2::kanMX4 vps4::ura4$^+$ ura- leu-*	This study

GG3136	*h? cbs2::kanMX4 vps32::ura4+ ura- leu- ade-*	This study
GG3137	*h? ssp1::kanMX4 vps36::ura4+ ura- leu-*	This study
GG3138	*h? ssp1::kanMX4 vps36::ura4+ ura- leu-*	This study
GG3139	*h? ssp1::kanMX4 vps32::ura4+ ura- leu-*	This study
GG3140	*h? ssp1::kanMX4 vps32::ura4+ ura- leu- ade-*	This study
GG3141	*h? ssp1::kanMX4 vps32::ura4+ ura- leu- ade-*	This study
GG3142	*h? ssp1::kanMX4 vps32::ura4+ ura- leu-*	This study
GG3144	*h? amk2::kanMX4 plo1-ts18::ura4+ ura- leu- ade-*	This study
GG3145	*h? amk2::kanMX4 plo1-ts18::ura4+ ura- leu- ade-*	This study
GG3146	*h? amk2::kanMX4 plo1-ts18::ura4+ ura- leu- ade-*	This study
GG3147	*h? amk2::kanMX4 plo1-ts18::ura4+ ura- leu- ade-*	This study
GG3148	*h? cbs2::kanMX4 plo1-ts18::ura4+ ura- leu- ade-*	This study
GG3149	*h? amk2::kanMX4 plo1-ts18::ura4+ ura- leu- ade-*	This study
GG3150	*h? amk2::kanMX4 plo1-ts18::ura4+ ura- leu- ade-*	This study
GG3151	*h? amk2::kanMX4 plo1-ts18::ura4+ ura- leu- ade-*	This study
GG3152	*h? ssp1::kanMX4 plo1-ts18::ura4+ ura- leu- ade-*	This study
GG3153	*h? ssp1::kanMX4 plo1-ts18::ura4+ ura- leu-*	This study
GG3134	*h? ssp1::kanMX4 plo1-ts18::ura4+ ura- leu-*	This study

GG3155	*h? ssp1::kanMX4 plo1-ts18::ura4+ ura- leu-*	This study
GG3160	*h? ssp1::kanMX4 mid1::ura4+ ura- leu-ade-*	This study
GG3161	*h? ssp1::kanMX4 mid1::ura4+ ura- leu-ade-*	This study
GG3162	*h? ssp1::kanMX4 mid1::ura4+ ura- leu-ade-*	This study
GG3163	*h? ssp1::kanMX4 vps2::LEU2 ura- leu-*	This study
GG3164	*h? ssp1::kanMX4 vps2::LEU2 ura- leu-*	This study
GG3165	*h? ssp1::kanMX4 vps2::LEU2 ura- leu-*	This study
GG3166	*h? ssp2::ura4+ dmf1::kanMX4 ura- leu-*	This study
GG3167	*h? ssp2::ura4+ dmf1::kanMX4 ura- leu-*	This study
GG3168	*h? ssp2::ura4+ dmf1::kanMX4 ura- leu-*	This study
GG3169	*h? ssp2::ura4+ plo1-ts18:: ura4+ ura- leu- ade-*	This study
GG3170	*h? ssp2::ura4+ plo1-ts18:: ura4+ ura- leu- ade-*	This study
GG3171	*h? ssp2::ura4+ plo1-ts35 ura- leu-*	This study
GG3172	*h? ssp2::ura4+ plo1-ts35 ura- leu-*	This study
GG3173	*h? ssp2::ura4+ plo1-ts35 ura- leu-*	This study
GG3174	*h? ssp2::ura4+ plo1-ts35 ura- leu-*	This study
GG3175	*h? amk2::ura4+ vps36:: ura4+ ura- leu- ade-*	This study
GG3176	*h? amk2::ura4+ vps36:: ura4+ ura- leu- ade-*	This study

GG3177	*h? amk2::ura4+ vps36:: ura4+ ura- leu- ade-*	This study
GG3178	*h? cbs2::ura4+ vps32:: ura4+ ura- leu- ade-*	This study
GG3179	*h? cbs2::ura4+ vps32:: ura4+ ura- leu- ade-*	This study
GG3180	*h? cbs2::ura4+ vps32:: ura4+ ura- leu- ade-*	This study
GG3225	*h- plo1::GFP-NatR*	YGRC, FY20279
GG3227	*h- ark1::GFP-leu1+ leu1-32*	YGRC, FY9431 (Okazaki and Niwa, 2008)

Table 7-1. *S. pombe* strain list
Strains were stored in 30% (v/v) glycerol at -80ºC. YGRC represents the Yeast Genetic Resource Centre, National BioResource Project, Japan.

8 Appendix 2-Negative genetic interactions between AMPK and ESCRT components in *S. pombe*

8.1 Negative interactions between *ssp2* and ESCRT components

Figure 8-1. No growth rate defects were observed in *ssp2Δ vps25Δ* double mutant cells
Wild type (GG1278), *vps25Δ* (GG1618), *ssp2Δ* (GG3080), and two separate isolates of *ssp2Δ vps25Δ* (GG2064, 3065). Strains were suspended at $1.5x10^6$ cell per ml and subjected to 10-fold serial dilution. Cell suspension was pipetted onto solid YE media and for 3 days.

8.2 Negative interactions between *amk2* and ESCRT components

Figure 8-2. No growth rate defects were observed in *amk2Δ sst4Δ* double mutant cells
Wild type (GG1278), *amk2Δ* (GG2979), *sst4Δ* (GG1623) and three separate isolates of *ssp2Δ sst4Δ* (GG2995, GG2996, GG 2997). Strains were suspended at 1.5×10^6 cell per ml and subjected to 10-fold serial dilution. Cell suspension was pipetted onto solid YE media and for 3 days.

Figure 8-3. No growth rate defects were observed in *amk2Δ sst6Δ* double mutant cells
Wild type (GG1278), *sst6Δ* (GG1615), *amk2Δ* (GG2979) and three separate isolates of *ssp2Δ sst6Δ* (GG3006, GG3007, GG3075). Strains were suspended at 1.5×10^6 cell per ml and subjected to 10-fold serial dilution. Cell suspension was pipetted onto solid YE media and for 3 days.

Figure 8-4. No growth rate defects were observed in *amk2Δ vps28Δ* double mutant cells
Wild type (GG1278), *vps28Δ* (GG1616), *amk2Δ* (GG2979) and three separate isolates of *ssp2Δ vps28Δ* (GG3008, GG3055, GG3076). Strains were suspended at 1.5×10^6 cell per ml and subjected to 10-fold serial dilution. Cell suspension was pipetted onto solid YE media and for 3 days.
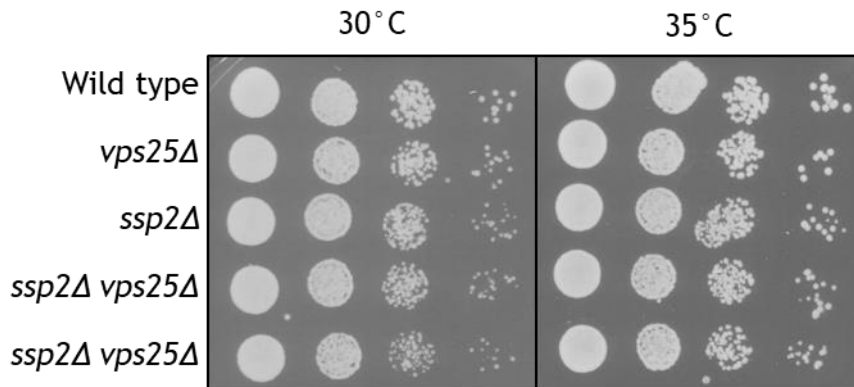

Figure 8-5. No growth rate defects were observed in *amk2Δ vps36Δ* double mutant cells
Wild type (GG1278), *vps36Δ* (GG1617), *amk2Δ* (GG2979) and three separate isolates of *ssp2Δ vps36Δ* (GG3173, GG3176, GG3177). Strains were suspended at 1.5×10^6 cell per ml and subjected to 10-fold serial dilution. Cell suspension was pipetted onto solid YE media and for 3 days.
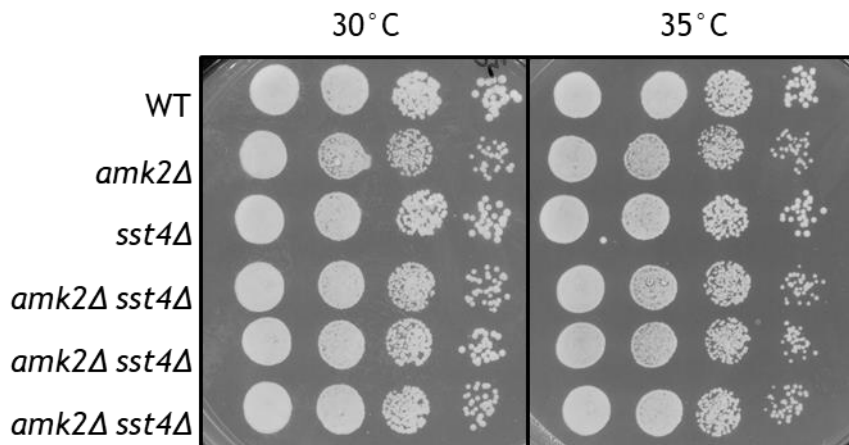
Figure 8-6. No growth rate defects were observed in *amk2Δ vps25Δ* double mutant cells
Wild type (GG1278), *vps25Δ* (GG1618), *amk2Δ* (GG2979) and three separate isolates of *ssp2Δ vps25Δ* (GG3044, GG3045, GG3046). Strains were suspended at 1.5×10^6 cell per ml and subjected to 10-fold serial dilution. Cell suspension was pipetted onto solid YE media and for 3 days.

Figure 8-7. No growth rate defects were observed in *amk2Δ vps20Δ* double mutant cells
Wild type (GG1278), *vps20Δ* (GG1619), *amk2Δ* (GG2979) and three separate isolates of *ssp2Δ vps20Δ* (GG2998, GG2999, GG3000). Strains were suspended at 1.5×10^6 cell per ml and subjected to 10-fold serial dilution. Cell suspension was pipetted onto solid YE media and for 3 days.

Figure 8-8. No growth rate defects were observed in *amk2Δ vps32Δ* double mutant cells
Wild type (GG1278), *vps32Δ* (GG2540), *amk2Δ* (GG2979) and three separate isolates of *ssp2Δ vps32Δ* (GG3009, GG3010, GG3058). Strains were suspended at 1.5x10^6 cell per ml and subjected to 10-fold serial dilution. Cell suspension was pipetted onto solid YE media and for 3 days.
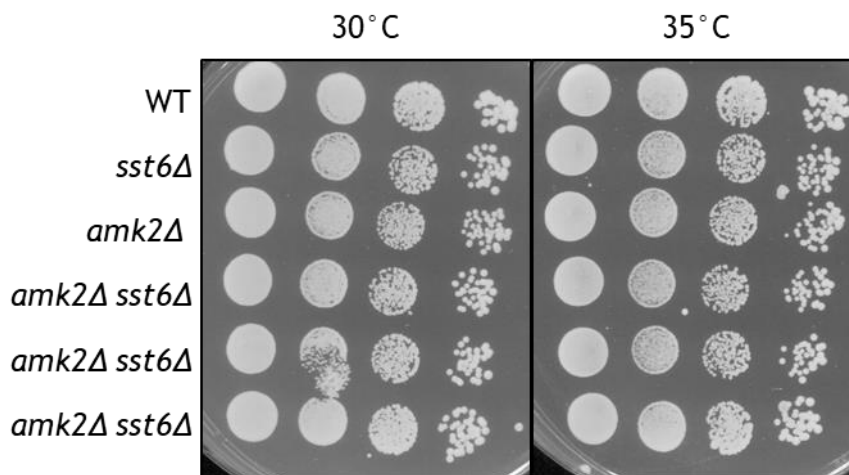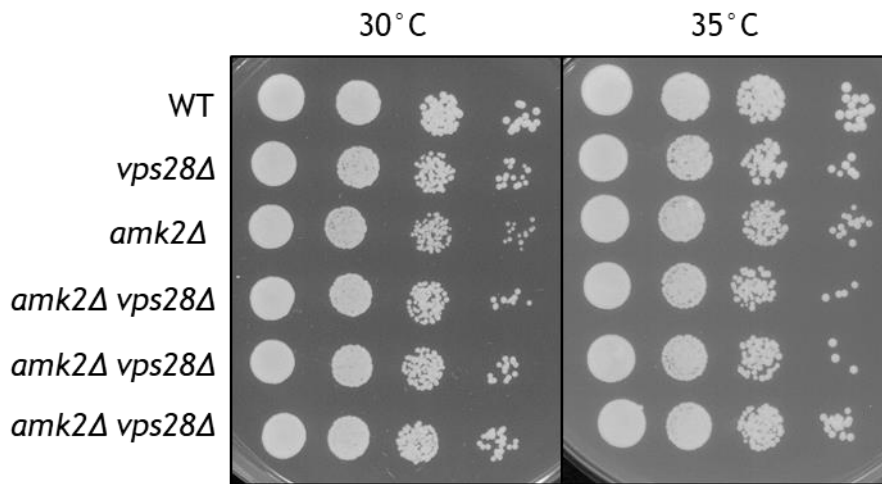

Figure 8-9. No growth rate defects were observed in *amk2Δ vps2Δ* double mutant cells
Wild type (GG1278), *amk2Δ* (GG2979), *vps2Δ* (GG1621) and three separate isolates of *ssp2Δ vps2Δ* (GG3002, GG3003, GG3004). Strains were suspended at 1.5x10^6 cell per ml and subjected to 10-fold serial dilution. Cell suspension was pipetted onto solid YE media and for 3 days.
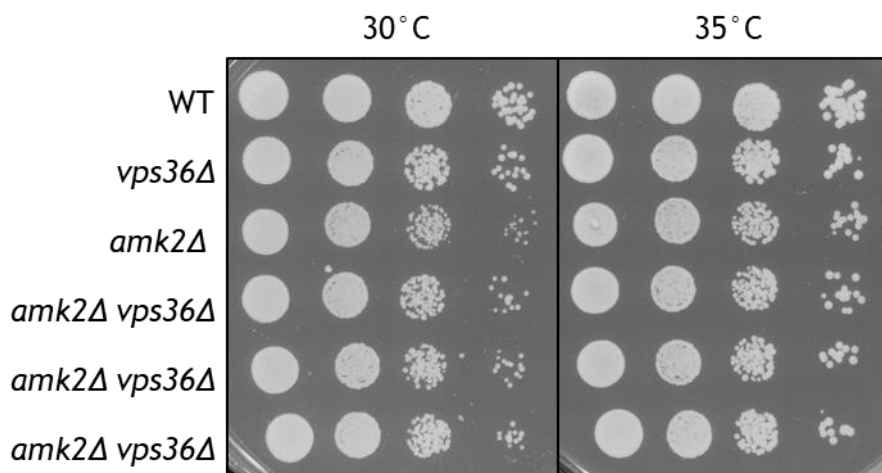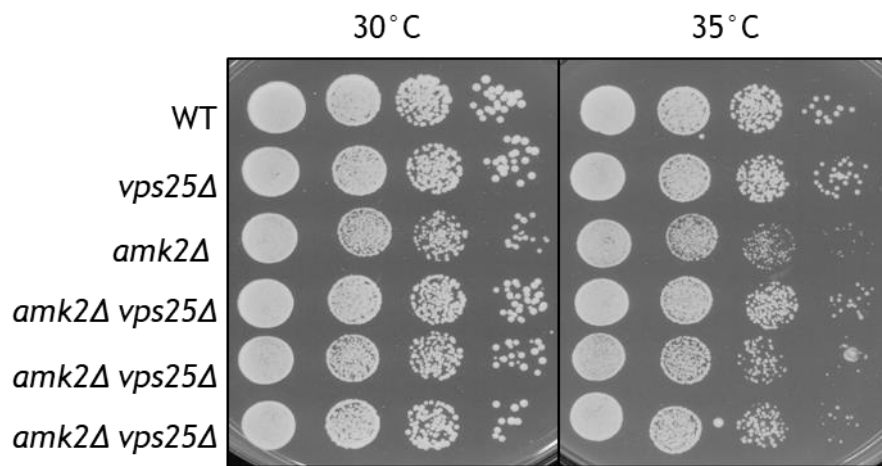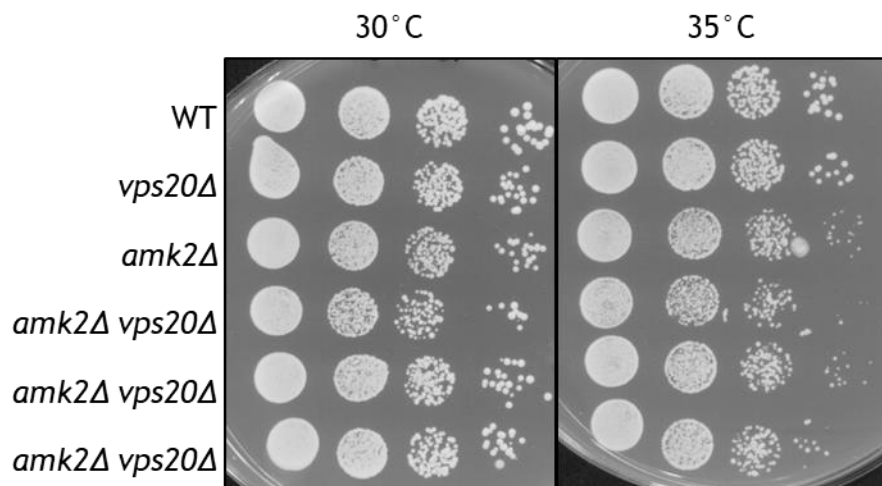
Figure 8-10. No growth rate defects were observed in *amk2Δ vps4Δ* double mutant cells
Wild type (GG1278), *vps4Δ* (GG1622), *amk2Δ* (GG2979) and three separate isolates of *ssp2Δ vps4Δ* (GG3050, GG3051, GG3071). Strains were suspended at 1.5×10^6 cell per ml and subjected to 10-fold serial dilution. Cell suspension was pipetted onto solid YE media and for 3 days.

8.3 Negative interactions between *cbs2* and ESCRT components
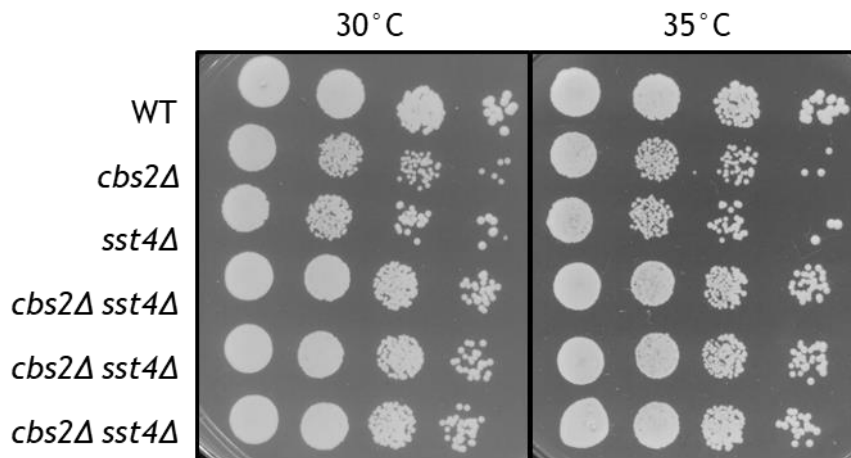
Figure 8-11. No growth rate defects were observed in *cbs2Δ sst4Δ* double mutant cells
Wild type (GG1278), *cbs2Δ* (GG2981), *sst4Δ* (GG1623) and three separate isolates of *cbs2Δ sst4Δ* (GG3012, GG3013, GG3014). Strains were suspended at 1.5×10^6 cell per ml and subjected to 10-fold serial dilution. Cell suspension was pipetted onto solid YE media and for 3 days.

Figure 8-12. No growth rate defects were observed in *cbs2Δ sst6Δ* double mutant cells
Wild type (GG1278), *sst6Δ* (GG1615), *cbs2Δ* (GG2981) and three separate isolates of *cbs2Δ sst6Δ* (GG3108, GG3109, GG3110). Strains were suspended at 1.5×10^6 cell per ml and subjected to 10-fold serial dilution. Cell suspension was pipetted onto solid YE media and for 3 days.

Figure 8-13. No growth rate defects were observed in *cbs2Δ vps28Δ* double mutant cells
Wild type (GG1278), *vps28Δ* (GG1616), *cbs2Δ* (GG2981) and three separate isolates of *cbs2Δ vps28Δ* (GG3084, GG3085, GG3086). Strains were suspended at 1.5×10^6 cell per ml and subjected to 10-fold serial dilution. Cell suspension was pipetted onto solid YE media and for 3 days.
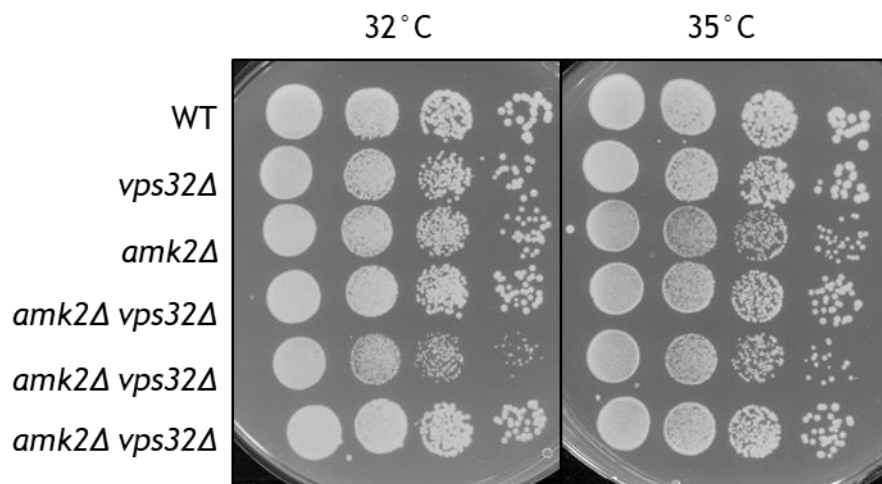

Figure 8-14. No growth rate defects were observed in *cbs2Δ vps36Δ* double mutant cells
Wild type (GG1278), *vps36Δ* (GG1617), *cbs2Δ* (GG2981) and three separate isolates of *cbs2Δ vps36Δ* (GG3029, GG3030, GG3031). Strains were suspended at 1.5×10^6 cell per ml and subjected to 10-fold serial dilution. Cell suspension was pipetted onto solid YE media and for 3 days.
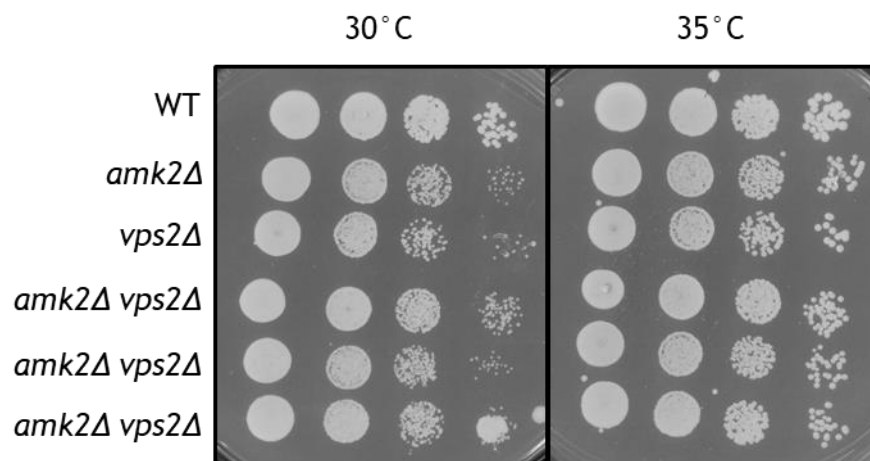
Figure 8-15. No growth rate defects were observed in *cbs2Δ vps25Δ* double mutant cells
Wild type (GG1278), *cbs2Δ* (GG2981), *vps25Δ* (GG1618) and three separate isolates of *cbs2Δ vps25Δ* (GG3068, GG3069, GG3083). Strains were suspended at 1.5×10^6 cell per ml and subjected to 10-fold serial dilution. Cell suspension was pipetted onto solid YE media and for 3 days.
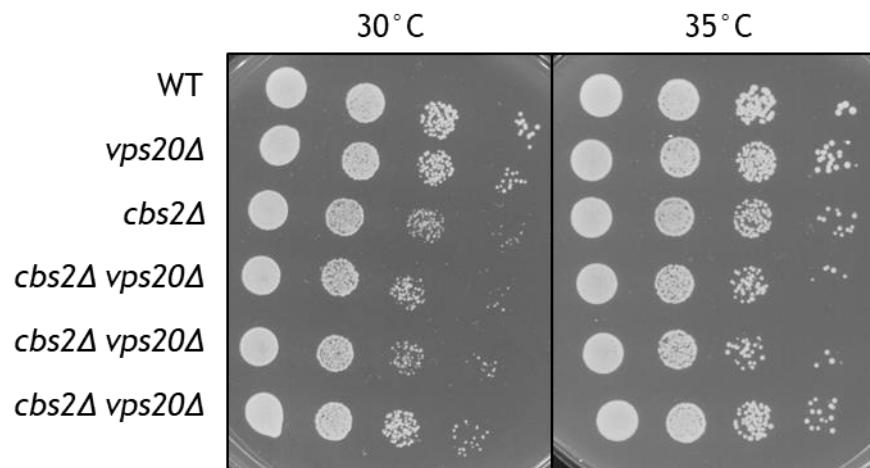
Figure 8-16. No growth rate defects were observed in *cbs2Δ vps20Δ* double mutant cells
Wild type (GG1278), *vps20Δ* (GG1619), *cbs2Δ* (GG2981) and three separate isolates of *cbs2Δ vps20Δ* (GG3015, GG3016, GG3017). Strains were suspended at 1.5×10^6 cell per ml and subjected to 10-fold serial dilution. Cell suspension was pipetted onto solid YE media and for 3 days.
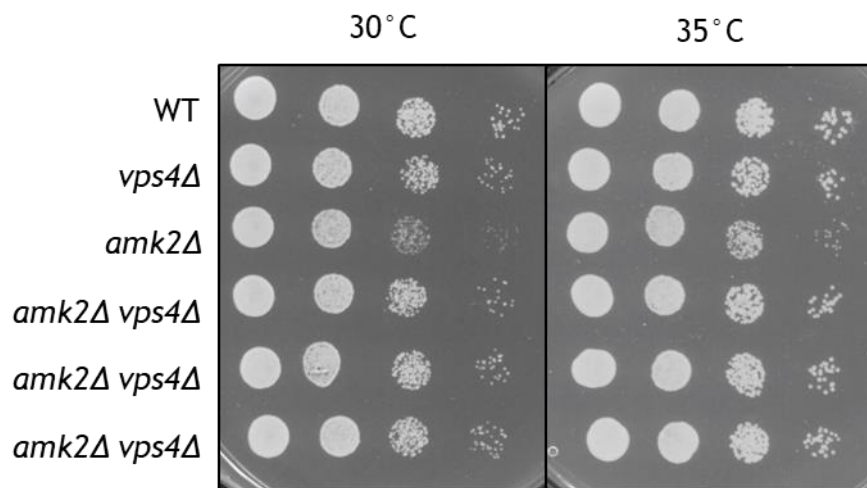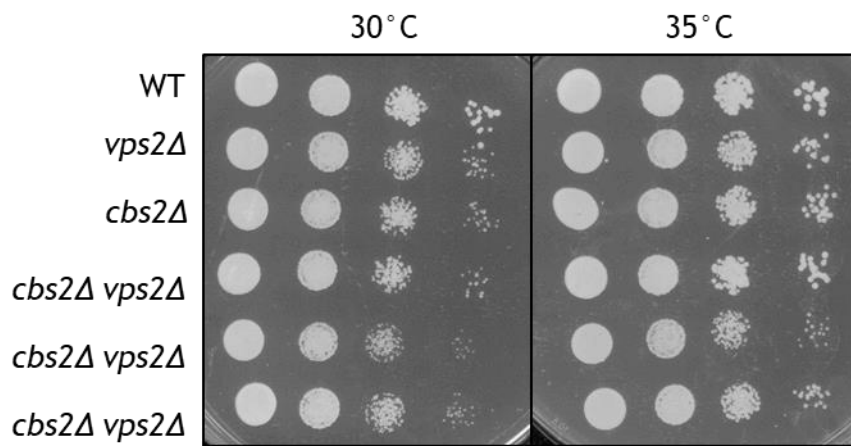
Figure 8-17. No growth rate defects were observed in *cbs2Δ vps2Δ* double mutant cells
Wild type (GG1278), *vps2Δ* (GG1621), *cbs2Δ* (GG2981) and three separate isolates of *cbs2Δ vps2Δ* (GG352, GG3053, GG3054). Strains were suspended at 1.5×10^6 cell per ml and subjected to 10-fold serial dilution. Cell suspension was pipetted onto solid YE media and for 3 days.
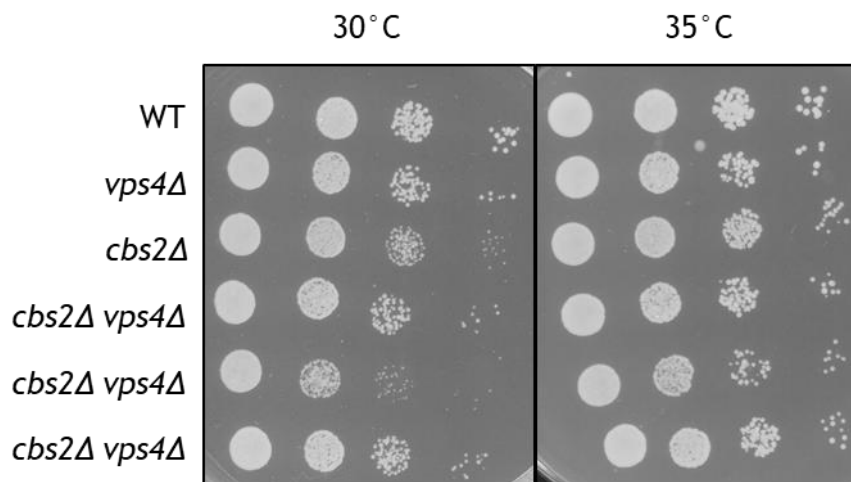
Figure 8-18. No growth rate defects were observed in *cbs2Δ vps4Δ* double mutant
Wild type (GG1278), *vps4Δ* (GG1622), *cbs2Δ* (GG2981) and three separate isolates of *cbs2Δ vps4Δ* (GG2052, GG3131, GG3135). Strains were suspended at 1.5×10^6 cell per ml and subjected to 10-fold serial dilution. Cell suspension was pipetted onto solid YE media and for 3 days.

## 8.4 Negative interactions between *ssp1* and ESCRT components
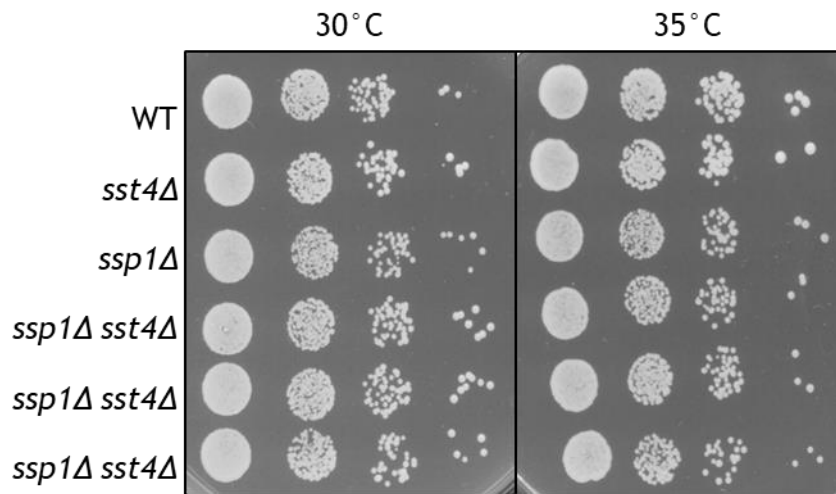
Figure 8-19. No growth rate defects were observed in *ssp1Δ sst4Δ* double mutant
Wild type (GG1278), *sst4Δ* (GG1623), *ssp1Δ* (GG3080) and three separate isolates of *ssp1Δ sst4Δ* (GG3128, GG3129, GG3130). Strains were suspended at 1.5×10^6 cell per ml and subjected to 10-fold serial dilution. Cell suspension was pipetted onto solid YE media and for 3 days.
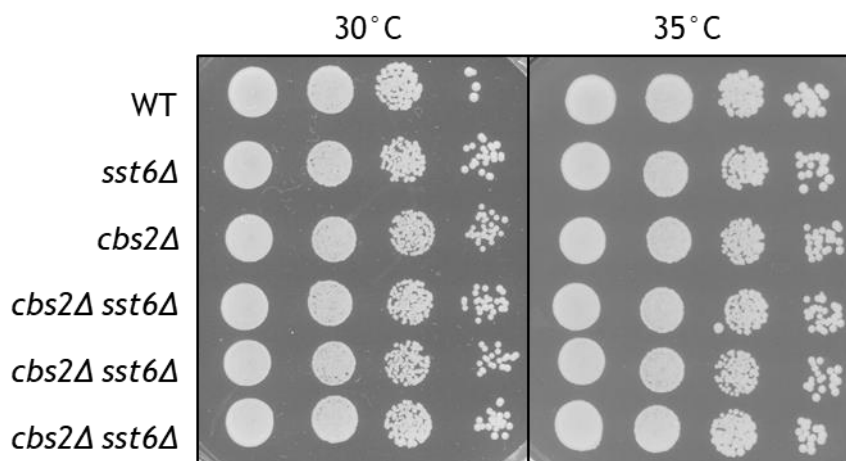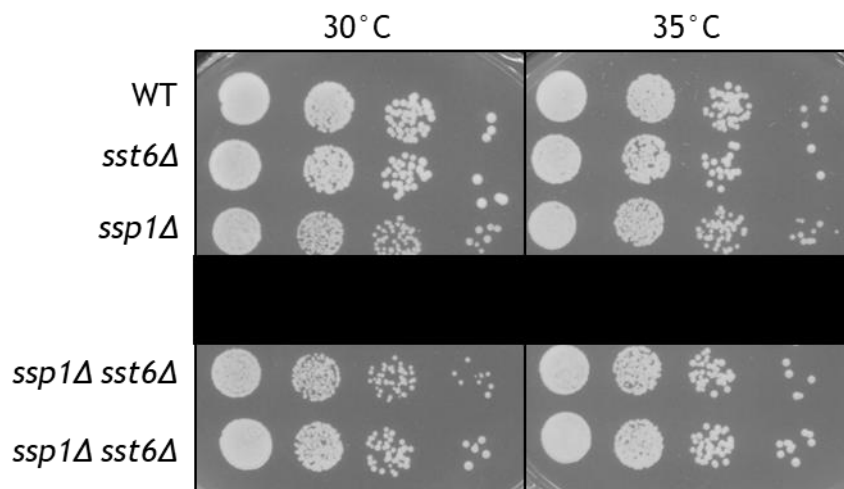

Figure 8-20. No growth rate defects were observed in *ssp1Δ sst6Δ* double mutant cells
Wild type (GG1278), *sst6Δ* (GG1615), *ssp1Δ* (GG3080) and three separate isolates of *ssp1Δ sst6Δ* (GG3090, GG3121, GG3122). Strains were suspended at 1.5×10^6 cell per ml and subjected to 10-fold serial dilution. Cell suspension was pipetted onto solid YE media and for 3 days.
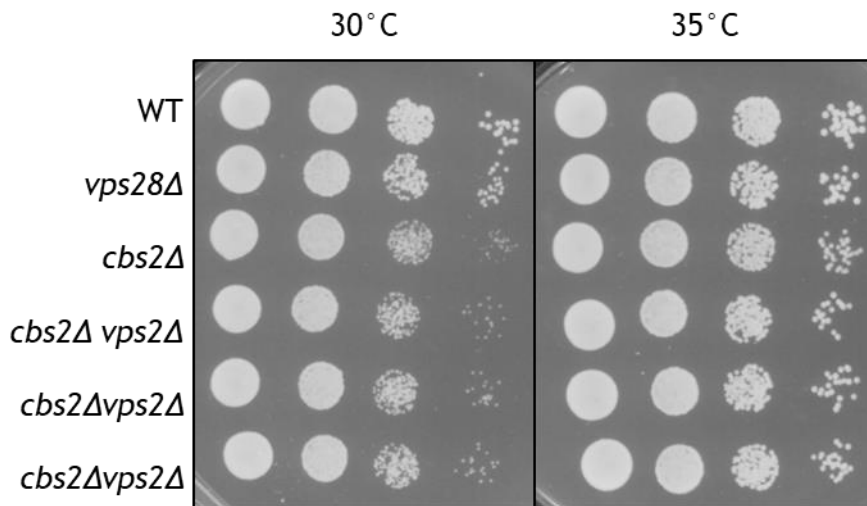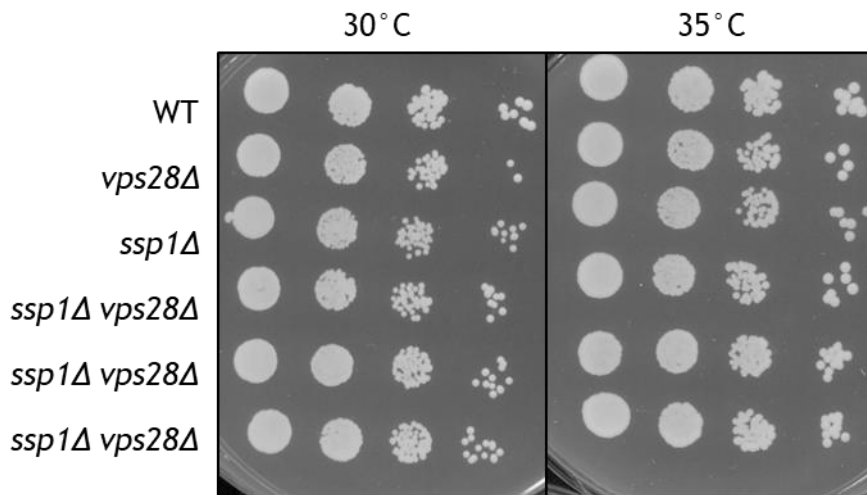
Figure 8-21. No growth rate defects were observed in *ssp1Δ vps28Δ* double mutant cells
Wild type (GG1278), *vps28Δ* (GG1616), *ssp1Δ* (GG3080) and three separate isolates of *ssp1Δ vps28Δ* (GG3087, GG3088, GG3089). Strains were suspended at 1.5×10^6 cell per ml and subjected to 10-fold serial dilution. Cell suspension was pipetted onto solid YE media and for 3 days.
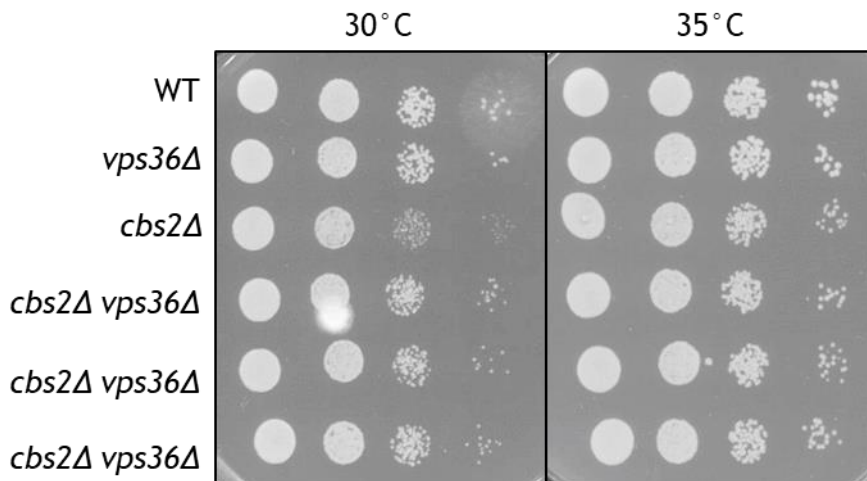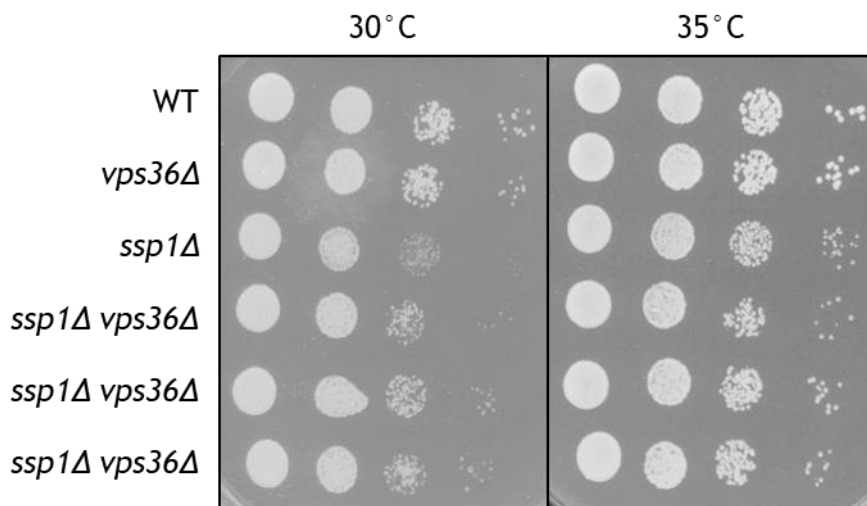

Figure 8-22. No growth rate defects were observed in *ssp1Δ vps36Δ* double mutant cells
Wild type (GG1278), *vps36Δ* (GG1617), *ssp1Δ* (GG3080) and three separate isolates of *ssp1Δ vps36Δ* (GG3137, GG3138, GG3139). Strains were suspended at 1.5×10^6 cell per ml and subjected to 10-fold serial dilution. Cell suspension was pipetted onto solid YE media and for 3 days.
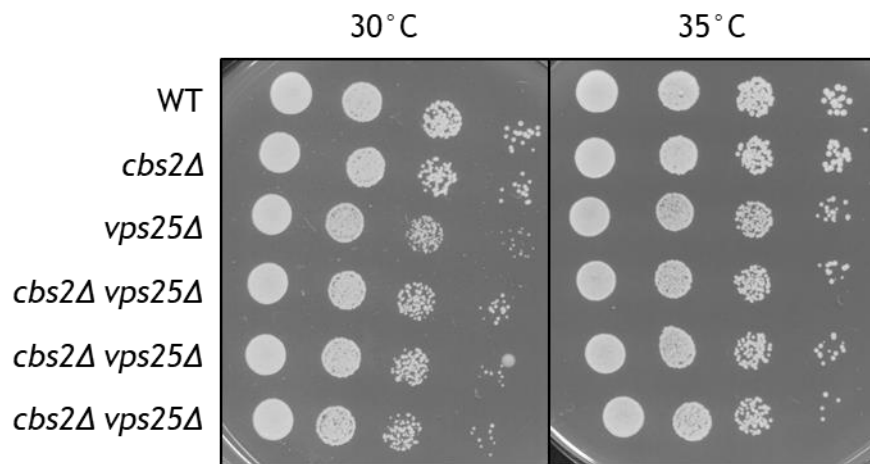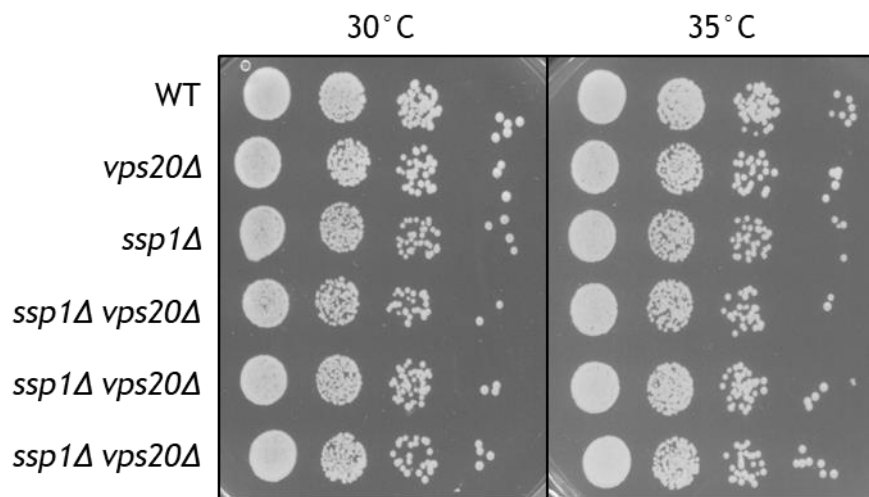
Figure 8-23. No growth rate defects were observed in *ssp1Δ vps20Δ* double mutant
Wild type (GG1278), *vps20Δ* (GG1619), *ssp1Δ* (GG3080) and three separate isolates of *ssp1Δ vps20Δ* (GG3116, GG3132, GG3124). Strains were suspended at 1.5×10^6 cell per ml and subjected to 10-fold serial dilution. Cell suspension was pipetted onto solid YE media and for 3 days.
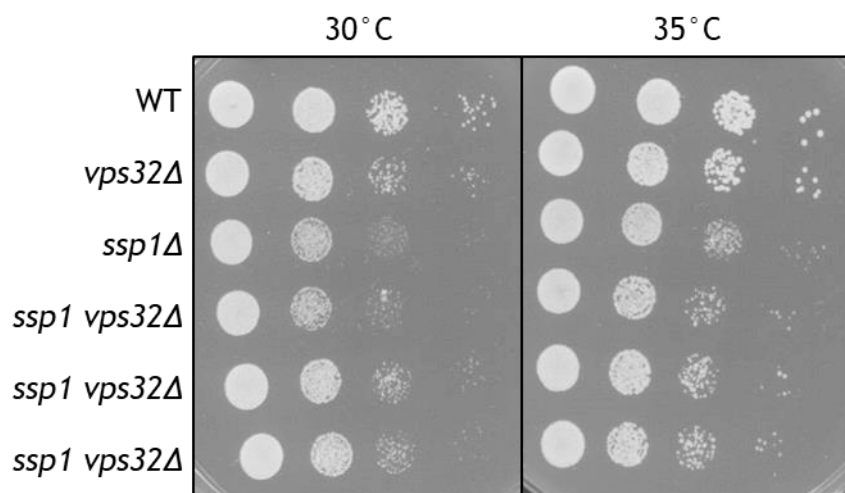
Figure 8-24. No growth rate defects were observed in *ssp1Δ vps32Δ* double mutant cells
Wild type (GG1278), *vps32Δ* (GG2540), *ssp1Δ* (GG3080) and three separate isolates of *ssp1Δ vps32Δ* (GG3131, GG3163, GG3133). Strains were suspended at 1.5×10^6 cell per ml and subjected to 10-fold serial dilution. Cell suspension was pipetted onto solid YE media and for 3 days.

9 References

Abrieu, A. *et al.* (1998) 'The Polo-like kinase Plx1 is a component of the MPF amplification loop at the G2/M-phase transition of the cell cycle in *Xenopus* eggs.', *Journal of cell science*, 111 (Pt 12), pp. 1751–7.

Abu-Elheiga, L. *et al.* (2000) 'The subcellular localization of acetyl-CoA carboxylase 2.', *Proceedings of the National Academy of Sciences of the United States of America*. National Academy of Sciences, 97(4), pp. 1444–9. doi: 10.1073/pnas.97.4.1444.

Adam, R. D. (2000) 'The Giardia lamblia genome.', *International journal for parasitology*, 30(4), pp. 475–84.

Al-Feel, W., DeMar, J. C. and Wakil, S. J. (2003) 'A Saccharomyces cerevisiae mutant strain defective in acetyl-CoA carboxylase arrests at the G2/M phase of the cell cycle.', *Proceedings of the National Academy of Sciences of the United States of America*. National Academy of Sciences, 100(6), pp. 3095–100. doi: 10.1073/pnas.0538069100.

Alberts, B. *et al.* (2012) 'The cell cycle', in *Molecular Biology of the Cell*. Garland Science, pp. 1054–1114.

Almonacid, M. *et al.* (2011) 'Temporal Control of Contractile Ring Assembly by Plo1 Regulation of Myosin II Recruitment by Mid1/Anillin', *Current Biology*, 21(6), pp. 473–479. doi: 10.1016/j.cub.2011.02.003.

Amemiya, T. *et al.* (2017) 'Primordial oscillations in life: Direct observation of glycolytic oscillations in individual HeLa cervical cancer cells', *Chaos: An Interdisciplinary Journal of Nonlinear Science*. AIP Publishing LLC , 27(10), p. 104602. doi: 10.1063/1.4986865.

An, R. *et al.* (2018) 'Plk1 interacts with RNF2 and promotes its ubiquitin-dependent degradation', *Oncology Reports*. Spandidos Publications, 39(5), pp. 2358-2364. doi: 10.3892/or.2018.6326.

Anderson, M. *et al.* (2002) 'Plo1(+) regulates gene transcription at the M-G(1) interval during the fission yeast mitotic cell cycle.', *The EMBO journal*. EMBO Press, 21(21), pp. 5745–55. doi: 10.1093/EMBOJ/CDF564.

Ando, Y. *et al.* (2007) 'Inactivation of Rho GTPases with *Clostridium difficile* Toxin B Impairs Centrosomal Activation of Aurora-A in G2/M Transition of HeLa Cells', *Molecular Biology of the Cell*. Edited by Y. Zheng, 18(10), pp. 3752–3763. doi: 10.1091/mbc.e07-03-0281.

Andrysik, Z. *et al.* (2010) 'The novel mouse Polo-like kinase 5 responds to DNA damage and localizes in the nucleolus', *Nucleic Acids Research*. Oxford University Press, 38(9), p. 2931. doi: 10.1093/NAR/GKQ011.

Arnaud, L., Pines, J. and Nigg, E. A. (1998) 'GFP tagging reveals human Polo-like kinase 1 at the kinetochore/centromere region of mitotic chromosomes.', *Chromosoma*, 107(6–7), pp. 424–9.

Bahassi, E. M. *et al.* (2002) 'Mammalian Polo-like kinase 3 (Plk3) is a multifunctional

protein involved in stress response pathways', *Oncogene*, 21(43), pp. 6633–6640. doi: 10.1038/sj.onc.1205850.

Bähler, Jürg *et al.* (1998) 'Heterologous modules for efficient and versatile PCR-based gene targeting in *Schizosaccharomyces pombe*', *Yeast*, 14(10), pp. 943–951. doi: 10.1002/(SICI)1097-0061(199807)14

Bähler, J *et al.* (1998) 'Role of polo kinase and Mid1p in determining the site of cell division in fission yeast.', *The Journal of cell biology*, 143(6), pp. 1603–16.

Bain, J. *et al.* (2007) 'The selectivity of protein kinase inhibitors: a further update.', *The Biochemical journal*. Portland Press Ltd, 408(3), pp. 297–315. doi: 10.1042/BJ20070797.

Bak, A. L., Zeuthen, J. and Crick, F. H. (1977) 'Higher-order structure of human mitotic chromosomes.', *Proceedings of the National Academy of Sciences*, 74(4), pp. 1595–1599. doi: 10.1073/pnas.74.4.1595.

Banerjee, S. *et al.* (2014) 'Interplay between Polo kinase, LKB1-activated NUAK1 kinase, PP1ßMYPT1 phosphatase complex and the SCFßTrCP E3 ubiquitin ligase.', *The Biochemical journal*. Portland Press Ltd, 461(2), pp. 233–45. doi: 10.1042/BJ20140408.

Banko, M. R. *et al.* (2011) 'Chemical Genetic Screen for AMPKα2 Substrates Uncovers a Network of Proteins Involved in Mitosis', *Molecular Cell*, 44(6), pp. 878–892. doi: 10.1016/j.molcel.2011.11.005.

Beach, D. H. (1983) 'Cell type switching by DNA transposition in fission yeast', *Nature*. Nature Publishing Group, 305(5936), pp. 682–688. doi: 10.1038/305682a0.

Bertolin, G. *et al.* (2016) 'A FRET biosensor reveals spatiotemporal activation and functions of aurora kinase A in living cells', *Nature Communications*, 7(1), p. 12674. doi: 10.1038/ncomms12674.

Bhutta, M. S. *et al.* (2014) 'A complex network of interactions between mitotic kinases, phosphatases and ESCRT proteins regulates septation and membrane trafficking in *S. pombe*.', *PloS one*. Public Library of Science, 9(10), p. e111789. doi: 10.1371/journal.pone.0111789.

Bischoff, J. R. *et al.* (1998) 'A homologue of *Drosophila* aurora kinase is oncogenic and amplified in human colorectal cancers.', *The EMBO journal*. European Molecular Biology Organization, 17(11), pp. 3052–65. doi: 10.1093/emboj/17.11.3052.

Bradford, M. M. (1976) 'A rapid and sensitive method for the quantitation of microgram quantities of protein utilizing the principle of protein-dye binding.', *Analytical biochemistry*, 72, pp. 248–54.

Burkard, M. E. *et al.* (2007) 'Chemical genetics reveals the requirement for Polo-like kinase 1 activity in positioning RhoA and triggering cytokinesis in human cells', *Proceedings of the National Academy of Sciences*, 104(11), pp. 4383–4388. doi: 10.1073/pnas.0701140104.

Calabrese, M. F. *et al.* (2014) 'Structural Basis for AMPK Activation: Natural and

Synthetic Ligands Regulate Kinase Activity from Opposite Poles by Different Molecular Mechanisms', *Structure*. Cell Press, 22(8), pp. 1161–1172. doi: 10.1016/J.STR.2014.06.009.

Cao, L. G. and Wang, Y. L. (1996) 'Signals from the spindle midzone are required for the stimulation of cytokinesis in cultured epithelial cells.', *Molecular biology of the cell*, 7(2), pp. 225–32.

Capalbo, L. *et al.* (2019) 'The midbody interactome reveals new unexpected roles for PP1 phosphatases in cytokinesis', *bioRxiv*. Cold Spring Harbor Laboratory, p. 569459. doi: 10.1101/569459.

de Carcer, G. *et al.* (2011) 'Plk5, a Polo Box Domain-Only Protein with Specific Roles in Neuron Differentiation and Glioblastoma Suppression', *Molecular and Cellular Biology*, 31(6), pp. 1225–1239. doi: 10.1128/MCB.00607-10.

Carlton, J. G., Agromayor, M. and Martin-Serrano, J. (2008) 'Differential requirements for Alix and ESCRT-III in cytokinesis and HIV-1 release', *Proceedings of the National Academy of Sciences*, 105(30), pp. 10541–10546. doi: 10.1073/pnas.0802008105.

Carlton, J. G. and Martin-Serrano, J. (2007) 'Parallels Between Cytokinesis and Retroviral Budding: A Role for the ESCRT Machinery', *Science*, 316(5833), pp. 1908–1912. doi: 10.1126/science.1143422.

Carlson, M. *et al.*(1981) 'Mutants of yeast defective in sucrose utilization', *Genetics, 98 (1), 25-40*

Celenza, J. L. and Carlson, M. (1989) 'Mutational analysis of the Saccharomyces cerevisiae SNF1 protein kinase and evidence for functional interaction with the SNF4 protein.', *Molecular and cellular biology*, 9(11), pp. 5034–44. doi: 10.1128/mcb.9.11.5034.

Chan, C. S. and Botstein, D. (1993) 'Isolation and characterization of chromosome-gain and increase-in-ploidy mutants in yeast.', *Genetics*, 135(3), pp. 677–91.

Chan, E. Y. (2009) 'mTORC1 Phosphorylates the ULK1-mAtg13-FIP200 Autophagy Regulatory Complex', *Science Signaling*, 2(84), pp. pe51–pe51. doi: 10.1126/scisignal.284pe51.

Chang, F., Woollard, A. and Nurse, P. (1996) 'Isolation and characterization of fission yeast mutants defective in the assembly and placement of the contractile actin ring.', *Journal of cell science*, 109 (Pt 1), pp. 131–42.

Chen, L. *et al.* (2012) 'AMP-activated protein kinase undergoes nucleotide-dependent conformational changes', *Nature Structural & Molecular Biology*. Nature Publishing Group, 19(7), pp. 716–718. doi: 10.1038/nsmb.2319.

Chen, L. *et al.* (2013) 'Conserved regulatory elements in AMPK', *Nature*, 498(7453), pp. E8–E10. doi: 10.1038/nature12189.

Cheung, P. C. *et al.* (2000) 'Characterization of AMP-activated protein kinase gamma-subunit isoforms and their role in AMP binding.', *The Biochemical journal*. Portland

Press Ltd, 346 Pt 3(Pt 3), pp. 659–69.

Cool, B. *et al.* (2006) 'Identification and characterization of a small molecule AMPK activator that treats key components of type 2 diabetes and the metabolic syndrome', *Cell Metabolism*, 3(6), pp. 403–416. doi: 10.1016/j.cmet.2006.05.005.

Corton, J. M. *et al.* (1995) '5-aminoimidazole-4-carboxamide ribonucleoside. A specific method for activating AMP-activated protein kinase in intact cells?', *European journal of biochemistry*, 229(2), pp. 558–65.

Crosio, C. *et al.* (2002) 'Mitotic Phosphorylation of Histone H3: Spatio-Temporal Regulation by Mammalian Aurora Kinases', *Molecular and Cellular Biology*. American Society for Microbiology (ASM), 22(3), p. 874. doi: 10.1128/MCB.22.3.874-885.2002.

Davie, E., Forte, G. M. A. and Petersen, J. (2015) 'Nitrogen regulates AMPK to control TORC1 signaling.', *Current biology : CB*. Elsevier, 25(4), pp. 445–54. doi: 10.1016/j.cub.2014.12.034.

Davies, S. P. *et al.* (1994) 'Purification of the AMP-activated protein kinase on ATP-gamma-sepharose and analysis of its subunit structure.', *European journal of biochemistry / FEBS*, 223(2), pp. 351–7.

Davies, S. P. *et al.* (1995) '5′-AMP inhibits dephosphorylation, as well as promoting phosphorylation, of the AMP-activated protein kinase. Studies using bacterially expressed human protein phosphatase-2Cα and native bovine protein phosphatase-2Ac', *FEBS Letters* 377(3), pp. 421–425. doi: 10.1016/0014-5793(95)01368-7.

Day, P. *et al.* (2007) 'Structure of a CBS-domain pair from the regulatory γ1 subunit of human AMPK in complex with AMP and ZMP', *Acta Crystallographica Section D Biological Crystallography*, 63(5), pp. 587–596. doi: 10.1107/S0907444907009110.

Dekker, N. *et al.* (2004) 'Role of the α-Glucanase Agn1p in Fission-Yeast Cell Separation', *Molecular Biology of the Cell*, 15(8), pp. 3903–3914. doi: 10.1091/mbc.e04-04-0319.

Deng, L. *et al.* (2014) 'Dueling kinases regulate cell size at division through the SAD kinase Cdr2', *Current biology : CB*. NIH Public Access, 24(4), p. 428. doi: 10.1016/J.CUB.2014.01.009.

Deng, L. *et al.* (2017) 'Phosphatases Generate Signal Specificity Downstream of Ssp1 Kinase in Fission Yeast', *Molecular and Cellular Biology*, 37(10). doi: 10.1128/MCB.00494-16.

Ding, R. *et al.* (1997) 'The spindle pole body of Schizosaccharomyces pombe enters and leaves the nuclear envelope as the cell cycle proceeds.', *Molecular Biology of the Cell*, 8(8), pp. 1461–1479. doi: 10.1091/mbc.8.8.1461.

Dite, T. A. *et al.* (2018) 'AMP-activated protein kinase selectively inhibited by the type II inhibitor SBI-0206965.', *The Journal of biological chemistry*. American Society for Biochemistry and Molecular Biology, 293(23), pp. 8874–8885. doi: 10.1074/jbc.RA118.003547.

Eckley, D. M. *et al.* (1997) 'Chromosomal proteins and cytokinesis: patterns of cleavage furrow formation and inner centromere protein positioning in mitotic heterokaryons and mid-anaphase cells.', *The Journal of cell biology*, 136(6), pp. 1169–83.

Egan, D. *et al.* (2011) 'The autophagy initiating kinase ULK1 is regulated via opposing phosphorylation by AMPK and mTOR', *Autophagy*, 7(6), pp. 643–644. doi: 10.4161/auto.7.6.15123.

Egan, D. F. *et al.* (2015) 'Small Molecule Inhibition of the Autophagy Kinase ULK1 and Identification of ULK1 Substrates.', *Molecular cell*. NIH Public Access, 59(2), pp. 285–97. doi: 10.1016/j.molcel.2015.05.031.

Egel, R. and Egel-Mitani, M. (1974) 'Premeiotic DNA synthesis in fission yeast.', *Experimental cell research*, 88(1), pp. 127–34.

Egel, R. and Gutz, H. (1981) 'Gene activation by copy transposition in mating-type switching of a homothallic fission yeast', *Current Genetics*, 3(1), pp. 5–12. doi: 10.1007/BF00419574.

Eggert, U. S., Mitchison, T. J. and Field, C. M. (2006) 'Animal Cytokinesis: From Parts List to Mechanisms', *Annual Review of Biochemistry*, 75(1), pp. 543–566. doi: 10.1146/annurev.biochem.74.082803.133425.

Elia, N. *et al.* (2011) 'Dynamics of endosomal sorting complex required for transport (ESCRT) machinery during cytokinesis and its role in abscission', *Proceedings of the National Academy of Sciences*, 108(12), pp. 4846–4851. doi: 10.1073/pnas.1102714108.

Elia, N. *et al.* (2012) 'Computational model of cytokinetic abscission driven by ESCRT-III polymerization and remodeling.', *Biophysical journal*. The Biophysical Society, 102(10), pp. 2309–20. doi: 10.1016/j.bpj.2012.04.007.

Elion, E. A., Brill, J. A. and Fink, G. R. (1991) 'FUS3 represses CLN1 and CLN2 and in concert with KSS1 promotes signal transduction.', *Proceedings of the National Academy of Sciences*, 88(21), pp. 9392–9396. doi: 10.1073/pnas.88.21.9392.

Emerling, B. M. *et al.* (2007) 'Compound C inhibits hypoxic activation of HIF-1 independent of AMPK', *FEBS Letters*, 581(29), pp. 5727–5731. doi: 10.1016/j.febslet.2007.11.038.

Esfahanian, N. *et al.* (2012) 'Effect of metformin on the proliferation, migration, and MMP-2 and -9 expression of human umbilical vein endothelial cells.', *Molecular medicine reports*. Spandidos Publications, 5(4), pp. 1068–74. doi: 10.3892/mmr.2012.753.

Eskelinen, E.-L. *et al.* (2002) 'Inhibition of autophagy in mitotic animal cells.', *Traffic (Copenhagen, Denmark)*, 3(12), pp. 878–93.

Fantes, P. A. and Hoffman, C. S. (2016) 'A Brief History of *Schizosaccharomyces pombe* Research: A Perspective Over the Past 70 Years.', *Genetics*. Genetics Society of America, 203(2), pp. 621–9. doi: 10.1534/genetics.116.189407.

Fantes, P. and Nurse, P. (1977) 'Control of cell size at division in fission yeast by a

growth-modulated size control over nuclear division.', *Experimental cell research*, 107(2), pp. 377–86.

Fediuc, S., Gaidhu, M. P. and Ceddia, R. B. (2006) 'Regulation of AMP-activated protein kinase and acetyl-CoA carboxylase phosphorylation by palmitate in skeletal muscle cells.', *Journal of lipid research*. American Society for Biochemistry and Molecular Biology, 47(2), pp. 412–20. doi: 10.1194/jlr.M500438-JLR200.

Field, C. M. and Alberts, B. M. (1995) 'Anillin, a contractile ring protein that cycles from the nucleus to the cell cortex.', *The Journal of cell biology*. Rockefeller University Press, 131(1), pp. 165–78. doi: 10.1083/jcb.131.1.165.

Fuller, B. G. *et al.* (2008) 'Midzone activation of aurora B in anaphase produces an intracellular phosphorylation gradient', *Nature*, 453(7198), pp. 1132–1136. doi: 10.1038/nature06923.

Furuya, T. *et al.* (2010) 'Negative regulation of Vps34 by Cdk mediated phosphorylation.', *Molecular cell*. NIH Public Access, 38(4), pp. 500–11. doi: 10.1016/j.molcel.2010.05.009.

Garoff, H., Hewson, R. and Opstelten, D. J. (1998) 'Virus maturation by budding.', *Microbiology and molecular biology reviews : MMBR*, 62(4), pp. 1171–90.

Giet, R. and Prigent, C. (1999) 'Aurora/Ipl1p-related kinases, a new oncogenic family of mitotic serine-threonine kinases.', *Journal of cell science*, 112 (Pt 21), pp. 3591–601.

Glatzel, D. K. *et al.* (2018) 'Acetyl-CoA carboxylase 1 regulates endothelial cell migration by shifting the phospholipid composition.', *Journal of lipid research*. American Society for Biochemistry and Molecular Biology, 59(2), pp. 298–311. doi: 10.1194/jlr.M080101.

Glover, D. M. *et al.* (1995) 'Mutations in aurora prevent centrosome separation leading to the formation of monopolar spindles', *Cell*. Cell Press, 81(1), pp. 95–105. doi: 10.1016/0092-8674(95)90374-7.

Goeckeler, Z. M. *et al.* (2000) 'Phosphorylation of Myosin Light Chain Kinase by p21-activated Kinase PAK2', *Journal of Biological Chemistry*, 275(24), pp. 18366–18374. doi: 10.1074/jbc.M001339200.

Goepfert, T. M. *et al.* (2002) 'Centrosome amplification and overexpression of aurora A are early events in rat mammary carcinogenesis.', *Cancer research*, 62(14), pp. 4115–22.

Göransson, O. *et al.* (2007) 'Mechanism of action of A-769662, a valuable tool for activation of AMP-activated protein kinase.', *The Journal of biological chemistry*. Europe PMC Funders, 282(45), pp. 32549–60. doi: 10.1074/jbc.M706536200.

Gowans, G. J. *et al.* (2013) 'AMP is a true physiological regulator of AMP-activated protein kinase by both allosteric activation and enhancing net phosphorylation.', *Cell metabolism*. Elsevier, 18(4), pp. 556–66. doi: 10.1016/j.cmet.2013.08.019.

Guertin, D. A., Trautmann, S. and McCollum, D. (2002) 'Cytokinesis in eukaryotes.',

Microbiology and molecular biology reviews : MMBR. American Society for Microbiology (ASM), 66(2), pp. 155–78. doi: 10.1128/MMBR.66.2.155-178.2002.

Guizetti, J. *et al*. (2011) 'Cortical Constriction During Abscission Involves Helices of ESCRT-III-Dependent Filaments', *Science*, 331(6024), pp. 1616–1620. doi: 10.1126/science.1201847.

Gurumurthy, S. *et al*. (2008) 'LKB1 deficiency sensitizes mice to carcinogen-induced tumorigenesis.', *Cancer research*. NIH Public Access, 68(1), pp. 55–63. doi: 10.1158/0008-5472.CAN-07-3225.

Gwinn, D. M. *et al*. (2008) 'AMPK phosphorylation of raptor mediates a metabolic checkpoint.', *Molecular cell*. Elsevier, 30(2), pp. 214-26. doi: 10.1016/j.molcel.2008.03.003.

Ha, J. *et al*. (1994) 'Critical phosphorylation sites for acetyl-CoA carboxylase activity.', *The Journal of biological chemistry*, 269(35), pp. 22162–8.

Habedanck, R. *et al*. (2005) 'The Polo kinase Plk4 functions in centriole duplication', *Nature Cell Biology*, 7(11), pp. 1140–1146. doi: 10.1038/ncb1320.

Hall, P. A. *et al*. (2005) 'The Septin-Binding Protein Anillin Is Overexpressed in Diverse Human Tumors', *Clinical Cancer Research*. American Association for Cancer Research, 11(19), pp. 6780–6786. doi: 10.1158/1078-0432.CCR-05-0997.

Hannak, E. *et al*. (2001) 'Aurora-A kinase is required for centrosome maturation in Caenorhabditis elegans.', *The Journal of cell biology*. Rockefeller University Press, 155(7), pp. 1109–16. doi: 10.1083/jcb.200108051.

Hanyu, Y. *et al*. (2009) '*Schizosaccharomyces pombe* cell division cycle under limited glucose requires Ssp1 kinase, the putative CaMKK, and Sds23, a PP2A-related phosphatase inhibitor', *Genes to Cells*, 14(5), pp. 539–554. doi: 10.1111/j.1365-2443.2009.01290.x.

Hardie, D. G. *et al*. (2003) 'Management of cellular energy by the AMP-activated protein kinase system', *FEBS Letters*. John Wiley & Sons, Ltd, 546(1), pp. 113–120. doi: 10.1016/S0014-5793(03)00560-X.

Hardie, D. G. (2011) 'AMP-activated protein kinase: an energy sensor that regulates all aspects of cell function.', *Genes & development*. Cold Spring Harbor Laboratory Press, 25(18), pp. 1895–908. doi: 10.1101/gad.17420111.

Hardie, D. G., Carling, D. and Carlson, M. (1998) 'the AMP-avtivated.SNF1 protein kinase subfamily: Metabolic Sensors of the Eukaryotic Cell?', *Annual Review of Biochemistry*, 67(1), pp. 821–855. doi: 10.1146/annurev.biochem.67.1.821.

Hartwell, L. H. *et al*. (1973) 'Genetic Control of the Cell Division Cycle in Yeast: V. Genetic Analysis of cdc Mutants.', *Genetics*. Genetics Society of America, 74(2), pp. 267–86.

Hawley, S. A. *et al*. (2003a) 'Complexes between the LKB1 tumor suppressor, STRAD alpha/beta and MO25 alpha/beta are upstream kinases in the AMP-activated protein

kinase cascade.', *Journal of biology*, 2(4), p. 28. doi: 10.1186/1475-4924-2-28.

Hawley, S. A. *et al.* (2003b) 'Complexes between the LKB1 tumor suppressor, STRADα/ß and MO25α/ß are upstream kinases in the AMP-activated protein kinase cascade', *Journal of Biology*. BioMed Central, 2(4), p. 28. doi: 10.1186/1475-4924-2-28.

Hawley, S. A. *et al.* (2005) 'Calmodulin-dependent protein kinase kinase-beta is an alternative upstream kinase for AMP-activated protein kinase.', *Cell metabolism*, 2(1), pp. 9–19. doi: 10.1016/j.cmet.2005.05.009.

Hawley, S. A. *et al.* (2012) 'The Ancient Drug Salicylate Directly Activates AMP-Activated Protein Kinase', *Science*, 336(6083), pp. 918–922. doi: 10.1126/science.1215327.

Hawley, S. A. *et al.* (2016) 'The Na+/Glucose Cotransporter Inhibitor Canagliflozin Activates AMPK by Inhibiting Mitochondrial Function and Increasing Cellular AMP Levels.', *Diabetes*. Europe PMC Funders, 65(9), pp. 2784–94. doi: 10.2337/db16-0058.

He, G. *et al.* (2014) 'AMP-activated protein kinase induces p53 by phosphorylating MDMX and inhibiting its activity.', *Molecular and cellular biology*, 34(2), pp. 148–57. doi: 10.1128/MCB.00670-13.

He, R. *et al.* (2013) 'Cep57 Protein Is Required for Cytokinesis by Facilitating Central Spindle Microtubule Organization', *Journal of Biological Chemistry*, 288(20), pp. 14384–14390. doi: 10.1074/jbc.M112.441501.

Hemminki, A. *et al.* (1998) 'A serine/threonine kinase gene defective in Peutz–Jeghers syndrome', *Nature*, 391(6663), pp. 184–187. doi: 10.1038/34432.

Hengeveld, R. C. C. *et al.* (2012) 'Development of a Chemical Genetic Approach for Human Aurora B Kinase Identifies Novel Substrates of the Chromosomal Passenger Complex', *Molecular & Cellular Proteomics*, 11(5), pp. 47–59. doi: 10.1074/mcp.M111.013912.

Higgs, G. A. *et al.* (1987) 'Pharmacokinetics of aspirin and salicylate in relation to inhibition of arachidonate cyclooxygenase and antiinflammatory activity.', *Proceedings of the National Academy of Sciences*, 84(5), pp. 1417–1420. doi: 10.1073/pnas.84.5.1417.

Hoffman, C. S., Wood, V. and Fantes, P. A. (2015) 'An Ancient Yeast for Young Geneticists: A Primer on the *Schizosaccharomyces pombe* Model System', *Genetics*. Genetics Society of America, 201(2), p. 403. doi: 10.1534/GENETICS.115.181503.

Högnäs, G. *et al.* (2012) 'Cytokinesis failure due to derailed integrin traffic induces aneuploidy and oncogenic transformation *in vitro* and *in vivo*', *Oncogene*. Nature Publishing Group, 31(31), pp. 3597–3606. doi: 10.1038/onc.2011.527.

Hong, S.-P. *et al.* (2003) 'Activation of yeast Snf1 and mammalian AMP-activated protein kinase by upstream kinases', *Proceedings of the National Academy of Sciences*, 100(15), pp. 8839–8843. doi: 10.1073/pnas.1533136100.

Horisberger, M. and Rouvet-Vauthey, M. (1985) 'Cell wall architecture of the fission

yeastSchizosaccharomyces pombe', *Experientia*. Birkhäuser-Verlag, 41(6), pp. 748–750. doi: 10.1007/BF02012578.

Humbel, B. M. *et al*. (2001) '*In situ* localization of ß-glucans in the cell wall of *Schizosaccharomyces pombe*', *Yeast*, 18(5), pp. 433–444. doi: 10.1002/yea.694.

Inoki, K. *et al*. (2002) 'TSC2 is phosphorylated and inhibited by Akt and suppresses mTOR signalling', *Nature Cell Biology*, 4(9), pp. 648–657. doi: 10.1038/ncb839.

Inoki, K., Zhu, T. and Guan, K.-L. (2003) 'TSC2 mediates cellular energy response to control cell growth and survival.', *Cell*, 115(5), pp. 577–90.

Isakovic, A. *et al*. (2007) 'Dual antiglioma action of metformin: cell cycle arrest and mitochondria-dependent apoptosis', *Cellular and Molecular Life Sciences*, 64(10), pp. 1290–1302. doi: 10.1007/s00018-007-7080-4.

Iwaki, T. *et al*. (2007) 'Essential roles of class E Vps proteins for sorting into multivesicular bodies in *Schizosaccharomyces pombe*.', *Microbiology (Reading, England)*. Microbiology Society, 153(Pt 8), pp. 2753–64. doi: 10.1099/mic.0.2007/006072-0.

Jackman, M. *et al*. (2003) 'Active cyclin B1–Cdk1 first appears on centrosomes in prophase', *Nature Cell Biology*, 5(2), pp. 143–148. doi: 10.1038/ncb918.

Jimenez, A. J. *et al*. (2014) 'ESCRT Machinery Is Required for Plasma Membrane Repair', *Science*, 343(6174), pp. 1247136–1247136. doi: 10.1126/science.1247136.

Jin, X., Townley, R. and Shapiro, L. (2007) 'Structural Insight into AMPK Regulation: ADP Comes into Play', *Structure*, 15(10), pp. 1285–1295. doi: 10.1016/j.str.2007.07.017.

Johnson, D. S., Bleck, M. and Simon, S. M. (2018) 'Timing of ESCRT-III protein recruitment and membrane scission during HIV-1 assembly', *eLife*, 7. doi: 10.7554/eLife.36221.

Jones, R. G. *et al*. (2005) 'AMP-Activated Protein Kinase Induces a p53-Dependent Metabolic Checkpoint', *Molecular Cell*, 18(3), pp. 283–293. doi: 10.1016/j.molcel.2005.03.027.

Kahn, B. B. *et al*. (2005) 'AMP-activated protein kinase: Ancient energy gauge provides clues to modern understanding of metabolism', *Cell Metabolism*, 1(1), pp. 15–25. doi: 10.1016/j.cmet.2004.12.003.

Katzmann, D. J., Babst, M. and Emr, S. D. (2001) 'Ubiquitin-dependent sorting into the multivesicular body pathway requires the function of a conserved endosomal protein sorting complex, ESCRT-I.', *Cell*, 106(2), pp. 145–55.

Kemp, B. E. (2004) 'Bateman domains and adenosine derivatives form a binding contract.', *The Journal of clinical investigation*. American Society for Clinical Investigation, 113(2), pp. 182–4. doi: 10.1172/JCI20846.

Kimura, M. *et al*. (1999) 'Cell cycle-dependent expression and centrosome localization of a third human aurora/Ipl1-related protein kinase, AIK3.', *The Journal of biological*

chemistry. American Society for Biochemistry and Molecular Biology, 274(11), pp. 7334–40. doi: 10.1074/JBC.274.11.7334.

Koch, A. *et al.* (2011) 'Mitotic substrates of the kinase aurora with roles in chromatin regulation identified through quantitative phosphoproteomics of fission yeast.', *Science signaling*. American Association for the Advancement of Science, 4(179), p. rs6. doi: 10.1126/scisignal.2001588.

Komatsu, S. *et al.* (2000) 'Effects of the Regulatory Light Chain Phosphorylation of Myosin II on Mitosis and Cytokinesis of Mammalian Cells', *Journal of Biological Chemistry*, 275(44), pp. 34512–34520. doi: 10.1074/jbc.M003019200.

Kothe, M. *et al.* (2007) 'Structure of the Catalytic Domain of Human Polo-like Kinase 1', *Biochemistry*, 46(20), pp. 5960-5971. doi: 10.1021/bi602474j.

Kukidome, D. *et al.* (2006) 'Activation of AMP-activated protein kinase reduces hyperglycemia-induced mitochondrial reactive oxygen species production and promotes mitochondrial biogenesis in human umbilical vein endothelial cells.', *Diabetes*, 55(1), pp. 120-7.

Kurth-Kraczek, E. J. *et al.* (1999) '5' AMP-activated protein kinase activation causes GLUT4 translocation in skeletal muscle', *Diabetes*, 48(8), pp. 1667–1671. doi: 10.2337/diabetes.48.8.1667.

Laderoute, K. R. *et al.* (2006) '5'-AMP-activated protein kinase (AMPK) is induced by low-oxygen and glucose deprivation conditions found in solid-tumor microenvironments.', *Molecular and cellular biology*, 26(14), pp. 5336–47. doi: 10.1128/MCB.00166-06.

Lane, H. A. (1996) 'Antibody microinjection reveals an essential role for human polo-like kinase 1 (Plk1) in the functional maturation of mitotic centrosomes', *The Journal of Cell Biology*, 135(6), pp. 1701–1713. doi: 10.1083/jcb.135.6.1701.

Lee, H. H. *et al.* (2008) 'Midbody targeting of the ESCRT machinery by a noncanonical coiled coil in CEP55.', *Science*. NIH Public Access, 322(5901), pp. 576–80. doi: 10.1126/science.1162042.

Lee, J. O. *et al.* (2012) 'Metformin regulates glucose transporter 4 (GLUT4) translocation through AMP-activated protein kinase (AMPK)-mediated Cbl/CAP signaling in 3T3-L1 preadipocyte cells.', *The Journal of biological chemistry*. American Society for Biochemistry and Molecular Biology, 287(53), pp. 44121–9. doi: 10.1074/jbc.M112.361386.

Leech, A. *et al.* (2003) 'Isolation of mutations in the catalytic domain of the snf1 kinase that render its activity independent of the snf4 subunit.', *Eukaryotic cell*, 2(2), pp. 265–73. doi: 10.1128/ec.2.2.265-273.2003.

Li, X. *et al.* (2015) 'Structural basis of AMPK regulation by adenine nucleotides and glycogen', *Cell Research*. Nature Publishing Group, 25(1), pp. 50-66. doi: 10.1038/cr.2014.150.

Lindon, C. and Pines, J. (2004) 'Ordered proteolysis in anaphase inactivates Plk1 to

contribute to proper mitotic exit in human cells.', *The Journal of cell biology*. The Rockefeller University Press, 164(2), pp. 233–41. doi: 10.1083/jcb.200309035.

Lioutas, A. and Vernos, I. (2013) 'Aurora A kinase and its substrate TACC3 are required for central spindle assembly', *EMBO reports*, 14(9), pp. 829–836. doi: 10.1038/embor.2013.109.

Littlepage, L. E. *et al.* (2002) 'Identification of phosphorylated residues that affect the activity of the mitotic kinase Aurora-A.', *Proceedings of the National Academy of Sciences of the United States of America*. National Academy of Sciences, 99(24), pp. 15440–5. doi: 10.1073/pnas.202606599.

Liu, Q. and Ruderman, J. V. (2006) 'Aurora A, mitotic entry, and spindle bipolarity', *Proceedings of the National Academy of Sciences*, 103(15), pp. 5811–5816. doi: 10.1073/pnas.0601425103.

Liu, X. *et al.* (2014) 'The AMPK inhibitor compound C is a potent AMPK-independent antiglioma agent.', *Molecular cancer therapeutics*. NIH Public Access, 13(3), pp. 596–605. doi: 10.1158/1535-7163.MCT-13-0579.

Liu, Y. *et al.* (2019) 'Multi-omic measurements of heterogeneity in HeLa cells across laboratories', *Nature Biotechnology*, 37(3), pp. 314–322. doi: 10.1038/s41587-019-0037-y.

Lizcano, J. M. *et al.* (2004) 'LKB1 is a master kinase that activates 13 kinases of the AMPK subfamily, including MARK/PAR-1', *The EMBO Journal*, 23(4), pp. 833–843. doi: 10.1038/sj.emboj.7600110.

Ma, S., Charron, J. and Erikson, R. L. (2003) 'Role of Plk2 (Snk) in Mouse Development and Cell Proliferation', *Molecular and Cellular Biology*, 23(19), pp. 6936-6943. doi: 10.1128/MCB.23.19.6936-6943.2003.

MacIver, F. H., Glover, D. M. and Hagan, I. M. (2003) 'A ?marker switch? approach for targeted mutagenesis of genes in *Schizosaccharomyces pombe*', *Yeast*, 20(7), pp. 587–594. doi: 10.1002/yea.983.

Mancini, S. J. *et al.* (2018) 'Canagliflozin inhibits interleukin-1β-stimulated cytokine and chemokine secretion in vascular endothelial cells by AMP-activated protein kinase-dependent and -independent mechanisms', *Scientific Reports*. Nature Publishing Group, 8(1), p. 5276. doi: 10.1038/s41598-018-23420-4.

Mao, L. *et al.* (2013) 'AMPK phosphorylates GBF1 for mitotic Golgi disassembly.', *Journal of cell science*, 126(Pt 6), pp. 1498–505. doi: 10.1242/jcs.121954.

Marin, T. L. *et al.* (2015) 'Identification of AMP-activated protein kinase targets by a consensus sequence search of the proteome', *BMC Systems Biology*. BioMed Central, 9(1), p. 13. doi: 10.1186/s12918-015-0156-0.

Marks, J., Hagan, I. M. and Hyms, J. S. (1986) 'Growth Polarity and Cytokinesis in Fission Yeast: The Role of the Cytoskeleton', *Journal of Cell Science*. The Company of Biologists Ltd, 1986(Supplement 5), pp. 229-241. doi: 10.1242/jcs.1986.Supplement_5.15.

Maroto, B. *et al*. (2008) 'P21-activated kinase is required for mitotic progression and regulates Plk1', *Oncogene*, 27(36), pp. 4900–4908. doi: 10.1038/onc.2008.131.

Marumoto, T. *et al*. (2003) 'Aurora-A kinase maintains the fidelity of early and late mitotic events in HeLa cells.', *The Journal of biological chemistry*. American Society for Biochemistry and Molecular Biology, 278(51), pp. 51786–95. doi: 10.1074/jbc.M306275200.

Matsumoto, T. *et al*. (2009) 'Polo-like kinases mediate cell survival in mitochondrial dysfunction.', *Proceedings of the National Academy of Sciences of the United States of America*. National Academy of Sciences, 106(34), pp. 14542–6. doi: 10.1073/pnas.0904229106.

Matsusaka, T. *et al*. (1995) 'A novel protein kinase gene ssp1+ is required for alteration of growth polarity and actin localization in fission yeast.', *The EMBO journal*. European Molecular Biology Organization, 14(14), pp. 3325–38.

Matsuzawa, T. *et al*. (2012) 'Snf1-Like Protein Kinase Ssp2 Regulates Glucose Derepression in *Schizosaccharomyces pombe*', *Eukaryotic Cell*, 11(2), pp. 159–167. doi: 10.1128/EC.05268-11.

May, M. *et al*. (2014) 'Rac1-dependent recruitment of PAK2 to G2 phase centrosomes and their roles in the regulation of mitotic entry.', *Cell cycle (Georgetown, Tex.)*. Taylor & Francis, 13(14), pp. 2211–21. doi: 10.4161/cc.29279.

McGarry, J. D. (2002) 'Banting lecture 2001: dysregulation of fatty acid metabolism in the etiology of type 2 diabetes.', *Diabetes*. American Diabetes Association, 51(1), pp. 7–18. doi: 10.2337/diabetes.51.1.7.

McGee, S. L. *et al*. (2008) 'AMP-Activated Protein Kinase Regulates GLUT4 Transcription by Phosphorylating Histone Deacetylase 5', *Diabetes*, 57(4), pp. 860–867. doi: 10.2337/db07-0843.

Meraldi, P., Honda, R. and Nigg, E. A. (2002) 'Aurora-A overexpression reveals tetraploidization as a major route to centrosome amplification in p53-/- cells.', *The EMBO journal*, 21(4), pp. 483–92.

Miller, K. G., Field, C. M. and Alberts, B. M. (1989) 'Actin-binding proteins from Drosophila embryos: a complex network of interacting proteins detected by F-actin affinity chromatography.', *The Journal of Cell Biology*. Rockefeller University Press, 109(6), pp. 2963–2975. doi: 10.1083/JCB.109.6.2963.

Minoshima, Y. *et al*. (2003) 'Phosphorylation by aurora B converts MgcRacGAP to a RhoGAP during cytokinesis.', *Developmental cell*. Elsevier, 4(4), pp. 549-60. doi: 10.1016/S1534-5807(03)00089-3.

Mitchelhill, K. I. *et al*. (1997) 'Posttranslational modifications of the 5'-AMP-activated protein kinase beta1 subunit.', *The Journal of biological chemistry*. American Society for Biochemistry and Molecular Biology, 272(39), pp. 24475–9. doi: 10.1074/jbc.272.39.24475.

Mitchison, J. M. and Nurse, P. (1985) 'Growth in cell length in the fission yeast

Schizosaccharomyces pombe.', *Journal of cell science*, 75, pp. 357–76.

Mizrachy-Schwartz, S. *et al*. (2011) 'Up-regulation of AMP-activated protein kinase in cancer cell lines is mediated through c-Src activation.', *The Journal of biological chemistry*. American Society for Biochemistry and Molecular Biology, 286(17), pp. 15268–77. doi: 10.1074/jbc.M110.211813.

Moreno, S., Klar, A. and Nurse, P. (1991) 'Molecular genetic analysis of fission yeast Schizosaccharomyces pombe.', *Methods in enzymology*, 194, pp. 795–823.

Morita, E. *et al*. (2007) 'Human ESCRT and ALIX proteins interact with proteins of the midbody and function in cytokinesis.', *The EMBO journal*. European Molecular Biology Organization, 26(19), pp. 4215–27. doi: 10.1038/sj.emboj.7601850.

Moseley, J. B. *et al*. (2009) 'A spatial gradient coordinates cell size and mitotic entry in fission yeast', *Nature*, 459(7248), pp. 857–860. doi: 10.1038/nature08074.

Munday, M. R. (2002) 'Regulation of mammalian acetyl-CoA carboxylase.', *Biochemical Society transactions*. Portland Press Limited, 30(Pt 6), pp. 1059–64. doi: 10.1042/.

Nam, M. *et al*. (2008) 'Compound C inhibits clonal expansion of preadipocytes by increasing p21 level irrespectively of AMPK inhibition', *Archives of Biochemistry and Biophysics*, 479(1), pp. 74–81. doi: 10.1016/j.abb.2008.07.029.

Nasmyth, K., Nurse, P. and FRASER, R. S. S. (1979) 'The Effect of Cell Mass on the Cell Cycle Timing and Duration of S-Phase in Fission Yeast', *Journal of Cell Science*, 39(1).

Neto, H. *et al*. (2013) 'Syntaxin 16 is a master recruitment factor for cytokinesis.', *Molecular biology of the cell*. American Society for Cell Biology, 24(23), pp. 3663–74. doi: 10.1091/mbc.E13-06-0302.

Nicastro R. *et al*. (2015) 'enhanced amino acid utalization sustains growth of cells lacking Snf1/AMPK' *Biochemica et Biophysica Acta*, 1853*(7) 1615– 1625. https://doi.org/10.1016/j.bbamcr.2015.03.014*

Oegema, K. *et al*. (2000) 'Functional analysis of a human homologue of the Drosophila actin binding protein anillin suggests a role in cytokinesis.', *The Journal of cell biology*. Rockefeller University Press, 150(3), pp. 539–52. doi: 10.1083/jcb.150.3.539.

Okazaki, K. and Niwa, O. (2008) 'Dikaryotic Cell Division of the Fission Yeast *Schizosaccharomyces pombe*', *Bioscience, Biotechnology, and Biochemistry*, 72(6), pp. 1531–1538. doi: 10.1271/bbb.80035.

Oliveras-Ferraros, C., Vazquez-Martin, A. and Menendez, J. A. (2009) 'Genome-wide inhibitory impact of the AMPK activator metformin on [*kinesins, tubulins, histones, auroras* and *polo-like kinases*] M-phase cell cycle genes in human breast cancer cells', *Cell Cycle*, 8(10), pp. 1633–1636. doi: 10.4161/cc.8.10.8406.

Olmos, Y. *et al*. (2015) 'ESCRT-III controls nuclear envelope reformation', *Nature*, 522(7555), pp. 236–239. doi: 10.1038/nature14503.

Owen, M. R., Doran, E. and Halestrap, A. P. (2000) 'Evidence that metformin exerts its

anti-diabetic effects through inhibition of complex 1 of the mitochondrial respiratory chain.', *The Biochemical journal*, 348 Pt 3, pp. 607–14.

Pal, D. *et al.* (2010) 'Role of a novel coiled-coil domain-containing protein CCDC69 in regulating central spindle assembly.', *Cell cycle (Georgetown, Tex.)*. Taylor & Francis, 9(20), pp. 4117–29. doi: 10.4161/cc.9.20.13387.

Paoletti, A. and Chang, F. (2000) 'Analysis of mid1p, a Protein Required for Placement of the Cell Division Site, Reveals a Link between the Nucleus and the Cell Surface in Fission Yeast', *Molecular Biology of the Cell*. Edited by T. Stearns, 11(8), pp. 2757–2773. doi: 10.1091/mbc.11.8.2757.

Petretti, C. *et al.* (2006) 'The PITSLRE/CDK11p58 protein kinase promotes centrosome maturation and bipolar spindle formation.', *EMBO reports*. European Molecular Biology Organization, 7(4), pp. 418–24. doi: 10.1038/sj.embor.7400639.

Peyton, K. J. *et al.* (2012) 'Activation of AMP-activated protein kinase inhibits the proliferation of human endothelial cells.', *The Journal of pharmacology and experimental therapeutics*. American Society for Pharmacology and Experimental Therapeutics, 342(3), pp. 827–34. doi: 10.1124/jpet.112.194712.

Pickett-Heaps and JD (1969) 'The evolution of the mitotic apparatus : an attempt at comparative ultrastructural cytology in dividing plant cells', *Cytobios*, 1, pp. 257–280.

Piekny, A. J. and Glotzer, M. (2008) 'Anillin Is a Scaffold Protein That Links RhoA, Actin, and Myosin during Cytokinesis', *Current Biology*, 18(1), pp. 30–36. doi: 10.1016/j.cub.2007.11.068.

Pines, J. and Hunter, T. (1989) 'Isolation of a human cyclin cDNA: Evidence for cyclin mRNA and protein regulation in the cell cycle and for interaction with p34cdc2', *Cell*. Cell Press, 58(5), pp. 833–846. doi: 10.1016/0092-8674(89)90936-7.

Pinter, K. *et al.* (2012) 'Subunit composition of AMPK trimers present in the cytokinetic apparatus: Implications for drug target identification.', *Cell cycle (Georgetown, Tex.)*. Europe PMC Funders, 11(5), pp. 917–21. doi: 10.4161/cc.11.5.19412.

Platara, M. *et al.* (2006) 'The Transcriptional Response of the Yeast Na$^+$-ATPase *ENA1* Gene to Alkaline Stress Involves Three Main Signaling Pathways', *Journal of Biological Chemistry*, 281(48), pp. 36632–36642. doi: 10.1074/jbc.M606483200.

Polekhina, G. *et al.* (2003) 'AMPK beta subunit targets metabolic stress sensing to glycogen.', *Current biology : CB*, 13(10), pp. 867–71.

Pollard, T. D. and Wu, J.-Q. (2010) 'Understanding cytokinesis: lessons from fission yeast.', *Nature reviews. Molecular cell biology*. NIH Public Access, 11(2), pp. 149–55. doi: 10.1038/nrm2834.

Portillo, F., Mulet, J. M. and Serrano, R. (2005) 'A role for the non-phosphorylated form of yeast Snf1: tolerance to toxic cations and activation of potassium transport', *FEBS Letters*, 579(2), pp. 512–516. doi: 10.1016/j.febslet.2004.12.019.

Protein Phosphorylation and Ubiquitination unit, University of Dundee, MRC,

n.d.. Accessed 30 January 2020. https://www.ppu.mrc.ac.uk/

Qian, Y. W., Erikson, E. and Maller, J. L. (1999) 'Mitotic effects of a constitutively active mutant of the Xenopus polo-like kinase Plx1.', *Molecular and cellular biology*. American Society for Microbiology (ASM), 19(12), pp. 8625–32. doi: 10.1128/mcb.19.12.8625.

Raab, M. *et al.* (2016) 'ESCRT III repairs nuclear envelope ruptures during cell migration to limit DNA damage and cell death', *Science*, 352(6283), pp. 359–362. doi: 10.1126/science.aad7611.

Ralser, M. *et al.* (2012) 'The *Saccharomyces cerevisiae* W303-K6001 cross-platform genome sequence: insights into ancestry and physiology of a laboratory mutt', *Open Biology*, 2(8), pp. 120093–120093. doi: 10.1098/rsob.120093.

Raymond, C. K. *et al.* (1992) 'Morphological classification of the yeast vacuolar protein sorting mutants: evidence for a prevacuolar compartment in class E vps mutants.', *Molecular Biology of the Cell*, 3(12), pp. 1389–1402. doi: 10.1091/mbc.3.12.1389.

Reboutier, D. *et al.* (2013) 'Aurora A is involved in central spindle assembly through phosphorylation of Ser 19 in P150Glued', *The Journal of Cell Biology*, 201(1), pp. 65–79. doi: 10.1083/jcb.201210060.

Reihill, J. A., Ewart, M.-A. and Salt, I. P. (2011) 'The role of AMP-activated protein kinase in the functional effects of vascular endothelial growth factor-A and -B in human aortic endothelial cells.', *Vascular cell*. BioMed Central, 3, p. 9. doi: 10.1186/2045-824X-3-9.

Rezig, I. M. *et al.* (2019) 'Genetic and Cytological Methods to Study ESCRT Cell Cycle Function in Fission Yeast', in *Methods in molecular biology (Clifton, N.J.)*, pp. 239–250. doi: 10.1007/978-1-4939-9492-2_18.

Robbins, E., Jentzsch, G. and Micali, A. (1968) 'The centriole cycle in synchronized HeLa cells.', *The Journal of cell biology*. The Rockefeller University Press, 36(2), pp. 329–39. doi: 10.1083/jcb.36.2.329.

Rosenwasser, R. F. *et al.* (2013) 'SGLT-2 inhibitors and their potential in the treatment of diabetes.', *Diabetes, metabolic syndrome and obesity : targets and therapy*. Dove Press, 6, pp. 453–67. doi: 10.2147/DMSO.S34416.

Sagona, A. P. *et al.* (2010) 'PtdIns(3)P controls cytokinesis through KIF13A-mediated recruitment of FYVE-CENT to the midbody', *Nature Cell Biology*, 12(4), pp. 362–371. doi: 10.1038/ncb2036.

Sagona, A. P. *et al.* (2011) 'A tumor-associated mutation of FYVE-CENT prevents its interaction with Beclin 1 and interferes with cytokinesis.', *PloS one*. Public Library of Science, 6(3), p. e17086. doi: 10.1371/journal.pone.0017086.

Saitoh, S. *et al.* (1996) 'Aberrant mitosis in fission yeast mutants defective in fatty acid synthetase and acetyl CoA carboxylase.', *The Journal of cell biology*, 134(4), pp. 949–61.

Saitoh, S. *et al.* (2015) 'Mechanisms of expression and translocation of major fission yeast glucose transporters regulated by CaMKK/phosphatases, nuclear shuttling, and TOR', *Molecular Biology of the Cell*. Edited by D. J. Lew, 26(2), pp. 373–386. doi: 10.1091/mbc.E14-11-1503.

Sakamoto, K. *et al.* (2004) 'Activity of LKB1 and AMPK-related kinases in skeletal muscle: effects of contraction, phenformin, and AICAR', *American Journal of Physiology-Endocrinology and Metabolism*, 287(2), pp. E310–E317. doi: 10.1152/ajpendo.00074.2004.

Saksena, S. *et al.* (2009) 'Functional reconstitution of ESCRT-III assembly and disassembly.', *Cell*. NIH Public Access, 136(1), pp. 97–109. doi: 10.1016/j.cell.2008.11.013.

Salt, I. *et al.* (1998) 'AMP-activated protein kinase: greater AMP dependence, and preferential nuclear localization, of complexes containing the alpha2 isoform.', *The Biochemical journal*. Portland Press Ltd, 334 (Pt 1(Pt 1), pp. 177–87.

Salt, I. P., Connell, J. M. and Gould, G. W. (2000) '5-aminoimidazole-4-carboxamide ribonucleoside (AICAR) inhibits insulin-stimulated glucose transport in 3T3-L1 adipocytes', *Diabetes*, 49(10), pp. 1649–1656. doi: 10.2337/diabetes.49.10.1649.

Sanders, L. C. *et al.* (1999) 'Inhibition of myosin light chain kinase by p21-activated kinase.', *Science (New York, N.Y.)*, 283(5410), pp. 2083–5.

Sanders, M. J. *et al.* (2007) 'Defining the Mechanism of Activation of AMP-activated Protein Kinase by the Small Molecule A-769662, a Member of the Thienopyridone Family', *Journal of Biological Chemistry*, 282(45), pp. 32539-32548. doi: 10.1074/jbc.M706543200.

Sapkota, G. P. *et al.* (2002) 'Ionizing radiation induces ataxia telangiectasia mutated kinase (ATM)-mediated phosphorylation of LKB1/STK11 at Thr-366', *Biochemical Journal*, 368(2), pp. 507–516. doi: 10.1042/bj20021284.

Scaglia, N. *et al.* (2014) 'De novo fatty acid synthesis at the mitotic exit is required to complete cellular division.', *Cell cycle (Georgetown, Tex.)*. Taylor & Francis, 13(5), pp. 859-68. doi: 10.4161/cc.27767.

Scheffer, L. L. *et al.* (2014) 'Mechanism of Ca2+-triggered ESCRT assembly and regulation of cell membrane repair', *Nature Communications*, 5(1), p. 5646. doi: 10.1038/ncomms6646.

Schmidt, K. and Nichols, B. J. (2004) 'A Barrier to Lateral Diffusion in the Cleavage Furrow of Dividing Mammalian Cells', *Current Biology*, 14(11), pp. 1002–1006. doi: 10.1016/j.cub.2004.05.044.

Schutt, K. L. and Moseley, J. B. (2017) 'Transient activation of fission yeast AMPK is required for cell proliferation during osmotic stress', *Molecular Biology of the Cell*. Edited by D. Lew, p. mbc.E17-04-0235. doi: 10.1091/mbc.E17-04-0235.

Scott, J. W. *et al.* (2008) 'Thienopyridone Drugs Are Selective Activators of AMP-Activated Protein Kinase β1-Containing Complexes', *Chemistry & Biology*, 15(11), pp.

1220–1230. doi: 10.1016/j.chembiol.2008.10.005.

Scott, J. W. *et al.* (2014) 'Small Molecule Drug A-769662 and AMP Synergistically Activate Naive AMPK Independent of Upstream Kinase Signaling', *Chemistry & Biology*, 21(5), pp. 619–627. doi: 10.1016/j.chembiol.2014.03.006.

Shieh, S. Y. *et al.* (1997) 'DNA damage-induced phosphorylation of p53 alleviates inhibition by MDM2.', *Cell*, 91(3), pp. 325-34.

Shimada, M. *et al.* (2016) 'Essential role of autoactivation circuitry on Aurora B-mediated H2AX-pS121 in mitosis', *Nature Communications*, 7(1), p. 12059. doi: 10.1038/ncomms12059.

Sipiczki, M. and Bozsik, A. (2000) 'The use of morphomutants to investigate septum formation and cell separation in *Schizosaccharomyces pombe*.', *Archives of microbiology*, 174(6), pp. 386–92.

Sohrmann, M. *et al.* (1996) 'The *dmf1/mid1* gene is essential for correct positioning of the division septum in fission yeast.', *Genes & development*, 10(21), pp. 2707–19.

Straight, A. F., Field, C. M. and Mitchison, T. J. (2005) 'Anillin Binds Nonmuscle Myosin II and Regulates the Contractile Ring', *Molecular Biology of the Cell*, 16(1), pp. 193–201. doi: 10.1091/mbc.e04-08-0758.

Su, M. *et al.* (2017) 'Mechanism of Vps4 hexamer function revealed by cryo-EM', *Science Advances*, 3(4), p. e1700325. doi: 10.1126/sciadv.1700325.

Sugawara, T. *et al.* (2003) 'In situ localization of cell wall -1,3-glucan in the fission yeast Schizosaccharomyces pombe', *Journal of Electron Microscopy*. Oxford University Press, 52(>2), pp. 237–242. doi: 10.1093/jmicro/52.2.237.

Sugimoto, K. *et al.* (2002) 'Molecular dynamics of Aurora-A kinase in living mitotic cells simultaneously visualized with histone H3 and nuclear membrane protein importinalpha.', *Cell structure and function*, 27(6), pp. 457–67.

Sullivan, J. E. *et al.* (1994) 'Inhibition of lipolysis and lipogenesis in isolated rat adipocytes with AICAR, a cell-permeable activator of AMP-activated protein kinase.', *FEBS letters*, 353(1), pp. 33-6.

Sumara, I. *et al.* (2004) 'Roles of Polo-like Kinase 1 in the Assembly of Functional Mitotic Spindles', *Current Biology*, 14(19), pp. 1712–1722. doi: 10.1016/j.cub.2004.09.049.

Sunkel, C. E. and Glover, D. M. (1988) '*polo*, a mitotic mutant of Drosophila displaying abnormal spindle poles.', *Journal of cell science*, 89 (Pt 1), pp. 25–38.

Suter, M. *et al.* (2006) 'Dissecting the Role of 5′-AMP for Allosteric Stimulation, Activation, and Deactivation of AMP-activated Protein Kinase', *Journal of Biological Chemistry*, 281(43), pp. 32207–32216. doi: 10.1074/jbc.M606357200.

Sutherland, C. M. *et al.* (2003) 'Elm1p is one of three upstream kinases for the *Saccharomyces cerevisiae* SNF1 complex.', *Current biology : CB*, 13(15), pp. 1299–305.

Tanner, M. M. *et al*. (2000) 'Frequent amplification of chromosomal region 20q12-q13 in ovarian cancer.', *Clinical cancer research : an official journal of the American Association for Cancer Research*, 6(5), pp. 1833–9.

Thaiparambil, J. T., Eggers, C. M. and Marcus, A. I. (2012) 'AMPK regulates mitotic spindle orientation through phosphorylation of myosin regulatory light chain.', *Molecular and cellular biology*. American Society for Microbiology, 32(16), pp. 3203–17. doi: 10.1128/MCB.00418-12.

Thelander, M., Olsson, T. and Ronne, H. (2004) 'Snf1-related protein kinase 1 is needed for growth in a normal day–night light cycle', *The EMBO Journal*, 23(8), pp. 1900–1910. doi: 10.1038/sj.emboj.7600182.

Thornton, C., Snowden, M. A. and Carling, D. (1998) 'Identification of a novel AMP-activated protein kinase beta subunit isoform that is highly expressed in skeletal muscle.', *The Journal of biological chemistry*, 273(20), pp. 12443–50.

Tokumitsu, H. *et al*. (2002) 'STO-609, a specific inhibitor of the Ca(2+)/calmodulin-dependent protein kinase kinase.', *The Journal of biological chemistry*. American Society for Biochemistry and Molecular Biology, 277(18), pp. 15813–8. doi: 10.1074/jbc.M201075200.

Townley, R. and Shapiro, L. (2007) 'Crystal Structures of the Adenylate Sensor from Fission Yeast AMP-Activated Protein Kinase', *Science*, 315(5819), pp. 1726–1729. doi: 10.1126/science.1137503.

Treitel, M. *et al*. (1998). Snf1 protein kinase regulates phosphorylation of the Mig1 repressor in Saccharomyces cerevisiae. Molecular and Cellular Biology, 18(11), 6273–6280. https://doi.org/10.1128/MCB.18.11.6273

Tuazon, P. T. and Traugh, J. A. (1984) 'Activation of actin-activated ATPase in smooth muscle by phosphorylation of myosin light chain with protease-activated kinase I.', *The Journal of biological chemistry*, 259(1), pp. 541–6.

Lopold, U. (1949) 'Die Vererbung von Homothallie und Heterothallie bei *Schizosaccharomyces pombe*', *Compt. Rend.*, 24, pp. 381–480.

Umesono, K. *et al*. (1983) 'Visualization of chromosomes in mitotically arrested cells of the fission yeast Schizosaccharomyces pombe', *Current Genetics*. Springer-Verlag, 7(2), pp. 123–128. doi: 10.1007/BF00365637.

Valbuena, N. and Moreno, S. (2012) 'AMPK phosphorylation by Ssp1 is required for proper sexual differentiation in fission yeast', *Journal of Cell Science*, 125(11).

Vazquez-Martin, A. *et al*. (2009) 'AMPK: Evidence for an energy-sensing cytokinetic tumor suppressor.', *Cell cycle (Georgetown, Tex.)*, 8(22), pp. 3679–83. doi: 10.4161/cc.8.22.9905.

Vazquez-Martin, A. *et al*. (2011) 'Polo-like kinase 1 regulates activation of AMP-activated protein kinase (AMPK) at the mitotic apparatus.', *Cell cycle (Georgetown, Tex.)*, 10(8), pp. 1295–302. doi: 10.4161/cc.10.8.15342.

Vazquez-Martin, A. *et al.* (2012) 'Polo-like kinase 1 directs the AMPK-mediated activation of myosin regulatory light chain at the cytokinetic cleavage furrow independently of energy balance.', *Cell cycle (Georgetown, Tex.)*, 11(13), pp. 2422–6. doi: 10.4161/cc.20438.

Vazquez-Martin, A. *et al.* (2013) 'Serine79-phosphorylated acetyl-CoA carboxylase, a downstream target of AMPK, localizes to the mitotic spindle poles and the cytokinesis furrow.', *Cell cycle (Georgetown, Tex.)*. Landes Bioscience, 12(10), pp. 1639–41. doi: 10.4161/cc.24700.

Vazquez-Martin, A., Oliveras-Ferraros, C. and Menendez, J. A. (2009) 'The active form of the metabolic sensor: AMP-activated protein kinase (AMPK) directly binds the mitotic apparatus and travels from centrosomes to the spindle midzone during mitosis and cytokinesis.', *Cell cycle (Georgetown, Tex.)*, 8(15), pp. 2385–98. doi: 10.4161/cc.8.15.9082.

Vincent, M. F. *et al.* (1991) 'Inhibition by AICA Riboside of Gluconeogenesis in Isolated Rat Hepatocytes', *Diabetes*, 40(10), pp. 1259–1266. doi: 10.2337/diab.40.10.1259.

Vincent, M. F., Bontemps, F. and Van den Berghe, G. (1992) 'Inhibition of glycolysis by 5-amino-4-imidazolecarboxamide riboside in isolated rat hepatocytes', *Biochemical Journal*, 281(1), pp. 267–272. doi: 10.1042/bj2810267.

Wang, P., Henning, S. M. and Heber, D. (2010) 'Limitations of MTT and MTS-Based Assays for Measurement of Antiproliferative Activity of Green Tea Polyphenols', *PLoS ONE*. Public Library of Science, 5(4), p. e10202. doi: 10.1371.

Wang, Z. *et al.* (2001) 'Antagonistic controls of autophagy and glycogen accumulation by Snf1p, the yeast homolog of AMP-activated protein kinase, and the cyclin-dependent kinase Pho85p.', *Molecular and cellular biology*, 21(17), pp. 5742–52. doi: 10.1128/mcb.21.17.5742-5752.2001.

Warburg, O. (1925) 'The Metabolism of Carcinoma Cells', *The Journal of Cancer Research*. American Association for Cancer Research Journals, 9(1), pp. 148–163. doi: 10.1158/jcr.1925.148.

Van de Weerdt, B. C. M. *et al.* (2005) 'Uncoupling anaphase-promoting complex/cyclosome activity from spindle assembly checkpoint control by deregulating polo-like kinase 1.', *Molecular and cellular biology*. American Society for Microbiology (ASM), 25(5), pp. 2031–44. doi: 10.1128/MCB.25.5.2031-2044.2005.

Werle, K. *et al.* (2014) 'Liver kinase B1 regulates the centrosome via PLK1', *Cell Death & Disease*. Nature Publishing Group, 5(4), pp. e1157–e1157. doi: 10.1038/cddis.2014.135.

Wilson, W. A., Hawley, S. A. and Hardie, D. G. (1996) 'Glucose repression/derepression in budding yeast: SNF1 protein kinase is activated by phosphorylation under derepressing conditions, and this correlates with a high AMP:ATP ratio.', *Current biology : CB*, 6(11), pp. 1426–34.

Wollert, T. and Hurley, J. H. (2010) 'Molecular mechanism of multivesicular body biogenesis by ESCRT complexes.', *Nature*. NIH Public Access, 464(7290), pp. 864–9. doi: 10.1038/nature08849.

Wood, V. *et al.* (2002) 'The genome sequence of Schizosaccharomyces pombe', *Nature*. Nature Publishing Group, 415(6874), pp. 871–880. doi: 10.1038/nature724.

Woods, A *et al.* (1996) 'The alpha1 and alpha2 isoforms of the AMP-activated protein kinase have similar activities in rat liver but exhibit differences in substrate specificity in vitro.', *FEBS letters*, 397(2–3), pp. 347–51.

Woods, Angela *et al.* (1996) 'The α1 and α2 isoforms of the AMP-activated protein kinase have similar activities in rat liver but exhibit differences in substrate specificity in vitro', *FEBS Letters*. No longer published by Elsevier, 397(2–3), pp. 347–351. doi: 10.1016/S0014-5793(96)01209-4.

Woods, A. *et al.* (2000) 'Characterization of the role of AMP-activated protein kinase in the regulation of glucose-activated gene expression using constitutively active and dominant negative forms of the kinase.', *Molecular and cellular biology*, 20(18), pp. 6704–11.

Woods, A. *et al.* (2005) 'Ca2+/calmodulin-dependent protein kinase kinase-β acts upstream of AMP-activated protein kinase in mammalian cells', *Cell Metabolism*, 2(1), pp. 21–33. doi: 10.1016/j.cmet.2005.06.005.

Wu, J.-Q. *et al.* (2006) 'Assembly of the cytokinetic contractile ring from a broad band of nodes in fission yeast', *The Journal of Cell Biology*, 174(3), pp. 391–402. doi: 10.1083/jcb.200602032.

Wu, Z. *et al.* (1999) 'Mechanisms Controlling Mitochondrial Biogenesis and Respiration through the Thermogenic Coactivator PGC-1', *Cell*, 98(1), pp. 115–124. doi: 10.1016/S0092-8674(00)80611-X.

Xiao, B. *et al.* (2011) 'Structure of mammalian AMPK and its regulation by ADP', *Nature*. Nature Publishing Group, 472(7342), pp. 230–233. doi: 10.1038/nature09932.

Yang, X., Jiang, R. and Carlson, M. (1994) 'A family of proteins containing a conserved domain that mediates interaction with the yeast SNF1 protein kinase complex.', *The EMBO journal*. European Molecular Biology Organization, 13(24), pp. 5878–86.

You, S. Y. *et al.* (2016) 'Beclin-1 knockdown shows abscission failure but not autophagy defect during oocyte meiotic maturation.', *Cell cycle (Georgetown, Tex.)*. Taylor & Francis, 15(12), pp. 1611–9. doi: 10.1080/15384101.2016.1181235.

Zagorska, A. *et al.* (2010) 'New Roles for the LKB1-NUAK Pathway in Controlling Myosin Phosphatase Complexes and Cell Adhesion', *Science Signaling*, 3(115), pp. ra25–ra25. doi: 10.1126/scisignal.2000616.

Zhao, X. *et al.* (2014) 'Peroxisome proliferator-activated receptor γ coactivator 1α and FoxO3A mediate chondroprotection by AMP-activated protein kinase.', *Arthritis & rheumatology (Hoboken, N.J.)*. NIH Public Access, 66(11), pp. 3073–82. doi: 10.1002/art.38791.

Zhao, Z. *et al.* (2005) 'The GIT-Associated Kinase PAK Targets to the Centrosome and Regulates Aurora-A', *Molecular Cell*, 20(2), pp. 237–249. doi: 10.1016/j.molcel.2005.08.035.

Zheng, X. *et al.* (2018) 'Aurora-A-mediated phosphorylation of LKB1 compromises LKB1/AMPK signaling axis to facilitate NSCLC growth and migration', *Oncogene*, 37(4), pp. 502–511. doi: 10.1038/onc.2017.354.

Zhou, G. *et al.* (2001) 'Role of AMP-activated protein kinase in mechanism of metformin action.', *The Journal of clinical investigation*. American Society for Clinical Investigation, 108(8), pp. 1167–74. doi: 10.1172/JCI13505.